INVESTIGATIONS INTO RAT HEPATOBILIARY DRUG CLEARANCE PATHWAYS IN EARLY DRUG DISCOVERY

A thesis submitted to the University of Manchester for the degree of Doctor of Philosophy in the Faculty of Medical and Human Sciences

2014

CAROLINE RYNN

Manchester Pharmacy School

LIST OF CONTENTS

LIST OF FIGURES 6
LIST OF TABLES 9
ABBREVIATIONS 11
ABSTRACT 15
DECLARATION 16
COPYRIGHT STATEMENT 17
ACKNOWLEDGEMENTS 18
1 CHAPTER ONE: INTRODUCTION 19
1.1 Optimising pharmacokinetics in drug discovery 19
1.1.1 Drug clearance 20
1.2 Liver physiology and hepatobiliary drug disposition pathways 21
1.3 Hepatic drug metabolism 23
1.3.1 Cytochrome P450 enzymes 25
1.3.2 Prediction of hepatic metabolic clearance 25
1.4 Hepatic drug transport 27
1.4.1 Uptake transporters expressed at the sinusoidal membrane of hepatocytes 28
1.4.2 Efflux transporters expressed at the bile canalicular membrane of hepatocytes 31
1.4.3 Tools to investigate hepatobiliary drug transport 34
1.4.4 Prediction of hepatic transporter-mediated clearance 38
1.5 Biopharmaceutics drug disposition classification system 39
1.6 Species differences in hepatobiliary clearance 40
1.6.1 Species differences in metabolism 41
1.6.2 Species differences in biliary clearance 41
1.7 Aims and objectives 42
2 CHAPTER TWO: MATERIALS AND METHODS 44
2.1 Materials 44
2.2 Metabolic clearance in rat liver microsomes 45
2.2.1 Assessment of metabolic stability in rat liver microsomes 45
2.2.2 Quantitation of drug by liquid chromatography tandem mass spectrometry 46
2.2.3 Calculation of stability, half-life and intrinsic clearance 46
2.2.4 Calculation of scaled metabolic $CL_{int,met}$ to normalise for whole liver microsomal and hepatocyte content 47
2.2.5 Prediction of *in vivo* hepatic clearance 47
2.2.6 Statistical analysis of clearance predictions 48
2.2.7 Rat physiological blood flow used for clearance predictions 48
2.3 Isolation of primary rat liver hepatocytes 48
2.3.1 Rat liver excision 48
2.3.2 *Ex-vivo* rat liver perfusion 49
2.3.3 Isolation of rat parenchymal hepatocytes 49
2.3.4 Measurement of primary rat hepatocyte viability and yield 50
2.4 Metabolic clearance in primary rat liver hepatocytes 50
2.4.1 Metabolic stability in primary rat hepatocytes 50
2.5 Metabolic clearance in rat plasma 51
2.6 Drug uptake studies in primary rat hepatocytes 52
2.6.1 Cell culture of primary rat hepatocytes 52
2.6.2 *In vitro* drug uptake in cultured primary rat hepatocytes 52

2.6.3 Determination of protein content of cultured primary rat hepatocytes using the DC protein assay 53
2.6.4 Calculation of initial uptake rates at 37°C and 4°C in cultured primary rat hepatocytes 54
2.6.5 Calculation of intrinsic uptake clearance and scaled uptake clearance in cultured primary rat hepatocytes 54
2.7 Measurement of biliary efflux using a sandwich-cultured primary rat hepatocyte model 55
2.7.1 Cell culture of primary rat hepatocytes in a Collagen I/Matrigel® sandwich 55
2.7.2 Assessment of the viability of sandwich-cultured primary rat hepatocytes 56
2.7.3 Transport of unlabelled drugs in sandwich-cultured rat hepatocytes 57
2.7.4 Transport of fluorescent drugs in sandwich-cultured rat hepatocytes 58
2.7.5 Radiolabelled drug transport studies in sandwich-cultured rat hepatocytes 59
2.7.6 Determination of protein content of sandwich-cultured rat hepatocytes using the DC protein assay 59
2.7.7 Calculation of accumulation, biliary efflux index and biliary clearance 60
2.8 Measurement of plasma protein binding 61
2.8.1 Calculation of unbound fraction, stability in plasma and assay recovery 62
2.9 *In vivo* pharmacokinetic studies in rat 62
2.9.1 *In vivo* blood clearance studies in rat 62
2.9.2 *In vivo* excretion studies in rat 63
2.10 Measurement of drug permeability in MDCKII LE cells and PAMPA 64
2.10.1 The MDCKII LE assay 64
2.10.2 The parallel artificial membrane permeability assay (PAMPA) 65
2.11 *In silico* prediction of p*K*a 67
3 CHAPTER THREE: RESULTS – *IN VITRO-IN VIVO* EXTRAPOLATION OF CLEARANCE IN RAT 68
3.1 Background 68
3.2 Early drug discovery at Novartis Basel 68
3.2.1 Clearance optimization in early drug discovery 69
3.3 Exploring hepatobiliary disposition of early drug discovery NCEs 73
3.3.1 Physicochemical properties of the NCE set 74
3.3.2 IVIVE of rat clearance for the NCE set 76
3.3.3 Comparison of IVIVE methods for predicting hepatic metabolic clearance 83
4 CHAPTER FOUR: RESULTS – DRUG UPTAKE STUDIES IN CULTURED PRIMARY RAT HEPATOCYTES 86
4.1 Background 86
4.2 Development and characterization of a drug uptake model using cultured primary rat hepatocytes 87
4.2.1 Time course of d_8-taurocholic acid and pitavastatin uptake in cultured primary rat hepatocyte monolayers 87
4.2.2 Concentration-dependence of d_8-TCA and pitavastatin in cultured primary rat hepatocyte monolayers 88
4.2.3 Temperature dependence of passive uptake into cultured primary rat hepatocyte monolayers 90
4.2.4 Cultured primary rat hepatocyte uptake assay reproducibility 92
4.3 Measurement of drug uptake in cultured primary rat hepatocytes 94
4.3.1 Distribution of chemical class for substrates and non-substrates of active uptake into cultured primary rat hepatocytes 100

5 CHAPTER FIVE: RESULTS – DRUG HEPATOBILIARY EFFLUX STUDIES IN PRIMARY RAT HEPATOCYTES CULTURED IN A SANDWICH CONFIGURATION 102
5.1 Background 102
5.2 Development and characterisation of a drug efflux model using primary rat hepatocytes cultured in a sandwich configuration 102
5.2.1 Assessment of viability of primary rat hepatocytes maintained in culture for up to 96 h 104
5.2.2 Determination of functional biliary excretion in sandwich cultured rat hepatocytes 105
5.2.3 Optimisation of cell culture conditions for sandwich cultured rat hepatocytes 108
5.3 Measurement of biliary efflux of drugs in sandwich cultured rat hepatocytes..... 127
5.3.1 Distribution of chemical class for substrates and non-substrates of active efflux in sandwich cultured rat hepatocytes. 131
6 CHAPTER SIX: RESULTS – SINGLE AND MULTIPLE PATHWAY IVIVE OF HEPATIC CLEARANCE INVOLVING ACTIVE TRANSPORT 133
6.1 Single pathway IVIVE of hepatic clearance involving active uptake 133
6.2 Single pathway IVIVE of hepatic clearance involving biliary efflux 134
6.3 Multiple pathway IVIVE of hepatic clearance involving metabolism and transport 136
6.3.1 Multiple pathway IVIVE of hepatic clearance involving metabolism and active uptake 136
6.3.2 Multiple pathway IVIVE of hepatic clearance involving metabolism and biliary efflux 138
7 CHAPTER SEVEN: RESULTS – STRUCTURAL AND MOLECULAR ANALYSES OF HEPATIC DRUG TRANSPORT IN RAT 142
7.1 Structural analysis of hepatic drug transport using Bayesian Modelling 142
7.1.1 Structural analysis of substrates of active uptake in cultured primary rat hepatocytes 142
7.1.2 Structural analysis of substrates of biliary efflux in sandwich cultured rat hepatocytes 147
7.2 Molecular analysis of hepatic drug transport using *in silico* computational modelling 152
7.2.1 Molecular analysis of substrates of drug uptake into culture primary rat hepatocytes 152
7.2.2 Molecular analysis of substrates of biliary efflux in sandwich cultured rat hepatocytes 155
8 CHAPTER EIGHT: RESULTS – INVESTIGATION OF THE RELATIONSHIP BETWEEN DRUG PHYSICOCHEMICAL PROPERTIES AND DISPOSITION PATHWAYS 159
8.1 Background 159
8.2 Relationship between clearance and permeability 159
8.3 Relationship between clearance and physicochemical parameters molecular weight, calculated partition coefficient, polar surface area and hydrogen bonding ability. 161
8.4 Relationship between active drug transport and passive permeability 162
8.4.1 Relationship between passive permeability and active uptake in cultured primary rat hepatocytes 162

8.4.2 Relationship between passive permeability and biliary efflux in sandwich cultured rat hepatocytes 164
8.4.3 Cooperativity of active uptake and efflux processes in rat hepatocytes 166
8.5 Investigating disposition permeability relationships in rat 168
9 CHAPTER NINE: DISCUSSION 173
9.1 IVIVE methods for predicting hepatic metabolic clearance in rat 173
9.2 Development and characterisation of a drug uptake model using cultured primary rat hepatocytes 174
9.3 Development and characterization of a drug efflux model using primary rat hepatocytes cultured in a sandwich configuration 176
9.4 Analysis of single and multiple pathway IVIVE of hepatic clearance involving active transport 178
9.5 Structural and molecular analysis of hepatic drug transport 180
9.6 Investigation of the relationship between drug physicochemical properties and disposition pathways 182
9.7 Investigation of disposition permeability relationships in rat 183
10 CHAPTER TEN: CONCLUSIONS AND FUTURE WORK 184
11 APPENDIX 188
11.1 *In vivo*, *in vitro* and *in silico* values for the NCE set 188
11.2 Physicochemical properties of the marketed drug se 194
11.3 Transport of marketed drugs across MDCKII LE cells 196
12 REFERENCES 200

Total word count: 57192

LIST OF FIGURES

Figure 1-1 Key pharmacokinetic parameters which determine dose regimens (van de Waterbeemd and Gifford, 2003) 20
Figure 1-2 Arrangement of hepatocytes, sinusoids and bile ducts in a liver lobule (Ganong, 1995) 22
Figure 1-3 Hepatobiliary drug disposition pathways 23
Figure 1-4 Location of phase I and phase II enzymes in the hepatocyte 24
Figure 1-5 Human drug transporters expressed at the sinusoidal and bile canalicular membranes of hepatocytes (Giacomini et al., 2010) 28
Figure 3-1 Distribution of chemical class for Novartis NCEs. 68
Figure 3-2 Range of lipophilicity values and molecular weights for Novartis NCEs 69
Figure 3-3 Rat IVIVC analysis of Novartis NCEs: Distribution of clearance predictions 70
Figure 3-4 Prediction of rat clearance using rat liver microsomes and cryopreserved hepatocytes for Novartis NCEs 71
Figure 3-5 Distribution of chemical class in the NCE set 74
Figure 3-6 Lipophilicity and molecular weight range for the NCE set 75
Figure 3-7 Physiochemical property space for the NCE set 76
Figure 3-8 Comparison of observed and predicted clearance categories for the NCE set 77
Figure 3-9 Prediction of rat clearance using rat liver microsomes and fresh rat hepatocytes for the NCE set 79
Figure 3-10 Comparison of predicted clearance from rat liver microsomes and fresh rat hepatocytes for the NCE set 82
Figure 3-11 Comparison of three IVIVE methods to predict rat clearance from rat liver microsomes 84
Figure 4-1 Time course of d_8-TCA uptake in cultured primary rat hepatocyte monolayer cultures 87
Figure 4-2 Time course of pitavastatin uptake in cultured primary rat hepatocyte monolayer cultures 88
Figure 4-3 Concentration dependence of d_8-TCA uptake in cultured primary rat hepatocytes 89
Figure 4-4 Concentration dependence of pitavastatin uptake in cultured primary rat hepatocytes 90
Figure 4-5 Effect of incubation temperature on passive uptake of propranolol in cultured primary rat hepatocytes 91
Figure 4-6 Effect of incubation temperature on passive uptake of alprenolol in cultured primary rat hepatocytes 92
Figure 4-7 Distribution of chemical class for substrates and non-substrates of active uptake into cultured primary rat hepatocytes 101
Figure 5-1 Phase contrast images of primary rat hepatocytes cultured in BioCoat™ Matrigel® 6-well plates for 24 h 103

Figure 5-2 Phase contrast images of sandwich cultured rat hepatocytes cultured in BioCoat™ Matrigel® 6-well plates for 96 h 104
Figure 5-3 Assessment of viability of primary rat hepatocytes maintained in culture up to 96 h 105
Figure 5-4 Fluorescent images of CDF inside sandwich cultured rat hepatocytes cultured in BioCoat™ Matrigel® 6-well plates for 96 h following pre-treatment with Ca^{2+}/Mg^{2+}-free buffer 106
Figure 5-5 Fluorescent images of CDF inside sandwich cultured rat hepatocytes cultured in BioCoat™ Matrigel® 6-well plates for 96 h following pre-treatment with standard buffer 107
Figure 5-6 Accumulation of hydrolysed carboxydichlorfluorescein in sandwich cultured rat hepatocytes 108
Figure 5-7 Influence of cell seeding density on the transport of [^{3}H]TCA in sandwich cultured rat hepatocytes 110
Figure 5-8 Time dependence of cellular accumulation and biliary excretion of [^{3}H] TCA in sandwich cultured rat hepatocytes 112
Figure 5-9 Influence of extracellular matrix type on the accumulation and biliary excretion of [^{3}H]TCA and [^{3}H]Digoxin in sandwich cultured rat hepatocytes 114
Figure 5-10 Influence of extracellular matrix type on the accumulation and biliary excretion of [^{3}H]DPDPE and rosuvastatin in sandwich culture rat hepatocytes 115
Figure 5-11 Prediction of biliary clearance for marketed drugs using sandwich cultured rat hepatocytes 121
Figure 5-12 Comparison of *in vitro* and *in vivo* biliary efflux index of marketed drugs using sandwich cultured rat hepatocytes 122
Figure 5-13 Comparison of in-house and reference biliary excretion index of marketed drugs using sandwich cultured rat hepatocytes 123
Figure 5-14 Distribution of chemical class for substrates and non-substrates of active efflux in sandwich cultured rat hepatocytes 131
Figure 6-1 Single pathway IVIVE analysis: Prediction of rat clearance for substrates of active uptake 133
Figure 6-2 Single pathway IVIVE analysis: Prediction of rat clearance for substrates of biliary efflux 135
Figure 6-3 Comparison of single and multiple pathway IVIVE analysis: Prediction of rat clearance for substrates of active uptake 137
Figure 6-4 Comparison of single and multiple pathway IVIVE analysis: Prediction of rat clearance for substrates of biliary efflux 140
Figure 7-1 Activity scores of active and inactive compounds of hepatic uptake transporters 143
Figure 7-2 Structures of marketed drugs with high calculated activity score for hepatic uptake transporters 144
Figure 7-3 Example substructures with high calculated fragment score for hepatic uptake transporters 145

Figure 7-4 Predicted activity score of active and inactive compounds of hepatic uptake transporters 146
Figure 7-5 Activity scores of active and inactive molecules of biliary efflux 148
Figure 7-6 Structures of marketed drugs with high calculated activity score for biliary efflux 149
Figure 7-7 Example substructures with high calculated fragment score for biliary efflux 150
Figure 7-8 Predicted activity score of active and inactive molecules of biliary efflux 151
Figure 7-9 Coefficient plot of the 4 descriptors used to define the discriminant model of drug uptake 154
Figure 7-10 Discriminant PLS model of drug uptake into cultured primary rat hepatocytes 155
Figure 7-11 Coefficient plot of the 3 descriptors used to define the discriminant model of biliary efflux 156
Figure 7-12 Discriminant PLS model of biliary efflux in sandwich cultured rat hepatocytes 157
Figure 8-1 Prediction of rat clearance from *in vitro* $CL_{int,met}$ for NCEs with low, medium and high passive permeability 160
Figure 8-2 Range in measured passive permeability for non-substrates and substrates of active uptake in cultured primary rat hepatocytes 163
Figure 8-3 Range in measured permeability for non-substrates and substrates of biliary efflux in sandwich cultured rat hepatocytes 165
Figure 8-4 Influence of passive permeability on the cooperative relationship of active transport processes in rat hepatocytes 167
Figure 8-5 Prediction of rat clearance using rat liver microsomes for the 12 NCEs profiled in bile duct-cannulated rat studies 170
Figure 11-1 Distribution of chemical class for the marketed drug set used to explore rat IVIVE of drug clearance 194
Figure 11-2 Lipophilicity and molecular weight range for the marketed drug set 195
Figure 11-3 Physiochemical property space for the marketed drug set 196
Figure 11-4 Comparison of MDCKII LE P_{app} values with reference data for 13 marketed drugs 198

LIST OF TABLES

Table 1-1 Solute carrier uptake transporters at the sinusoidal membrane of hepatocytes 30

Table 1-2 Hepatic efflux transport proteins expressed at the bile canalicular membrane 32

Table 1-3 Summary of model systems used to study hepatobiliary drug transport (adapted from Annaert, 2007) 35

Table 1-4 The BDDCS System: Predicting drug disposition. 40

Table 2-1 LC-MS/MS gradient conditions 46

Table 2-2 PAMPA permeability categories 67

Table 3-1 Comparison of clearance predictions for Novartis NCEs using rat liver microsomes and hepatocytes 72

Table 3-2 Statistical analysis of clearance predictions in rat liver microsomes and fresh rat hepatocytes for the NCE set 80

Table 3-3 Statistical analysis for three different IVIVE methods to predict clearance in rat liver microsomes for the NCE set 85

Table 4-1 Intra- and inter-assay variability in pitavastatin uptake in cultured primary rat hepatocytes 93

Table 4-2 Intra- and inter-assay variability in propranolol uptake in cultured primary rat hepatocytes 94

Table 4-3 Uptake of NCEs and marketed drugs into cultured primary rat hepatocytes 95

Table 5-1 Calculated biliary efflux index and predicted biliary clearance data for [^{3}H]TCA in sandwich cultured rat hepatocytes 112

Table 5-2 Influence of cell seeding density on the accumulation, biliary efflux index and predicted CL_b of 10 µM [^{3}H]TCA in 12- and 24-well BioCoat™ Collagen I plates 117

Table 5-3 Comparison of accumulation, biliary efflux index and predicted biliary clearance of drugs in 6, 12- and 24-well BioCoat™ Collagen I plates 118

Table 5-4 Assessment of BEI and predicted biliary clearance in sandwich cultured rat hepatocytes for a range of marketed drugs and comparison to reference *in vitro* and *in vivo* rat biliary excretion data 120

Table 5-5 Statistical data comparing the accuracy of in-house CL_b predictions and biliary efflux index with observed values in rat 123

Table 5-6 Intra- and inter-assay variability in d_8-TCA accumulation and biliary efflux in primary rat hepatocytes cultured in a sandwich configuration. 125

Table 5-7 Intra- and inter-assay variability in pitavastatin accumulation and biliary efflux in primary rat hepatocytes cultured in a sandwich configuration. 126

Table 5-8 Intra- and inter-assay variability in propranolol accumulation and biliary efflux in primary rat hepatocytes cultured in a sandwich configuration. 127

Table 5-9 Measurement of biliary efflux and biliary clearance of NCEs and marketed drugs in sandwich cultured rat hepatocytes 128

Table 6-1 Statistical data comparing the accuracy of clearance predictions for substrates of active uptake. 134
Table 6-2 Statistical data comparing the accuracy of clearance predictions for substrates of biliary efflux..... 136
Table 6-3 Statistical data comparing the accuracy of clearance predictions for substrates of active uptake: Comparison of single and multiple pathway IVIVE analysis. 138
Table 6-4 Statistical data comparing the accuracy of clearance predictions for substrates of biliary efflux: Comparison of single and multiple pathway IVIVE analysis 141
Table 7-1 Predictivity of the hepatic uptake classification model 147
Table 7-2 Predictivity of the biliary efflux classification model..... 152
Table 7-3 Predictivity of the *in silico* model of drug uptake into cultured primary rat hepatocytes..... 155
Table 7-4 Predictivity of the *in silico* model of biliary efflux in sandwich cultured rat hepatocytes..... 157
Table 8-1 Statistical analysis of predictions of rat clearance from rat liver microsomes for low, medium and high permeability NCEs..... 161
Table 8-2 Statistical analysis of predictions of rat clearance from rat liver microsomes: Relationship between predictability and physicochemical parameters 163
Table 8-3 Comparison of passive permeability category for substrates and non-substrates of active uptake in cultured primary rat hepatocytes 164
Table 8-4 Comparison of passive permeability categories for substrates and non-substrates of biliary efflux in sandwich cultured rat hepatocytes 166
Table 8-5 Cooperativity of active uptake and biliary efflux processes in rat hepatocytes..... 167
Table 8-6 *In vivo, in vitro* and physicochemical properties for the 12 NCEs profiled in BDC rat studies 169
Table 11-1 *In vivo, in vitro* and *in silico* values for the NCE set 188
Table 11-2 Permeability results for marketed drugs with MDCKII LE cells and comparison to reference MDCKII P_{app} data and human intestinal absorption..... 197
Table 11-3 Reproducibility of P_{app} values and percentage assay recovery of quality control standards in MDCKII LE cells 199

ABBREVIATIONS

A	Accessible filter area of PAMPA hexadecane membrane
ABC	ATP-binding cassette
ADME	Absorption, distribution, metabolism, excretion
afe	Average fold error
AUC	Area under the curve
AUC_{extrap}	Extrapolated area under the curve
AUC_{last}	Area under the curve based on the last time point
AUMC	Area under the moment curve
BCS	Biopharmaceutics classification system
BDDCS	Biopharmaceutics drug disposition classification system
BCRP (Bcrp)	Breast cancer related protein
BEI	Biliary efflux index
BSA	Bovine serum albumin
BSEP (Bsep)	Bile salt efflux protein
Ca^{2+}	Calcium ion
$CaCl_2$	Calcium chloride
CDFDA	Carboxydichlorofluorescein diacetate
CDF	Carboxydichlorofluorescein
CL	Clearance
CL_b	Biliary clearance
CL_H	Hepatic clearance
CL_{int}	Intrinsic clearance
$CL_{int,act}$	Active uptake intrinsic clearance
$CL_{int,met}$	Metabolic intrinsic clearance
$CL_{int,pas}$	Passive uptake intrinsic clearance
$CL_{int,sec}$	Biliary (secretion) intrinsic clearance
$CL_{int,upt}$	Total uptake intrinsic clearance
CO	Collagen I coating
CO_2	Carbon dioxide
CV	Coefficient of variation
CYP450	Cytochrome P450
d_8-TCA	Deuterium-labelled taurocholic acid
DC	Detergent compatible
DMEM	Dulbecco's modified Eagle medium
DMSO	Dimethyl sulphoxide
DPBS	Dulbecco’s phosphate buffered saline
DPDPE	[D-Pen2,5]-Enkephalin hydrate
dpm	disintegrations per minute

EBSS	Earl's balanced salt solution
EGTA	Ethylene glycol tetra acetic acid
FA_{calc}	Calculated fraction absorbed
F_I	Ionisation factor
Fu	Fraction unbound
Fu_p	Fraction unbound in plasma
fu_b	Fraction unbound in blood
fu_{inc}	Fraction unbound in the incubation
fu_{liver}	Fraction unbound in liver
fu_p	Fraction unbound in plasma
$Fu_{p\text{-}app}$	Apparent fraction unbound in plasma
G	Gram
GI	Gastro-intestinal
GSH	Glutathione
H	Hour
[^{3}H]	Tritium labelled substrate
HBSS	Hank's balanced salt solution
HDM	Hexadecane membrane
HEPES	4-(2-Hydroxyethyl)piperazine-1-ethanesulfonic acid
HPLC	High performance liquid chromatography
HTS	High throughput screening
I.D.	Inner diameter
ITS	Insulin-transferrin-selenium (solution)
i.v.	Intra-venous
IVIVC	*In vitro-in vivo* clearance correlation
IVIVE	*In vitro-in vivo* clearance extrapolation
k_{el}	Initial rate of elimination
Kg	Kilogram
K_m	Substrate concentration that yields half maximal reaction velocity
LC-MS/MS	Liquid chromatography tandem mass spectrometry
LOQ	Limit of quantitation
M	Incubation protein content
MB	Mass balance
MDR	Multiple drug resistance protein
MG	Matrigel®
Mg	Milligram
Mg^{2+}	Magnesium ion
µl	Microlitres
Min	Minutes
Ml	Millilitre
MRP (Mrp)	Multidrug resistance associated protein 2

MRT	Mean residence time
MTS	[3-(4,5-dimethylthiazol-2-yl)-5-(3-carboxymethoxyphenyl)-2-(4-sulfophenyl)-2H-tetrazolium
NADPH	β-nicotinamide adenine dinucleotide 2′-phosphate reduced tetrasodium salt hydrate
NCE	New chemical entity
nd	No data
NMP	N-Methyl-2-pyrrolidone
nr	No result
NSB	Non-specific binding
NTCP (Ntcp)	Sodium taurocholate co-transporting polypeptide
OCT (Oct)	Organic cation transporter
OAT (Oat)	Organic anion transporter
OATP (Oatp)	Organic anion transporting polypeptide
O_2	Oxygen
P.A.R.	Peak area ratio
Pa	Apparent permeability
PAMPA	Parallel artificial membrane permeability assay
PBS	Phosphate buffered saline
PC	Phosphatidylcholine
*Pc*50	PAMPA permeability at 50% fraction absorbed
PD	Pharmacodynamic
P_e	Effective membrane permeability
P-gp	P-glycoprotein
PK	Pharmacokinetic
p*K*a	The negative logarithm of the acid dissociation constant, *K*a
PEG	Polyethylene glycol
PPB	Plasma protein binding
Q_H	Hepatic blood flow rate
Q_P	Hepatic plasma flow rate
r	Ratio
r^2	R squared, coefficient of variation
RED	Rapid equilibrium dialysis
RLM	Rat liver microsomes
RH	Rat hepatocytes
rmse	Root mean squared prediction error
rpm	Revolutions per minute
s.c.	Sub-cutaneous
SCRH	Sandwich cultured rat hepatocytes
S.D.	Standard deviation
SDS	Sodium dodecyl sulfate

SF	Scaling factor
SLC (SLCO)	Solute carrier
TCA	Taurocholic acid
T	time point
*t*1/2	Half-life
UGT	5'-Uridine diphosphate-glucuronosyltransferase
V	Incubation volume
V_d	Volume of distribution
V_D	Volume of the donor compartment
v/v	Volume to volume
Vmax	Maximal rate of velocity of reaction
V_R	Volume of the receiver compartment
V_{ss}	Volume of distribution at steady state
WEM	Williams E medium

ABSTRACT

Conventional 'well-stirred' extrapolation methodology using intrinsic metabolic clearance data from rat liver microsomes poorly predicts *in vivo* clearance for approximately half of drug discovery compounds. The aim of this present study was to gain a more detailed understanding of the hepatobiliary disposition pathways which influence drug clearance. A set of 77 new chemical entities (NCEs), demonstrating a range of physicochemical properties and *in vitro-in vivo* clearance correlations (IVIVC), were employed to explore relationships between hepatobiliary disposition pathways in rat and physicochemical, structural and molecular properties of the NCEs.

Primary rat hepatocytes with >80% cell viability were successfully isolated from male Han Wistar rats and used to establish *in vitro* models of drug uptake and biliary efflux. Preliminary studies with cultured primary rat hepatocytes indicated that uptake of d_8-taurocholic acid and pitavastatin was time, concentration and temperature dependent. Initial studies with sandwich cultured primary rat hepatocytes demonstrated that cellular accumulation and biliary efflux of [^{3}H]-Taurocholic acid was time and concentration dependent. These *in vitro* rat hepatocyte models were then used to investigate drug uptake and biliary efflux for all NCEs. In general, NCEs with high (passive) permeability showed better IVIVC and a lower incidence of active uptake and biliary efflux compared to NCEs with lower permeability, suggesting permeability is a key property influencing hepatobiliary drug disposition in rat. Preliminary *in silico* models analysing structural and molecular descriptors of substrates of active transport in rat hepatocytes were developed and indicated modest potential to highlight clearance pathways beyond hepatic metabolism but further follow up work with larger, more diverse compound sets is warranted to gain confidence in these models.

Extended clearance models were investigated to estimate the effect of hepatic transporters on clearance and to predict the overall hepatic clearance of the NCEs. None of these models resulted in a 1 to 1 correlation but in general, improvements in clearance predictions were made when drug transport processes were accounted for.

In vivo excretion studies using bile duct cannulated rats demonstrated that NCEs with high permeability and good IVIVC were not directly eliminated in bile or urine as unchanged drug, whereas NCEs with lower permeability and poor IVIVC (> 3-fold under predicted) were all directly eliminated unchanged indicating key drivers of clearance beyond metabolism.

In conclusion these investigations confirmed a role for hepatic transporters in clearance but the complex nature of active transport mechanisms and a lack of robust *in vitro* tools create challenges in the quantitative prediction of hepatobiliary clearance. However, one of the key findings from this research, which is highly applicable in early drug discovery, was to identify the existence of disposition permeability relationships. These can be anticipated by observing physicochemical parameters of NCEs in conjunction with conventional IVIVC, since NCEs that are not highly permeable, possess some hydrophobic characteristics, and which are poor substrates of cytochrome P450 enzymes are more likely to be good substrates of transporters and be directly eliminated in bile and/or urine.

The present study focused on exploring hepatobiliary disposition pathways using rat as the investigative species. Whilst there is no guarantee that pathways relevant to rat will be similar to other preclinical species or even humans, an early diagnosis of dominant clearance pathways can guide a more efficient use of the ADME-PK toolbox.

DECLARATION

That no portion of the work referred to in the thesis has been submitted in support of an application for another degree or qualification of this or any other university or other institute of learning.

COPYRIGHT STATEMENT

ACKNOWLEDGEMENTS

Firstly, I would like to express my appreciation to my supervisors, Dr. Jeff Penny for his valuable advice, support, patience, encouragement and diligence throughout my PhD studies and Dr. Bernard Faller for his expert knowledge and facilitation of my part-time PhD research program within Novartis.

I would also like to express my sincere gratitude to my colleagues; Gaëlle Chenal and Cornelia Schluep for their assistance with isolation of fresh rat hepatocytes, Gaëlle Chenal and Yannick Friche for their help with the *in silico* modelling of active transport and Dr. Peter Ertl for his expertise and collaboration with the Bayesian modelling of active transport. In addition, there are numerous colleagues in the Metabolism and Pharmacokinetics department at Novartis in Basel that I am grateful for their assistance, scientific input and challenge.

I would also like to thank my friends and family, especially my sister Diane, for their love, support and encouragement.

Finally, I would like to thank Novartis Institute of Biomedical Research for this development opportunity and for their financial support.

Caroline Rynn

1 CHAPTER ONE: INTRODUCTION

1.1 Optimising pharmacokinetics in drug discovery

Pharmacokinetics describes the time course of drug concentration within the body. Pharmacokinetic characteristics are influenced by intrinsic properties like solubility and permeability which confer the absorption, distribution, metabolism and excretion characteristics of compounds (Lipinski et al., 1997) and determine the pharmacokinetic (PK) profile. High attrition rates in drug discovery and development coupled with rising complexity and costs to deliver new medicines to market in a shorter time frame constitute a huge challenge to the pharmaceutical industry. Back in the late 1980's, analysis of success rates of bringing new medicines to man between 1964 and 1985 indicated that ~40% of new chemical entities (NCEs) displayed poor PK properties and this was the main reason for attrition (Prentis et al., 1988). Consequently, drug discovery functions invested heavily to optimise the PK properties of NCEs to minimize risk and reduce attrition. By 2000, attrition through poor pharmacokinetics had reduced dramatically to less than 10% (Kola and Landis, 2004).

The dose response of a drug also includes a pharmacodynamic (PD) phase involving engagement of drug with the target, which requires sufficient exposure of drug. A balance of both PK and PD properties determine the success of a drug and the prediction and optimization of PK remains a central component of modern drug discovery. Pharmacokinetic parameters may be derived from the measurement of drug concentrations in blood following administration of drug to pre-clinical species or man. Most drugs are given orally for reasons of convenience. The drug dissolves in the gastro-intestinal (GI) tract and is absorbed through the gut wall into the portal circulation before passing into the liver. There are 5 key PK parameters which determine the size of dose and frequency (dosing regimen) required to achieve target engagement and efficacy; volume of distribution, clearance, absorption, half-life and oral bioavailability (Figure 1-1).

Figure 1-1 Key pharmacokinetic parameters which determine dose regimens (van de Waterbeemd and Gifford, 2003)

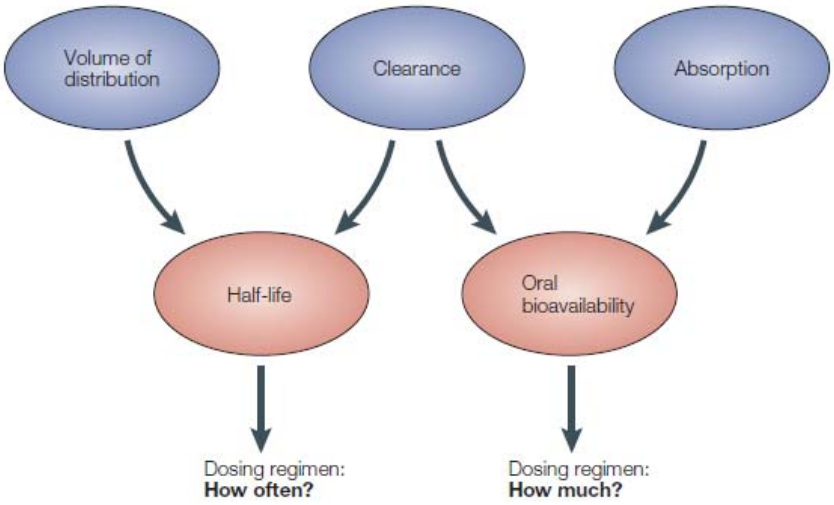

The volume of distribution at steady state (V_d or V_{ss} at steady state) is a theoretical concept relating the concentration of a drug in the blood to the total amount in the body and provides a term which reflects the extent of distribution and tissue affinity. This parameter is reasonably predictable from physicochemical properties and *in vitro* data (Lombardo et al., 2002). Clearance refers to the volume of blood cleared of drug per unit time and describes the efficiency of irreversible elimination of drug from the systemic circulation. The clearance rate together with the volume of distribution determine the half-life of drug elimination (the time taken for the amount of drug in the body to fall by half) and thus the frequency of dosing. Absorption is the extent to which intact drug is absorbed across the gut wall into the portal circulation and is determined by many factors including dissolution rate in the stomach, gastric emptying rate, intestinal motility and passage through the gut wall. Oral bioavailability of drugs is the product of the fraction of drug absorbed and the fraction of drug cleared prior to reaching the systemic circulation, which in turn determines the size of dose required.

1.1.1 Drug clearance

The major drug elimination routes in pre-clinical species and humans are metabolism, renal and biliary. Elimination in this context refers to two processes; the first is the metabolic conversion of parent drug to more polar metabolites, predominantly in the liver, and the second refers to direct excretion of unchanged drug into bile and urine. Clearance may be referred to by a particular organ, such as liver clearance or kidney clearance,

whereas total clearance is the sum of all elimination processes that occur for a given drug. Both hepatic metabolic and biliary elimination are covered in more detail in subsequent sections of this introductory chapter.

1.1.1.1 Renal excretion

Renal excretion of unchanged drug can be a major elimination route for some drugs, especially those demonstrating low hepatic clearance. In addition, excretion via the renal route can also be an important elimination route for polar metabolites of drugs. Renal excretion of drugs can involve passive and active processes. If drug is cleared from the blood into the renal proximal tubule via passive filtration then renal clearance is determined by glomerular filtration rate and the unbound fraction of drug in the blood. Passive reabsorption from urine into blood is dependent on passive permeability and is influenced by urine flow and pH. Reabsorption back into the blood is highly correlated with lipophilicity, consequently, higher lipophilicity generally improves passive permeability, reducing tubular secretion into urine. Typically, only compounds with a negative log $D_{7.4}$ will be passively renally cleared (Smith et al., 1996).

Active renal excretion is more complex and can involve several processes. Transporters polarized to the basolateral membrane of renal proximal tubules can mediate uptake of substrates from the blood into the tubule. Efflux transporters expressed on the apical membrane may then pump substrate from the tubule to the renal collecting ducts, with subsequent elimination in the urine.

1.2 Liver physiology and hepatobiliary drug disposition pathways

The liver, a primary organ of elimination and the largest glandular organ of the body, performs many complex functions including formation of bile, urea and plasma proteins, cholesterol metabolism and detoxification of many drugs and toxins. The liver is organized into lobules. Hepatocytes, which are the predominant cell type in the liver, are polarised cells with distinct basolateral (sinusoidal) and apical (canalicular) domains that extend in chord like arrays throughout the liver. Terminal branches of the hepatic portal vein and hepatic artery empty together and mix as they enter into sinusoids either side of single layers of hepatic cells (Figure 1-2). The sinusoidal membrane of the hepatocyte contains many microvilli creating a large surface area for passive diffusion of lipophilic compounds from blood into the hepatocyte. Each hepatocyte is in contact with adjacent hepatocytes and has access to a bile canaliculus. In comparison, the bile canalicular

membrane has a comparatively small surface area for diffusion at ~10-15% of the total hepatocyte surface area (Fenner et al., 2012).

Figure 1-2 Arrangement of hepatocytes, sinusoids and bile ducts in a liver lobule (Ganong, 1995)

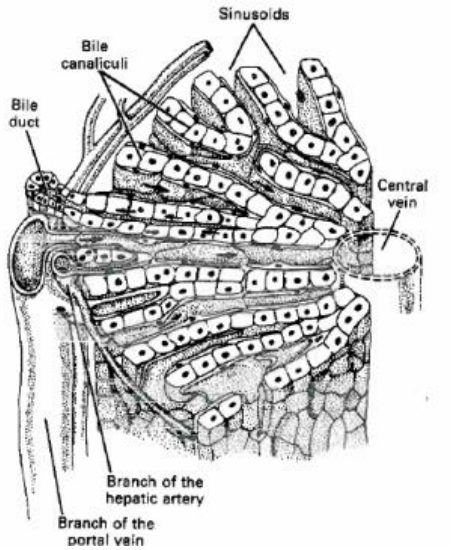

Drug elimination in the liver consists of 4 pathways: (1) Uptake of drug from sinusoidal blood into hepatocyte, (2) metabolism and/or (3) excretion into the bile canaliculi and (4) sinusoidal efflux from inside the hepatocyte to the sinusoidal blood, as detailed in Figure 1-3. Drug uptake, metabolism and biliary efflux pathways are the focus of this thesis and are described in more detail in subsequent sections.

Figure 1-3 Hepatobiliary drug disposition pathways

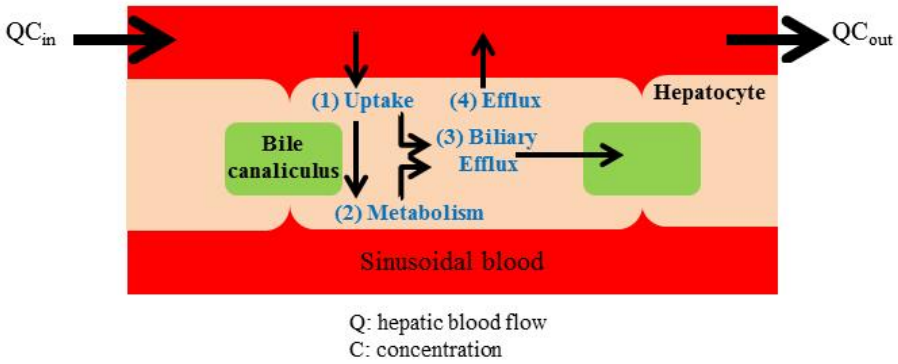

Pathways involved in hepatobiliary drug disposition. Uptake and efflux of drug molecules across the sinusoidal membrane can involve both passive and active processes. Drug molecules inside the hepatocyte may be metabolized by phase I and II enzymes. Efflux of unchanged drug or metabolites across the bile canalicular membrane into bile is primarily an active process.

1.3 Hepatic drug metabolism

In most cases, the role of metabolism is to convert drugs into more water soluble molecules that may be excreted in the urine. Drugs which are directly eliminated in the urine are typically polar and poorly permeable, whereas, lipophilic drugs may require metabolism into more polar, membrane impermeable metabolites prior to excretion. Hepatocytes contain the principal metabolic machinery responsible for metabolic drug clearance. Drug metabolism occurs in two phases, phase I reactions typically create more polar metabolites which may be directly eliminated into bile or further metabolised or conjugated following phase II reactions. Phase I enzymes are predominantly cytochrome P450 (CYP450) enzymes which catalyse hydroxylation of a wide variety of structurally diverse drugs and chemicals which requires molecular oxygen and reduced β-nicotinamide adenine dinucleotide 2′-phosphate tetrasodium salt hydrate (NADPH) cofactor. Phase II conjugation reactions involve a diverse group of enzymes. Glucuronidation, the most common phase II reaction, is catalysed by uridine 5′-diphosphate-glucuronosyltransferases (UGTs) and results in production of glucuronide metabolites which are excreted into bile. Direct glucuronidation of drugs can also be an important pathway for drugs which already possess functional groups like –OH, -COOH or $-NH_2$. The routes by which drugs may be metabolized are many and varied and many phase I and II reactions may compete for the same substrate.

Isolated primary hepatocytes are recognised as one of the most relevant *in vitro* models with which to study drug metabolism since they contain a full complement of

phase I and II hepatic enzymes and respective cofactors. They can fully substitute for microsomes and have been shown to provide improved *in vitro-in vivo* extrapolation (IVIVE) when hepatic metabolism involves more than CYP450 mediated metabolism such as aldehyde oxidation, glucuronidation, sulfation etc (Hewitt et al., 2007; McGinnity et al., 2004). Microsomes and hepatocytes constitute the traditional metabolism toolbox used in early drug discovery along with recombinant CYP450s and liver S9 and cytosolic fractions which can all be utilized in a systematic manner to explore and understand metabolic clearance. The location of phase I and II enzymes in hepatocytes is illustrated in Figure 1-4.

Figure 1-4 Location of phase I and phase II enzymes in the hepatocyte

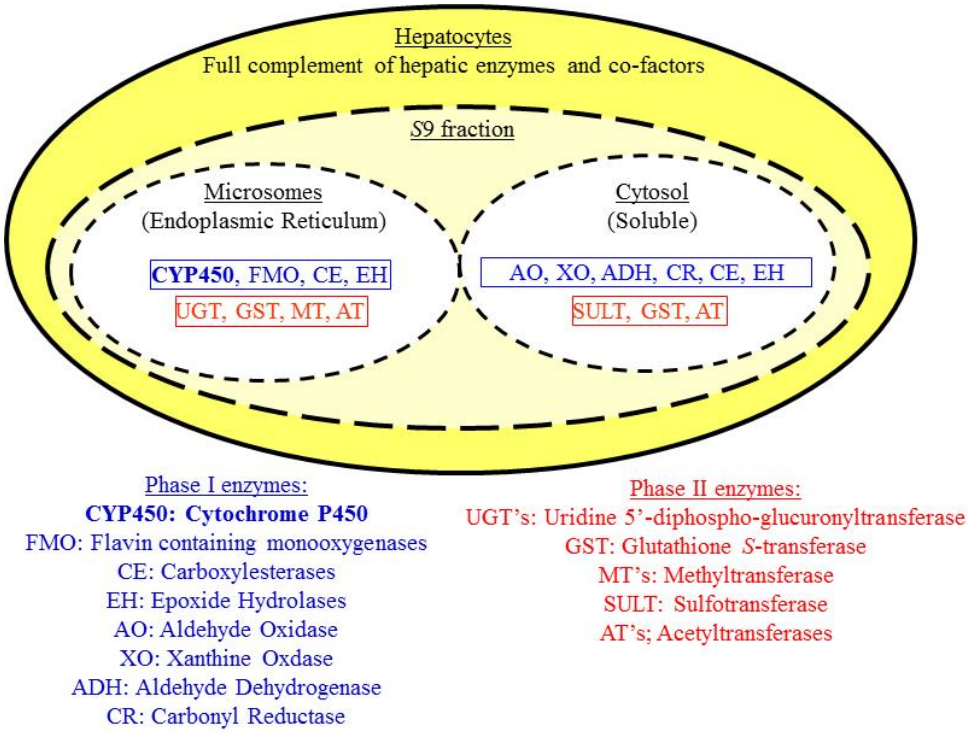

Hepatic metabolic enzymes are located either in the endoplasmic reticulum or cytosolic fractions. Hepatocytes contain all cofactors required to enable catalysis. These cofactors are lost during the preparation of microsome and cytosolic fractions and assay incubations need to be supplemented with co-factors relevant to the enzyme. Metabolic reactions involving xanthine oxidase, carboxylesterase and epoxide hydrolase do not require cofactors.

1.3.1 Cytochrome P450 enzymes

Metabolism is listed as a clearance mechanism for three quarters of the top 200 prescribed drugs in the USA in 2002 and of these metabolized drugs, about three-quarters are metabolized by the CYP450 superfamily of enzymes (Williams et al., 2004). CYP450s catalyse a variety of oxidation (and some reduction) reactions for a diverse range of substrates. The central features of the catalytic cycle are the ability of the haem iron to undergo cyclic oxidation and reduction reactions in conjunction with substrate binding and oxygen activation. Many CYP450 isoenzymes have been discovered although a relatively small subset account for the majority of drug oxidations in humans, with CYP3A being the most abundant isoenzyme in the human liver catalysing the vast majority of oxidative metabolism. Species differences in CYP450 metabolism are also well known and substrates of the major human CYP450s can be metabolized in other species, but the rate and the precise CYP450 subfamily involved may differ (Nishimuta et al., 2013). Optimisation of clearance in early drug discovery has driven the development of a range of well validated, robust, *in vitro* tools but the emphasis remains focused on CYP450 screening systems, with liver microsomes providing a common and convenient *in vitro* tool of choice within industry as a first line metabolism screen.

1.3.2 Prediction of hepatic metabolic clearance

In vitro in vivo extrapolation (IVIVE) strategies were first introduced more than 20 years ago following seminal publications describing the inter-relationship between hepatic clearance, intrinsic clearance, blood flow and unbound fraction of drug in blood (fu_b) known as the well-stirred model (Houston, 1994; Wilkinson and Shand, 1975). This model assumes (1) that drug distribution from blood into the liver is perfusion rate limited and active transport systems are generally disregarded, (2) that only unbound drug can cross membranes to reach the active enzyme site and (3) that there is an homogenous distribution of metabolic enzymes throughout the liver. Intrinsic clearance (CL_{int}) is a pure measure of the ability of enzymes to metabolise compounds and the pivotal parameter for the extrapolation of *in vitro* data to the *in vivo* situation. Intrinsic clearance is expressed in terms µl/min/mg microsomal protein or µl/min/10^6 cells and converted to ml/min/kg body weight using species specific physiological scaling factors which account for the recovery ratio of microsomal protein/g liver or hepatocellularity and liver weights (Davies and Morris, 1993; Iwatsubo et al., 1997; Sohlenius-Sternbeck, 2006).

Systematic under prediction of clearance is frequently associated with the conventional well-stirred approach. One of the most controversial aspects in the general understanding of this model is the inclusion, or not, of drug binding terms in either blood (fu_b) or plasma (fu_p) or non-specific binding to the incubation constituents such as microsomes or hepatocytes (fu_{inc}) into the prediction and many reviews have been published on this subject with mixed success. Generally, underestimates with extrapolated clearance can occur if only fu_b (or fu_p) is taken into account, particularly for basic and neutral compounds. Whereas inclusion of both fu_b (or fu_p) and fu_{inc} can result in a better agreement between extrapolated and observed clearance values, especially for acidic compounds (Obach, 1997; Obach, 1999; Riley et al., 2005).

Recently, newer approaches have been developed in an attempt to remove the systematic bias observed with the conventional well-stirred approach. For ionisable drugs, the predicted clearance may be improved by adjusting the binding terms for the ionisation factor F_I which is the ratio of unionised drug at pH 7.4 and pH 7 which accounts for the pH difference inside (intracellular tissue water, pH 7) and outside of the hepatocyte (plasma, pH 7.4) by applying an ionisation factor (Berezhkovskiy, 2011). Another novel method which improved clearance predictions for a small number of drugs highly bound to albumin adjusts the binding terms to account for the unbound fraction in liver (fu_{liver}). The fu_{liver} is calculated by converting the fu_p adjusted by F_I ($Fu_{p\text{-}app}$) into a whole-liver-plasma ratio (Poulin et al., 2012b). However, prior knowledge of the main binding protein is required to enable estimation of the fu_{liver}. Additionally, the regression offset approach where empirical correction factors derived from regression analyses of *in vivo* and *in vitro* CL_{int} are applied to predict *in vivo* clearance has also shown promise (Sohlenius-Sternbeck et al., 2012). Key requirements for inclusion in a hepatocyte regression line are that the principle route of elimination should be metabolism whereas compounds reliant on uptake transporters for entry into the hepatocyte along with those with *in vivo* blood clearance approaching liver blood flow should be avoided. In their application, improved clearance predictions were obtained with these newer approaches providing appropriate attention to detail was made, however they are not easily applicable in an early drug discovery setting as detailed knowledge of the major protein binding partners and information on elimination routes are typically not available.

1.4 Hepatic drug transport

For drug molecules to reach therapeutic targets in the body, they must be able to permeate phospholipid bilayers membranes. Passive diffusion is the most important permeability mechanism for drug molecules, and the extent of passive diffusion is governed by the concentration gradient across the membrane. To gain access into hepatocytes, drug molecules carried in portal blood need to pass through the non-polar lipid bilayer of the hepatocyte membrane. Typically, lipophilic and neutral molecules are more membrane permeable compared to hydrophilic molecules and molecules which are ionized at physiological pH tend to interact with the charged membrane which results in reduced passive permeability. Molecules may also pass through the intercellular pores between adjacent cells, i.e. via the paracellular route but this route is limited to polar molecules with low molecular weight.

Membrane-associated transporter proteins expressed on the sinusoidal membrane can mediate uptake of substrates into the hepatocyte. Transporters are also expressed on the bile canalicular membrane, and these require energy to actively extrude substrates from the hepatocyte into the bile. Most drug transporters can be classified as members of either the solute carrier (SLC) or ATP-binding cassette (ABC) superfamily. ABC transporters require ATP hydrolysis for the transport of substrates across the membrane and are classed as primary active transporters. Some SLC transporters utilise ion or proton gradients across the membrane to transport substrates against an electrochemical gradient and are classed as secondary active transporters. The location of ABC and SLC transporters in the human hepatocyte is illustrated in Figure 1-5.

Figure 1-5 Human drug transporters expressed at the sinusoidal and bile canalicular membranes of hepatocytes (Giacomini et al., 2010)

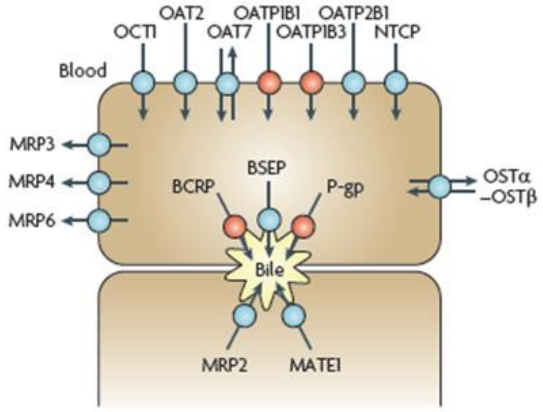

Human hepatic transporters on the sinusoidal (blood) and bile canalicular membranes.

The coordinated action of uptake and efflux processes serves to keep the hepatocyte intracellular drug concentration low, maintaining a favourable concentration gradient for the entry of more drug. Hepatobiliary drug transporters are therefore extremely important components of total drug clearance *in vivo*.

For many years, drug discovery efforts have focused on reducing CYP450-mediated metabolism of NCEs leading to a shift in physicochemical properties of NCEs and a surgence of NCEs developed which are reliant on active transport for their disposition (Funk, 2008; Parker and Houston, 2008; Soars et al., 2009). With the increasing awareness of the role of transporters in drug clearance, it is obvious there are instances where assumptions of the well stirred model are violated leading to significant under prediction of clearance. Several *in vitro* methods have been developed in the last decade to explore active drug transport in hepatocytes which can be used to interrogate emerging IVIVC and diagnose root causes of disconnects with conventional metabolism methods.

1.4.1 Uptake transporters expressed at the sinusoidal membrane of hepatocytes

Drug uptake into the hepatocyte may be mediated by non-saturable passive and saturable active processes, both of which are influenced by the physicochemical properties of drugs. The sinusoidal membranes of the hepatocyte contain many microvilli with a large surface area for diffusion of permeable drugs from the sinusoidal blood into the hepatocyte. The

localization of transporters on the sinusoidal membrane gives them a key 'gatekeeper' function, controlling the entry of substrates into the hepatocyte, access to metabolizing enzymes and excretory pathways, indicating a key role in mediating drug disposition (Shugarts and Benet, 2009). The direction of drug transport is governed by the intracellular hepatocyte concentration; uptake is favoured at low intracellular concentrations due to the downhill gradient from blood to hepatocyte whereas at high intracellular concentrations, sinusoidal transporters can act as efflux transporters trafficking drug out of the hepatocyte into the blood (Faber et al., 2003). The SLC gene family, containing SLC10 and SLC22 subfamilies, and the SLCO gene family represent the predominant transporter proteins which mediate uptake of drug molecules from blood across the sinusoidal hepatocyte. For uniformity and ease of use a new standardised system was introduced and accepted by the HUGO Gene Nomenclature Committee (HUGO, 2014) which classifies solute carriers into either SLC or SLCO gene families which are illustrated in Table 1-1 where all lower case nomenclature represents rodent genes and gene products while upper case nomenclature denotes human genes and gene products.

Table 1-1 Solute carrier uptake transporters at the sinusoidal membrane of hepatocytes

New gene symbol*	New protein name	Old protein name
Slco1a1	Oatp1a1	Oatp1, Oatp
Slco1a4	Oatp1a4	Oatp2
Slco1b2	Oatp1b2	Oatp4, Lst-1
Slc10a1	Ntcp	Ntcp
Slc22a7	Oat2	Oat2
Slc22a1	Oct1	Oct1
SLCO1A2	OATP1A2	OATP-A, OATP
SLCO2B1	OATP2B1	OATP-B
SLCO1B1	OATP1B1	OATP-C, OATP2, LST-1
SLCO1B3	OATP1B3	OATP8
SLC10A1	NTCP	NTCP
SLC22A7	OAT2	OAT2
SLC22A1	OCT1	OCT1

*All lower case nomenclature represents rodent genes and gene products while upper case nomenclature denotes human genes and gene products.

1.4.1.1 Organic Anion Transporting Polypeptides

Organic Anion Transporting Polypeptides (OATP, Oatp) mediate the sodium-independent transport of a wide spectrum of bile salts, organic anions and cations including therapeutic drugs such as statins (Ieiri et al., 2007; Kitamura et al., 2008; Nezasa et al., 2003; Sasaki et al., 2004). OATP1A2 (SLCO1A2), OATP2B1 (SLCO2B1) and OATP1B1 (SLCO1B1) transporters are expressed on the sinusoidal membrane. For many substrates, uptake by these transporters can be the rate-limiting step controlling hepatic elimination and/or oral bioavailability. OATP–mediated transport appears to involve bicarbonate anion exchange, coupling the uptake of substrate with the efflux of bicarbonate in a pH-dependent manner (Leuthold et al., 2009). It has also been proposed that some OATP isoforms may mediate the bidirectional transport of organic anions by a glutathione (GSH)-sensitive mechanism (Li et al., 2000).

1.4.1.2 Organic Anion Transporters

Organic Anion Transporter 2 (OAT2, SLC22A7) mediates uptake of molecules that are primarily negatively charged at physiological pH (pKa < 7) into the hepatocyte in exchange for dicarboxylate ions (Zhou and You, 2007). Typical substrates of OAT2 include salicylate, prostaglandin E_2 and *p*-aminohippurate (Anzai et al., 2006).

1.4.1.3 Organic Cation Transporters

Organic Cation Transporter 1 (OCT1, SLC22A1) mainly transports relatively hydrophilic, low molecular mass organic cations that are positively charged at physiological pH in a Na^+-independent fashion. In human or rat, OCT1 (Oct1) is highly expressed on the sinusoidal membrane of the hepatocyte and substrates include verapamil, quinidine, 1-methyl-4-phenylpyridinium and tetraethylammonium (Koepsell et al., 2007).

1.4.1.4 Sodium-dependent Taurocholate Co-transporting Polypeptide

Sodium-dependent taurocholate co-transporting polypeptide (NTCP, SLC10A1) is expressed exclusively on the sinusoidal membrane of hepatocytes where it mediates the hepatic uptake of bile salts (Faber et al., 2003). The driving force of NTCP-mediated transport is the downhill sodium gradient between blood and hepatocyte. NTCP accounts for an estimated 80% of total hepatic uptake of conjugated bile acids from the portal blood to help maintain plasma concentrations at a minimum. Additionally NTCP substrate specificity extends beyond bile acids and structurally related compounds as this protein can also transport the cholephilic compounds bromosulfophthalein and estrone-3-sulfate, and the statins rosuvastatin, pitavastatin, atorvastatin and fluvastatin (Doring et al., 2012; Faber et al., 2003).

1.4.2 Efflux transporters expressed at the bile canalicular membrane of hepatocytes

Drug molecules which exit the hepatocyte across the canalicular membrane are eliminated in bile which flows through fine tubular canals between adjacent hepatocytes. Given the small surface area of the bile canalicular membrane for passive diffusion, unchanged drug or metabolites are transported into the bile primarily by an active process mediated by efflux transporters on the bile canalicular membrane. These efflux proteins belong to the ABC family of transport proteins which mediate ATP-dependent transfer of substrates into bile.

A list of ABC transporters expressed in the liver are presented in Table 1-2. A standardised gene symbol nomenclature system (HUGO, 2014) is used where all lower case nomenclature represents rodent genes and gene products while upper case nomenclature denotes human genes and gene products.

Table 1-2 Hepatic efflux transport proteins expressed at the bile canalicular membrane

Gene symbol*	Protein name	Old protein name
Abcb1a	Mdr1a	P-gp
Abcg2	Bcrp	Mxr
Abcb4	Mdr2	Phospholipid floppase
Abcb11	Bsep	Spgp
Abcc2	Mrp2	Cmoat
Abcc1 , Abcc3, Abcc4 & Abcc6	Mrp1, Mrp3, Mrp4 & Mrp6	-
ABCB1	MDR1	P-gp
ABCG2	BCRP	MXR
ABCB4	MDR3	Phospholipid floppase
ABCB11	BSEP	SPGP
ABCC2	MRP2	CMOAT
ABCC1, ABCC3, ABCC4 & ABCC6	MRP1, MRP3, MRP4 & MRP6	GS-X, MOATD, MOATB, MOATE

*All upper case nomenclature denotes human genes and gene products while lower case nomenclature represents rodent genes and gene products.

1.4.2.1 P-glycoprotein

P-glycoprotein (P-gp, ABCB1), a 170 kDa protein, was the original ABC transporter identified over 30 years ago and represents the most studied ABC transporter. It has been reported that drug substrates diffuse through the lipid bilayer of the membrane and enter the drug binding pocket of P-gp which stimulates ATP hydrolysis to release energy. This in turn causes the drug binding pocket to undergo a conformational change and the drug substrate is subsequently effluxed out of the cell (Loo and Clarke, 2005). P-gp is responsible for the biliary efflux of hundreds of structurally diverse substrates which are generally bulky and hydrophobic and mostly cationic or neutral. Typical substrates include digoxin, verapamil, fexofenadine and the chemotherapeutics doxorubicin, methotrexate and etoposide (Faber et al., 2003).

1.4.2.2 Breast Cancer Resistance Protein

Breast Cancer Resistance Protein (BCRP, ABCG2), a 72kDa protein, was originally considered a half-transporter and thought to homodimerise in order to function, however more recently human BCRP was reported to exist as a homotramer, a 4-subunit complex (Lepper et al., 2005). It has also been reported that BCRP contains a low-affinity and a high-affinity binding site (Huang et al., 2006). BCRP is highly expressed on the canalicular membrane of the hepatocyte and is reported to mediate hepatobiliary disposition of a broad range of endogenous and exogenous substrates including sulfate conjugates, porphyrins, anticancer drugs methotrexate, doxorubicin and etoposide and statins pravastatin and rosuvastatin (Choi and Yu, 2014).

1.4.2.3 Bile Salt Export Protein

The Bile Salt Export protein (BSEP, ABCB11) is predominantly responsible for mediating the rate-limiting step of detergent-like bile salt transport across the canalicular membrane and constitutes the major driving force for the generation of bile flow so any impairment can lead to intracellular accumulation of cytotoxic bile salts inside the hepatocyte (Hillgren et al., 2013). Bile is composed of small ions, organic salts and bile salts which are amphipathic molecules and it provides a vehicle for excretion of poorly water soluble substances. BSEP has a narrow substrate specificity, largely restricted to conjugated and unconjugated bile salts but other substrates include cyclosporin A, tamoxifen, bosentan, rifampicin and pravastatin (Faber et al., 2003; Giacomini et al., 2010).

1.4.2.4 Multidrug Resistance-associated Protein 2

Multidrug Resistance-associated Protein 2 (MRP2, ABCC2) functions to mediate the uni-directional efflux into bile of a wide variety of substrates including organic anions including glutathione and bilirubin-glucuronide conjugates, sulfated bile salts and divalent bile salt conjugates. Numerous drugs, and drug metabolites, including estradiol-17-ß-glucuronide, doxorubicin, methotrexate and valsartan are also substrates of MRP2 (Faber et al., 2003). Dubin-Johnson syndrome is associated with the absence of MRP2 and a defect in the ability of hepatocytes to efflux conjugated bilirubin into the bile due causing increased blood levels of conjugated bilirubin (Tsujii et al., 1999). MRP2 exhibits similar substrate specificity to OATP1B1 (SLCO1B1) and it has been suggested that a synergy exists between these two proteins involved in hepatobiliary dispositions of some anionic drugs such as the statins (Sasaki et al., 2004).

1.4.2.5 Multi-Drug Resistance protein 3

Multidrug Resistance Protein 3 (MDR3, ABCB4) is highly expressed on the canalicular membrane of the hepatocyte. MDR3 is defined as a floppase for phosphatidylcholine (PC) as it functions to 'flop' PC from the inner leaflet to the outer leaflet of the membrane and into the bile. Following PC excretion into bile, it is taken up into bile salt micelles which reduces the detergent activity of these micelles, thus protecting cell membranes facing the bile (Oude Elferink and Paulusma, 2007). Other substrates of MDR3 include digoxin, vinblastine and paclitaxel (Faber et al., 2003). Dysfunctions of MDR3 due to genetic variations can cause hepatic disease in humans including low phospholipid-associated cholelithiasis, familial intrahepatic cholestasis type 3 and drug induced liver injury (Kim et al., 2013).

1.4.2.6 Sinusoidal efflux proteins

Members of the MRP subfamily represent a major class of efflux proteins expressed on the hepatic sinusoidal membrane which translocate substrates from the hepatocyte into sinusoidal blood. MRP1 (ABCC1), MRP3 (ABCC3), MRP4 (ABCC4) and MRP6 (ABCC6) are responsible for efflux of various organic anions, including glucuronide-, glutathione and sulfate-conjugated drugs, methotrexate and doxorubicin (Annaert, 2007). The expression of both MRP1 and MRP3 is normally low but is inducible when transport across the canalicular membrane is blocked, thus providing a back-up system during cholestasis or in patients with MRP2 deficiencies such as Dubin-Johnson syndrome (Faber et al., 2003; Ros et al., 2003).

1.4.3 Tools to investigate hepatobiliary drug transport

Several *in vitro* models have been applied successfully to study hepatobiliary drug transport ranging from relatively simple models utilising membrane vesicles possessing transporters to more complex and physiologically relevant models like the sandwich cultured rat hepatocyte (SCRH) model. A summary of some of the models with which to study hepatobiliary drug transport is given in Table 1-3 Essentially, all of these models have advantages and disadvantages and the data generated from them must be interpreted cautiously but often also in conjunction with complementary model systems.

Table 1-3 Summary of model systems used to study hepatobiliary drug transport (adapted from Annaert, 2007)

Model System	Major Applications	(+) Advantages / (-) Disadvantages	Reference
Inside out membrane vesicles prepared from transfected systems	High throughput screening for substrates and inhibitors of selective transporter	+ High throughput - Limited information on single transport protein	(Saito et al., 2006)
Purified membrane vesicles prepared from liver tissue	Mechanistic studies of specific transporters at particular membrane domain e.g. basolateral and canalicular membrane vesicles	+ All relevant transporters expressed + No interference from metabolism - Technically challenging to prepare	(Meier et al., 1984; Shilling et al., 2006)
Non-polarised transfected cells (HeLa, CHO) expressing transporter of interest	High throughput screening for substrates and inhibitors	+ High throughput cell-based model - Non-hepatic cellular context	(Annaert et al., 2010)
Polarised transfected cells (MDCKII, LLC-PK1, HEK293)	Measure vectorial transport across whole cells. Can be used to express uptake and/ or efflux transporters.	+ Polarised phenotype mimics hepatocyte polarity - Use of non-hepatic host cells - Difficult to standardise relative expression levels	(Sasaki et al., 2004)
Isolated hepatocytes (discussed in more detail in section 1.4.3.1)	Investigate hepatic uptake kinetics of substrates	+ Physiologically relevant model + Broad complement of hepatic enzymes & uptake transporters - Short viability (within few h after isolation) - Not suitable for study of canalicular efflux proteins	(Menochet et al., 2012; Shimada et al., 2003; Soars et al., 2007)
Sandwich cultured hepatocytes (discussed in more detail	Mechanistic studies on hepatobiliary disposition, drug interactions and transporter	+ Most comprehensive cell-based model (transporters & hepatic enzymes expressed) - Static model (no bile or blood flow)	(Abe et al., 2008; Wolf et al., 2008)

Model System	Major Applications	(+) Advantages / (-) Disadvantages	Reference
in section 1.4.3.2)	regulation at the molecular level	- Gradual loss of phenotype with time	
Liver slices	Mechanistic studies on interplay of hepatic metabolism and transport	+ In vivo architecture maintained at cellular level - Viability limited to a few h	(Godoy et al., 2013; Jung et al., 2007)
Isolated perfused liver	Study mechanism of hepatocyte uptake, metabolism and biliary excretion	+ Intact organ physiology - Low throughput, high animal consumption, limited viability	(Godoy et al., 2013; Hobbs et al., 2012)
Bile duct cannulated rat model	Most physiologically relevant model	+ Studies may be conducted in freely moving animals - Lowest throughput	(Rioux et al., 2013; Tonsberg et al., 2010)

1.4.3.1 Measurement of hepatic uptake transport processes

Isolated hepatocytes are recognised as one of the most physiologically relevant and practical models with which to study hepatic drug clearance. Primary hepatocytes may be isolated from liver lobes following a 2-step enzymatic digestion of the liver using a calcium-free buffer to disrupt the tight junctions followed by perfusion with collagenase to digest the liver collagen matrix (Seglen, 1976). Isolated hepatocytes are then suspended into an isotonic Percoll™ buffer and centrifuged to yield a high percentage of viable cells (>85%) and may be diluted into an appropriate supplemented buffer ready to use immediately.

Unfortunately, hepatocytes lose their cellular polarity rapidly upon isolation resulting in loss of efflux transporter function, however uptake transporter function is retained making them an ideal tool for short-term drug uptake studies. Primary hepatocytes, both in suspension or plated in an appropriate media to enhance cell attachment, are widely used to assess if drug uptake into the hepatocyte could be a rate determining step in hepatic elimination for compounds with poor permeability (Noe et al., 2007; Parker and Houston, 2008; Shimada et al., 2003). At physiological temperature (37°C), drug uptake into the hepatocyte may involve both passive and active processes, whereas parallel incubations at 4°C to disable any transport protein may also be conducted to assess passive diffusion of drug into the hepatocyte.

1.4.3.2 Measurement of hepatic efflux transport processes

Modifications to culture conditions have resulted in dramatic improvements to longevity and functionality of hepatocytes in culture. One successful approach is to mimic the native extracellular matrix geometry by maintaining hepatocytes between two layers of Collagen I or Collagen I/Matrigel® in a sandwich configuration (LeCluyse et al., 1994). Hepatocytes cultured long term in a collagen or Matrigel® sandwich configuration repolarise and re-establish a bile canalicular network but also show both a better maintenance of drug uptake and better enzyme induction potential.

In this thesis, primary rat hepatocytes cultured in a sandwich configuration (employing Collagen I/Matrigel®) are ready after 96 h of culture. The functional activity of the canalicular transport proteins has been demonstrated using a technique to quantitate the amount of substrate inside the hepatocyte and the bile canaliculi by determination of substrate accumulation in the presence and absence of Ca^{2+} in the incubation medium.

Previous studies have demonstrated that a 10 minute incubation of SCRHs in Ca^{2+}/Mg^{2+}-free buffer disrupted the integrity of the tight junctions of the bile canaliculi (Liu et al., 1999c). The SCRH model represents a gold standard *in vitro* model with which to simultaneously study drug uptake and efflux since both sinusoidal and canalicular transport proteins have been shown to be functional in this model.

1.4.4 Prediction of hepatic transporter-mediated clearance

Based on Novartis rat pharmacokinetic data, the rat *in vivo* clearance of half of NCEs remains poorly predicted by rat liver microsomes or RLM (Bell and Wang, 2012). A number of recent reports have indicated that drugs with poorly predicted clearance are often transporter substrates (Huang et al., 2010; Shitara et al., 2006; Webborn et al., 2007). Of particular interest are uptake transporters, since they may modulate the rate of hepatic metabolism and biliary excretion by elevating the free intracellular concentrations of drug exposed to the eliminating process(es). Several *in vitro* methods using the tools illustrated in Table 1-3, have been developed to explore uptake into hepatocytes and or biliary efflux which has advanced our knowledge of the role of transporters in drug clearance. Essentially, all of these models have their own advantages and disadvantages and the data generated must be interpreted cautiously since forecasting hepatic clearance using the measured intrinsic clearance data from a single pathway may lead to a false outcome when other hepatobiliary processes become rate limiting.

Improvement in clearance predictions for substrates of active hepatic transport requires accurate measurement of the intrinsic uptake and/or efflux processes in the hepatocyte using detailed kinetic study designs. These kinetic data may be incorporated into more complex *in vitro-in vivo* extrapolation methods accounting for all four hepatobiliary pathways; uptake, sinusoidal efflux, metabolism and biliary efflux (Liu and Pang, 2005; Umehara and Camenisch, 2012; Webborn et al., 2007) and comprehensive mechanistic compartmental models or physiologically-based pharmacokinetic models to predict *in vivo* clearance (Menochet et al., 2012; Paine et al., 2008; Poirier et al., 2008). In most cases, successful predictions were obtained but these methods require more detailed information and understanding of the disposition processes involved and are therefore not easily applied in early drug discovery to address the high incidence of IVIVC disconnects. However, given the important role that both uptake and/or efflux transporters in the hepatocyte may have in modulating hepatic clearance, transporter assays with adequate throughput may be frontloaded in early drug discovery to identify if hepatic uptake or

biliary efflux is the rate-determining step in hepatic clearance. When high hepatic transporter-mediated clearance is implicated, modifying the structural and/or physicochemical properties of NCEs which confer active uptake or efflux in hepatocytes may provide an efficient means of clearance optimisation which complements the more traditional metabolism screens.

1.5 Biopharmaceutics drug disposition classification system

Amidon and co-workers recognized the fundamental parameters controlling the rate and extent of oral absorption of drugs were solubility and permeability and proposed a Biopharmaceutics Classification System (BCS) which categorized drugs accordingly into 4 classes (Amidon et al., 1995). A modified version of the BCS system, the Biopharmaceutics Drug Disposition Classification System (BDDCS) presented in Table 1-4, was proposed some 10 years later to serve as a basis for predicting the importance of drug transporters in determining disposition (Wu and Benet, 2005):

Table 1-4 The BDDCS System: Predicting drug disposition.

		High Solubility	Low Solubility
High Permeability		**Class 1** Metabolism	**Class 2** Metabolism
Low Permeability		**Class 3** Renal +/or Biliary elimination of unchanged drug	**Class 4** Renal +/or Biliary elimination of unchanged drug

The Biopharmaceutics Drug Disposition Classification System for predicting drug disposition. (Adapted from Wu and Benet 2005).

The premise of this proposed system is that highly permeable, lipophilic class 1 and 2 drugs capable of crossing biological membranes, make good substrates for CYP450 enzymes and metabolism is the major route of elimination. The impact of any active uptake on hepatic extraction of highly permeable drugs is reduced due to diminished ability to increase the ratio of the intracellular and extracellular free concentrations in the hepatocyte. In contrast for the poorly permeable, less lipophilic Class 3 and 4 compounds, metabolism only plays a minor role in drug elimination. Uptake transporters may modulate the rate of hepatic metabolism and biliary secretion by elevating the free intracellular concentration relative to that in blood for these poorly permeable drugs and both uptake and efflux transporters could be important for drug elimination.

1.6 Species differences in hepatobiliary clearance

Pharmacotoxicological properties of NCEs have to be extensively studied in pre-clinical species prior to administration to humans. However, the expression, substrate specificity and activities of drug metabolism enzymes and drug transporters in humans differ from pre-clinical species, so it is unlikely that any animal model can appropriately model all aspects of human hepatobiliary disposition of NCEs. Thus, it is important that information on the pathways involved in hepatobiliary clearance can be incorporated into the decision-

making process at an early stage in order to aid the selection of the appropriate tools, models and species to use to aid extrapolation of clearance to man.

1.6.1 Species differences in metabolism

There are a number of animal species that have been used as pre-clinical models of drug metabolism and mouse, rat, dog, and monkey see the most widespread use. CYP450s are the most important drug metabolising enzyme family contributing to metabolism of the majority of drugs in humans. CYP450s are encoded by a superfamily of genes which show a high sequence homology among species but small changes in the amino acid sequences can result in profound differences in substrate specificity and catalytic activity (Dekeyser, 2012).

Whilst CYP3A isoforms are the most important drug metabolising isoforms in all species, the various CYP3A isoforms expressed show different substrate specificities across species. Moreover, the CYP3A isoforms are highly inducible but induction may be species-specific (Martignoni et al., 2006) which may pose problems when making the extrapolation from animal to human.

Hepatic metabolic clearance data may be extrapolated to humans reasonably well using allometric scaling, a concept which states that anatomical, physiological and biochemical variables in mammals (such as organ weights, organ blood flow, organ process rates and lifespan potential) can be scaled across species as a function of body weight (Mahmood and Balian, 1996a; Mahmood and Balian, 1996b).

1.6.2 Species differences in biliary clearance

Biliary clearance is a major issue in drug discovery because it can result in high drug clearance and ultimately low systemic exposure. Several efflux transporters present on the bile canalicular membrane are responsible for the biliary elimination of substrates into the bile. Transporter-mediated biliary excretion is most common for acids and zwitterions, although some basic compounds are also eliminated via this route. Typical characteristics of substrates being low passive permeability, high molecular mass > 400 Da, large polar surface area and a high hydrogen bond count.

Whilst *in vitro* models of biliary excretion such as the sandwich cultured hepatocyte model (Liu et al., 1999b) are available to explore biliary excretion, *in vitro-in vivo* models for prediction of biliary excretion remain immature as the absolute differences in transporter expression in the *in vitro* models are unknown (Li et al., 2009b). Assembly

of large and chemically diverse datasets have enabled extensive examination of the physicochemical profiles of compounds that are extensively excreted into bile and *in silico* models to discriminate substrates from non-substrates of biliary excretion have been reported (Varma et al., 2012).

Inter-species differences in MRP2 transporter activity have been reported (Ninomiya et al., 2006; Ninomiya et al., 2005) but inter-species differences for other biliary transporters remain obscure. Drugs which are substrates of both active uptake transporters and biliary efflux transporters tend to be very efficiently eliminated in the bile. Active uptake of drugs into the liver increases the exposure of the drug to efflux transporters at the bile canalicular membrane, which can result in liver blood flow limited clearances which may be difficult to predict across species. It was recently postulated that there are fairly insignificant differences in rat, dog and human biliary clearance of drugs when they do not require active uptake to access the liver, but when OATPs are involved, a discrepancy in rat to human of up 10-fold may be expected (Grime and Paine, 2013). Species differences in active hepatic uptake of substrates have also been reported indicating it is an important factor to be considered when attempting to translate across species. Pravastatin, a known OATP1B1 and OATP1B3 substrate which is predominantly non-metabolised and whose active uptake is the rate limiting step in biliary excretion in humans, showed comparable active uptake in dog, monkey and human cryopreserved hepatocytes but uptake rates were 2-5-fold higher in rodent species (Li et al., 2013).

There is not a wealth of literature on the subject of predicting human biliary clearance of drug candidates and relevant clinical data is scarce. Allometric interspecies scaling has been applied to predict human biliary clearance from at least three pre-clinical species with reasonable accuracy using the rule of exponents and a correction factor to account for species differences in bile flow rate (Mahmood, 2012). However, biliary excretion studies are generally conducted in rat in early drug discovery and it is somewhat over-reaching to assume that drugs which are excreted efficiently in rats will also be excreted to the same extent or even at all in humans. Hence prediction of biliary clearance remains as a largely unresolved problem.

1.7 Aims and objectives

The overall aim of this thesis is to analyse IVIVC to gain a more detailed understanding of the processes involved in rat hepatobiliary disposition of NCEs. Of particular interest is

identification of potential mechanisms beyond metabolism for underestimation of *in vivo* clearance. The specific objectives are:

- To establish and characterise models of drug uptake and biliary efflux in primary rat hepatocytes.
- To measure active uptake and biliary efflux for a set of NCEs and commercially available drugs.
- Assess clearance predictions from single pathway IVIVE using intrinsic metabolic clearance, intrinsic uptake clearance and intrinsic secretory clearance and compare to more complex multiple pathway IVIVE models, assuming either biliary efflux or biliary efflux and metabolism are primary processes driving clearance.
- To identify physicochemical properties which confer active transport in rat hepatocytes and build and evaluate discriminant *in silico* and classification models of uptake and efflux.
- To explore how passive permeability influences hepatobiliary drug disposition of NCEs in rat.

These studies should help clarify the mechanisms that dominate *in vivo* clearance, diagnose IVIVC disconnects and guide refinement of *in vitro* absorption, distribution, metabolism and excretion (ADME) strategies in early drug discovery.

2 CHAPTER TWO: MATERIALS AND METHODS

2.1 Materials

1M calcium chloride solution, dexamethasone, diazepam, ethylene glycol tetra acetic acid (EGTA), Hank's balanced salts solution (HBSS), HPLC grade ethanol and acetonitrile, 1M 4-(2-hydroxyethyl)piperazine-1-ethanesulfonic acid (HEPES) solution, NADPH, *N*-methyl-2-pyrrolidone (NMP)**,** Percoll®, polyethylene glycol (PEG200), potassium chloride (4 M solution), potassium phosphate monobasic, sodium bicarbonate 7.5% (w/v) solution, sodium chloride (5 M solution), sodium phosphate dibasic, Triton™ X-100 solution, trypan blue 0.4% (w/v) solution, trypsin inhibitor from soybean, warfarin and 1x Williams E medium (WEM) were all obtained from Sigma-Aldrich Chemie GmbH (Buchs, Switzerland).

Dulbecco's Modified Eagle Medium (DMEM), DMEM plus Glutamax™-I medium, Dulbecco's phosphate buffered saline (DPBS), Earl's balanced salt solution (EBSS), fetal bovine serum (FBS), insulin (human recombinant, 4 mg/ml zinc solution), 100x insulin-transferrin-selenium (ITS) solution, 100x non-essential amino acid solution and penicillin (5000 units/ml)/streptomycin (5000 µg/ml) solution were all obtained from Life Technologies Europe B.V. (Zug, Switzerland).

Bovine serum albumin (BSA), 2 mg/ml solution, Corning Microtitre 96-well polystyrene plates (flat- and conical-bottomed) and HTS Transwell® 96 well insert plates and feeder trays, dimethyl sulfoxide (DMSO, HPLC grade), Masterflex™ Tygon LFL tubing, 3.2mm inner diameter (I.D.), methanol (HPLC grade), NUNC U96 polypropylene 2 ml deep-well plate, Phenomenex Synergi RP Polar C18 5cm x 3mm ID (4 µm) liquid chromatography columns and rapid equilibrium dialysis (RED) Teflon® base plates and inserts were all obtained from Thermo Fisher Scientific (Switzerland) AG (Reinach, Switzerland). BioCoat™ Collagen I cell culture plates 1 (12 and 24-well), cell strainer (100 µm nylon filter), Matrigel® basement membrane and pooled male rat liver microsomes were all obtained from Becton Dickinson AG, Allschwil, Switzerland. Cannulae of 0.9 mm diameter were obtained from Solomon Scientific (Plymouth, USA). Carbogen gas was obtained from Carbogas (Basel, Switzerland). Collagenase H from *Clostridium histolyticum* was obtained from Roche Diagnostics (Zug, Switzerland). Detergent compatible (DC) protein assay kit II was obtained from Biorad Laboratories AG (Cressier, Switzerland). Fast Read 102 counting chambers were obtained from ISL

(Devon, UK). Han Wistar rats (male) were obtained from Charles River (Iffa Credo, France). Multiscreen cell culture trays and Multiscreen Permeability plate, 0.4 μm polycarbonate membrane were purchased from Millipore AG (Zug, Switzerland). Miniature polyethylene pony vials (6 ml), Irga Safe liquid scintillant and [^{3}H]taurocholic acid, [^{3}H]digoxin and [^{3}H][D-Pen2,5]-Enkephalin hydrate (DPDPE) all with specific activity between 1 and 5 Ci/mmol and a concentration of 1 mCi/ml were obtained from Perkin Elmer (Schwerzenbach, Switzerland). Pooled mixed gender Sprague Dawley rat plasma was obtained from SLI International (Bolney, UK).

2.2 Metabolic clearance in rat liver microsomes

2.2.1 Assessment of metabolic stability in rat liver microsomes

The metabolic stability data for Novartis compounds using male Sprague Dawley rat liver microsomes were generated in the course of Medicinal Chemistry project support and not generated by the candidate. Metabolic stability was assessed using a compound depletion method to generate the *in vitro* half-life (*t*1/2). The fully automated, generic method was used for the incubations (Hamilton Robotics GmbH, Martinsried, Germany). The assay was assumed to be conducted under linear reaction conditions using a low microsomal protein concentration of 0.5 mg/ml and low compound concentration (1 μM, assumed to be lower than the K_m of the substrate). Compounds were prepared as 10 mM stock solutions in DMSO and dispensed into incubation plates using an Echo® acoustic dispenser (Labcyte Europe, Dublin, Ireland)

Incubations were supplemented with NADPH co-factor prepared in DPBS at a final concentration of 1 mM. Reactions were initiated by addition of a suspension of microsomes and NADPH cofactor in DPBS. The final solvent concentration in the assay was <0.1% (v/v) DMSO. At specific reaction time points (nominally 0, 5, 15, 30, 45 and 60 minutes) aliquots were sampled and reactions terminated by addition of 1 volume of ice cold acetonitrile containing analytical internal standard. Samples were mixed and centrifuged at approximately 3000 x g for 15 minutes to pellet the microsomal protein. Peak area ratios (P.A.R.) of analyte:internal standard in the supernatants were analysed by liquid chromatography tandem mass spectrometry (LC-MS/MS) as detailed in Section 2.2.2. Metabolic clearance data for marketed drugs using rat liver microsomes was generated in the course of this thesis research. The final assay conditions used were the same as those detailed above.

2.2.2 Quantitation of drug by liquid chromatography tandem mass spectrometry

The levels of drugs in extracted samples were quantified via LC-MS/MS using a TSQ quantum discovery MAX mass spectrometer with Xcalibur and QuickQuan 2.1 software (Thermo Fisher Scientific Inc., Wohlen, Switzerland). The analytical column used was a Phenomenex Synergi RP Polar C18 5cm x 3 mm ID (4 µm) at ambient temperature. The mobile phases used were A= HPLC grade acetonitrile with 0.1% (v/v) formic acid and B= HPLC grade water with 0.1% (v/v) formic acid and the gradient is detailed below:

Table 2-1 LC-MS/MS gradient conditions

Time (min)	% A	% B	Flow rate (µl/min)
0	5	95	400
0.5	5	95	400
0.6	95	5	400
2.8	95	5	400
2.9	5	95	400
3.5	5	95	400

The first minute of eluent was allowed to drain to waste to prevent mass spectrometer source fouling. Mass spectrometry was performed using an electrospray source in positive or negative ion mode.

2.2.3 Calculation of stability, half-life and intrinsic clearance

Following LC-MS/MS quantitation of parent compound in the supernatant, stability was determined semi-quantitatively from P.A.R. of analyte:internal standard which were used to determine the percentage stability at all pre-defined time points in relation to a zero minute time point (*t*0) set to 100%. For example, the percentage stability of a compound at time point *t*5 (5 minutes) was calculated as follows:

$$\%\ Stability = \frac{P.A.R.(t5)}{P.A.R.(t0)} * 100$$

Percentage stability data was log transformed and plotted against time points to define the initial phase of the slope, also known as the initial rate of elimination, k_{el}. The half-life or *t*1/2 (min) was obtained by dividing the natural log of 2 (0.693) by the k_{el}:

$$Half\ life\ (minutes) = \frac{0.693}{k_{el}}$$

In vitro metabolic intrinsic clearance ($CL_{int,met}$) is a pure measure of enzyme activity towards a drug and is calculated to standardise the observed *t*1/2 for *in vitro* reaction conditions. *V* is the incubation volume (µl) and *M* is the microsomal protein content (mg) or hepatocyte concentration (10^6 cells) in the incubation:

$$CL_{\text{int,met}}\ (\mu l/min/mg\ protein) = half\ life * \frac{V}{M}$$

2.2.4 Calculation of scaled metabolic $CL_{int,met}$ to normalise for whole liver microsomal and hepatocyte content

$CL_{int,met}$ was scaled to account for microsomal protein content in the whole liver of a rat, where physiological scaling factor SF1 approximates 45 mg microsomal protein per gram liver (Iwatsubo et al., 1997). $CL_{int,met}$ was also scaled to account for hepatocyte content in the whole liver of a rat, where physiological scaling factor SF1 approximates 117 million cells/g liver (Sohlenius-Sternbeck, 2006). Scaling factor SF2 approximates 40 gram of liver per kg body weight of a rat (Davies and Morris, 1993). The scaled $CL_{int,met}$ parameter forms the cornerstone for the extrapolation of *in vitro* data to the *in vivo* situation as it is not influenced by other physiological scaling parameters such as liver blood flow or correction factors such as blood:plasma distribution ratio or plasma or blood protein binding. $CL_{int,met}$ is calculated as follows:

$$CL_{int,met}(ml/min/kg) = \frac{CL_{int,met}\ (\mu l/min/mg\ protein) * SF1 * SF2}{1000}$$

2.2.5 Prediction of *in vivo* hepatic clearance

To further predict the *in vivo* hepatic clearance (CL_H) from the scaled $CL_{int,met}$, a well stirred model was used which describes the inter-relationship between scaled $CL_{int,met}$ liver blood flow (Q_H) and unbound fraction (fu_b) in blood (Houston, 1994):

$$CL_H\ (ml/min/kg) = \frac{Q_H * fu * CL_{int,met}\ (ml/min/kg)}{Q_H + fu * CL_{int,met}\ (ml/min/kg)}$$

However, during early drug discovery, protein binding data are not readily available so the fraction unbound was disregarded for estimating hepatic clearance, CL_H. This model is called the direct scaling model and simplifies the equation:

$$CL_H\ (ml/min/kg) = \frac{Q_H * CL_{int,met}\ (ml/min/kg)}{Q_H + CL_{int,met}\ (ml/min/kg)}$$

Further investigations into the IVIVE of clearance have also accounted for the difference in drug ionisation in extracellular and intracellular tissues where an ionisation correction factor F_I, corresponding to the ratio of unionized drug in blood and intracellular tissue water, is applied to the conventional well stirred model (Berezhkovskiy, 2011):

$$CL_H\,(ml/min/kg) = \frac{Q_H * CL_{int,met}\,(ml/min/kg) * F_I}{Q_H + CL_{int,met}\,(ml/min/kg) * F_I}$$

2.2.6 Statistical analysis of clearance predictions

The Bias parameter explains how data are related to the line of unity, bias greater than 1 indicates over prediction whereas if the bias tends to 0, this indicates under prediction:

$$Bias = 10^{\left|\frac{1}{N}\sum log\frac{Predicted}{Observed}\right|}$$

In order to compare the accuracy of clearance predictions, the root mean squared prediction error (*rmse*), and average fold error (*afe*) were estimated from the prediction error (difference between predicted and observed *in vivo* values) as a measure of precision:

$$rmse = \sqrt{\left|\frac{1}{N}\sum(Predicted - Observed)^2\right|}$$

$$afe = 10^{rmse}$$

2.2.7 Rat physiological blood flow used for clearance predictions

The male Sprague Dawley rat liver blood flow for the Novartis rat colony is estimated to be approximately 150 ml/min/kg which is approximately 2-fold higher than the historical value of ~ 77 ml/min/kg reported in the literature (Boxenbaum, 1980). This is based on in-house blood clearance data generated for high extraction compounds like propranolol and indocyanine green. Clearance predictions were calculated using a rat liver blood flow (Q_H) of 150 ml/min/kg to calculate predicted clearance from rat liver microsomes and hepatocytes.

2.3 Isolation of primary rat liver hepatocytes

2.3.1 Rat liver excision

All animal handling and dissection was performed by qualified animal technicians in the Novartis Metabolism and Pharmacokinetic group in Basel and performed according to an experimental license granted by Canton Basel-City, Switzerland. Male Han Wistar rats weighing approximately 200 g were used as liver donors. Animals were allowed free

access to food and water. Prior to liver excision, 500 units of heparin i.v. (0.1 ml of a 5000 units/ml solution) was administered to each rat to prevent blood clotting. Ten minutes after heparin administration, the rat was anaesthetized with isoflurane and the liver excised and placed into ice cold DPBS buffer.

2.3.2 *Ex-vivo* rat liver perfusion

A two-stage buffer perfusion, collagenase dispersion technique was applied. The pH of both perfusion buffers was adjusted to 7.4. Perfusion buffers were pre-warmed to 37°C inside a Grant GD100 waterbath (Thermo Fisher Scientific Inc., Wohlen, Switzerland) and maintained under constant gassing with carbogen (5% CO_2/95% O_2). The carbogen gassing served to maintain the pH of the buffers by facilitating a CO_2/bicarbonate system and preventing acidification of recirculated buffer which is critical since the activity of collagenase in liver dispersion exhibits a sharp optimum at pH 7.5.

The perfusion apparatus was set up using Masterflex™ Tygon LFL tubing and a Minipuls 3 peristaltic pump (Gilson Switzerland, Mettmenstetten, Switzerland) set to a flow rate of 28 ml/min. A single tubing line was inserted into buffer bottles residing in a water bath maintained at 37°C and used to transfer buffer through an air trap and into a four-way line splitter connected to 0.9 mm diameter cannula (Solomon Scientific, Plymouth, USA) by Masterflex™ Tygon LFL tubing, 3.2 mm inner diameter (I.D.). The flow rate per cannula was approximately 7 ml/min. One cannula was placed into each of the four liver lobes resting on a perforated support plate.

The first buffer, EBSS containing sodium bicarbonate 0.23% (w/v) and EGTA (0.5 mM) to remove the calcium-containing junctions between the hepatocytes, was perfused until the lobes were completely blanched (approximately 12 minutes). The perfusion line was then transferred into the second EBSS buffer containing sodium bicarbonate (0.23% w/v), trypsin inhibitor (0.06 mg/ml) and collagenase H (1 mg/ml) activated with calcium (calcium chloride at 2 mM), to digest the collagen matrix between hepatocytes. The second buffer was recirculated until liver lobes obtained a ‘cauliflower appearance’ under the capsule membrane (approximately 10-12 minutes).

2.3.3 Isolation of rat parenchymal hepatocytes

Following perfusion, lobes were transferred to a cell culture tray containing 50 ml ice cold WEM and cells were isolated or teased away from digested liver lobes using surgical tweezers and glass pipettes. Cells were then filtered through a BD Falcon™ 100 μm cell

strainer into a 50 ml BD Falcon™ tube (Becton Dickinson AG, Allschwil, Switzerland) and centrifuged at low speed (50 x g, 5 minutes, 4°C) using a Thermo Heraeus Multifuge 3S-R centrifuge (Thermo Fisher Scientific Inc., Wohlen, Switzerland). The cells then underwent an additional three wash steps, to separate parenchymal from haematopoietic cells, the latter mostly remaining in suspension (Osypiw et al., 1994; Seglen, 1976). For the second wash step, the cell pellet was resuspended in a sterile isotonic Percoll® solution in WEM (18% v/v) followed by centrifugation (100 x g, 6 minutes, 4°C). In the third step, the cell pellet was resuspended in WEM and the cell suspension centrifuged at 50 x g, 3 minutes, 4°C. The final pellet was resuspended in medium appropriate for purpose, i.e. WEM for hepatocyte clearance assays or DMEM if cells were to be cultured.

2.3.4 Measurement of primary rat hepatocyte viability and yield

Cell yield and viability of the isolated hepatocytes were measured using a trypan blue exclusion technique which is based on the principle that live cells possess an intact cell membrane to exclude trypan blue dye, whereas dead cells do not (Strober, 2001). A 50 µl aliquot of cells was diluted in 200 µl WEM and 100 µl 0.4% (w/v) trypan blue solution added. Samples were gently mixed, an aliquot transferred to a Fast Read 102 counting chamber (ISL, Devon, UK) and viewed under a Zeiss Axiovert 40 CFL light microscope (Zeiss, Zurich, Switzerland). The cells were counted and the average number of viable cells with a clear cytoplasm and non-viable cells with a blue cytoplasm were calculated from four 4 x 4 grids. The percentage cell viability was determined as follows:

$$\%\ viability = \frac{viable\ cells}{viable + non\ viable\ cells} * 100$$

A minimum cell viability of 85% was required for all subsequent experiments. The number of viable cells/ml was calculated accounting for the initial cell dilution factor of 7 and the volume of a 4 x 4 grid which is 10^{-4} ml:

$$Viable\ cells = Average\ number\ of\ viable\ cells * 7(dilution\ factor) * 10^{-4}\ ml$$

2.4 Metabolic clearance in primary rat liver hepatocytes

2.4.1 Metabolic stability in primary rat hepatocytes

Metabolic stability of compounds with suspensions of fresh isolated primary rat hepatocytes was assessed using a substrate depletion method to generate the *in vitro* half-life (*t*1/2). Hepatocytes were isolated from male Han Wistar rats according to the method detailed in Section 2.3 and suspended in WEM (supplemented with 10mM HEPES) at a

final concentration of 1 million cell/ml. The assay was assumed to be conducted under linear reaction conditions using a fresh hepatocyte cell count of 0.99 million cell/ml and a low compound concentration of 1 µM (assumed to be lower than the K_m of the substrate). Compounds were prepared as 10 mM stock solutions in DMSO and subsequently diluted 100-fold in methanol to achieve a 100 µM methanolic stock.

Using NUNC U96 polypropylene 2 ml deep-well plates, 990 µl freshly isolated hepatocytes (1 million cells/ml) were added to the wells and pre-warmed to 37°C for approximately 10 minutes in a shaking waterbath at 100 rpm (Julabo SW23, Julabo Labortechnik, Seebach, Germany). Reactions were initiated by addition of 10 µl of pre-warmed 100 µM methanolic compound stock. At specific reaction time points (0, 5, 15, 30, 60, 120 minutes) aliquots were removed to a fresh 96-well microtitre plate and reactions terminated by addition of 1 volume of ice cold internal standard solution (acetonitrile containing internal standards diazepam (0.1 µM) and warfarin (1 µM)). Samples were mixed and centrifuged at ~3400 x g, 4°C for 15 minutes using a Thermo Heraeus Multifuge 3S-R centrifuge. Peak area ratios of analyte:internal standard in the supernatants were calculated following LC-MS/MS analysis as detailed in Section 2.2.

Following LC-MS/MS quantitation of parent compound in the supernatant, stability, t1/2, $CL_{int,met}$ and CL_H were all calculated and the accuracy of the clearance predictions were also assessed as detailed in Sections 2.2.3 to 2.2.6.

2.5 Metabolic clearance in rat plasma

Metabolic stability of compounds in rat plasma was assessed using a compound depletion method to generate the *in vitro* *t*1/2. Fresh frozen pooled Sprague Dawley rat plasma of mixed gender was thawed quickly at 37°C and centrifuged 100 x g for 5 minutes to remove the fibrin clot and then diluted 2-fold in isotonic phosphate buffered saline (PBS). PBS was prepared containing 85 mM Na_2HPO_4, 15 mM KH_2PO_4, 3 mM KCl and 137 mM NaCl and adjusted to pH7.4.

The assay was assumed to be conducted under linear reaction conditions using 50% (v/v) plasma in PBS and a low compound concentration (1 µM, assumed to be lower than the K_m of the substrate). Compounds were prepared as 10 mM stock solutions in DMSO and subsequently diluted 100-fold in methanol to achieve a 100 µM methanolic stock. Using NUNC U96 polypropylene 2 ml deep-well plates, 990 µl of 50% plasma in PBS (v/v) was added and pre-warmed to 37°C for approximately 10 minutes on a Tecan

T-shake incubator (Tecan, Männedorf, Switzerland). Reactions were initiated by addition of 10 µl of pre-warmed 100 µM methanolic compound stock. At specific reaction time points (0, 5, 15, 30, 60, 120 minutes) aliquots were removed to a fresh 96-well microtitre plate and reactions terminated by addition of 4 volumes of ice cold internal standard solution (acetonitrile containing internal standards diazepam (0.1 µM) and warfarin (1 µM)). Samples were mixed and centrifuged at ~3400 x g, 4°C for 15 minutes using a Thermo Heraeus Multifuge 3S-R centrifuge. Peak area ratios of analyte:internal standard in the supernatants were analysed by LC-MS/MS as detailed in Section 2.2.2. Following LC-MS/MS quantitation of parent compound in the supernatant, stability and t1/2 were calculated as detailed in Section 2.2.3.

2.6 Drug uptake studies in primary rat hepatocytes

2.6.1 Cell culture of primary rat hepatocytes

Hepatocytes were freshly isolated from male Han Wistar rats according to the method detailed in Section 2.3 and suspended in plating medium at a final concentration of 0.2 million cell/ml. The plating medium contained DMEM supplemented with 5% (v/v) fetal bovine serum, 1% (v/v) non-essential amino acids, 25 mM HEPES, 1 µM dexamethasone, 4 µg/ml insulin, 50 units/ml penicillin and 50µg/ml streptomycin. Hepatocytes were seeded into BioCoat™ Collagen I 24-well plates at a final concentration of 0.2 million cells/well and cultured in a Hera Cell 150 incubator at 37°C (5% CO_2, 95% air). After approximately 2 h culture time, cells were viewed under a Zeiss Axiovert 40 CFL light microscope (Zeiss, Zurich, Switzerland) to check they had attached to the Collagen I coating on the bottom of the wells of the culture plate.

2.6.2 *In vitro* drug uptake in cultured primary rat hepatocytes

Compounds were prepared as 10 mM stock solutions in DMSO and subsequently diluted 2000-fold in WEM medium supplemented with 10 mM HEPES (WEM + HEPES) containing 0.45% (v/v) acetonitrile to make the 'dosing solutions', which were pre-warmed to 37°C. Before initiation of the uptake study, the cultured primary rat hepatocytes were washed 3 times with WEM + HEPES buffer pre-warmed to 37°C and pre-incubated with 0.5 ml of the same buffer at 37°C. After 10 minutes pre-incubation at 37°C (5% CO_2, 95% O_2) inside a Hera Cell 150 incubator, the uptake study was initiated by replacing the WEM + HEPES buffer with 0.5 ml of the dosing solution (triplicate wells per compound) and hepatocytes were incubated at 37°C. After 2 minutes incubation, the

plate was removed from the incubator, dosing solutions were discarded to waste and cells washed rapidly 3 times with ice cold WEM + HEPES buffer to stop the active transport activity and to remove any drug not taken up into the hepatocytes. Parallel incubations of each compound were also conducted at 4°C (on ice). In these studies cells were washed rapidly 3 times and equilibrated with ice cold WEM + HEPES buffer pre-chilled to 4°C. Dosing solutions were also pre-chilled to 4°C.

Following the uptake experiment, cells were then lysed by addition of 250 µl of ice-cold water into each well and freezing at -20°C overnight. Plates were then transferred to a MaxQ 2000 plate shaker set to 100 rpm and thawed at ambient temperature. Plates were viewed under a Zeiss Axiovert 40 CFL light microscope to check for cell membrane lysis. Aliquots of 50 µl supernatant were then transferred to a Corning v-bottomed 96-well microtitre plate containing 50 µl of ice cold internal standard solution (acetonitrile containing internal standards diazepam (0.1 µM) and warfarin (1 µM)). Samples were mixed and centrifuged at ~3400 x g, 4°C for 15 minutes using a Thermo Heraeus Multifuge 3S-R centrifuge. The amount of drug that had accumulated inside the cells was quantified using standard curves for each compound. Five concentrations ranging from 0 to 1000 nM were prepared in water and internal standard solution (1:1 v/v). The limit of quantification (LOQ) was defined by the smallest concentration of each analyte that could be reliably measured (within 30% of the theoretical concentration). Peak area ratios of analyte:internal standard in the supernatants were calculated following LC-MS/MS analysis as detailed in Section 2.2.2.

2.6.3 Determination of protein content of cultured primary rat hepatocytes using the DC protein assay

To enable determination of the protein content per well used in the uptake studies, three extra wells of primary rat hepatocytes were cultured according to the method detailed in Section 2.6.3. Once cells had attached to the Collagen I coating of the plates (after ~ 2 h culture time), medium was removed and wells were rinsed 6 times with ice-cold WEM + HEPES buffer. Cells were then lysed by addition of 250 µl of ice-cold 1% (v/v) Triton™ X-100 solution in water into each well and freezing at -20°C overnight. Plates were then transferred to a MaxQ 2000 plate shaker set to 100rpm and thawed at ambient temperature. Plates were viewed under a Zeiss Axiovert 40 CFL light microscope to check for cell membrane lysis.

Protein content of the wells was determined using the DC protein assay. This is a calorimetric assay for quantification of total protein and is similar to the well-documented Lowry assay (Lowry et al., 1951). Under alkaline conditions, cupric ions (Cu^{2+}) chelate with peptide bonds in proteins resulting in the reduction of cupric ions to cuprous ions (Cu^{+}). Reduction of Folin reagent with Cu+ produces a characteristic blue colour with a maximum absorbance at 750nm, where the amount of colour produced is proportional to the amount of protein in the sample. Bovine serum albumin (BSA) was used as the protein standard at final concentrations of 0, 23, 47, 94, 187, 375, 750 and 1500 µg/ml in 1% (v/v) Triton™ X-100® solution in water. A working reagent was prepared by adding 50 parts of alkaline copper tartrate solution (Reagent A) with 1 part of Reagent S (50:1 v/v, Reagent A:S) and 25 µl of this working reagent was added to the wells of a flat-bottomed 96-well polystyrene plate (Corning Incorporated, Corning, NY). Five microliters of lysed cell samples and BSA standards (in duplicate) was added to the wells followed by 200µl of Folin reagent (Reagent B). Absorbance was measured at 750nm using a Tecan Safire 2 monochromator plate reader and Tecan XFLUOR4SAFIREII Version: V 4.62n software with temperature controlled at 37°C. Plates were shaken on the plate reader for 5 seconds and allowed to stand for 15 minutes prior to absorbance measurements. The protein content of samples was determined using the standard curve derived from BSA.

2.6.4 Calculation of initial uptake rates at 37°C and 4°C in cultured primary rat hepatocytes

Following quantitation of drug accumulated in cultured primary rat hepatocytes at 37°C and 4°C, the initial uptake rate of compounds (pmol/min/mg protein) was expressed as the amount of drug accumulated in the cell in pmols divided by the average protein content (mg/ml) of the well divided by the incubation time in minutes. Uptake rate ratios (37°C:4°C) were then calculated by dividing the initial uptake rate at 37°C by initial uptake rate at 4°C.

2.6.5 Calculation of intrinsic uptake clearance and scaled uptake clearance in cultured primary rat hepatocytes

Uptake intrinsic clearance ($CL_{int,upt}$), accounting for total uptake (passive and active) may be calculated from the initial uptake rate (pmol/min/mg protein) at 37°C and dividing by the assay substrate concentration [S] in pmol/µL:

$$CL_{int,upt}(\mu l/min/mg\ protein) = \frac{Initial\ uptake\ rate\ @\ 37°C}{Assay\ [S]}$$

The passive intrinsic clearance ($CL_{int,pas}$), accounting for passive uptake may be calculated from the initial uptake rate (pmol/min/mg protein) at 4°C and dividing by the assay substrate concentration in pmol/µl:

$$CL_{int,pas}(\mu l/min/mg\ protein) = \frac{Initial\ uptake\ rate\ @\ 4°C}{Assay\ [S]}$$

Active uptake intrinsic clearance ($CL_{int,act}$) may be calculated as follows:

$$CL_{int,act}(\mu l/min/mg\ protein) = CL_{int,upt} - CL_{int,pas}$$

The intrinsic clearance ($CL_{int,upt}$, $CL_{int,pas}$ or $CL_{int,act}$), may then be scaled to account for the protein content in the whole liver of a rat, where physiological scaling factor SF1 approximates 200 mg protein per gram liver and SF2 approximates 40 gram of liver per kg body weight of a rat (Liu et al., 1999a).

Scaled intrinsic clearance (ml/min/kg) was then calculated for $CL_{int,upt}$, $CL_{int,pas}$ or $CL_{int,act}$ using the following equation and $CL_{int,upt}$ (µl/min/mg protein) as an example:

$$CL_{int,upt}(ml/min/kg) = \frac{CL_{int,upt}\ (\mu l/min/mg\ protein) * SF1 * SF2}{1000}$$

The predicted clearance (CL_H) values based on total uptake intrinsic clearance were calculated based on the well-stirred model of hepatic disposition Q_H represents the hepatic blood flow in rats:

$$CL_H\ (ml/min/kg) = \frac{Q_H * CL_{int,upt}\ (ml/min/kg)}{Q_H + CL_{int,upt}\ (ml/min/kg)}$$

2.7 Measurement of biliary efflux using a sandwich-cultured primary rat hepatocyte model

2.7.1 Cell culture of primary rat hepatocytes in a Collagen I/Matrigel® sandwich

Hepatocytes were freshly isolated from male Han Wistar rats according to the method detailed in Section 2.3 and suspended in plating medium. The plating medium contained DMEM supplemented with 5% (v/v) foetal bovine serum, 1% (v/v) non-essential amino acids, 25 mM HEPES, 1 µM dexamethasone, 4 µg/ml insulin, 50 units/ml penicillin and 50µg/ml streptomycin.

Hepatocytes were seeded into BioCoat™ Collagen I plates at final concentrations of 100,000, 250,000 and 1000,000 cells/well for 24-, 12- or 6-well plate formats

respectively and cultured for approximately 2 h in a Hera Cell 150 incubator at 37°C (5% CO_2, 95% air) after which cells were viewed under a Zeiss Axiovert 40 CFL light microscope to check they had attached to the Collagen I coating on the bottom of the wells of the culture plate. The medium was then aspirated to waste and fresh pre-warmed plating medium added prior to further culturing. Approximately 24 h after seeding, cells were viewed again under a light microscope to check that they had spread to form a confluent monolayer. To prepare sandwich-cultured hepatocytes, BD Matrigel® Basement Membrane Matrix, phenol red free was diluted to 0.25 mg/ml in ice cold feeding medium and added to each well to achieve a final Matrigel® concentration of approximately 0.06 mg/cm^2 growth area. The feeding medium contained DMEM supplemented with 1% (v/v) non-essential amino acids, 25 mM HEPES, 0.1 µM dexamethasone, 1% (v/v) ITS solution, 50 units/ml penicillin and 50µg/ml streptomycin. Cells were then cultured for a further 72 h with feeding medium changed on a daily basis. After approximately 96 h of culture time, cells were again viewed under a light microscope to check for formation of bile canaliculi between the cells.

2.7.2 Assessment of the viability of sandwich-cultured primary rat hepatocytes

The viability of hepatocytes cultured for up to 96 h on BioCoat™ Matrigel® 6-well plates was assessed using a CellTiter 96® AQ_{ueous} one solution cell proliferation MTS assay (Promega, Dübendorf, Switzerland). The CellTiter 96® AQ_{ueous} one solution or MTS reagent contains an MTS tetrazolium compound (Owen's reagent) which is bioreduced by NADPH in living cells into a coloured formazan product with an maximum absorbance at 490 nm, where the amount of colour produced is proportional to the viability of cells in the sample.

Primary rat hepatocytes with viability >85% were seeded onto BioCoat™ Matrigel® 6-well plates and cultured for up to 96 h in a sandwich-configuration according to the method detailed in Section 2.7.1. To each well, 200 µl of MTS reagent was added and the plate was incubated for 1.5 h in a humidified incubator (37°C, 95% air, 5% CO_2). The quantity of formazan formed was then measured by UV absorbance at 490nm using a Tecan Safire 2 monochromator plate reader and Tecan XFLUOR4SAFIREII Version: V 4.62n software. The viability of primary rat hepatocytes cultured at 24 h post-seeding (prior to overlay with Matrigel®) and in a Collagen I/Matrigel® sandwich configuration at 48, 72 and 96 hour post-seeding was calculated in relation to the viability of primary rat

hepatocytes cultured for 2 h (at *t*2, prior to overlay with Matrigel®, viability was assumed to be at the maximum of 100%) where *t* = culture time (h):

$$\%\ viability = \frac{Cell\ viability\ at\ t}{Cell\ viability\ at\ t2h} * 100$$

2.7.3 Transport of unlabelled drugs in sandwich-cultured rat hepatocytes

Hepatocytes cultured for 96 h in a sandwich-configuration according to the method detailed in Section 2.7 were used. Wells were washed 3 times with buffer; one half of the plate with 0.5 ml of standard buffer and the other half with 0.5 ml $Ca^{2+/}Mg^{2+}$-free buffer and pre-incubated for 10 minutes inside a Hera Cell 150 incubator at 37°C (5% CO_2, 95% air). The standard buffer was a Hank's balanced salt solution (HBSS) containing $Ca^{2+/}Mg^{2+}$ supplemented with 4.2 mM $NaHCO_3$ and the pH adjusted to 7.4. The $Ca^{2+/}Mg^{2+}$-free buffer (HBSS without $Ca^{2+/}Mg^{2+}$) was supplemented with 1 mM ethylene glycol tetra acetic acid (EGTA) and 4.2 mM $NaHCO_3$ and the pH adjusted to 7.4.

Compounds were prepared as 10 mM stocks in DMSO and subsequently diluted 2000-fold in standard buffer containing 0.45% (v/v) acetonitrile to make the 'dosing solutions' which were pre-warmed to 37°C. A substrate uptake assay was initiated by adding 0.5 ml of the dosing solution containing drug to the wells (in triplicate per standard or $Ca^{2+/}Mg^{2+}$-free buffer type). Plates were transferred to a MaxQ 2000 plate shaker set to 100 rpm and incubated for 10 at 37°C (5% CO_2, 95% air). The dosing solutions, before and after incubation, were sampled and diluted 10-fold in methanol in water (70:30% v/v). Uptake reactions were then terminated by rinsing all wells 3 times with ice cold standard buffer. The cells were lysed by addition of 0.5 ml methanol in water (70:30% v/v) and agitated for approximately 30 minutes at ambient temperature on a MaxQ 2000 orbital plate shaker set to 100 rpm.

Fifty micolitre aliquots of all samples were then transferred to a v-bottomed 96-well microtitre plate containing 50 µl of ice cold internal standard solution (acetonitrile containing internal standards diazepam (0.1 µM) and warfarin (1 µM)). Samples were mixed and centrifuged at ~3400 x g, 4°C for 15 minutes using a Thermo Heraeus Multifuge 3S-R centrifuge. The amount of drug that had accumulated inside the cells and bile canaliculi was quantified using standard curves for each compound. Five standard concentrations ranging from 0 to 10,000 nM were prepared in methanol in water (70:30% v/v) and mixed 1:1 (v/v) with internal standard solution. The limit of quantification (LOQ) was defined by the smallest concentration of each analyte that could be reliably

measured (within 30% of the theoretical concentration). Peak area ratios of analyte:internal standard in the supernatants and standard curves were analysed by LC-MS/MS as detailed in Section 2.2.2.

Non-specific binding of compound to plastic-ware and/or Collagen I/Matrigel® sandwich in the absence of hepatocytes was assessed in parallel. Wells were treated as detailed in Section 2.7.1 but hepatocytes were omitted. The cell washing, incubation and cell lysis steps as detailed in this section were followed for the non-specific binding assessment.

2.7.4 Transport of fluorescent drugs in sandwich-cultured rat hepatocytes

Carboxydichlorofluorescein diacetate (CDFDA) readily permeates into hepatocytes and is hydrolysed to form fluorescent carboxydichlorofluorescein (CDF) which is transported into bile canaliculi via Mrp2 (Zamek-Gliszczynski et al., 2003). CDFDA was prepared as a 10 mM stock in DMSO and subsequently diluted 1000-fold in standard buffer containing 0.45% (v/v) acetonitrile to make the 'dosing solutions' containing drug which was pre-warmed to 37°C prior to use. Hepatocytes cultured for 96 h in a sandwich-configuration according to the method detailed in Section 2.7 were used. Following pre-treatment with either standard or $Ca^{2+/}Mg^{2+}$-free buffer, CDFDA (10 μM) was added to primary rat hepatocytes cultured in a sandwich configuration and incubated for 10 minutes inside a Hera Cell 150 incubator at 37°C (5% CO_2, 95% air). Uptake reactions were then terminated by rinsing all wells 3 times with ice cold standard buffer.

CDF fluorescence was imaged in the cells possessing intact bile canaliculi (standard buffer) or cells with disrupted bile canaliculi ($Ca^{2+/}Mg^{2+}$ - free buffer) using a Zeiss Axiovert 40 CFL fluorescent microscope, a Zeiss filter set 10 (excitation: 450-490 nm, emission: 515-565 nm) and beam splitter FT510 and imaged using Axiovision v4.6.1.0 software connected to a Zeiss Axiocam MRm digital camera (Carl Zeiss AG, Switzerland).

CDF biliary transport was also quantified. Prior to fluorescence analysis, cell lysates were disrupted using Adaptive Focused Acoustic (AFA) technology (60 second burst) using a Covaris E210 instrument (Covaris, Woburn, Massachusetts, USA). Samples were centrifuged at approximately 2600 x g for 15 minutes at 4°C using an Heraeus Microfuge 3S-R centrifugeand the supernatants were then analysed to quantify CDF present in hepatocytes with intact bile canaliculi (standard buffer) or cells with disrupted bile canaliculi (Ca^{2+}/Mg^{2+}-free buffer). CDF fluorescence was quantified using a Tecan

Safire II fluorescent plate reader (excitation: 504nm; emission 529nm, gain 52) and Tecan XFLUOR4SAFIREII Version: V 4.62n software.

2.7.5 Radiolabelled drug transport studies in sandwich-cultured rat hepatocytes

Tritiated substrates with specific activity between 1- and 5 Ci/mmol and a stock concentration of 1 mCi/ml were used. Radiolabelled dosing solutions were prepared in standard buffer containing the unlabelled version of the compound. Unlabelled compounds were prepared as 10 mM stocks in DMSO and subsequently diluted in standard buffer containing 0.45% (v/v) acetonitrile. Five microliters of radiolabelled compounds were then added per millilitre of unlabelled compound solution to result in the desired final concentration (nominally 5 µM). These radiolabelled dosing solutions were then pre-warmed to 37°C.

Hepatocytes cultured for 96 h in a sandwich-configuration according to the method detailed in Section 2.7.1 were used. Following pre-treatment with either standard or $Ca^{2+/}Mg^{2+}$-free buffer, radiolabelled dosing solutions were added to primary rat hepatocytes cultured in a sandwich configuration and incubated for 10 minutes inside a Hera Cell 150 incubator at 37°C (5% CO_2, 95% air). Uptake reactions were then terminated by rinsing all wells 3 times with ice cold standard buffer.

Cells were lysed with 0.5 ml 1% (v/v) Triton™ X-100 in standard buffer by shaking for approximately 30 minutes at ambient temperature on a MaxQ 2000 orbital plate shaker set to 100 rpm. Samples of the dosing solutions, before and after incubation were also analysed following a 10-fold dilution in 1% (v/v) Triton™ X-100 in standard buffer. Aliquots (100 µl) of samples were then transferred to 6 ml pony scintillation vials (Perkin Elmer, Schwerzenbach, Switzerland), 5 ml of Irga Safe Plus scintillant added and tritium radioactivity counted (disintegrations per minute, dpm) using a Packard Tri-carb 2200CA liquid scintillation analyser (Perkin Elmer, Schwerzenbach, Switzerland).

2.7.6 Determination of protein content of sandwich-cultured rat hepatocytes using the DC protein assay

To enable determination of the protein content per well used in the sandwich cultured rat hepatocyte studies, three extra wells of sandwich cultured rat hepatocytes were cultured according to the method detailed in Section 2.7.1. Following 96 h of culture time, the sandwich cultured rat hepatocytes were rinsed 6 times in 0.5 ml of standard buffer. Cells were lysed with 0.5 ml 1% (v/v) Triton™ X-100 in standard buffer by shaking for approximately 30 minutes at ambient temperature on a MaxQ 2000 orbital plate shaker at

100 rpm. The protein content of the sandwich-cultured rat hepatocytes in the wells was determined using the DC protein assay detailed in Section 2.6.3.

2.7.7 Calculation of accumulation, biliary efflux index and biliary clearance

The amount of compound accumulated in samples was quantitatively determined and divided by the average protein content/well (values are expressed as pmol/mg protein). The biliary efflux index (BEI) was calculated by comparing accumulation in cells pre-treated with standard and $Ca^{2+/}Mg^{2+}$-free buffer. The accumulation in cells pre-treated with standard buffer ($accumulation_{standard}$) equates to the amount of compound inside the hepatocytes plus bile canaliculi. Whereas, the accumulation in cells pre-treated with $Ca^{2+/}Mg^{2+}$-free buffer ($accumulation_{Ca2+/Mg2+-free}$) equates to the amount of compound inside the hepatocytes only since the bile canaliculi has been disrupted using this buffer pre-treatment:

$$BEI\ \% = \frac{\text{accumulation}_{\text{standard}} - \text{accumulation}_{\text{Ca2+Mg2+ -free}}}{\text{accumulation}_{\text{standard}}} * 100$$

Intrinsic secretory biliary clearance $CL_{int,sec}$ was calculated where AUC_{media} (pmol/ml · min) represents the area under the substrate concentration-time curve, determined by dividing the sum of the substrate concentration in the incubation medium at the beginning and end of the incubation period by 2 and multiplying by the incubation time (10 minutes):

$$CL_{int,sec}(ml/min/mg) = \frac{\text{accumulation}_{\text{standard}} - \text{accumulation}_{\text{Ca2+Mg2+ -free}}}{AUC_{media}}$$

$CL_{int,sec}$ may be scaled to account for the protein content in the whole liver of a rat, where physiological scaling factor SF1 approximates 200 mg protein per gram liver and SF2 approximates 40 gram of liver per kg body weight of a rat (Liu et al., 1999a):

$$Scaled\ CL_{int,sec}\ (ml/min/kg) = \frac{CL_{int,sec} * SF1 * SF2}{1000}$$

The predicted biliary clearance (CL_b) values were calculated based on the well-stirred model of hepatic disposition, assuming biliary excretion is the predominant elimination pathway and where Q_p represents the hepatic plasma flow in rats of 40 ml/min/kg (Liu et al., 1999a):

$$Predicted\ CL_b\ (ml/min/kg) = \frac{Q_p * scaled\ CL_{int,sec}}{Q_p + scaled\ CL_{int,sec}}$$

2.8 Measurement of plasma protein binding

Plasma protein binding (PPB) data were generated in the course of Medicinal Chemistry project support and not generated by the candidate. Data were collected from the Novartis Avalon database. Plasma protein binding was measured by equilibrium dialysis using a rapid equilibrium device (RED) (Thermo Fisher Scientific Inc., Wohlen, Switzerland) consisting of a Teflon base plate which holds up to 48 disposable dialysis inserts. Each dialysis insert is made up of two side-by-side chambers separated by a vertical cylinder of dialysis membrane made of regenerated cellulose (with a low glycerol content as a humectant, molecular weight cut off 8000), with a high membrane surface area-to-volume ratio offering the possibility of reduced equilibration times and higher assay throughput compared to standard equilibrium dialysis methods. The RED Teflon base plate was soaked in 20% (v/v) ethanol for a minimum of 20 minutes prior to use. RED Device inserts were used without any pre-treatment.

Fresh frozen Sprague Dawley rat plasma of mixed gender (SeraLab International, Bolney, UK) was thawed quickly at 37°C and centrifuged 100 x g for 5 minutes to remove the fibrin clot. The plasma was spiked with test compound solutions in DMSO to give a final concentration of 5 µM compound and 1% (v/v) DMSO. To enable assessment of compound stability in plasma and assay recovery, aliquots (50 µl) of plasma were taken immediately after compound spiking (pre-incubation samples). Aliquots (300 µl) of the spiked plasma were then added in triplicate to the plasma chamber of the insert. Isotonic PBS was added in 500 µl aliquots into each corresponding buffer chamber insert. The plate was sealed with a gas permeable adhesive seal (Thermo Fisher Scientific Inc., Wohlen, Switzerland) and placed on a dynamic shaker (model V 2000, Kisker Biotech, Steinfurt, Germany) set at 750 rpm. The shaker was placed inside an incubator set at 37 °C, 5% CO_2 and without added humidity for approximately 4 h.

At the end of the incubation, 50 µl aliquots were removed from the buffer and plasma chambers into a NUNC U96 polypropylene 2 ml deep well plate (post-incubation samples). A 50 µl aliquot of the opposite matrix was added to enable all samples to be matrix matched. Six volumes of quench solution (ice cold acetonitrile containing internal standard) were then added, samples mixed to precipitate proteins, and the deep well plate was centrifuged at ~3400 x g, 4°C for 15 minutes using a Thermo Heraeus Multifuge 3S-R centrifuge. A 50 µl aliquot of supernatant from each well was transferred to a clean 96-well plate and further diluted with 25 µl HPLC grade water. The samples were analysed

by LC-MS/MS for quantitation of drug in plasma (total drug, i.e. bound and unbound drug) and buffer (free drug, i.e. unbound drug). Peak area ratios of analyte to internal standard were calculated in all samples. Analytical conditions used are detailed in Section 2.2.2.

2.8.1 Calculation of unbound fraction, stability in plasma and assay recovery

The percentage unbound fraction in plasma (% fu) was calculated as follows:

$$\%\, fu = \frac{\text{P.A.R. buffer}_{(\text{post-incubation})}}{\text{P.A.R. plasma}_{(\text{post-incubation})}} * 100$$

The stability of compound in plasma following incubation was calculated according to:

$$\%\, plasma\ stability = \frac{\text{P.A.R. plasma}_{(\text{post-incubation})}}{\text{P.A.R. plasma}_{(\text{pre-incubation})}} * 100$$

The assay recovery, or mass balance, of compound was calculated to identify any issues of non-specific binding of compound to the RED apparatus (in particular to the membrane) following incubation according to:

$$\%\, recovery = \frac{\text{P.A.R. buffer}_{(\text{post-incubation})} + \text{P.A.R. plasma}_{(\text{post-incubation})}}{\text{P.A.R. plasma}_{(\text{pre-incubation})}} * 100$$

2.9 *In vivo* pharmacokinetic studies in rat

2.9.1 *In vivo* blood clearance studies in rat

All rat blood clearance data were generated in the course of Medicinal Chemistry project support and not generated by the candidate. Data were collected from the Novartis Avalon database. Male SD rats weighing approximately 300-350g were used for these experiments. Five days before drug administration, rats were anesthetized and catheters were surgically implanted into the femoral artery (for blood collection) and femoral vein (for intravenous injection). The catheters were exteriorized at the neck where they were fixed via a tether and flexible spring to a Harvard swivel system (Harvard Apparatus, MA, USA), which allowed blood sampling and intravenous injections without disturbing the freely-moving animal. Animals were kept individually in Makrolon cages, with free access to food and water throughout the experiment. Compounds were administered i.v. to the rats (nominally 4 rats per study), either discretely (1 compound per application) or in a cassette format (multiple compounds per application).

All compounds were solubilized in NMP:PEG200 (30:70 v/v) at 2 mg/ml and a volume of 0.5 ml/kg was administered resulting in a final dose of 1 mg/kg. Blood samples were taken at pre-defined time points (nominally 0.08; 0.25; 0.5; 1.0; 2.0; 3.0; 4.0; 6.0; 8.0; 24.0; 48.0 h). Prior to analysis, the protein in the blood samples was precipitated by mixing 1 volume of blood with approximately 8 volumes of acetonitrile and centrifuging at approximately 3500 x g at 4°C. A volume of supernatant was transferred into a microtitre plate and mixed with 1 volume of 0.1% (v/v) formic acid in water. Samples were then analysed by LC-MS/MS using individually optimized chromatographic conditions based on compound physicochemistry to determine the blood concentration/time profiles.

2.9.1.1 Pharmacokinetic calculations

Data analysis was done using an in-house Excel macro utilising a non-compartmental PK approach. For calculation of the intravenous area under the curve (AUC), the first measured time point at 5 minutes was used as a surrogate of the concentration at time zero. AUC was calculated using the linear trapezoidal method. Total blood clearance (CL) was calculated as Dose/AUC following i.v. dosing. The extrapolated AUC (AUCextrap) was used if the value was within 25% of the AUC based on the last time point (AUClast). Steady state volume of distribution (Vss) was calculated as mean residence time (MRT)*CL following i.v. dosing where MRT was calculated as AUMCextrap/AUCextrap and AUMC or area under the moment curve and calculated using the linear trapezoidal method. All calculations were based on the compounds' free basic form.

2.9.2 *In vivo* excretion studies in rat

Male SD rats weighing approximately 300-350g were used for these experiments. A day before drug administration, rats were anesthetized and catheters were surgically implanted into the femoral artery (for blood collection), femoral vein (for intravenous injection) and bile duct (for bile collection). Animals were kept individually in metabolic cages, with free access to food and water throughout the experiment. Compounds were administered i.v. to the rats (1 rat per study). All compounds were solubilized in NMP:PEG200 (30:70 v/v) and a volume of 0.5 ml/kg was administered resulting in a final dose of either 1 or 3 mg/kg. Sparse blood samples were taken at pre-defined time points. Bile, urine and faeces were collected over an 8 hour period. Faecal pellets were homogenised in methanol/water (1:1 v/v) using a Dispomix® homogeniser to yield a 20-fold diluted faecal homogenate (5% w/v). Prior to analysis, all blood and excreta samples were precipitated

with acetonitrile and centrifuged at approximately 3500 x g at 4°C. A volume of supernatant was transferred into a microtitre plate and mixed with 1 volume of 0.1% (v/v) formic acid in water. Samples were then analysed by LC-MS/MS using individually optimized chromatographic conditions based on compound physicochemistry to determine the concentration of parent in blood and excreta samples and the percentage dose eliminated as parent in the excreta.

2.10 Measurement of drug permeability in MDCKII LE cells and PAMPA

2.10.1 The MDCKII LE assay

Cellular permeability of NCEs was assessed using a subpopulation of low efflux cells from MDCKII wild type cells. The MDCKII wild type cells were originally obtained from Professor Anton Berns at the Netherlands Cancer Institute, Amsterdam. The low efflux sub population of MDCKII cells (MDCKII LE) was previously identified and validated in-house using methodology similar to that previously reported in the literature (Di et al., 2011). MDCKII LE cells were cultured at 37°C, 5% CO_2, 95% relative humidity in growth medium (DMEM plus Glutamax™-I medium containing 5% FBS) and passaged weekly at approximately 80% confluency in sterile petri dishes. Cells were removed from petri dishes following trypsinisation, counted using a haemocytometer and diluted to 4 x 10^5 cells/ml in growth media. Cells were then plated onto Corning HTS Transwell® 96-well polycarbonate membrane inserts (0.4µm pore size) at a volume of 75 µl per apical well. The inserts were placed into a pre-filled feeder tray containing 35 ml of growth medium and incubated for 4 days.

The fluorescent substrate, Lucifer yellow was prepared as a 1 mg/ml stock in HPLC grade water. Compounds were prepared as 10 mM stock solutions in DMSO and subsequently diluted in Lucifer yellow and transport buffer (Williams E medium containing 10mM HEPES and 0.52% acetonitrile (v/v)) to achieve a final concentration of 5 µM compound and 100 µM Lucifer yellow. The final solvent concentration in the dosing solutions was 0.05% DMSO and 0.45% acetonitrile (v/v). After 4 days culturing, Transwell® membrane inserts were rinsed in transport buffer and transferred into a Transwell® 96 well receiver plate containing 235 µl transport buffer per well. Transport assays were performed in the apical to basolateral direction and 75 µl dosing solutions were added to the apical wells in triplicate and plates incubated at 37°C (5% CO_2, 95% relative humidity). Samples were taken at 0 and 2 h from both apical and receiver

compartments. All samples were then mixed with 1 volume of acetonitrile containing an analytical internal standard. Transport of Lucifer yellow was assessed immediately by fluorescence spectrometry (excitation 430nm, emission 530nm) using a Tecan Safire 2 monochromator plate reader and Tecan XFLUOR4SAFIREII Version: V 4.62n software with temperature controlled at 37°C. Samples were subsequently analysed by LC-MS/MS to obtain peak area ratios of analyte:internal standard as detailed in Section 2.2.2.

2.10.1.1 Calculation of apparent permeability

Apparent permeability, P_{app}, values were calculated for Lucifer yellow and compounds as follows:

$$P_{app} = \frac{dQ}{dt} * \frac{1}{Area * C_D(0)}$$

Where d*Q*/d*t* is the permeability rate of the compound across the monolayer, Area is the growth area of the well (0.43cm^2), C_D (0) is the concentration in the donor samples at time 0 and *t* is time in seconds. Membrane integrity of the cell monolayer was assessed in each well by measuring exclusion of Lucifer yellow, an impermeable marker. Only monolayers with Lucifer yellow P_{app} (x 10^{-6} cm/s) values <1 were considered integral and used for further experimentation. Passages 24, 26 and 28 were used to generate cellular permeability data in this thesis.

2.10.1.2 Assay recovery of compounds

The assay recovery, or mass balance of compound was calculated to identify any issues of non-specific binding of compound (in particular to the membrane), malfunctioning of the assay or analytical failures. In general, recovery within 70-130% was accepted and was calculated where PAR_{rec2h}, PAR_{don2h} and PAR_{don0h} correspond to the peak area ratio of analyte:internal standard in the receiver and donor wells at 2h (post incubation) and in the donor well at 0h (pre-incubation) respectively:

$$\%\, recovery = \frac{P.A.R._{rec2h} + P.A.R._{don2h}}{P.A.R._{don0h}} * 100$$

2.10.2 The parallel artificial membrane permeability assay (PAMPA)

All PAMPA permeability data were generated in the course of Medicinal Chemistry project support and not generated by the candidate. Data were collected from the Novartis Avalon database. A parallel artificial membrane permeability assay using a hexadecane membrane (HDM-PAMPA) was used to predict the passive permeability of compounds

(Wohnsland and Faller, 2001). The PAMPA assay was carried out in 96-well microplates and measured the ability of compounds to diffuse across a microporous filter coated with a thin 9-10 μm hexadecane liquid layer separating pH buffered solutions in the donor and acceptor plates in a microplate sandwich configuration. To minimize solubility issues compounds were loaded at 5 μM in the donor compartment and the assay buffer contained 5% (v/v) DMSO. Permeability was measured at pH 4, pH 6.8 and pH 8 and was derived from the compound concentration (measured by LC-MS/MS) in the acceptor compartment after a 4-hour incubation time.

2.10.2.1 Calculation of transcellular permeability

The apparent membrane permeability value P_a was determined from the ratio of the peak area of compound found in the acceptor compartment divided by the theoretical equilibrium peak area (r, determined independently). V_R is the volume of the receiver compartment (0.3 cm^3), V_D is the volume of the donor compartment, A is the accessible filter area (0.24 cm^2 multiplied by a porosity of 20%) and *t* is the incubation time (4 h). In the absence of membrane retention, P_a is identical to P_e, the effective membrane permeability which is calculated at each of the three pHs used:

$$P_a(P_e) = \frac{V_D}{V_D + V_R} * \frac{V_R}{A * t} * \ln(1 - r)$$

2.10.2.2 Calculation of paracellular permeability

Typically, a well-functioning PAMPA assay mimics pure transcellular permeability only. However, a number of small, hydrophilic compounds can permeate across the gastro-intestinal tract via the paracellular route. Since overall permeability is the sum of both transcellular and paracellular contributions, the paracellular pathway is calculated mathematically using a modified version of the hydrodynamic model described in the literature (Adson et al., 1995; Adson et al., 1994) and is incorporated in the overall PAMPA permeability prediction. The following parameters are taken into account to model paracellular transport: molecular radius, cell junction pore radius, aqueous diffusion coefficient, electrostatic field, potential difference across the cell junction and gastro-intestinal wall. LogPAMPA refers to the log of the highest P_e value measured in the pH range tested and also includes the paracellular contribution and is used to classify permeability into low, medium or high categories.

2.10.2.3 Calculation of percent fraction absorbed

In-house data generated for more than 90 literature compounds indicated a sigmoidal relationship between LogPAMPA and the fraction absorbed in humans. The resultant permeability at 50% fraction absorbed ($Pc50$ = 7.63 10^{-6}) and slope factor (γ = 1.5) were used to derive a calculated fraction absorbed (FA_{calc}) for all NCEs:

$$FA_{calc} = \frac{100}{1 + (\frac{Pc50}{10^{LogPAMPA}})\gamma}$$

The LogPAMPA and percentage fraction absorbed data may be used to classify permeability into low, medium or high categories according to Table 2-2.

Table 2-2 PAMPA permeability categories

Permeability class	LogPAMPA	FA_{calc}
Low	< -5.3	< 35%
Medium	-4.8 to -5.3	35% to 75%
High	> -4.8	>75%

2.11 *In silico* prediction of p*K*a

The vast majority of drugs contain ionisable groups and the extent of ionisation of a compound is indicated by p*K*a, which is the negative log of the ionisation constant *K*a. The p*K*a of a compound is a major determinant of lipophilicity and solubility, two properties widely used to predict absorption and distribution of compounds. pKa values for the NCE set were predicted using an *in silico* computational approach, MoKa software version 2.0 (Molecular Discovery Ltd, UK). In brief, MoKa describes the molecular structure around an ionisable centre; atomic descriptors are used to map the chemical space of a molecule at different topological distances from the ionisable centre and the pKa is predicted by the 2D structure (Milletti et al., 2007). MoKa was also used to predict the charge type of each compound. All predicted pKa and charge type data were not generated by the candidate.

3 CHAPTER THREE: RESULTS – *IN VITRO-IN VIVO* EXTRAPOLATION OF CLEARANCE IN RAT

3.1 Background

Optimisation of clearance is typically one of the more significant challenges in drug discovery. Reliable assessment of metabolism in early drug discovery has driven the development of a range of robust, *in vitro* systems such as recombinant CYP450s, liver S9 fractions, microsomes and hepatocytes, which can be utilized in a systematic manner to explore and understand metabolic clearance. Much of the emphasis still remains focused on CYP450 screening systems, with liver microsomes used in a generic high throughout mode providing a common *in vitro* method of choice within industry as a first line metabolism screen. Hepatocytes can fully substitute for microsomes and have been shown to provide improved IVIVE when hepatic metabolism involves more than CYP450 reactions such as aldehyde oxidase, glucuronidation, sulfation etc (Hewitt et al., 2007; McGinnity et al., 2004).

3.2 Early drug discovery at Novartis Basel

Following review of the internal database of discovery molecules synthesized in 2013, pKa values were determined for ~6,400 NCEs. The distribution in chemical class is displayed in the pie chart in Figure 3-1. Bases are the most common class (44%), followed by ampholytes (29%), acids (16%), neutral (7%) and zwitterionic compounds (4%).

Figure 3-1 Distribution of chemical class for Novartis NCEs.

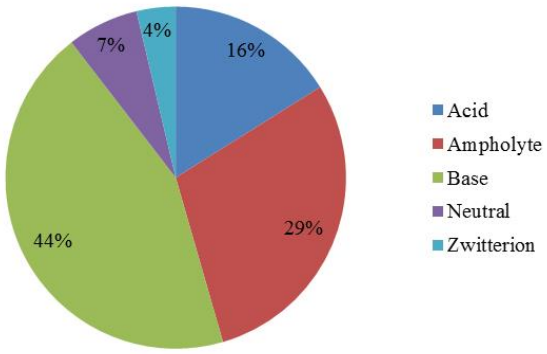

The range in lipohilicity (cLogP) and molecular weights of NCEs are illustrated in the box plots in Figure 3-2 below. The median calculated LogP was 3.1 and the median molecular weight was 424.

Figure 3-2 Range of lipophilicity values and molecular weights for Novartis NCEs

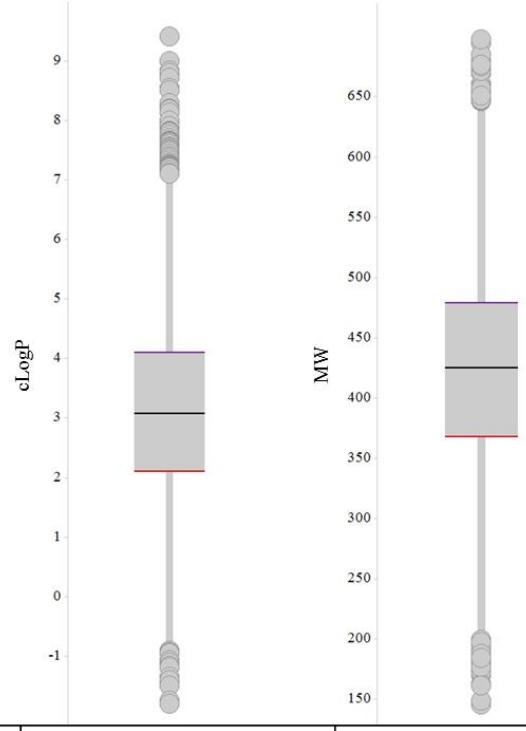

	cLogP	MW
Count	6396	6396
Median	3.1	424
Outliers	76	50

Box plot illustrating the range of lipophilicity (cLogP) values and molecular weights for NCEs (n= 6396). The purple and red horizontal lines represent the third quartile and first quartile respectively and the vertical lines (whiskers) extending from the boxes indicate variability outside the upper and lower quartiles. The grey circles represent outliers. Solid horizontal black lines indicate the median values (second quartile).

3.2.1 Clearance optimization in early drug discovery

In vitro $CL_{int,met}$ data may be extrapolated to the *in vivo* situation using the well-stirred model where fu_b and fu_{inc} (fraction unbound in the incubation, e.g. to liver microsomes) are incorporated to capture the effect of binding on drug available for extraction (Obach, 1999):

$$CL_H(mlminkg) = \frac{Q_H * \frac{fu_b}{fu_{inc}} * CL_{int,met}}{Q_H + \frac{fu_b}{fu_{inc}} * CL_{int,met}}$$

In Novartis during early drug discovery, prediction of rat hepatic clearance is commonly conducted using rat liver microsomes as a first line metabolism screen. The routine generation of fu_{inc} or fu_b data for all NCEs are impractical and initial extrapolations are made using a direct scaling model (where drug binding terms are not accounted for) to indicate the relationship of $CL_{int,met}$ and total clearance:

$$CL_H\,(ml/min/kg) = \frac{Q_H * CL_{int,met}\,(ml/min/kg)}{Q_H + CL_{int,met}\,(ml/min/kg)}$$

Historical *In vitro-in vivo* clearance correlation analysis for more than 1800 Novartis NCEs indicated that *in vivo* clearance of approximately half of all NCEs were poorly predicted from rat liver microsomes using a direct scaling model (Figure 3-3). Approximately 10% of NCEs had predicted clearance more than 2-fold higher than observed blood clearance. Of greater concern is the high frequency of NCEs that had predicted clearance more than 2-fold lower than observed clearance, occurring for approximately 40% of NCEs.

Figure 3-3 Rat IVIVC analysis of Novartis NCEs: Distribution of clearance predictions

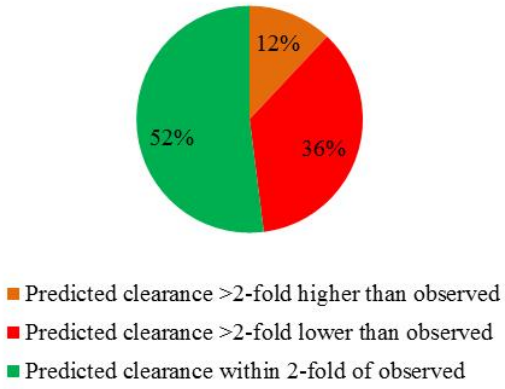

Rat IVIVC analysis of 1872 Novartis discovery NCEs comparing total rat blood clearance and predicted clearance from rat liver microsomes.

An hepatocyte clearance assay is often employed to explore metabolism when poor estimates of clearance occur with rat liver microsomes. The hepatocytes are cryopreserved but reference phase I and II activity marker substrates are incorporated into each assay run indicating functionality and reproducibility. With few exceptions, the hepatocyte assay typically does not appear to be adding extra value in line with investment to improve IVIVC. This is illustrated in Figure 3-4, which depicts the IVIVC for 194 Novartis NCEs where total blood clearance and predicted clearance from both rat liver microsome and hepatocytes were routinely generated.

Figure 3-4 Prediction of rat clearance using rat liver microsomes and cryopreserved hepatocytes for Novartis NCEs

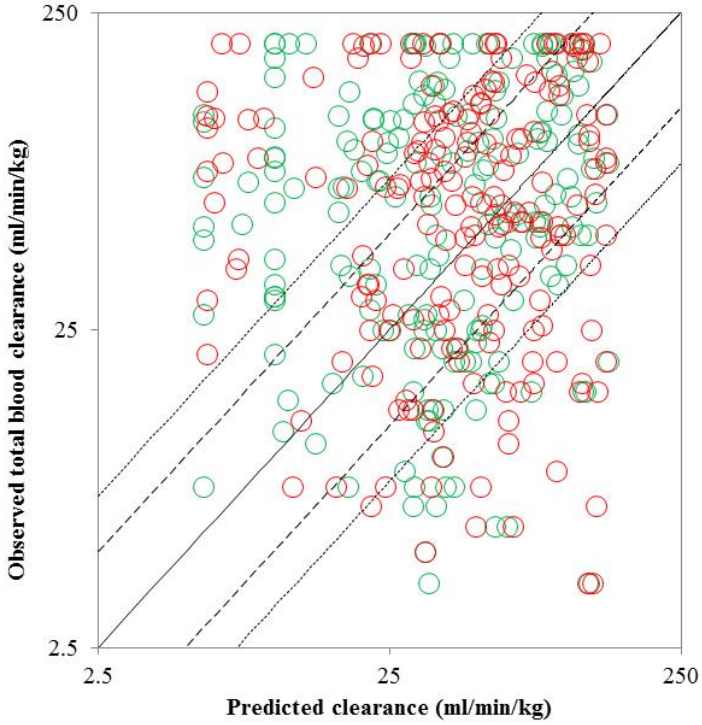

Prediction of rat clearance from rat liver microsomes and cryopreserved hepatocytes for Novartis NCEs (n=194). Red circles represent predicted clearance using rat liver microsomes. Green circles represent predicted clearance using cryopreserved rat hepatocytes. Solid line indicates the line of unity. Dashed and dotted lines represent 2-fold and 3-fold of the unity line respectively.

The molecules in this dataset show a range of observed rat blood clearance values from low (<50 ml/min/kg) to very high, with clearance exceeding 150 ml/min/kg (the upper end of the estimated liver blood flow in the Novartis rat colony). Where clearance values exceed liver blood flow, it is assumed that drugs may also be cleared via non-

hepatic routes including renal clearance. For NCEs where measured rat clearance values exceed estimated hepatic and renal blood flow in rat, the measured values have been capped and reported as '> 200 ml/min/kg' indicating very high total blood clearance.

Table 3-1 Comparison of clearance predictions for Novartis NCEs using rat liver microsomes and hepatocytes

Clearance prediction	Metabolism assay matrices	
	Rat liver microsomes	Rat hepatocytes
% Outside 2-fold	58	62
% Outside 3-fold	36	42
n	194	194
Bias	0.83	0.71
Rmse	0.59	0.58
afe	3.9	3.8

n: sample number, afe: average fold error, rmse: root mean squared prediction error

The statistical comparisons of these predictions are summarized in Table 3-1. When observed and predicted clearance values in rat are compared, there was a marginally lower percentage of compounds falling outside 2-fold and 3-fold error with rat liver microsomes compared to hepatocytes and this was consistent with the bias observed. Precision in predicted clearance was comparable in both matrices (similar *rmse* and *afe*). In general, rat cryopreserved hepatocytes do not appear to provide improved clearance predictions compared to rat liver microsomes. Given that hepatocytes contain a full complement of hepatic phase 1 and II enzymes and cofactors, it remains unclear why rat cryopreserved hepatocytes typically do not appear to give a significant improvement in IVIVE for clearance in rat compared to microsomes. Issues with co-factor exhaustion, rate-limiting permeability and reduced dynamic range in $CL_{int,met}$ due to scaling factors used (117 million hepatocytes/g liver compared to 45 mg of microsomal protein/g liver) may be partly responsible. However, similar to the microsomal assay, the hepatocyte method employed was originally validated and optimized to focus on reducing metabolic liability with little scope for assessing active transport. Hence, significant under-predictions of clearance could result for compounds that are actively transported in the liver.

3.3 Exploring hepatobiliary disposition of early drug discovery NCEs

Drug transporters are still an emerging area of interest but industry is clearly aware of the potential implications that transporters can have in drug clearance. Prior to changing IVIVE strategies in early drug discovery, there is a need to explore different techniques and models to gain a detailed understanding of the processes involved in hepatobiliary disposition of discovery compounds. Ideally, through appropriate experimental design and modelling of molecular and structural descriptors, the critical aspects of these innovations can be identified and effectively incorporated with sufficient throughput into a drug discovery setting to add value and improvements to IVIVE.

A set of 77 proprietary discovery compounds, hereon in referred to as the NCE set, were identified from the in-house database in order to explore the role of transporters in hepatobiliary drug disposition. Compounds were chosen based on existing *in vitro* and *in vivo* rat clearance data with an emphasis on compounds where predicted clearance in liver microsomes was > 2-fold lower than observed clearance in order to explore the impact of hepatic transporters on drug clearance. The *in vitro*, *in vivo* and *in silico* properties of the NCE set are presented in Table 11-1 in the appendix. Rat blood pharmacokinetic values (total blood clearance and V_{ss}), rat liver microsomal $CL_{int,met}$, fu_p, PAMPA permeability and aqueous solubility data was retrieved from the Novartis database. Prior to commencing *in vitro* hepatic transporter studies, the dataset was supplemented with *In silico* parameters, plasma stability, $CL_{int,met}$ and predicted CL_H in freshly isolated rat hepatocytes and cellular permeability (MDCKII LE) data all generated in the course of this thesis research. Additionally, a small set of 14 marketed drugs were compiled to test and validate the functionality of the *in vitro* hepatocyte uptake and efflux assays. These marketed drugs were chosen based on information available in the literature and most of these drugs have previously been documented as either uptake and/or efflux substrates of hepatic transporters. Rat liver microsomal and hepatocyte $CL_{int,met}$, PAMPA permeability, fu_p, aqueous solubility plasma stability and cellular permeability (MDCKII LE) data and *in silico* parameters were generated for these marketed drugs in the course of this PhD research and are also presented in Table 11-1 in the Appendix.

3.3.1 Physicochemical properties of the NCE set

The distribution in chemical class in the NCE set is displayed in the pie chart in Figure 3-5. Bases are the most common class (68%), followed by neutrals (21%). Whereas the number of acids, ampholytes and zwitterionic compounds are low (sum = 11%).

Figure 3-5 Distribution of chemical class in the NCE set

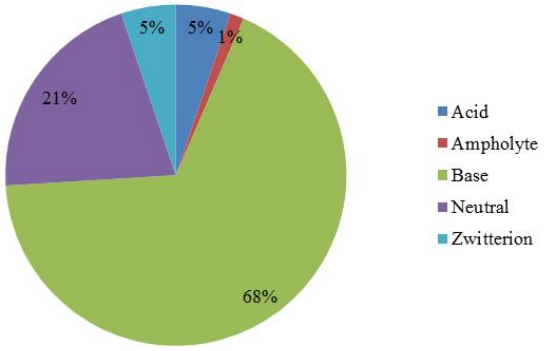

The range in lipophilicity (cLogP) and molecular weights for the NCE set are illustrated in the box plots in Figure 3-6 below. The median molecular weight was 450. The median calculated LogP was 2.5.

Figure 3-6 Lipophilicity and molecular weight range for the NCE set

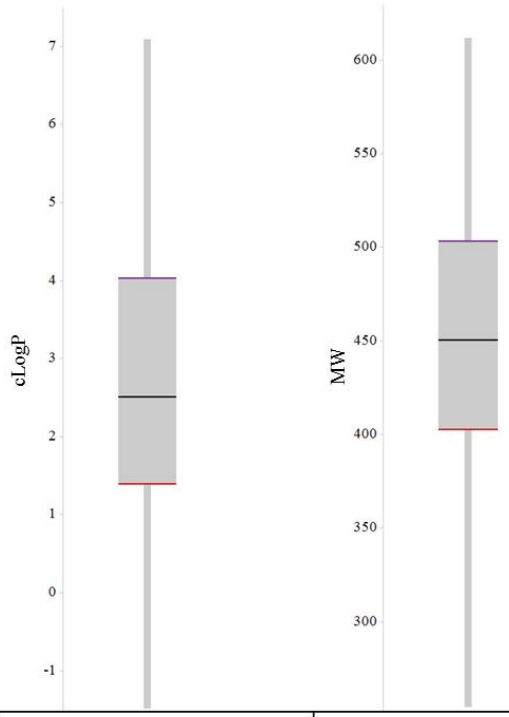

	cLogP	MW
Count	77	77
Median	2.5	450
Outliers	0	0

Box plot illustrating the range of lipophilicity (cLogP) values and molecular weights for the NCE set. The purple and red horizontal lines represent the third quartile and first quartile respectively and the vertical lines (whiskers) extending from the boxes indicate variability outside the upper and lower quartiles. Solid horizontal black lines indicate the median values (second quartile).

3.3.1.1 Physicochemical property space of the NCE set

ChemMAP is a navigational tool which was developed to navigate the physicochemical property space of bioactive molecules (Faller et al., 2011). Volsurf+ molecular descriptors from 240 representative marketed drugs covering the physicochemical property space are used as reference molecules and set the boundaries of the property space. 3D maps of molecular interaction fields are converted into 56 molecular descriptors that account for size, shape, hydrophilicity, hydrophobicity, H-bonding donor and acceptor capacities. Principal component analyses (PCA) was used to compress information contained in the 56 descriptors into 3 principal components accounting for 75% of the overall variance.

Additional drugs of interest can then be projected onto the ChemMAP to determine their relative position in the score plot.

Figure 3-7 Physiochemical property space for the NCE set

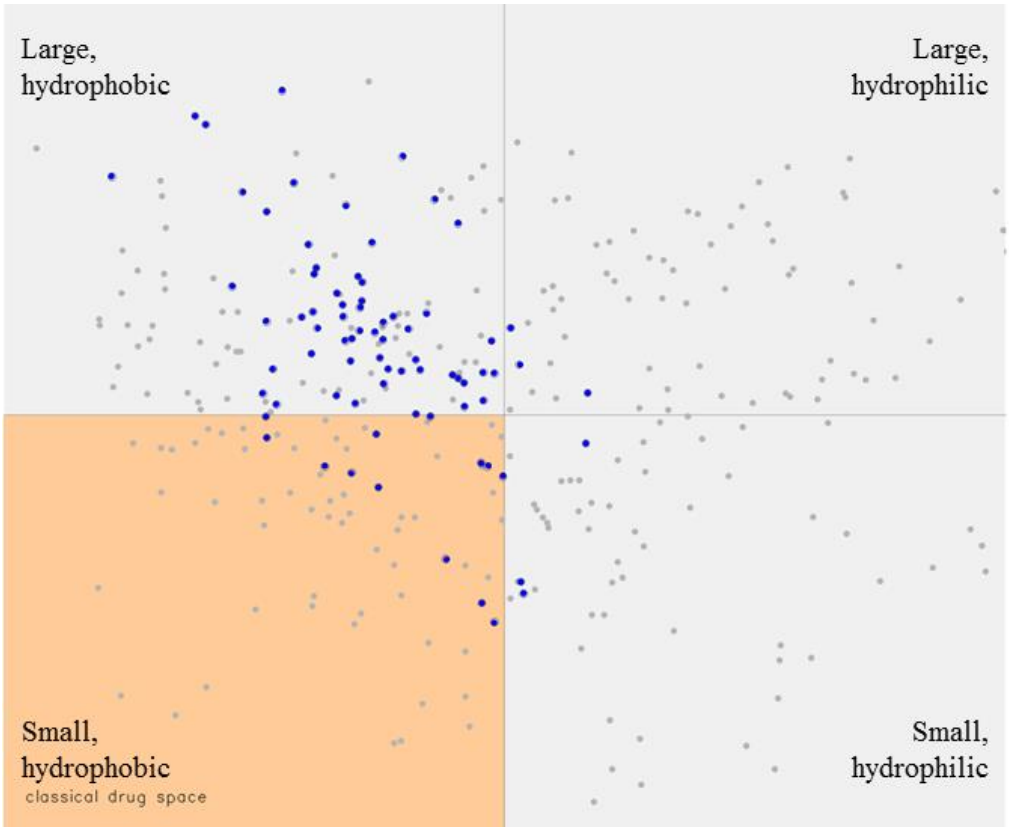

Physicochemical property space occupied by the NCE set used to explore IVIVE. Blue dots represent the 77 NCEs. Grey dots represent background ChemMAP molecules. Classical drug space denotes the property space held by traditional small molecule drugs approved prior to 2002.

The majority of the NCEs occupy the top left quadrant of ChemMAP indicating this compound set comprises a number of large hydrophobic compounds. The NCEs also occupy to a lesser degree, the remaining 3 quadrants suggesting modest diversity in the physicochemical property space for this compound set.

3.3.2 IVIVE of rat clearance for the NCE set

As previously highlighted, the 77 NCEs were chosen based on existing *in vitro* (rat liver microsome) and *in vivo* rat blood clearance data with an emphasis on compounds where predicted clearance in liver microsomes was > 2-fold lower than observed clearance in

order to explore the impact of hepatic transporters on drug clearance. Rat liver microsomal and total blood clearance data for the NCE set was obtained from the Novartis database.

The NCE set show a range of observed rat blood clearance values from low (<50 ml/min/kg) to very high (>150 ml/min/kg). For compounds where measured rat blood clearance values exceed estimated hepatic and renal blood flow in rat, the measured values have been capped and reported as '> 200 ml/min/kg' indicating very high total blood clearance. Observed rat blood clearance and predicted clearance values for the NCE set were categorised as either 'low' (CL<50 ml/min/kg), 'medium' (CL 50-100 ml/min/kg) or 'high' (CL 100-150 ml/min/kg) with the addition of a fourth category for observed clearance of 'very high' (CL>150 ml/min/kg). Comparison of the observed and predicted clearance categories in Figure 3-8 clearly indicates a large *in vitro-in vivo* clearance disconnect and a high incidence of under prediction of clearance from rat liver microsomes.

Figure 3-8 Comparison of observed and predicted clearance categories for the NCE set

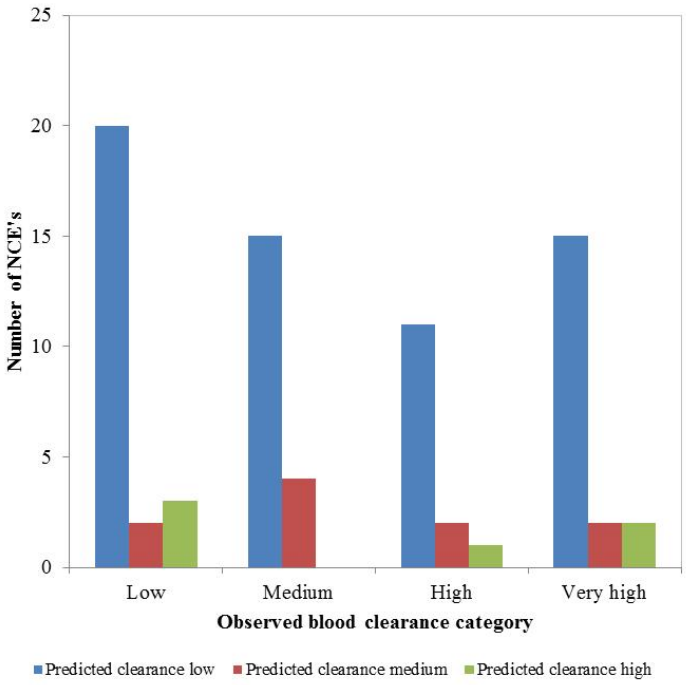

Observed rat blood clearance and predicted clearance values from rat liver microsomes for the NCE set were categorized into either 'low' (CL<50 ml/min/kg), 'medium' (CL 50-100 ml/min/kg) or 'high' (CL 100-150 ml/min/kg). A fourth category of 'very high' was used to describe observed blood clearance >150 ml/min/kg.

Additionally, clearance of the NCE set was measured in freshly isolated rat hepatocytes (in suspension) as detailed in Section 2.4.1. Primary rat hepatocytes were successfully isolated from freshly excised male Han Wistar rat livers and suspended in WEM (supplemented with 10mM HEPES) at a final concentration of 1 million cell/ml. Routinely, the cell viability was >85%. Parameters of $t1/2$, $CL_{int,met}$ and predicted CL_H were defined using the same methods of calculation as detailed in Section 2.2. The comparison of observed and predicted rat clearance for the Novartis compound set from fresh hepatocyte is presented in Figure 3-9. Additionally, predicted rat clearance data from rat liver microsomes was added for comparison.

Figure 3-9 Prediction of rat clearance using rat liver microsomes and fresh rat hepatocytes for the NCE set

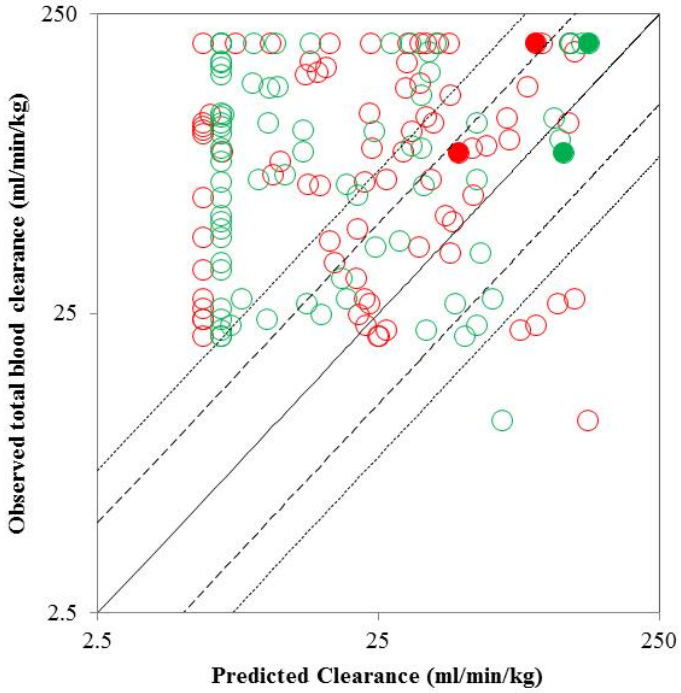

Prediction of rat clearance from rat liver microsomes and fresh rat hepatocytes for the NCE set (n=77) using the direct scaling model. Red circles represent predicted clearance values using rat liver microsomes where the 2 red filled circles represent 2 compounds (NCEs 1 & 5) which showed instability in rat plasma (half-lives of ≤ 35 minutes). Green circles represent predicted clearance values using fresh rat hepatocytes where the 2 green filled circles represent NCEs 1 &5 which were unstable in rat plasma. The black solid line indicate the line of unity whereas dashed and dotted black lines denote 2-fold and 3-fold of the unity respectively.

Comparison of observed and predicted clearance indicates a high incidence of under prediction of clearance with both rat liver microsomes and fresh rat liver hepatocytes.

Table 3-2 Statistical analysis of clearance predictions in rat liver microsomes and fresh rat hepatocytes for the NCE set

Clearance prediction	Metabolism assay matrices	
	Rat liver microsomes	Fresh rat hepatocytes
% Outside 2-fold	70	75
% Outside 3-fold	58	66
n	77	77
Bias	0.33	0.22
rmse	0.71	0.83
afe	5.1	6.8

n: sample number, rmse: root mean squared prediction error, afe: average fold error

The statistical comparisons of these predictions are summarized in Table 3-2. When observed and predicted clearance values in rat are compared, there was a lower percentage of compounds falling outside 2-fold and 3-fold error with rat liver microsomes compared to hepatocytes and this was consistent with the bias observed. Precision in predicted clearance was also higher with rat liver microsomes (lower *rmse* and *afe*). In general, clearance was substantially underestimated (> 3-fold lower than observed) from both microsomes and hepatocytes for ~60% of the NCEs. In such cases extra-hepatic metabolism may contribute to drug clearance. Drugs with certain functional groups including esters, amides, lactones, lactams, carbamides, sulfonamides and peptide mimetics may be more susceptible to hydrolysis by plasma amidases, esterases, carbonyl reductases and monoamine oxidases etc. Following review of rat plasma stability data it became evident that plasma stability data did not reconcile the IVIVE disconnect for these NCEs. Only NCEs 1 and 5 were found to show instability in plasma with half-lives ≤ 35 minutes and the clearance IVIVE in both microsomes and hepatocytes was already modestly good suggesting plasma metabolism may not be the main elimination pathway for these 2 NCEs (Figure 3-9).

MDCKII LE cell permeability of the NCE set was measured for all except 7 NCEs which remained undefined due to poor assay recovery (<70%). NCEs were grouped into low, medium and high passive permeability categories according to MDCKII LE P_{app} values with low permeability < 5 x 10^{-6} cm/s and high permeability ≥ 10 x 10^{-6} cm/s respectively. These cut off values were defined by the range of P_{app} values for marketed

drugs classified as having either low or high % human intestinal absorption in the literature (see Appendix section 11.3 for more details.)

With fresh rat hepatocytes, a higher percentage of NCEs showed predicted clearance outside 3-fold observed values (66% compared to 58% in rat liver microsomes). Compounds need to be able to permeate the hepatocyte membrane to gain access to intracellular enzymes hence NCEs with lower permeability could appear more stable in hepatocytes compared to microsomes. This permeability limited clearance is evident with direct correlation of predicted clearance from microsomes and hepatocytes as in Figure 3-10. Twelve NCEs with low and moderate permeability appeared stable in hepatocytes but showed metabolic instability in liver microsomes (as indicated by the red and orange data points with lowest predicted clearance values lined up horizontally on the Y axis). In comparison, there were fewer NCEs which appeared more stable in liver microsomes compared to hepatocytes (as indicated by the lowest predicted clearance values lined up vertically on the X axis). Given that hepatocytes contain a full complement of phase I and II enzymes and cofactors, metabolism of these compounds is more than likely catalysed mainly by non-NADPH dependent enzymes which are functionally active in hepatocytes but not microsomes.

Figure 3-10 Comparison of predicted clearance from rat liver microsomes and fresh rat hepatocytes for the NCE set

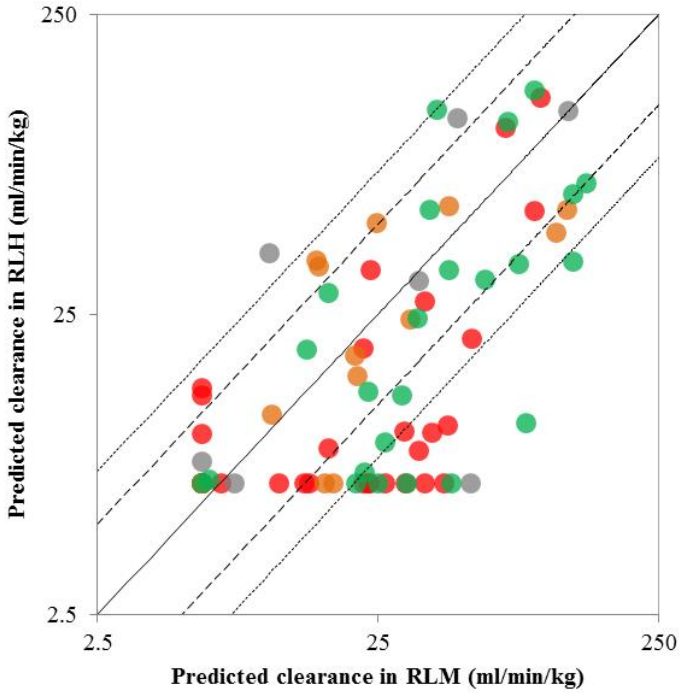

Comparison of predicted clearance in rat liver microsomes and fresh rat liver hepatocytes for the NCE set (n=77). NCEs are colour coded according to their MDCKII LE permeability category where red = low permeability, orange = medium permeability, green= high permeability and grey = permeability not measured. The black solid line indicates the line of unity whereas black dashed and dotted lines indicate 2-fold and 3-fold of the unity line respectively.

In summary, *in vitro* experiments with liver microsomes and fresh hepatocytes to predict the clearance of this NCE set led to significant under predictions of clearance and the reasons for this remain unclear. Inadequacies with the chosen experimental methods may have contributed since the 'metabolism' format used provides little scope for assessing active transport. More recently, novel methodological adaptations have been introduced to hepatocyte clearance studies to improve predictions of clearance when uptake transporters have a predominant role in drug clearance. (Nordell et al., 2013; Soars et al., 2007). Subsequently, established models of hepatic clearance IVIVE in the literature have also been adapted to incorporate these newer transporter concepts (Umehara and Camenisch, 2012; Webborn et al., 2007) which may provide some bandwidth for improving IVIVE in early drug discovery.

3.3.3 Comparison of IVIVE methods for predicting hepatic metabolic clearance

Systematic under-prediction of drug clearance from liver microsomes and hepatocytes using conventional 'well-stirred' extrapolation methodology has been well documented in the literature (Ito and Houston, 2004; Riley et al., 2005; Stringer et al., 2008). More recently newer approaches like the regression offset approach which applies empirical correction factors to improve clearance predictions have been applied with success (Sohlenius-Sternbeck et al., 2012) but these are not without limitations. Key requirements are that hepatic metabolism should be the principle route of elimination and compounds with observed blood clearance approaching liver blood flow should not be included. In the NCE set, 45% of compounds showed total blood clearances ≥ 100 ml/min/kg and the principal elimination routes are not fully elucidated which prevent the use of this extrapolation approach.

It was of interest to ascertain how blood binding terms might influence the IVIVE using the well stirred model. Rat plasma protein binding data was retrieved from the Novartis data base for 70 NCEs but was not measured for 7 NCEs. The fraction of drug unbound in plasma was corrected for the blood to plasma partition ratio to calculate the fraction unbound in blood (fu_b). Blood to plasma partition values are typically not available for early discovery NCEs so a value of 1.0 was assumed for basic and neutral compounds and a value of 0.55 (1- haematocrit) was assumed for acids. Predicted clearance accounting for blood binding terms was then calculated from rat liver microsome data. Additionally, an extrapolation method which accounts for the ionization properties of drug molecules was also investigated by applying a correction or ionization factor F_I, corresponding to the ratio of unionized drug in blood and intracellular tissue water, to the conventional well stirred model (Berezhkovskiy, 2011). A comparison of these 3 extrapolation methods to predict blood clearance from rat liver microsome data is presented in Figure 3-11.

Figure 3-11 Comparison of three IVIVE methods to predict rat clearance from rat liver microsomes

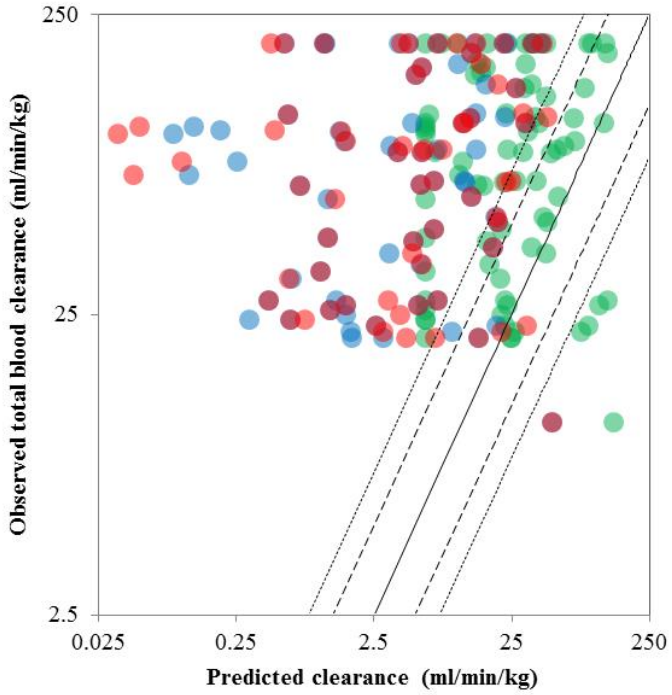

Comparison of 3 different IVIVE methods used to predict rat clearance from rat liver microsomes for the NCE set. Green circles represent predicted clearance using a direct scaling method (well stirred model disregarding binding, n=77). Blue circles denote predicted clearance using the conventional well stirred model accounting for fu_b only (n=70). Red circles indicate predicted clearance using the conventional well stirred model accounting for fu_b and F_I (n=70). The solid black line indicates the line of unity whereas dashed and dotted black lines denote 2-fold and 3-fold of the unity respectively.

It is clearly evident that accounting for drug binding to blood alone in the clearance prediction does not improve the IVIVE for this NCE set. Accounting for the difference in drug ionization in extracellular and intracellular tissue water into the IVIVE also did not yield improvements compared to the direct scaling method. The statistical comparisons of these predictions are summarized in Table 3-3. With the direct scaling method, predictivity, precision and bias were improved in comparison to the other 2 IVIVE methods were drug ionization and/or blood binding was accounted for.

Table 3-3 Statistical analysis for three different IVIVE methods to predict clearance in rat liver microsomes for the NCE set

Clearance prediction	IVIVE method (terms accounted for)		
	Well stirred (none, direct scaling)	Well stirred (fu_b)	Well stirred (fu_b and F_I)
% Outside 2-fold	70	97	96
% Outside 3-fold	58	91	87
N	77	70	70
Bias	0.33	0.05	0.06
Rmse	0.71	1.44	1.46
Afe	5.1	28	29

n: sample number, rmse: root mean squared prediction, afe: average fold error, error

Reports in the literature suggest that the extent of non-specific binding to microsomes can vary greatly from one compound to the next and the extent of this incubational binding (fu_{inc}) is an important parameter to obtain when attempting to relate *in vitro* intrinsic clearance to observed clearance *in vivo* (Obach, 1997). Fu_{inc} is not routinely measured in early drug discovery and in-house experience with the model based on logP/D to predict the extent of microsomal binding (Austin et al., 2002) has been unfavourable leading to poor predictions of fu_{inc}. Paucity of measured fu_{inc} and blood-plasma equilibrium concentration ratio data during early stages of drug discovery creates limitations to the IVIVE strategy that may be applied. Once these data become available during the later characterization stages of drug development, further investigations may then be conducted to capitalise on recent advances in IVIVE from the literature.

4 CHAPTER FOUR: RESULTS – DRUG UPTAKE STUDIES IN CULTURED PRIMARY RAT HEPATOCYTES

4.1 Background

In vitro systems such as liver microsomes are well established to study various aspects of drug metabolism and predict clearance. Hepatocytes, however have the major advantage of an intact structural integrity. Several uptake transporters including Oatp, Ntcp, Oat and Oct are expressed on the basolateral membrane of hepatocytes enabling investigation of transporter-mediated uptake of drug into the hepatocyte. Primary hepatocytes are widely used to assess if drug uptake into the hepatocyte could be a rate determining step in hepatic elimination for compounds with poor permeability (Noe et al., 2007; Parker and Houston, 2008; Shimada et al., 2003). At physiological temperature, drug uptake into the hepatocyte may involve both passive and active processes whereas parallel incubations at 4°C to disable transport proteins may also be conducted to assess passive diffusion of drug into the hepatocyte.

4.2 Development and characterization of a drug uptake model using cultured primary rat hepatocytes

Primary rat hepatocytes were successfully isolated from freshly excised male Han Wistar rat livers. Routinely, the cell viability was >85%. Hepatocytes were seeded onto 24-well Collagen I coated plates and cultured for approximately 2 h until they had attached on the bottom of the wells of the culture plate. Compounds were prepared as 10 mM stock solutions in DMSO and subsequently diluted in WEM medium supplemented with 10 mM HEPES and 0.45% acetonitrile (v/v) and were pre-warmed to 37°C.

4.2.1 Time course of d_8-taurocholic acid and pitavastatin uptake in cultured primary rat hepatocyte monolayers

Cultured primary rat hepatocyte monolayers were incubated at 37°C with d_8-taurocholic acid or d_8-TCA (0.3, 1, 3 and 10 µM) an Ntcp substrate (Wolf et al., 2010) or pitavastatin (0.3, 1, 3 and 10 µM), an Oatp substrate (Imaoka et al., 2013) for up to 30 minutes. Following termination of the incubation, cell washing and lysis, the amount of drug taken up into hepatocytes expressed as pmol drug/mg hepatocyte protein was determined in cell lysates following LC-MS/MS analysis as detailed in Section 2.2.2.

At all concentrations tested, the initial uptake of d_8-TCA into cultured primary rat hepatocytes was rapid (Figure 4-1). The rate of uptake appeared to slow from 60 seconds and had reached a maximum after 600 seconds of incubation.

Figure 4-1 Time course of d_8-TCA uptake in cultured primary rat hepatocyte monolayer cultures

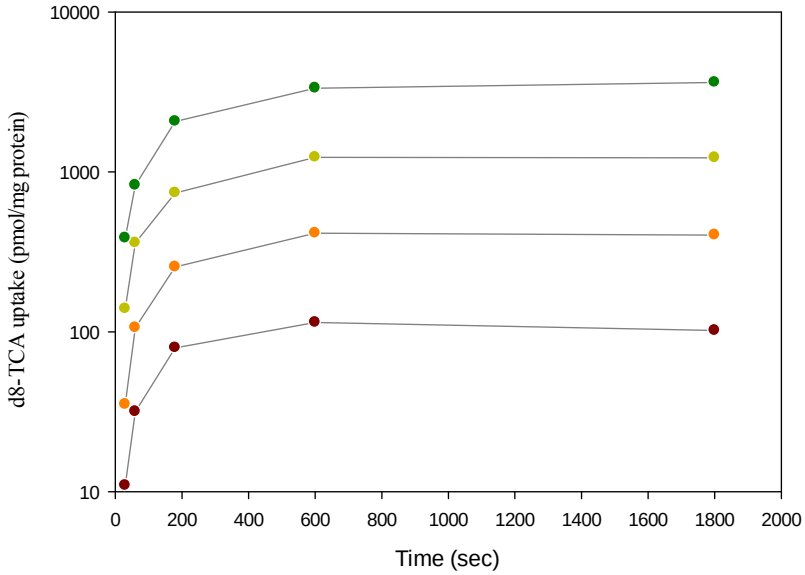

Monolayers of primary rat hepatocytes were cultured for 2 h in 24-well plates and incubated at 37°C in Williams E media containing 0.3 µM d_8-TCA (red circle), 1 µM d_8-TCA (orange circle), 3 µM d_8-TCA (yellow circle) and 10 µM d_8-TCA (green circle) for up to 1800 seconds (30, 60, 180, 600 & 1800 seconds). Each point represents 1 determinant per time point.

At all concentrations tested, the initial uptake of pitavastatin into cultured primary rat hepatocytes was rapid (Figure 4-2). The rate of uptake appeared to slow from 180 seconds and had reached a maximum after 600 seconds of incubation.

Figure 4-2 **Time course of pitavastatin uptake in cultured primary rat hepatocyte monolayer cultures**

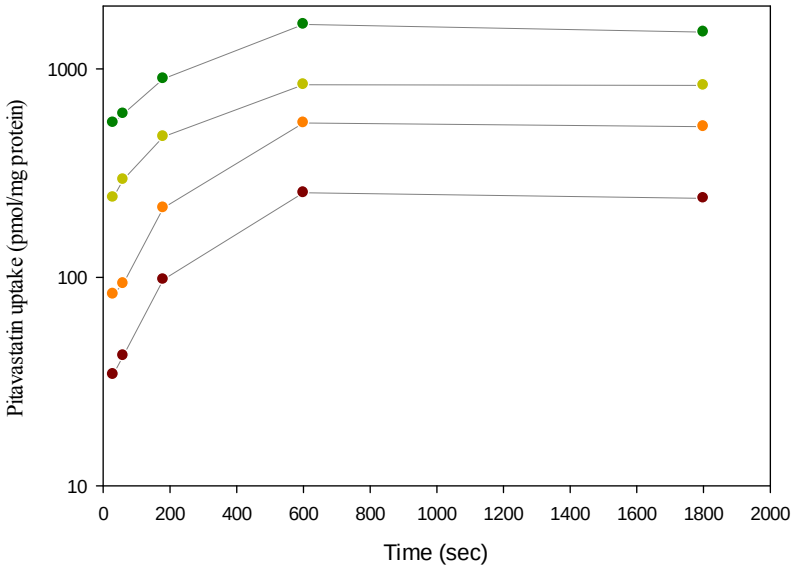

Monolayers of primary rat hepatocytes were cultured for 2 h in 24-well plates and incubated at 37°C in Williams E media containing 0.3 µM pitavastatin (red circle), 1 µM pitavastatin (orange circle), 3 µM pitavastatin (yellow circle) and 10 µM pitavastatin (green circle) for up to 1800 seconds (30, 60, 180, 600 & 1800 seconds). Each point represents 1 determinant per time point.

Based on the hepatocyte uptake data for both d_8-TCA and pitavastatin, an incubation time of 120 seconds was chosen for future drug uptake experiments as this was considered a good compromise between a technically achievable incubation time and one in which the uptake rate of either compounds had not yet reached maximum.

4.2.2 Concentration-dependence of d_8-TCA and pitavastatin in cultured primary rat hepatocyte monolayers

Cultured primary rat hepatocyte monolayers were incubated at 37°C and 4°C with 7 concentrations (0.3 to 100 µM) of either d_8-TCA or pitavastatin for 120 seconds. Following termination of the incubation, cell washing and lysis, the amount of drug taken up into hepatocytes, expressed as pmol/min/mg hepatocyte protein, was determined in cell lysates following LC-MS/MS analysis.

Following incubation of d_8-TCA in cultured primary rat hepatocytes at 37°C, the uptake velocity appeared linear to 10 µM and saturated at higher concentrations (≥ 60 µM). Following incubation of d_8-TCA in cultured primary rat hepatocytes at 4ºC, the

uptake velocity remained linear at all concentrations tested (Figure 4-3). The K_m and V_{max} for the uptake of d_8-TCA were found to be 26 ± 3.8 μM, and the maximal uptake rate, was 1435 ± 74 pmol/min/mg protein.

Figure 4-3 Concentration dependence of d_8-TCA uptake in cultured primary rat hepatocytes

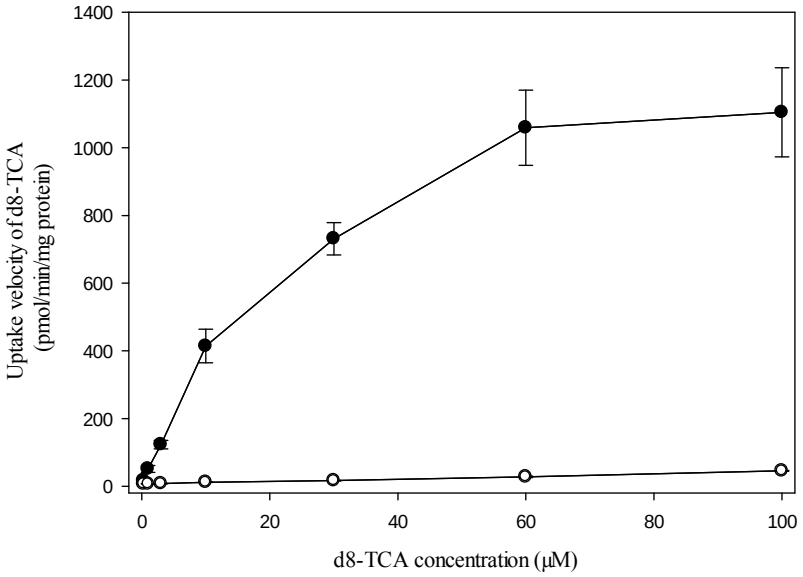

Monolayers of primary rat hepatocytes were cultured for 2 h in 24-well plates and incubated for 120 seconds with d_8-TCA at 37°C and 4°C. Closed circles represent uptake of d_8-TCA at 37°C and open circles represent uptake of d_8-TCA at 4°C (each value is the mean ± S.D. of 3 replicates.)

Following incubation of pitavastatin in cultured primary rat hepatocytes at 37°C, the uptake rate appeared linear to 10 μM and saturated at higher concentrations (≥ 60 μM Following incubation of pitavastatin in cultured primary rat hepatocytes at 4ºC, the uptake velocity remained linear at all concentrations tested (Figure 4-4). The K_m and V_{max} for the uptake of pitavastatin was 14 ± 1.2 μM and 1520 ± 36 pmol/min/mg protein respectively.

Figure 4-4 Concentration dependence of pitavastatin uptake in cultured primary rat hepatocytes

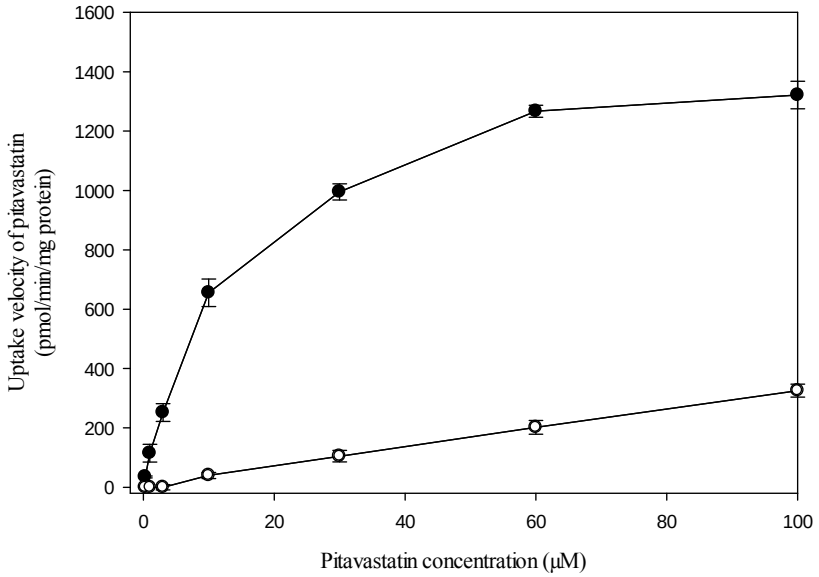

Monolayers of primary rat hepatocytes were cultured for 2 h in 24-well plates and incubated for 120 seconds with pitavastatin at 37°C and 4°C. Closed circles represent uptake of pitavastatin at 37°C and open circles represent uptake of pitavastatin at 4°C (each value is the mean ± S.D. of 3 replicates.)

4.2.3 Temperature dependence of passive uptake into cultured primary rat hepatocyte monolayers

Simple diffusion is the passive movement of solute across a membrane from a high concentration to a lower concentration until the concentration of the solute is uniform throughout and reaches equilibrium. Using primary hepatocytes, comparison of the rate of drug uptake at 37ºC and 4ºC are commonly made to distinguish active from passive drug transport processes since it is assumed that active drug transport is not functional at 4ºC. However, a potential limitation of conducting parallel control incubations at 4ºC is that membrane fluidity may decrease at lower temperatures (Frezard and Garnier-Suillerot, 1998) and permeability has been reported to be highly temperature-dependent in artificial (PAMPA) membranes and Chinese hamster ovary control cells (Poirier et al., 2008).

4.2.3.1 Effect of incubation temperature on passive diffusion of propranolol and alprenolol in cultured primary rat hepatocytes

Cultured primary rat hepatocytes were incubated at 37°C and 4°C with 7 concentrations (0.3 to 100 μM) of either propranolol or alprenolol for 120 seconds. Both

propranolol and alprenolol are known to have very high passive permeability and be highly absorbed with human oral absorption ≥ 90% (Irvine et al., 1999). Following termination of the incubation, cell washing and lysis, the amount of drug taken up into hepatocytes expressed as pmol/min/mg hepatocyte protein was determined in cell lysates following LC-MS/MS analysis (method detailed in Section 2.2.2).

The uptake velocity of propranolol at 37 and 4°C was linear and did not indicate saturation at the higher concentrations (Figure 4-5). The average fold increase in propranolol uptake at 37°C was found to be 2.5-fold higher compared to propranolol uptake at 4°C.

Figure 4-5 Effect of incubation temperature on passive uptake of propranolol in cultured primary rat hepatocytes

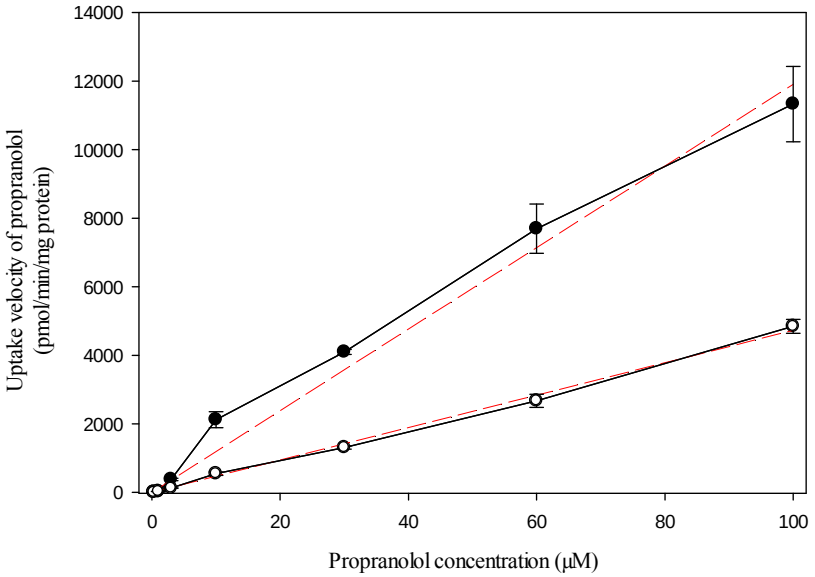

Monolayers of primary rat hepatocytes were cultured for 2 h in 24-well plates and incubated for 120 seconds with propranolol at 37°C and 4°C. Closed circles represent uptake of propranolol at 37°C and open circles represent uptake of propranolol at 4°C (each value is the mean ± S.D. of 3 replicates.) Lines of best fit (red dashed lines) revealed r^2 values > 0.98 for uptake of propranolol at both temperatures.

The uptake velocity of alprenolol at 37ºC and 4°C was linear and did not indicate saturation at the higher concentrations (Figure 4-6). The average fold increase in alprenolol uptake at 37°C was found to be 2.8-fold higher compared to alprenolol uptake at 4°C.

Figure 4-6 Effect of incubation temperature on passive uptake of alprenolol in cultured primary rat hepatocytes

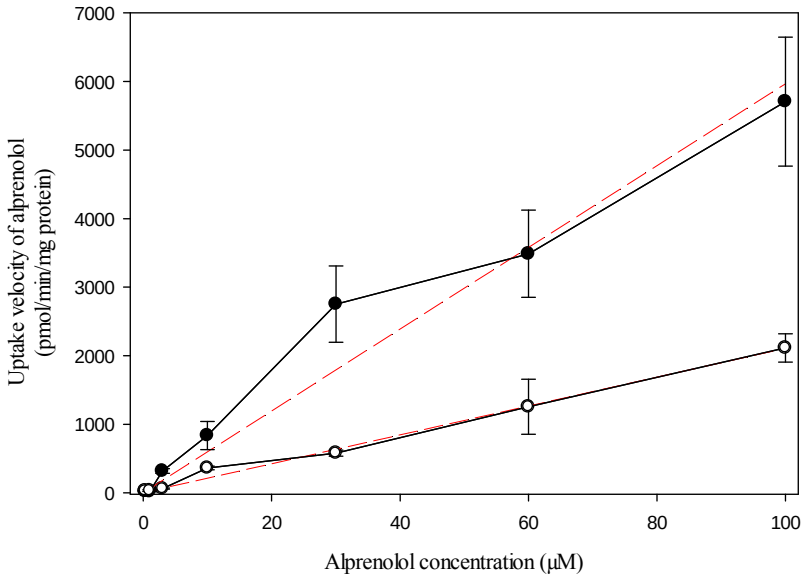

Monolayers of primary rat hepatocytes were cultured for 2 h in 24-well plates and incubated for 120 seconds with alprenolol at 37°C and 4°C. Closed and open circles represent uptake of alprenolol at 37°C and 4°C respectively (each value is the mean ± S.D. of 3 replicates.) Lines of best fit (red dashed lines) revealed r^2 values > 0.95 for uptake of alprenolol at both temperatures.

4.2.4 Cultured primary rat hepatocyte uptake assay reproducibility

The reproducibility of experimental assay runs was demonstrated by running multiple experiments with pitavastatin, a substrate of active uptake in rat hepatocytes (Shimada et al., 2003) and propranolol, a compound with very high passive permeability (Irvine et al., 1999). Cultured primary rat hepatocyte monolayers were incubated at 37°C and 4°C with 5 µM substrate for 120 seconds. Following termination of the incubation, cell washing and lysis, the amount of drug taken up into hepatocytes expressed as pmol/min/mg hepatocyte protein was determined in cell lysates following LC-MS/MS analysis. Initial uptake rates at 37°C and 4ºC, uptake rate ratios (37ºC:4ºC) and scaled total $CL_{int,upt}$ were then calculated and are presented in Table 4-1 and Table 4-2.

Table 4-1 Intra- and inter-assay variability in pitavastatin uptake in cultured primary rat hepatocytes

Experiment #	Initial uptake rate at 37ºC (pmol/min/mg protein)		Initial uptake rate at 4ºC (pmol/min/mg protein)		Uptake rate ratio (37ºC:4ºC)	Scaled total $CL_{int,upt}$ (ml/min/kg)	
	Mean	SD	Mean	SD		Mean	SD
1	330	36	20	1	17	529	57
2	251	23	14	3	18	402	37
3	279	21	21	2	30	446	34
4	504	22	21	2	24	806	36
Overall Mean	341		19		22	546	
Overall SD	113		3		6	181	
% CV	33		18		28	33	

On each experimental occasion, mean (± S.D.) pitavastatin uptake data were calculated from 3 replicates. Data from 4 individual experiments were used to calculate the overall inter-assay mean (± S.D.) and percentage coefficient of variation (%CV) values of initial uptake rates at 37ºC and 4ºC and the scaled total $CL_{int,upt}$.

Pitavastatin uptake into cultured primary rat hepatocytes was measured on 4 separate experimental occasions. Scaled total $CL_{int,upt}$ values for pitavastatin were high (>400 ml/min/kg) and uptake rates were considerably higher at 37ºC compared to 4ºC resulting in high uptake rate ratios (≥17) suggesting transport of pitavastatin into the hepatocytes involves an active uptake process. Inter-assay variability overall was modest and acceptable with percentage CV values ≤ 33.

Table 4-2 Intra- and inter-assay variability in propranolol uptake in cultured primary rat hepatocytes

Experiment #	Initial uptake rate at 37ºC (pmol/min/mg protein)		Initial uptake rate at 4ºC (pmol/min/mg protein)		Uptake rate ratio (37ºC:4ºC)	Scaled total $CL_{int,upt}$ (ml/min/kg)	
	Mean	SD	Mean	SD		Mean	SD
1	205	41	115	14	2	328	66
2	258	33	132	3	2	413	53
3	213	18	148	7	1	341	29
Overall Mean	226		132		2	361	
Overall SD	28		17		0.3	46	
% CV	13		13		15	13	

On each experimental occasion, mean (± S.D.) propranolol uptake data were calculated from 3 replicates. Data from 3 individual experiments were used to calculate the overall inter-assay mean (± SD) and percentage coefficient of variation (% CV) values of initial uptake rates at 37ºC and 4ºC and the scaled total $CL_{int,upt}$.

Propranolol uptake into cultured primary rat hepatocytes was measured on 3 separate experimental occasions. Scaled total $CL_{int,upt}$ values for propranolol were high (>300 ml/min/kg) and uptake rates were approximately 1-2-fold higher at 37ºC compared to 4ºC suggesting predominantly passive entry into the hepatocytes. Inter-assay variability overall was low with percentage CV values ≤ 15.

4.3 Measurement of drug uptake in cultured primary rat hepatocytes

Measurement of drug uptake was assessed in cultured primary rat hepatocytes for a compound set of 91 compounds comprising 77 NCEs and 14 marketed. Cultured primary rat hepatocyte were incubated at 37°C and 4°C with 5 µM compound in WEM medium supplemented with 10 mM HEPES and 0.45% acetonitrile (v/v) for 120 seconds. Following termination of the incubation, cell washing and lysis, the amount of drug taken up into hepatocytes expressed as pmol/min/mg hepatocyte protein was determined in cell lysates following LC-MS/MS analysis. Initial uptake rates at 37ºC and 4ºC, uptake rate ratios (37ºC:4ºC) and scaled total $CL_{int,upt}$ were then calculated and are presented in Table 4-3.

Table 4-3 Uptake of NCEs and marketed drugs into cultured primary rat hepatocytes

NCE# or drug name	Initial uptake rate at 37ºC (pmol/min/mg protein)		Initial uptake rate at 4ºC (pmol/min/mg protein)		Uptake rate ratio (37ºC:4ºC or 37ºC:LOQ)	Active uptake substrate	$CL_{int,upt}$ at 37°C (ml/min/kg)		$CL_{int,pas}$ at 4°C (ml/min/kg)	
	Mean	SD	Mean	SD			Mean	SD	Mean	SD
NCE 1	35	3	34	8	1.0	No	56	5	54	13
NCE 2	103	8	91	13	1.1	No	165	13	145	20
NCE 3	166	7	26	3	6.3	Yes	266	12	42	5
NCE 4	103	13	33	4	3.1	Yes	165	21	52	6
NCE 5	17	0.3	<LOQ		1.5	No	27	0	nr	
NCE 6	31	3	<LOQ		6.3	Yes	50	5	nr	
NCE 7	33	3	56	13	0.6	No	53	5	90	21
NCE 8	110	12	33	3	3.3	Yes	176	18	53	5
NCE 9	16	2	58	58	0.3	?	26	3	92	92
NCE 10	28	6	16	16	1.7	No	44	9	26	26
NCE 11	5	1	19	2	0.3	No	8	2	30	3
NCE 12	84	12	16	1	5.3	Yes	134	20	25	2
NCE 13	<LOQ		<LOQ			?	nr		nr	
NCE 14	111	8	8	1	14	Yes	177	13	13	2
NCE 15	56	2	12	1	4.8	Yes	90	3	19	2
NCE 16	50	3	22	3	2.3	No	80	5	35	5
NCE 17	28	2	17	5	1.7	No	45	3	27	8
NCE 18	164	19	25	7	6.5	Yes	262	30	40	11

NCE# or drug name	Initial uptake rate at 37ºC (pmol/min/mg protein)		Initial uptake rate at 4ºC (pmol/min/mg protein)		Uptake rate ratio (37ºC:4ºC or 37ºC:LOQ)	Active uptake substrate	$CL_{int,upt}$ at 37°C (ml/min/kg)		$CL_{int,pas}$ at 4°C (ml/min/kg)	
	Mean	SD	Mean	SD			Mean	SD	Mean	SD
NCE 19	171	10	9	1	18	Yes	274	16	15	1
NCE 20	12	2	13	1	1.4	No	19	3	21	2
NCE 21	<LOQ	0.0	<LOQ			?	nr		nr	
NCE 22	88	13	24	1	3.7	Yes	142	20	38	1
NCE 23	125	14	45	2	2.8	No	199	23	72	3
NCE 24	234	13	90	13	2.6	No	374	20	143	20
NCE 25	62	5	<LOQ		5.7	Yes	99	7	nr	
NCE 26	<LOQ		<LOQ			?	nr		nr	
NCE 27	29	4	13	3	2.3	No	47	7	21	4
NCE 28	298	16	77	4	3.9	Yes	477	26	122	7
NCE 29	22	3	36	3	0.6	No	35	5	57	5
NCE 30	252	26	49	5	5.1	Yes	403	41	79	7
NCE 31	<LOQ		<LOQ			?	nr		nr	
NCE 32	10	1	1	0.2	16	Yes	17	2	1	0
NCE 33	93	6	8	2	19	Yes	149	10	13	4
NCE 34	20	4	8	1	2.6	No	32	7	12	1
NCE 35	12	2	15	2	0.9	No	20	3	23	4
NCE 36	27	13	<LOQ		2.5	No	43	21	nr	
NCE 37	236	7	46	4	5.2	Yes	378	12	73	6
NCE 38	59	6	<LOQ		6.6	Yes	95	9	nr	

NCE# or drug name	Initial uptake rate at 37ºC (pmol/min/mg protein)		Initial uptake rate at 4ºC (pmol/min/mg protein)		Uptake rate ratio (37ºC:4ºC or 37ºC:LOQ)	Active uptake substrate	$CL_{int,upt}$ at 37°C (ml/min/kg)		$CL_{int,pas}$ at 4°C (ml/min/kg)	
	Mean	SD	Mean	SD			Mean	SD	Mean	SD
NCE 39	61	6	17	2	3.6	Yes	97	9	27	2
NCE 40	62	3	21	2	2.9	No	99	4	34	4
NCE 41	34	1	33	2	1.0	No	54	1	53	3
NCE 42	128	18	97	4	1.3	No	204	29	155	6
NCE 43	42	1	4	0.3	9.3	Yes	67	1	7	0
NCE 44	223	3	81	3	2.8	No	357	5	129	5
NCE 45	28	2	10	2	2.8	No	45	4	16	3
NCE 46	15	1	<LOQ		1.7	No	24	2	nr	
NCE 47	25	2	9	1	2.8	No	40	4	14	1
NCE 48	158	7	17	6	9.2	Yes	252	11	27	9
NCE 49	52	2	12	2	4.4	Yes	83	3	19	3
NCE 50	37	0.1	30	1	1.2	No	59	0	48	1
NCE 51	12	3	1	0.4	10	Yes	19	5	2	1
NCE 52	6	1	<LOQ		5.3	Yes	10	1	nr	
NCE 53	<LOQ		<LOQ			?	nr		nr	
NCE 54	12	1	8	0.1	11	Yes	19	1	13	0
NCE 55	15	2	<LOQ		15	Yes	24	3	nr	
NCE 56	40	6	<LOQ		4.0	Yes	64	9	nr	
NCE 57	168	14	<LOQ		17	Yes	268	23	nr	
NCE 58	12	1	1	0.4	11	Yes	19	1	2	1

NCE# or drug name	Initial uptake rate at 37ºC (pmol/min/mg protein)		Initial uptake rate at 4ºC (pmol/min/mg protein)		Uptake rate ratio (37ºC:4ºC or 37ºC:LOQ)	Active uptake substrate	$CL_{int,upt}$ at 37°C (ml/min/kg)		$CL_{int,pas}$ at 4°C (ml/min/kg)	
	Mean	SD	Mean	SD			Mean	SD	Mean	SD
NCE 59	59	1	<LOQ		5.9	Yes	95	2	nr	
NCE 60	112	15	<LOQ		11	Yes	179	24	nr	
NCE 61	48	10	<LOQ		4.8	Yes	77	16	nr	
NCE 62	71	14	58	13	1.2	No	114	22	93	21
NCE 63	8	2	4	1	2.1	No	13	3	6	2
NCE 64	61	11	<LOQ		6.1	Yes	97	18	nr	
NCE 65	211	33	8	3	25	Yes	338	52	13	4
NCE 66	265	36	<LOQ		27	Yes	424	57	nr	
NCE 67	290	15	57	4	5.1	Yes	464	25	91	7
NCE 68	42	2	<LOQ		4.2	Yes	68	3	nr	
NCE 69	52	5	18	0.4	2.9	No	84	8	29	1
NCE 70	<LOQ		<LOQ		nr	?	nr		nr	
NCE 71	24	4	8	1	2.9	No	38	6	13	1
NCE 72	27	5	7	1	3.7	Yes	43	7	12	2
NCE 73	32	7	10	2	3.2	Yes	51	11	16	4
NCE 74	26	1	8	1	3.4	Yes	42	1	13	2
NCE 75	121	3	78	9	1.6	No	194	4	125	14
NCE 76	55	6	12	1	4.5	Yes	87	10	20	2
NCE 77	37	2	<LOQ		3.7	Yes	59	3	nr	
atorvastatin	170	33	9	1	18	Yes	272	54	15	2

NCE# or drug name	Initial uptake rate at 37ºC (pmol/min/mg protein)		Initial uptake rate at 4ºC (pmol/min/mg protein)		Uptake rate ratio (37ºC:4ºC or 37ºC:LOQ)	Active uptake substrate	$CL_{int,upt}$ at 37°C (ml/min/kg)		$CL_{int,pas}$ at 4°C (ml/min/kg)	
	Mean	SD	Mean	SD			Mean	SD	Mean	SD
d8-TCA	360	34	6	0.4	58	Yes	576	54	10	1
digoxin	<LOQ		<LOQ		nr	?	nr		nr	
d-pen-enkephalin	139	11	14	3	10	Yes	222	17	22	5
erythromycin	44	6	<LOQ		4.0	Yes	70	9	nr	
fexofenadine	268	27	51	4	5.2	Yes	429	44	82	6
fluvastatin	368	20	24	1	15	Yes	589	32	39	2
methotrexate	17	2	12	1	1.4	No	27	2	19	1
pitavastatin	418	24	53	7	8.0	Yes	670	38	84	12
pravastatin	61	5	2	0.3	27	Yes	98	7	4	0.4
propranolol	258	33	132	3	2.0	No	413	53	210	5
quinidine	100	21	36	3	2.7	No	160	33	58	5
rosuvastatin	409	15	27	4	15	Yes	654	24	44	6
valsartan	133	11	3	1	39	Yes	213	18	5	1

nr: no result, <LOQ: Below analytical limit of quantification, ?: transport mechanism inconclusive

Drug uptake in cultured primary rat hepatocytes was assessed for the 77 NCEs and 14 marketed compounds. Drug uptake could not be quantified for NCEs 13, 21, 26, 31, 53 and 70 and digoxin as the amount of drug taken up into the hepatocytes at both 37 and 4ºC was less than the analytical LOQ for each of these analytes. Additionally, for many NCEs and erythromycin, the uptake into hepatocytes at 4ºC could not be quantified as the amount was less than the analytical LOQ. In such instances, a conservative approach was used to calculate the ratio of drug uptake rate by dividing the drug uptake rate at 37ºC by the LOQ for each analyte. NCEs were classed as active uptake substrates if the ratio (37ºC:4ºC or 37ºC:LOQ) of drug uptake rate into the hepatocyte was > 3 (the threshold value of 3 was defined to avoid 'active uptake substrate' assignation of compounds that show temperature dependent passive diffusion as previously defined in Section 4.2.3).

Marketed drugs previously reported in the literature to be substrates of active uptake into rat hepatocytes; statin compounds (atorvastatin, fluvastatin, pitavastatin, pravastatin and rosuvastatin), d-pen-enkephalin, erythromycin, fexofenadine, d_8-TCA and valsartan (Hoffmaster et al., 2005; Jemnitz et al., 2012; Yabe et al., 2011) all showed high uptake rate ratios in the range 8 - 58. Propranolol and quinidine, both highly permeable compounds with moderate to high initial uptake rates at 37°C (≥ 100 pmol/min/mg protein), resulted in uptake rate ratios of 2.0 and 2.7 respectively, indicating the main transport route into hepatocytes was passive diffusion. NCE 9 and NCE 11 both showed higher uptake rates into the hepatocyte at 4ºC compared to 37ºC which resulted in very low uptake rate ratios of 0.3. Both compounds are basic, completely unionized at pH7.4 and have good permeability, hence it would be anticipated that rapid equilibrium between incubation medium and intracellular compartments might be achieved mainly due to passive diffusion. To understand the processes involved which result in such low uptake rate ratios, further investigations into non-specific binding in the incubation (fu_{inc}) or assessing the contribution of passive and active efflux out of the hepatocyte at both 37ºC and 4ºC may be warranted which is out of scope in this present research.

4.3.1 Distribution of chemical class for substrates and non-substrates of active uptake into cultured primary rat hepatocytes

Following assessment of uptake into cultured primary rat hepatocytes, initial uptake rates were measurable for 71 out of 77 NCEs which were categorised as either substrates or non-substrates of active uptake based on their uptake rate ratios (> 3 or < 3 respectively). The distribution of chemical class for these NCEs is detailed in Figure 4-7.

Figure 4-7 Distribution of chemical class for substrates and non-substrates of active uptake into cultured primary rat hepatocytes

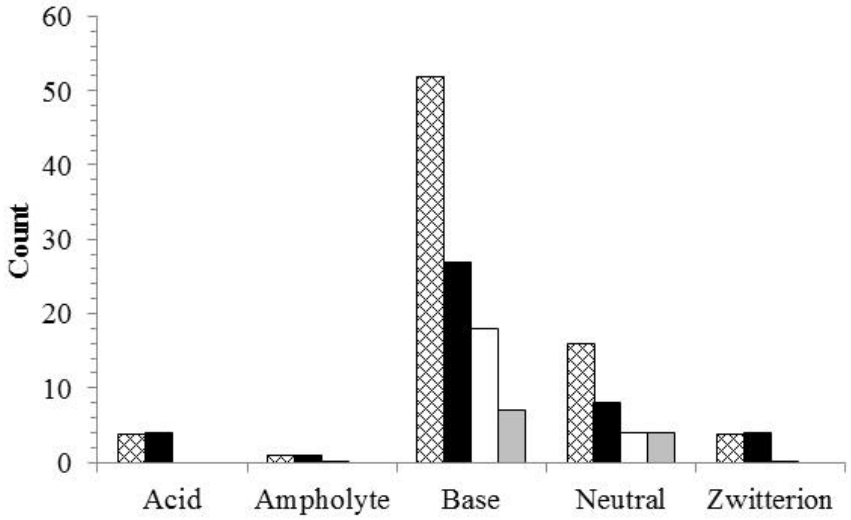

Hatched bars represent the total number of NCEs in each chemical class. Black bars represent the number of NCEs in each chemical class that were substrates of active uptake. White bars represent the number of NCEs in each chemical class that were non-substrates of active uptake. Grey bars represent the number of NCEs in each chemical class for which uptake data could not be measured.

In the NCE set, approximately half of the neutral and basic compounds were uptake substrates, whereas all acids, ampholytes and zwitterions (of which they were far fewer in the NCE set) were uptake substrates.

5 CHAPTER FIVE: RESULTS – DRUG HEPATOBILIARY EFFLUX STUDIES IN PRIMARY RAT HEPATOCYTES CULTURED IN A SANDWICH CONFIGURATION

5.1 Background

Hepatobiliary excretion is an important route of elimination from the body for many drugs and/or their metabolites and as such may impact drug exposure and efficacy (Rollins and Klaassen, 1979). Hepatocyte drug transporters play a key role in controlling intracellular drug concentrations in the hepatocyte to maintain a favourable gradient for the entry of new drugs. Uptake transporters on the sinusoidal membrane facilitate drug entry into the hepatocyte whilst several ABC efflux transporters including Bcrp, Bsep, Mrp2 and P-gp are expressed on the canalicular membrane and can facilitate the energy dependent transport of drugs from the hepatocyte into bile against an uphill concentration gradient.

Hepatocytes are highly polarized epithelial cells and their normal hepatic function is dependent on the maintenance of sinusoidal and apical membrane polarity (LeCluyse et al., 1994). Following isolation, the polarity of hepatocytes is lost which limits the utility of suspended primary hepatocytes to assess the potential for canalicular drug efflux. However, this polarity can be regenerated following culturing of hepatocytes in a sandwich configuration between layers of Collagen I or Matrigel® (Liu et al., 1999a). The sandwich cultured rat hepatocyte model allows a three-dimensional orientation, formation of bile canaliculi and proper localization of efflux transporters (Hoffmaster et al., 2004). Additionally, using this *in vitro* model, correlation between *in vitro* and *in vivo* biliary clearance in rat has been demonstrated for some drugs (Abe et al., 2008; Fukuda et al., 2008).

5.2 Development and characterisation of a drug efflux model using primary rat hepatocytes cultured in a sandwich configuration

Primary rat hepatocytes were successfully isolated and cultured from freshly excised male Han Wistar rat livers. Routinely, the cell viability was >85%. Hepatocytes were seeded into BioCoat™ plates and cultured (37°C, 95% air, 5% CO_2) for up to 96 h with medium changed daily. After approximately 24 h, the hepatocytes display basolateral surface contact with neighbouring cells (Figure 5-1).

Figure 5-1 Phase contrast images of primary rat hepatocytes cultured in BioCoat™ Matrigel® 6-well plates for 24 h

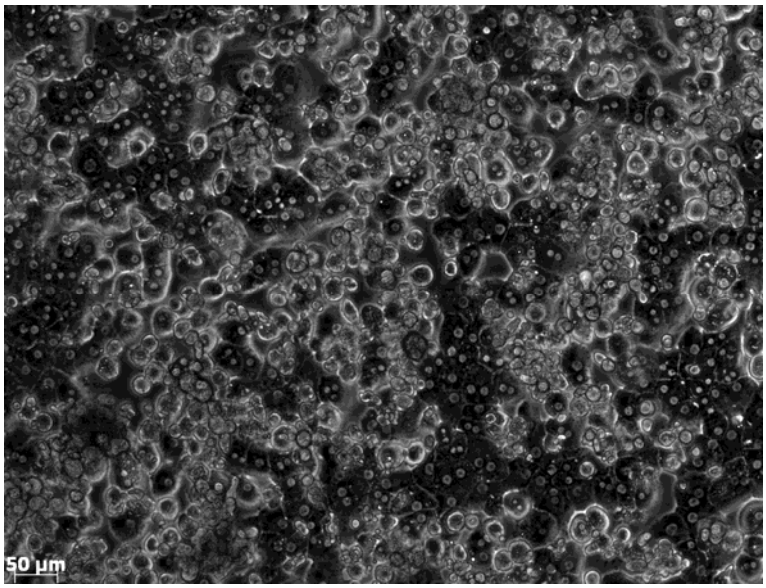

Phase contrast images of primary rat hepatocytes seeded at 1 million cells/well in BioCoat™ Matrigel® 6-well plates and cultured for 24 h (37°C, 95% air, 5% CO_2). Magnification 10x.

After approximately 96 h of total culture time, the sandwich cultured rat hepatocytes exhibited liver-like cell morphology and formed bile canalicular networks as indicated by the bright, white belt-like structures between cell tight junctions (Figure 5-2).

Figure 5-2 Phase contrast images of sandwich cultured rat hepatocytes cultured in BioCoat™ Matrigel® 6-well plates for 96 h

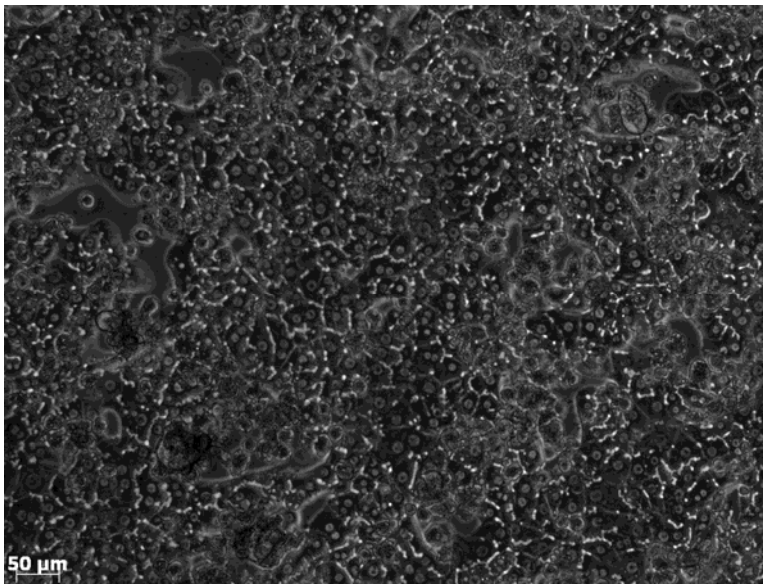

Phase contrast images of primary rat hepatocytes seeded at 1 million cells/well in BioCoat™ Matrigel® 6-well plates and cultured in a sandwich configuration for 96 h (37°C, 95% air, 5% CO_2). Magnification 10x.

5.2.1 Assessment of viability of primary rat hepatocytes maintained in culture for up to 96 h

Primary rat hepatocytes were seeded onto BioCoat™ Matrigel® 6-well plates at a cell density of 1 million cells per well and cultured for 2, 24, 48, 72 and 96 h (48, 72 and 96 h cultures were overlaid with Matrigel® at 24 h post seeding). Cell viability was assessed using an MTS cell proliferation assay and compared to viability of freshly isolated rat hepatocytes. The data are presented in Figure 5-3.

Figure 5-3 Assessment of viability of primary rat hepatocytes maintained in culture up to 96 h

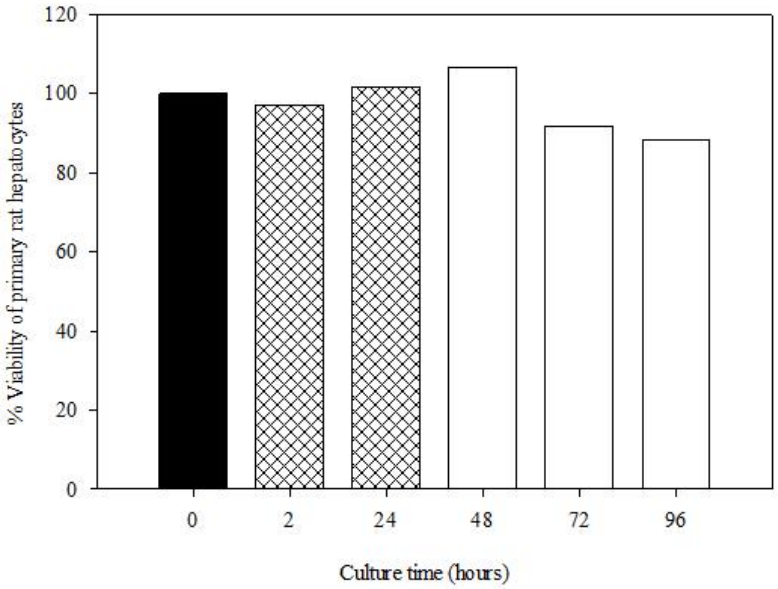

Primary rat hepatocytes were seeded at 1 million cells/well in BioCoat™ Matrigel® 6-well plates and cultured for up to 24 h as a monolayer or overlaid with Matrigel® at 24 h to form a Matrigel® sandwich configuration and cultured for a further 72 h with medium changed daily (37°C, 95% air, 5% CO_2). The filled bar represents the viability of primary rat hepatocytes freshly isolated in suspension at 0 hour. Hatched bars represent the viability of primary rat hepatocytes cultured as a monolayer for 2 and 24 h. Open bars represent the viability of primary rat hepatocytes primary rat hepatocytes cultured in a sandwich configuration for 48, 72 and 96 h (each value is the mean of 2 replicates and each replicate was within 30% of each other.)

Cell viability studies using an MTS assay revealed that primary rat hepatocytes maintained in monolayer culture for up to 24 h or in a sandwich configuration for up to 96 h retain good viability compared to freshly isolated primary rat hepatocytes.

5.2.2 Determination of functional biliary excretion in sandwich cultured rat hepatocytes

The excretory Mrp2 activity of primary rat hepatocytes cultured in a sandwich configuration was examined using Carboxydichlorofluorescein diacetate (CDFDA) which readily permeates into hepatocytes and is hydrolysed to form fluorescent carboxydichlorofluorescein (CDF) which is transported into bile canaliculi via Mrp2 (Liu et al., 1999b). Primary rat hepatocytes were seeded onto BioCoat™ Matrigel® 6-well plates at a cell density of 1 million cells per well and cultured for 96 h in a sandwich

configuration. The sandwich cultured rat hepatocytes were pre-treated with either standard or Ca^{2+}/Mg^{2+}-free buffer and then incubated with CDFDA (10μM) in standard buffer for 10 minutes at 37°C. Following cell washing, CDF was imaged using fluorescence microscopy. Representative fluorescent images are presented in Figure 5-4 and Figure 5-5.

Figure 5-4 Fluorescent images of CDF inside sandwich cultured rat hepatocytes cultured in BioCoat™ Matrigel® 6-well plates for 96 h following pre-treatment with Ca^{2+}/Mg^{2+}-free buffer

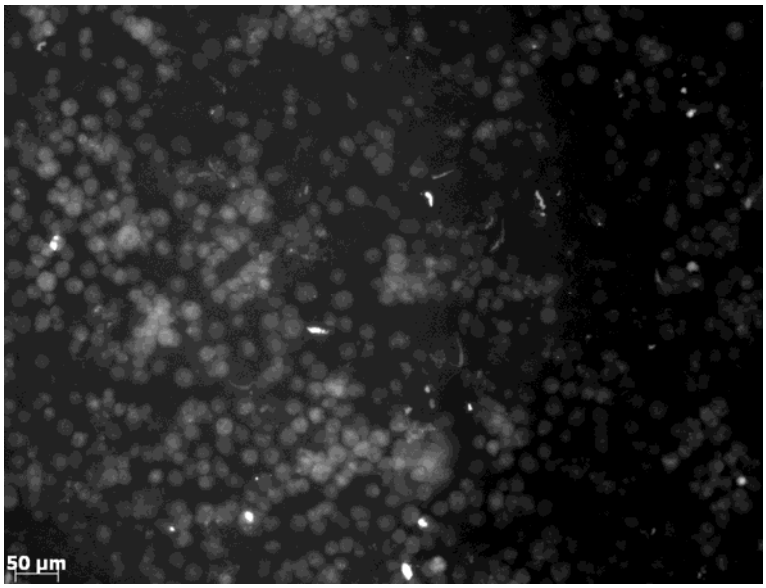

Fluorescent images of sandwich cultured rat hepatocytes following pre-treatment with Ca^{2+}/Mg^{2+}-free buffer and incubation with 10μM CDFDA. Magnification 10x.

After pre-treatment of sandwich cultured rat hepatocytes with Ca^{2+}/Mg^{2+}-free buffer followed by incubation with 10 μM CDFDA in standard buffer, fluorescent CDF is localized within the hepatocytes, indicating the lack of functional bile canalicular network.

Figure 5-5 Fluorescent images of CDF inside sandwich cultured rat hepatocytes cultured in BioCoat™ Matrigel® 6-well plates for 96 h following pre-treatment with standard buffer

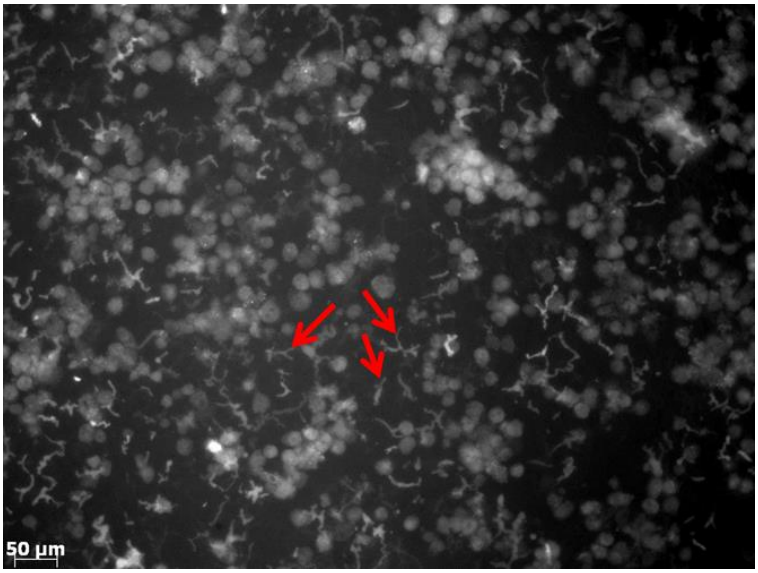

Fluorescent images of sandwich cultured rat hepatocytes following pre-treatment with standard buffer and incubation with 10µM CDFDA. Red arrows indicate fluorescent CDF localised within bile canaliculi. Magnification 10x.

After pre-treatment of sandwich cultured rat hepatocytes with standard buffer followed by incubation with 10 µM CDFDA in standard buffer, fluorescent CDF is localized within the hepatocyte and bile canaliculi (indicated by red arrows), demonstrating the functional activity of a bile canalicular network and Mrp2 in the canalicular membrane.

CDF biliary transport was also quantified. Prior to fluorescence analysis, cell lysates were disrupted using Covaris adaptive focused acoustic technology and samples were then centrifuged at approximately 2600 x g for 15 minutes at 4°C. The supernatants were analysed using a Tecan Safire II fluorescent plate reader (excitation: 504nm; emission 529nm, gain 52) to quantify CDF present in hepatocytes with intact bile canaliculi (standard buffer) or cells with disrupted bile canaliculi (Ca^{2+}/Mg^{2+}-free buffer). Biliary efflux index (BEI %) and predicted biliary clearance of CDF were then calculated as described in Section 2.7.7.

When sandwich cultured rat hepatocytes are exposed to a Ca^{2+}-free environment, efflux transporters on the bile canaliculi may still function to actively extrude drug from hepatocytes, but the bile canaliculi membrane loses its integrity and the contents of the

bile canaliculi will be released into the extracellular medium. Accumulation of hydrolysed CDF was higher following pre-treatment of sandwich cultured rat hepatocytes with standard buffer compared to Ca^{2+}/Mg^{2+}-free buffer (Figure 5-6). The biliary excretion index was estimated as the difference in accumulation of CDF in sandwich cultured rat hepatocytes pre-incubated in standard buffer and in Ca^{2+}/Mg^{2+}-free buffer. More than 50% of the hydrolysed CDF inside hepatocytes was excreted into the bile canaliculi yielding a BEI of 53% which compared favourably to a reference BEI value of 28% for CDF in sandwich cultured rat hepatocytes found in the literature (Turncliff et al., 2006) demonstrating the functional activity of a bile canalicular network and Mrp2 in this sandwich cultured rat hepatocyte model.

Figure 5-6 Accumulation of hydrolysed carboxydichlorfluorescein in sandwich cultured rat hepatocytes

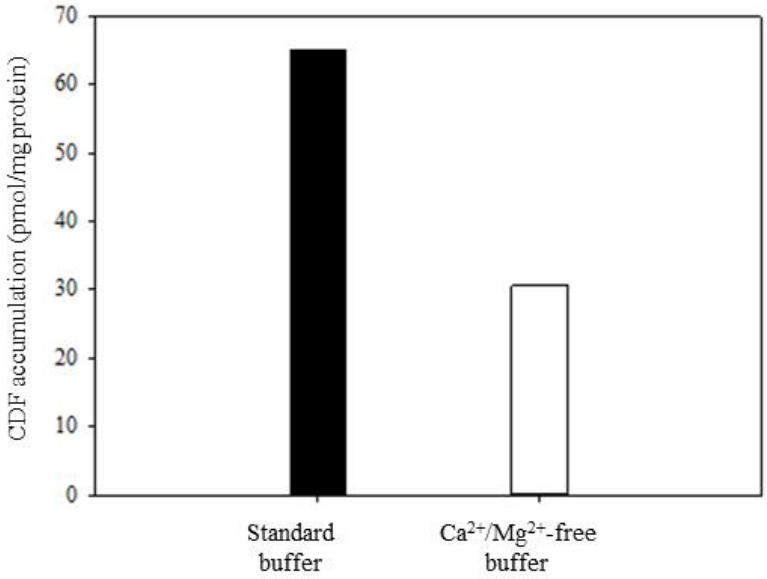

Sandwich cultured rat hepatocytes were seeded at 1 million cells/well in BioCoat™ Matrigel® 6-well plates and cultured in a sandwich configuration for up to 96 h prior to incubation with 10 µM CDFDA at 37°C for 10 minutes. Filled and open bars represent accumulation of hydrolysed CDF in cells and bile or cells only following pre-treatment with either standard or Ca^{2+}/Mg^{2+}-free buffer respectively at 37°C (each value is the mean of 2 replicates and each replicate was within 10% of each other).

5.2.3 Optimisation of cell culture conditions for sandwich cultured rat hepatocytes

As bile canalicular efflux may be the rate limiting step in the biliary excretion of drugs, the influence of cell seeding density, incubation time, substrate concentration and extracellular matrix coating of BioCoat™ plates on the functioning of the sandwich cultured rat

hepatocyte model was investigated using probe substrates of biliary efflux [^{3}H]taurocholic acid (TCA), [^{3}H]digoxin, [^{3}H][D-pen2,5]encephalin ([^{3}H]DPDPE) and rosuvastatin. Primary rat hepatocytes were seeded onto BioCoat™ plates and cultured for 96 h in a sandwich configuration. Sandwich cultured rat hepatocyte monolayers were pre-treated with either standard buffer or Ca^{2+}/Mg^{2+}-free buffer for 10 minutes at 37°C prior to incubation at 37°C with compound prepared in standard buffer for 10 minutes. Following termination of the incubation, cell washing and lysis, the amount of drug accumulation in cells expressed as pmol drug/mg hepatocyte protein with disrupted bile canaliculi (cells pre-treated with Ca^{2+}/Mg^{2+}-free buffer) or cells with intact bile canaliculi (cells pre-treated with standard buffer) was determined in cell lysates following LC-MS/MS analysis. Biliary efflux index (BEI %) and predicted biliary clearance were then calculated.

5.2.3.1 Influence of cell seeding density on transport of [^{3}H]TCA in sandwich cultured rat hepatocytes

Primary rat hepatocytes were seeded onto BioCoat™ Matrigel® 6-well plates at three different densities of 1, 1.5 and 2 million cells per well. Following a Matrigel® overlay at 24 h, cells were cultured for a further 72 h in a sandwich configuration with medium changed daily. Sandwich cultured rat hepatocytes were pre-treated with either standard or Ca^{2+}/Mg^{2+}-free buffer followed by a 10 minute incubation with 1 µM [^{3}H]TCA which is a substrate of the Ntcp uptake transporter on the sinusoidal membrane and the Bsep efflux transporter on the apical bile canalicular membrane of rat hepatocytes (Marion et al., 2007). The incubation was terminated by cell washing and lysis and the amount of [^{3}H]TCA remaining in the cell lysates was assessed by liquid scintillation analysis. Accumulation, biliary excretion index and predicted biliary clearance of [^{3}H]TCA were then calculated and the data are presented in Figure 5-7.

Figure 5-7 Influence of cell seeding density on the transport of [^{3}H]TCA in sandwich cultured rat hepatocytes

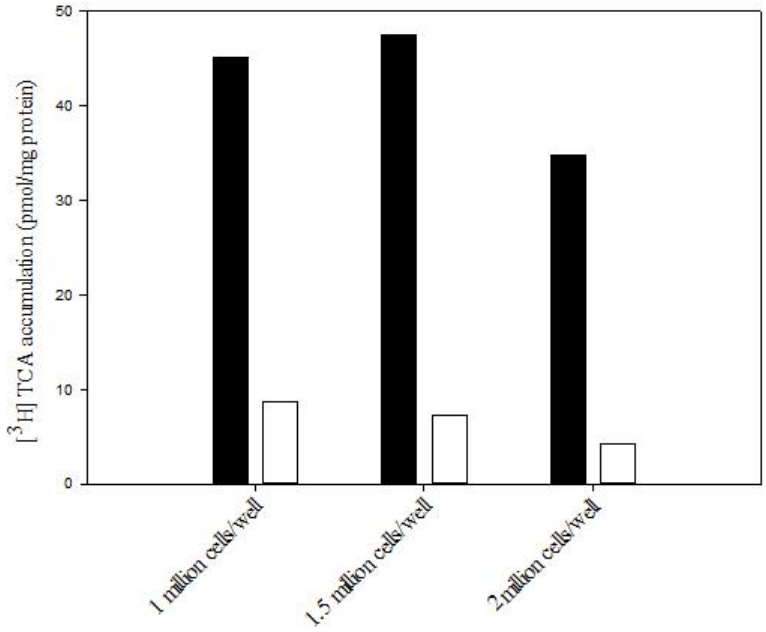

	1 million cells/well	1.5 million cells/well	2 million cells/well
BEI %	81	84	87
Predicted CL_b (ml/min/kg)	12	18	11

Sandwich cultured rat hepatocytes were seeded at 1, 1.5 and 2 million cells/well in BioCoat™ Matrigel® 6-well plates and cultured in a sandwich configuration for up to 96 h prior to incubation with 1 μM [^{3}H]TCA at 37°C for 10 minutes. Filled bars represent accumulation of [^{3}H]TCA following pre-treatment with standard buffer and open bars represent accumulation of [^{3}H]TCA following pre-treatment with Ca^{2+}/Mg^{2+}-free buffer at 37°C (each value is the mean of 2 replicates and each replicate was within 30% of each other). BEI and predicted CL_b determined at each cell density concentration are presented below the corresponding cell seeding density in the bar graph.

Cell density studies in sandwich cultured rat hepatocytes revealed that accumulation, BEI and CL_b values for [^{3}H]TCA remained comparable when primary rat hepatocytes were seeded at cell densities between 1 and 2 million cell/well. A final cell density concentration of 1 million cells/well was chosen for future studies as cell monolayers at this density formed the most uniform cell network across the entire culture when viewed under a light microscope (data not shown).

5.2.3.2 Influence of incubation time and dosing concentration on the accumulation and biliary excretion of [^{3}H]TCA in sandwich cultured rat hepatocytes

Primary rat hepatocytes were seeded onto BioCoat™ Matrigel® 6-well plates at 1 million cells per well. Following a Matrigel® overlay at 24 h, cells were cultured for a further 72 h in a sandwich configuration with medium changed daily. Sandwich cultured rat hepatocytes were pre-treated with either standard or Ca^{2+}/Mg^{2+}-free buffer followed by incubation for up to 20 minutes with [^{3}H]TCA either at 1 or 10 μM. Incubations were terminated by cell washing and lysis and the amount of [^{3}H]TCA remaining in the cell lysates was assessed by liquid scintillation analysis.

At concentrations of 1 and 10 μM [^{3}H]TCA, accumulation in standard and Ca^{2+}/Mg^{2+}-free buffer pre-treated sandwich cultured rat hepatocytes was time dependent, increasing approximately linearly up to 10 minutes, whereas at longer incubation times, accumulation appeared non-linear (Figure 5-8). Accumulation of [^{3}H]TCA in standard and Ca^{2+}/Mg^{2+}-free buffer pre-treated sandwich cultured rat hepatocytes was also concentration dependent and on average between 5- and 7-fold higher at 10 μM [^{3}H]TCA compared to 1 μM [^{3}H]TCA. For linearity reasons, a final incubation time of 10 minutes was chosen for future studies. In contrast, BEI and predicted CL_b values were comparable throughout (Table 5-1).

Figure 5-8 **Time dependence of cellular accumulation and biliary excretion of [^{3}H] TCA in sandwich cultured rat hepatocytes**

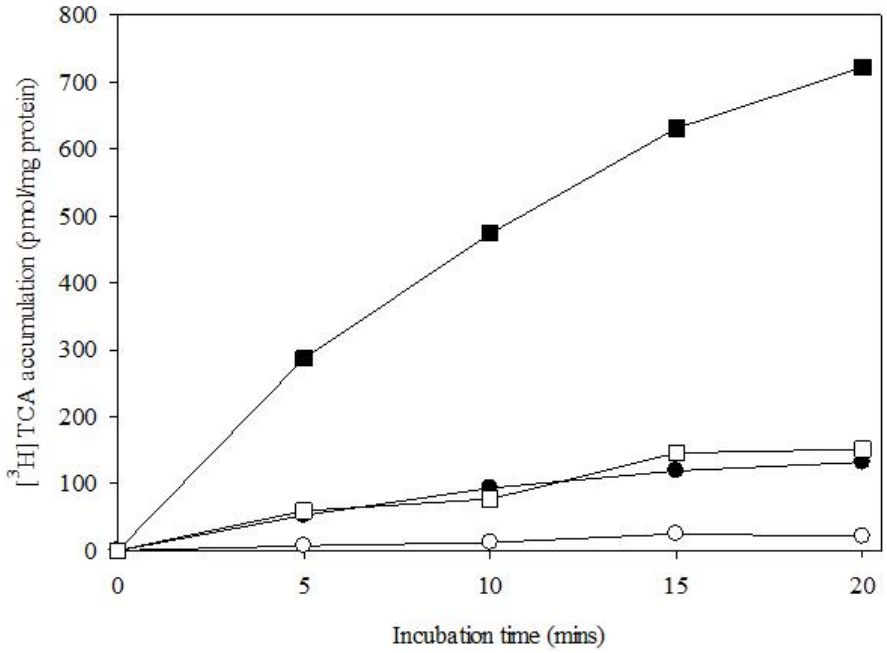

Sandwich cultured rat hepatocytes were seeded at 1 million cells/well in BioCoat™ Matrigel® 6-well plates and cultured in a sandwich configuration for up to 96 h prior to incubation with [^{3}H]TCA for up to 20 minutes. Filled circles represent accumulation of 1 µM [^{3}H]TCA following pre-treatment with standard buffer and open circles represent accumulation of 1 µM [^{3}H]TCA following pre-treatment with Ca^{2+}/Mg^{2+}-free buffer (singlicate value per timepoint). Filled squares represent accumulation of 10 µM [^{3}H]TCA following pre-treatment with standard buffer and open squares represent accumulation of 10 µM [^{3}H]TCA following pre-treatment with Ca^{2+}/Mg^{2+}-free buffer (singlicate value per timepoint).

Table 5-1 **Calculated biliary efflux index and predicted biliary clearance data for [^{3}H]TCA in sandwich cultured rat hepatocytes**

	1 µM [^{3}H]TCA Incubation time (mins)				10 µM [^{3}H]TCA Incubation time (mins)			
	5	10	15	20	5	10	15	20
BEI %	87	87	79	84	79	84	71	79
Predicted CL_b (ml/min/kg)	26	25	22	21	19	18	16	15

5.2.3.3 Influence of extracellular matrix plate type on the accumulation and biliary excretion of drugs in sandwich cultured rat hepatocytes

Primary rat hepatocytes were seeded onto either BioCoat™ Matrigel® or BioCoat™ Collagen I 6-well plates at 1 million cells per well. Following a Matrigel® overlay at 24 h, cells were cultured for a further 72 h in a sandwich configuration with medium changed daily. Four drugs; [^{3}H]TCA, [^{3}H]digoxin, [^{3}H][D-pen2,5]encephalin ([^{3}H]DPDPE) and rosuvastatin were chosen as model substrates of efflux transporters Bsep, P-gp, Mrp2, and Bcrp on the apical bile canalicular membrane of rat hepatocytes. Sandwich cultured rat hepatocytes were pre-treated with either standard or Ca^{2+}/Mg^{2+}-free buffer followed by incubation for 10 minutes with drug in standard buffer. Incubations were terminated by cell washing and lysis and the amount of drug remaining in the cell lysates was assessed by liquid scintillation analysis for triturated substrates or LC-MS/MS for unlabelled substrates.

Accumulation of 1 μM [^{3}H]TCA in standard and Ca^{2+}/Mg^{2+}-free buffer pre-treated sandwich cultured rat hepatocytes was approximately 2-fold higher with the BioCoat™ Collagen I plate compared to BioCoat™ Matrigel® plate however the BEI values remained comparable (Figure 5-9). Whereas, accumulation and BEI values for 10 μM [^{3}H]digoxin were all comparable in both BioCoat™ Matrigel® and BioCoat™ Collagen I plates. This data suggests extracellular matrix coating of BioCoat™ plates influenced the functioning of the sandwich cultured rat hepatocyte model using TCA (as accumulation was higher in the BioCoat™ Collagen I plate) but not for digoxin.

Figure 5-9 **Influence of extracellular matrix type on the accumulation and biliary excretion of [^{3}H]TCA and [^{3}H]Digoxin in sandwich cultured rat hepatocytes**

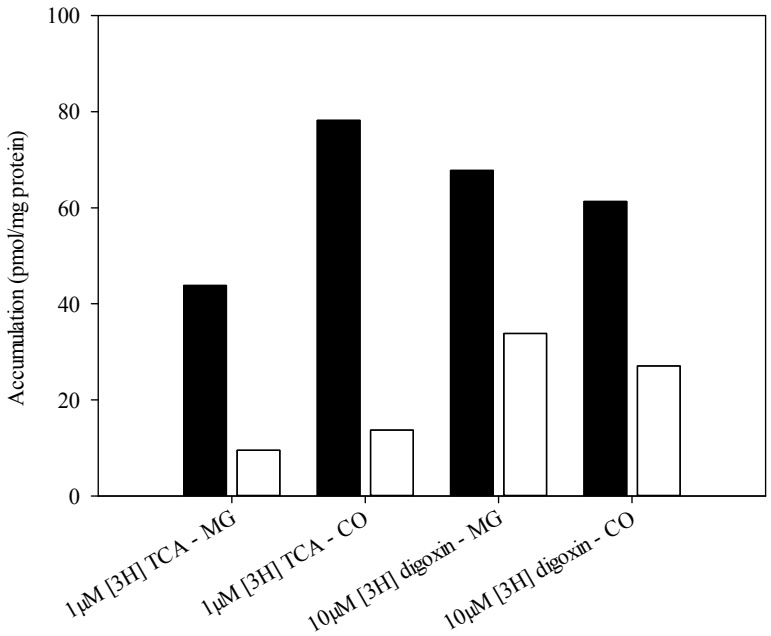

BEI %	78	82	50	56

Sandwich cultured rat hepatocytes were seeded at 1 million cells/well in either BioCoat™ Matrigel® (MG) or BioCoat™ Collagen I (CO) 6-well plates and cultured in a sandwich configuration for up to 96 h prior to prior to pre-treatment with either standard or Ca^{2+}/Mg^{2+}-free buffer at 37°C and then incubation with either 1 μM [^{3}H]TCA or 10 μM [^{3}H]Digoxin at 37°C for 10 minutes. Filled bars represent accumulation of drug following pre-treatment with standard buffer at 37°C and open bars represent accumulation of drug following pre-treatment with Ca^{2+}/Mg^{2+}-free buffer at 37°C (each value is the mean of 2 replicates and each replicate was within 20% of each other). Calculated BEI determined for both extracellular matrix types are presented below the figure.

Accumulation and BEI values for either 15 μM [^{3}H]DPDPE or 1 μM rosuvastatin were comparable in both BioCoat™ Matrigel® and Collagen I plates types suggesting extracellular matrix coating of BioCoat™ plates did not have an obvious impact on the functioning of the sandwich cultured rat hepatocyte model for either of these model substrates (Figure 5-10).

Figure 5-10 Influence of extracellular matrix type on the accumulation and biliary excretion of [^{3}H]DPDPE and rosuvastatin in sandwich culture rat hepatocytes

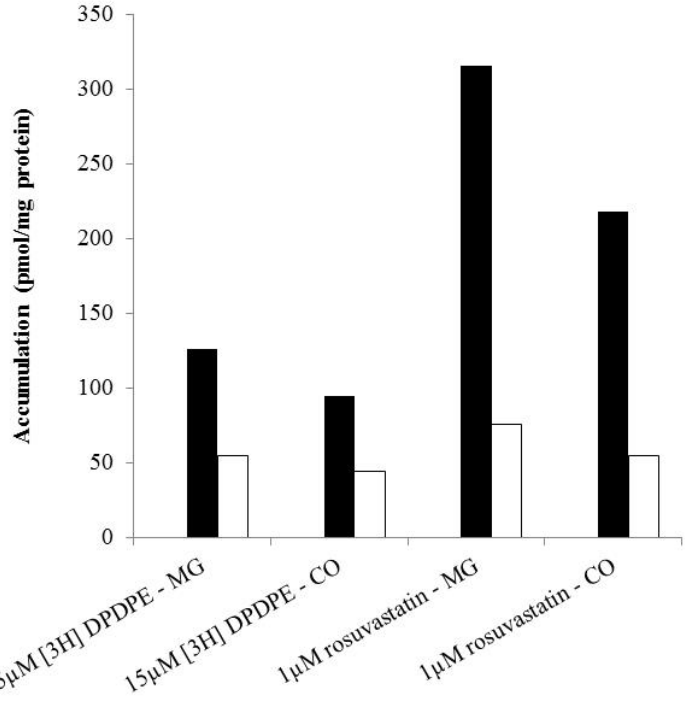

BEI %	56	54	76	81

Sandwich cultured rat hepatocytes were seeded at 1 million cells/well in either BioCoat™ Matrigel® (MG) or BioCoat™ Collagen I (CO) 6-well plates and cultured in a sandwich configuration for up to 96 h prior to prior to pre-treatment with either standard or Ca^{2+}/Mg^{2+}-free buffer at 37°C and then incubation with either 15 µM [^{3}H]DPDPE or 1 µM rosuvastatin at 37°C for 10 minutes. Filled bars represent accumulation of drug following pre-treatment with standard buffer at 37°C and open bars represent accumulation of drug following pre-treatment with Ca^{2+}/Mg^{2+}-free buffer at 37°C (each value is the mean of 2 replicates and each replicate was within 30% of each other.) Calculated BEI determined for both extracellular matrix types are presented below the figure.

In summary, extracellular matrix coating of BioCoat™ plates appeared to have very little overall impact on the accumulation and biliary efflux of digoxin, DPDPE or rosuvastatin. However, since accumulation of TCA was 2-fold higher in the BioCoat™ Collagen I plate (compared to Matrigel® coating) this plate type was selected for all future studies.

5.2.3.4 Assessment of biliary efflux of drugs in sandwich cultured rat hepatocytes cultured in different plate-well formats

It was highly desirable to increase the assay throughput as the 6-well plate format was low throughput, enabling assessment of only 1 compound per plate (in duplicate). BioCoat™ Collagen I plates with a higher well format (12- and 24-well) were investigated. An experiment was first conducted using different cell seeding densities in 12 and 24-well plate formats and compared to 6-well data using 1 million cells/well. Primary rat hepatocytes were cultured in a sandwich configuration. On day 4 (96 h post seeding) wells at all cell densities were visually inspected using a light microscope to check cell morphology and for formation of bile canaliculi. The sandwich cultured rat hepatocyte monolayers were then pre-treated with standard buffer or Ca^{2+}/Mg^{2+}-free buffer for 10 minutes at 37°C prior to incubation at 37°C with 10 µM [^{3}H]TCA in standard buffer for 10 minutes. Following termination of the incubation, cell washing and lysis, the amount of drug accumulation in cells only (cells pre-treated with Ca^{2+}/Mg^{2+}-free buffer) or cells plus intact bile canaliculi (cells pre-treated with standard buffer) expressed as pmol drug/mg hepatocyte protein was determined in cell lysates following liquid scintillation counting. Biliary efflux index (BEI %), scaled intrinsic biliary clearance and predicted biliary clearance were then calculated.

Table 5-2 Influence of cell seeding density on the accumulation, biliary efflux index and predicted CL_b of 10 µM [^{3}H]TCA in 12- and 24-well BioCoat™ Collagen I plates

Wells/plate format (surface area, cm^2)	Cell seeding density (million cells/well)	*Accumulation (pmol/mg protein) Mean	S.D.	BEI % Mean	S.D.	Predicted CL_b (ml/min/kg)
12 (3.8)	0.1	nr		nr		nr
	0.25	151	20	73	4	13
	0.5	34	8	36	17	1
24 (2)	0.05	nr		nr		nr
	0.075	141	8	57	2	6
	0.1	174	9	75	1	16
6 (9.6)	*1*	*157*	*4*	*86*	*0.3*	*14*

nr: no result, *cellular accumulation determined in standard buffer

Influence of cell seeding density on the accumulation, BEI and predicted CLb of 10 µM [^{3}H]TCA in sandwich cultured rat hepatocytes in 12 and 24-well BioCoat™ Collagen I plates (each value is the mean ± SD of 3 replicates.) For comparison, data from 6-well BioCoat™ Collagen I plates in italics was added.

Following visual inspection under a light microscope, sandwich cultured rat hepatocytes seeded at cell densities of 0.1 million cells/well in the 12-well plate format and 0.05 million cells/well in the 24 well plate format did not form integral cell monolayers and there was little evidence of bile canalicular network formation. Accumulation, biliary efflux and CL_b data for 10 µM [^{3}H]TCA in sandwich cultured rat hepatocytes at all other cell densities was assessed (Table 5-2). Sandwich cultured rat hepatocytes seeded at 0.25 million cells/well in 12-well plates and at 0.1 million cells/well in 24-well plates correlated best with 6-well plate data (1 million cells/well) and these cell densities were deemed optimal for the respective well plate format.

An additional experiment was conducted to compare the transport of drugs in sandwich cultured rat hepatocytes in 6-, 12- and 24-well plate formats. Primary rat hepatocytes were seeded onto BioCoat™ Collagen I 6-, 12- and 24-well plates at 1, 0.25 and 0.1 million cells per well respectively. Following a Matrigel® overlay at 24 h, cells were cultured for a further 72 h in a sandwich configuration with medium changed daily. Sandwich cultured rat hepatocytes were then pre-treated with either standard or Ca^{2+}/Mg^{2+}-free buffer followed by incubation for 10 minutes with either 5 µM d_8-TCA, pitavastatin or rosuvastatin in standard buffer. Incubations were terminated by cell

washing and lysis and the amount of drug remaining in the cell lysates was assessed by LC-MS/MS. Accumulation, BEI and CL_b values were then calculated and the data are presented in Table 5-3.

Table 5-3 Comparison of accumulation, biliary efflux index and predicted biliary clearance of drugs in 6, 12- and 24-well BioCoat™ Collagen I plates

Compound (5 µM)	Wells/ plate	*Accumulation (pmol/mg protein)		BEI %		Predicted CL_b (ml/min/kg)
		Mean	S.D.	Mean	S.D.	
d_8-TCA	6	134	5	84	0.6	11
	12	151	20	73	4	13
	24	174	9	75	1	16
(Wolf et al., 2008)	*6*	*nr*		*86*	*4*	*19*
pitavastatin	6	155	30	31	12	26
	12	469	68	38	8	14
	24	35	6	49	9	16
(Abe et al., 2008)	*6*	*nr*		*20*	*1*	*19*
rosuvastatin	6	31	6	56	7	21
	12	34	3	59	3	22
	24	15	2	68	3	16
(Abe et al., 2008)	*6*	*nr*		*45*	*6*	*21*

nr: no (reference) result, *cellular accumulation determined in standard buffer

Comparison of accumulation, BEI and predicted CL_b of 5µM d_8-TCA, pitavastatin or rosuvastatin in sandwich cultured rat hepatocytes in 6-, 12- and 24-well BioCoat™ Collagen I plates (each value is the mean ± SD of 3 replicates.) For comparison, 6-well plate reference data from literature was added in italics.

5.2.3.5 Comparison of *in vitro* and *in vivo* biliary clearance data of marketed drugs

Following optimisation of the sandwich cultured rat hepatocyte model, biliary transport was measured for 14 marketed drugs and the data compared to reference *in vitro* and *in vivo* data in the literature to check model functionality and predictivity. Primary rat hepatocytes were seeded onto BioCoat™ Collagen I 12-well plates at 0.25 million cells per well. Following a Matrigel® overlay at 24 h, cells were cultured for a further 72 h in a sandwich configuration with medium changed daily. Sandwich cultured rat hepatocytes were pre-treated with standard buffer or Ca^{2+}/Mg^{2+}-free buffer for 10 minutes at 37°C prior to incubation at 37°C with 5µM drug in standard buffer for 10 minutes. Following termination of the incubation, cell washing and lysis, the amount of drug accumulation in cells only (cells pre-treated with Ca^{2+}/Mg^{2+}-free buffer) or cells plus intact bile canaliculi (cells pre-treated with standard buffer) expressed as pmol drug/mg hepatocyte protein was

determined in cell lysates following LC-MS/MS analysis. Biliary efflux index (BEI %), $CL_{int,sec}$ and predicted biliary clearance were then calculated. Data are presented in Table 5-4 and Figure 5-11 to Figure 5-13.

Table 5-4 Assessment of BEI and predicted biliary clearance in sandwich cultured rat hepatocytes for a range of marketed drugs and comparison to reference *in vitro* and *in vivo* rat biliary excretion data

Compound	In house data			Reference data				Reference
	In vitro: BEI %		*In vitro:* Predicted CL_b (ml/min/kg)	*In vitro:* BEI %		*In vivo:* % Dose excreted in bile	*In vivo:* CL_b (ml/min/kg)	
	Mean	S.D.		Mean	S.D.			
atorvastatin	31	3	11	nr		nr	nr	nr
d_8-TCA	73	4	13	86	4	91	26	(Akashi et al., 2006; Watkins and Dykstra, 1987; Wolf et al., 2008)
digoxin	58	6	3	50	3	31	3	(Song et al., 1999; Wolf et al., 2008)
DPDPE	50	12	5	42	12	80	19	(Chen and Pollack, 1997; Liu et al., 1999a)
erythromycin	74	8	4	nr		30	17	(Lam et al., 2006; Zou et al., 2013)
fexofenadine	40	10	4	nr		40	11	(Tahara et al., 2005)
fluvastatin	38	6	27	nr		20	4	(Lindahl et al., 2004; Watanabe et al., 2010; Zou et al., 2013)
methotrexate	55	7	1	55	18	72	12	(Liu et al., 1999a; Masuda et al., 1997)
pitavastatin	38	8	12	20	1	73	5	(Abe et al., 2008; Hirano et al., 2005)
pravastatin	75	0.4	7	43	2	78	28	(Abe et al., 2008; Sasaki et al., 2004)
propranolol	0		0	nr		nr	nr	nr
quinidine	46	9	27	nr		nr	nr	nr
rosuvastatin	57	1	3	45	6	74	24	(Abe et al., 2008; Fukuda et al., 2008; Kitamura et al., 2008)
valsartan	39	6	7	16	11	70	13	(Fukuda et al., 2008; Yamashiro et al., 2006)

nr: no (reference) result.

Reference observed biliary clearance data in rat was identified for 11 of the 14 marketed drugs and compared to predicted biliary clearance data generated in this thesis (Table 5-4 and Figure 5-11). Five out of the eleven marketed drugs resulted in >3-fold under prediction of observed biliary clearance whereas one drug, fluvastatin, resulted in >3-fold over-prediction. The correlation of *in vitro* and *in vivo* data were poor with a resultant r^2 value was 0.14.

Figure 5-11 Prediction of biliary clearance for marketed drugs using sandwich cultured rat hepatocytes

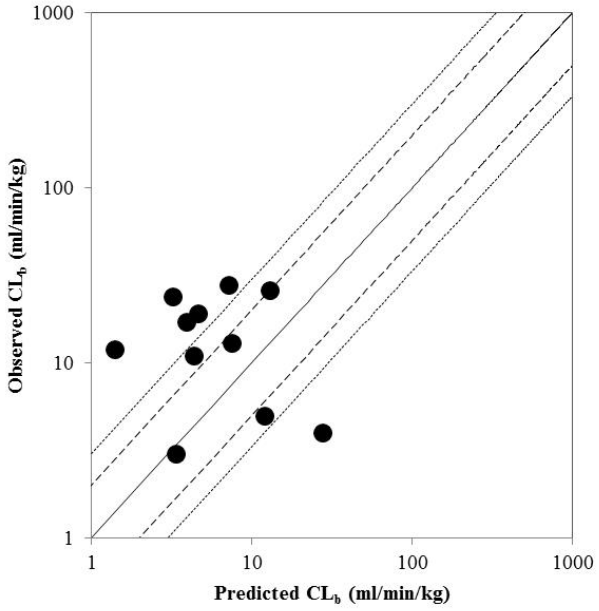

Prediction of biliary clearance using sandwich cultured rat hepatocytes for 11 marketed drugs. The solid black line indicates the line of unity and the black dashed and dotted lines represent 2-fold and 3-fold deviation of the line of unity respectively.

Reference observed percent dose excreted in bile in rat was identified for 11 out of the 14 marketed drugs and compared to BEI data generated in this thesis (Table 5-4 and Figure 5-12). *In vitro* BEI data compared favourably with observed percentage dose excreted in bile. Ten compounds indicated *in vitro* BEI values that were within 2-fold of observed values. Erythromycin was the exception, the *in vitro* BEI was 2.5 fold greater than observed. Whilst *in vitro* BEI data in general compares well with *in vivo* data, overall the distribution of biliary efflux data is uneven with all the data at the high end of the log scale and the resultant r^2 value was 0.31.

Figure 5-12 Comparison of *in vitro* and *in vivo* biliary efflux index of marketed drugs using sandwich cultured rat hepatocytes

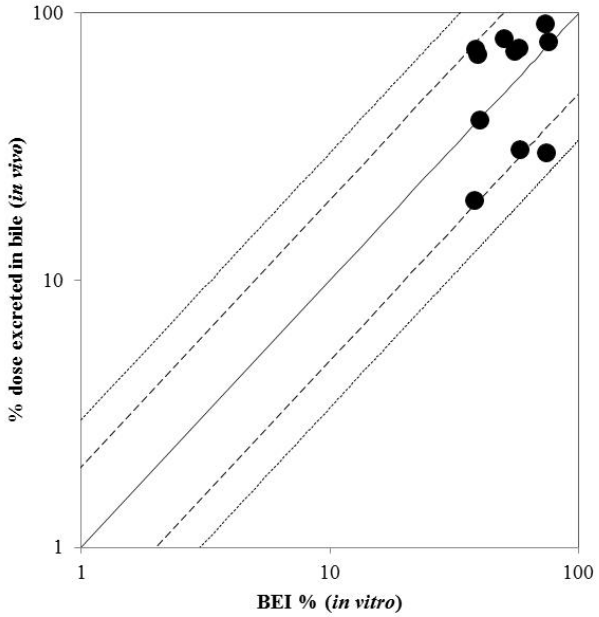

Comparison of *in vitro* BEI generated in sandwich cultured rat hepatocytes with observed percent dose excreted in bile in rat. The solid black line indicates the line of unity and black dashed and dotted lines represent 2-fold and 3-fold deviation of the line of unity respectively.

Reference BEI data in sandwich cultured rat hepatocytes was identified for 8 out of the 14 marketed drugs and compared to BEI data generated in this thesis (Table 5-4 and Figure 5-13). Seven compounds indicated *in vitro* BEI values that were within 2-fold of reference BEI values. Valsartan was the exception as in-house BEI data was 2.4-fold higher than reference data. Although the distribution of data is uneven with all the data at the high end of the log scale, the resultant r^2 value was 0.61 suggesting a modest to good correlation of BEI data and that the in-house biliary efflux model is functional.

Figure 5-13 Comparison of in-house and reference biliary excretion index of marketed drugs using sandwich cultured rat hepatocytes

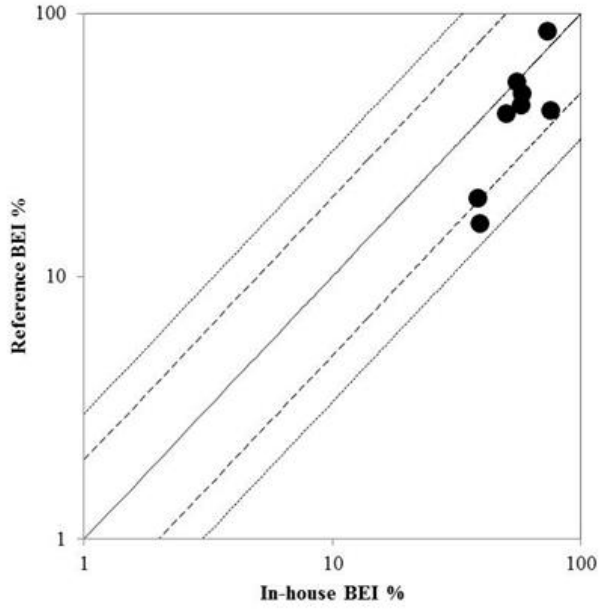

Comparison of in-house and reference *in vitro* BEI generated in sandwich cultured rat hepatocytes. The solid black line indicates the line of unity and the black dashed and dotted lines represent 2-fold and 3-fold deviation of the line of unity respectively.

Table 5-5 Statistical data comparing the accuracy of in-house CL_b predictions and biliary efflux index with observed values in rat

Predicted values	Predicted CL_b	BEI
% Outside 2-fold	82	9
% Outside 3-fold	55	0
n	11	11
Bias	0.56	0.97
rmse	0.62	0.22
afe	4.2	1.7

n: sample number, *afe*: average fold error, *rmse*: root mean squared prediction error

The statistical comparisons of these predictions are summarized in Table 5-5. The correlation of predicted versus observed CL_b clearly indicates a high incidence of under prediction with sandwich cultured rat hepatocytes. Whilst the data set is small, >50% predicted CL_b values fell outside 3-fold error of observed values. This suggests that predicted CL_b from the sandwich cultured rat hepatocyte model is not a reliable estimate of biliary clearance in rat. In contrast, the biliary excretion index appears to be predictive

of observed percentage dose excreted in bile in rat. All BEI data fell within 3-fold of observed values and this is consistent with the bias observed (Bias close to 1). In comparison to predicted CL_b, the precision of biliary excretion predictions was improved as indicated by lower *rmse* and *afe* values.

In summary, *in vitro* BEI data generated using sandwich cultured rat hepatocytes appears to be a reliable parameter for assessment of biliary elimination of unchanged drug.

5.2.3.6 Sandwich cultured rat hepatocyte model assay reproducibility

The reproducibility of experimental assay runs was demonstrated by running multiple experiments with either d_8-TCA and pitavastatin, substrates of active biliary uptake and efflux (Abe et al., 2008; Wolf et al., 2008) or propranolol, a compound with very high passive permeability (Irvine et al., 1999). Primary rat hepatocytes were seeded onto BioCoat™ Collagen I 12-well plates at 0.25 million cells per well. Following a Matrigel® overlay at 24 h, cells were cultured for a further 72 h in a sandwich configuration with medium changed daily. Sandwich cultured rat hepatocytes were pre-treated with standard buffer or Ca^{2+}/Mg^{2+}-free buffer for 10 minutes at 37°C prior to incubation at 37°C with 5µM drug in standard buffer for 10 minutes. Following termination of the incubation, cell washing and lysis, the amount of drug accumulation in cells only (cells pre-treated with Ca^{2+}/Mg^{2+}-free buffer) or cells plus intact bile canaliculi (cells pre-treated with standard buffer) expressed as pmol drug/mg hepatocyte protein was determined in cell lysates following LC-MS/MS analysis. Biliary efflux index (BEI %), scaled intrinsic biliary clearance and predicted biliary clearance were then calculated. Data are presented in Table 5-6, Table 5-7 and Table 5-8.

Table 5-6 **Intra- and inter-assay variability in d_8-TCA accumulation and biliary efflux in primary rat hepatocytes cultured in a sandwich configuration**

Experiment #	*Accumulation (pmol/mg protein)		BEI %		$CL_{int,sec}$ (ml/min/kg)		Predicted CL_b (ml/min/kg)
	Mean	S.D.	Mean	S.D.	Mean	S.D.	
1	151	20	73	4	19	3	13
2	87	11	83	2	11	2	9
3	80	14	84	3	10	2	8
Overall Mean	106		80		14		10
Overall S.D.	39		6		5		3
% CV	37		8		35		25

* accumulation determined in standard buffer

On each experimental occasion, mean (± S.D.) d_8-TCA cellular accumulation, BEI, $CL_{int,sec}$ and predicted CL_b data were calculated from 3 replicates. Data from 3 individual experiments were used to calculate the overall inter-assay mean (± SD) and percent coefficient of variation (% CV) values for d_8-TCA accumulation, BEI, scaled CL_b and predicted CL_b data.

Within each experiment, standard deviation of mean accumulation, BEI and $CL_{int,sec}$ values for d_8-TCA were low. Data from 3 individual experiments were used to calculate the overall mean (± SD) and percent coefficient of variation (% CV) of values. Inter-assay variability for BEI was low with percent CV ≤ 10%, whereas inter-assay variability of accumulation, $CL_{int,sec}$ and predicted CL_b data was higher with percent CV at 37%, 35% and 25% respectively.

Table 5-7 **Intra- and inter-assay variability in pitavastatin accumulation and biliary efflux in primary rat hepatocytes cultured in a sandwich configuration**

Experiment #	*Accumulation (pmol/mg protein)		BEI %		$CL_{int,sec}$ (ml/min/kg)		Predicted CL_b (ml/min/kg)
	Mean	S.D.	Mean	S.D.	Mean	S.D.	
1	469	68	38	8	17	6	12
2	470	10	40	1	19	1	13
3	404	59	46	2	26	2	16
Overall Mean	448		41		21		14
Overall S.D.	37		4		5		2
% CV	8		10		22		14

*accumulation determined in standard buffer

On each experimental occasion, mean (± S.D.) pitavastatin cellular accumulation, BEI, $CL_{int,sec}$ and predicted CL_b data were calculated from 3 replicates. Data from 3 individual experiments were used to calculate the overall inter-assay mean (± SD) and percent coefficient of variation (% CV) values for pitavastatin accumulation, BEI, $CL_{int,sec}$ and predicted CL_b data.

Within each experiment, standard deviation of mean accumulation, BEI and $CL_{int,sec}$ and predicted CL_b values were low to modest. Data from 3 individual experiments were used to calculate the overall mean (± SD) and percent CV values and the data indicates a modest to good inter-assay variability for accumulation, BEI, $CL_{int,sec}$ and predicted CL_b with percent CV values $\leq$ 22%.

Table 5-8 Intra- and inter-assay variability in propranolol accumulation and biliary efflux in primary rat hepatocytes cultured in a sandwich configuration

Experiment #	*Accumulation (pmol/mg protein)		BEI %		$CL_{int,sec}$ (ml/min/kg)		Predicted CL_b (ml/min/kg)
	Mean	S.D.	Mean	S.D.	Mean	S.D.	
1	4909	195	nr		nr		nr
2	9727	227	nr		nr		nr
3	7933	143	nr		nr		nr
Overall Mean	7523		nr		nr		nr
Overall S.D.	2435		nr		nr		nr
% CV	32		nr		nr		nr

nr: no result, *accumulation determined in standard buffer

On each experimental occasion, mean (± S.D.) propranolol accumulation was calculated from 3 replicates. Data from 3 individual experiments were used to calculate the overall inter-assay mean (± S.D.) and percent coefficient of variation (% CV) values for propranolol accumulation data.

Propranolol was not excreted into bile canaliculi in sandwich cultured rat hepatocytes. Accumulation was high which reflects the high passive permeability of propranolol. Within each experiment, standard deviation of mean cellular accumulation was low. Data from 3 individual experiments were used to calculate the overall mean (± SD) and percent CV of accumulation and the data indicates a modest inter-assay reproducibility (CV 32%).

5.3 Measurement of biliary efflux of NCEs and marketed drugs in sandwich cultured rat hepatocytes.

The biliary efflux of 91 compounds comprising 77 NCEs and 14 marketed drugs was assessed in sandwich cultured rat hepatocytes and data are presented in Table 5-9. Primary rat hepatocytes were seeded onto BioCoat™ Collagen I 12-well plates at 0.25 million cells per well. Following a Matrigel® overlay at 24 h, cells were cultured for a further 72 h in a sandwich configuration with medium changed daily. Sandwich cultured rat hepatocytes were pre-treated with standard buffer or Ca^{2+}/Mg^{2+}-free buffer for 10 minutes at 37°C prior to incubation at 37°C with 5µM drug in standard buffer for 10 minutes. Following termination of the incubation, cell washing and lysis, the amount of drug accumulation in cells only (cells pre-treated with Ca^{2+}/Mg^{2+}-free buffer) or cells plus intact bile canaliculi (cells pre-treated with standard buffer) expressed as pmol drug/mg hepatocyte protein was

determined in cell lysates following LC-MS/MS analysis (method detailed in Section 2.2.2). Biliary efflux index (BEI %), $CL_{int,sec}$ and predicted CL_b were then calculated. Drugs were classed as active efflux substrates if the BEI was ≥ 10% (the threshold value of 10% was defined to avoid 'active efflux substrate' assignation to non-substrates).

Table 5-9 Measurement of biliary efflux and biliary clearance of NCEs and marketed drugs in sandwich cultured rat hepatocytes

NCE# or drug name	BEI %		Active efflux substrate	$CL_{int,sec}$ (ml/min/kg)		Predicted CL_b (ml/min/kg)
	Mean	S.D.		Mean	S.D.	
NCE 1	nr (low MB)		?	nr	nr	nr
NCE 2	0	-	No	nr	nr	nr
NCE 3	45	5	Yes	20	13	13
NCE 4	57	12	Yes	3	2	3
NCE 5	nr (low MB)		?	nr	nr	nr
NCE 6	nr (low MB)		?	nr	nr	nr
NCE 7	0	-	No	-	-	-
NCE 8	20	7	Yes	179	33	33
NCE 9	0	-	No	nr	nr	nr
NCE 10	6	3	No	1	1	1
NCE 11	nr (low MB)		?	nr	nr	nr
NCE 12	0	-	No	-	-	-
NCE 13	nr (high NSB)		?	nr	nr	nr
NCE 14	28	2	Yes	12	10	9
NCE 15	0	-	No	nr	nr	nr
NCE 16	0	-	No	nr	nr	nr
NCE 17	24	4	Yes	2	4	2
NCE 18	27	5	Yes	4	4	4
NCE 19	46	0.2	Yes	8	13	7
NCE 20	0	-	No	nr	nr	nr
NCE 21	nr (<LOQ)		?	nr	nr	nr
NCE 22	0	-	No	nr	nr	nr
NCE 23	5	0.1	No	5	4	4
NCE 24	7	2	No	20	13	13
NCE 25	78	7	Yes	10	8	8
NCE 26	76	6	Yes	2	4	2
NCE 27	47	3	Yes	4	4	4
NCE 28	23	4	Yes	174	33	33
NCE 29	0	-	No	nr	nr	nr
NCE 30	18	5	Yes	77	26	26
NCE 31	64	4	Yes	127	30	30

NCE# or drug name	BEI %		Active efflux substrate	$CL_{int,sec}$ (ml/min/kg)		Predicted CL_b (ml/min/kg)
	Mean	S.D.		Mean	S.D.	
NCE 32	nr (high NSB)		?	nr	nr	nr
NCE 33	nr (high NSB)		?	nr	nr	nr
NCE 34	84	1	Yes	5	9	4
NCE 35	0	-	No	nr	nr	nr
NCE 36	nr (high NSB)		?	nr	nr	nr
NCE 37	14	6	Yes	72	26	26
NCE 38	30	4	Yes	62	24	24
NCE 39	47	1	Yes	6	5	5
NCE 40	0	-	No	nr	nr	nr
NCE 41	0	-	No	nr	nr	nr
NCE 42	0	-	No	nr	nr	nr
NCE 43	29	6	Yes	70	25	25
NCE 44	0	-	No	nr	nr	nr
NCE 45	0	-	No	nr	nr	nr
NCE 46	13	2	Yes	3	3	3
NCE 47	50	5	Yes	16	11	11
NCE 48	22	3	Yes	145	31	31
NCE 49	38	1	Yes	23	15	15
NCE 50	30	11	Yes	11	9	9
NCE 51	0	-	No	nr	nr	nr
NCE 52	0	-	No	nr	nr	nr
NCE 53	0	-	No	nr	nr	nr
NCE 54	40	1	Yes	315	35	35
NCE 55	24	3	Yes	4	3	4
NCE 56	94	0.3	Yes	10	8	8
NCE 57	44	3	Yes	50	22	22
NCE 58	41	6	Yes	17	12	12
NCE 59	66	0.3	Yes	7	6	6
NCE 60	34	1	Yes	27	16	16
NCE 61	33	5	Yes	15	11	11
NCE 62	nr (low MB)		?	nr	nr	nr
NCE 63	35	4	Yes	15	11	11
NCE 64	35	5	Yes	2	2	2
NCE 65	42	1	Yes	6	6	5
NCE 66	36	8	Yes	11	9	9
NCE 67	12	4	Yes	11	9	9
NCE 68	39	4	Yes	167	32	32
NCE 69	58	6	Yes	9	7	7
NCE 70	nr.(<LOQ)		?	nr	nr	nr

NCE# or drug name	BEI %		Active efflux substrate	$CL_{int,sec}$ (ml/min/kg)		Predicted CL_b
	Mean	S.D.		Mean	S.D.	(ml/min/kg)
NCE 71	35	1	Yes	14	1	11
NCE 72	39	6	Yes	7	2	6
NCE 73	67	3	Yes	12	2	9
NCE 74	78	1	Yes	9	1	7
NCE 75	26	6	Yes	53	16	23
NCE 76	56	6	Yes	32	8	18
NCE 77	0	-	No	nr	nr	nr
atorvastatin	31	3	Yes	16	2	11
d_8-TCA	83	2	Yes	19	3	9
digoxin	58	6	Yes	4	1	3
d-pen-enkephalin	50	12	Yes	5	3	5
erythromycin	74	8	Yes	4	2	4
fexofenadine	40	10	Yes	5	2	4
fluvastatin	38	6	Yes	87	25	27
methotrexate	55	7	Yes	1	0.4	1
pitavastatin	38	8	Yes	17	6	12
pravastatin	75	0.4	Yes	4	0.1	7
propranolol	0	0	No	nr	nr	nr
quinidine	46	9	Yes	79	29	27
rosuvastatin	57	1	Yes	3	0.3	3
valsartan	39	6	Yes	9	2	7

nr: no result, MB: mass balance low, NSB: non-specific binding high, <LOQ: Below analytical limit of quantification, ?: transport mechanism inconclusive.

Biliary efflux in sandwich cultured rat hepatocytes was assessed for 77 NCE compounds and 14 marketed drugs. *In vitro* biliary efflux (BEI %) and biliary clearance (scaled and predicted CL_b) data was measurable for 66 NCE compounds which were categorized as active efflux substrates when the BEI was > 10%. Recovery or mass balance of drug was measured and biliary efflux data reported when mass balance was ≥ 50%. For NCEs 1, 5, 6, 11 and 62, poor mass balance of drug in the assay prevented accurate assessment of *in vitro* biliary efflux. NCEs 1, 5, 11 and 62 were lipophilic (cLogP > 3) and the poor mass balance was likely a result of high metabolic instability (half-lives were ≤ 7 minutes following incubation in primary rat hepatocyte suspensions). NCE 6, whilst modestly stable in primary rat hepatocyte suspension incubations (half-life 37 minutes), is very lipophilic (cLogP 5) with low aqueous solubility (<0.004 mM) and these physicochemical properties may have contributed to the low mass balance for NCE

6. For NCEs 21 and 70, the accumulation of drug in the hepatocyte and bile canaliculi could not be quantified as the amount was less than the analytical LOQ. For NCEs 13, 32, 33 and 36, high non-specific binding in the control well (collagen/Matrigel® sandwich without cells) was observed and subtraction of drug non-specifically bound from the amount of drug accumulated in cells plus bile (standard buffer) or cells (Ca^{2+}/Mg^{2+}-free buffer), resulted in a negative value and biliary efflux could not be quantified.

5.3.1 Distribution of chemical class for substrates and non-substrates of active efflux in sandwich cultured rat hepatocytes.

Following assessment of biliary efflux in sandwich cultured rat hepatocytes, efflux data was measured for 66 out of 77 NCEs which were categorized as active efflux substrates when the BEI was > 10%. The distribution of chemical class for these NCEs is detailed in Figure 5-14.

Figure 5-14 Distribution of chemical class for substrates and non-substrates of active efflux in sandwich cultured rat hepatocytes

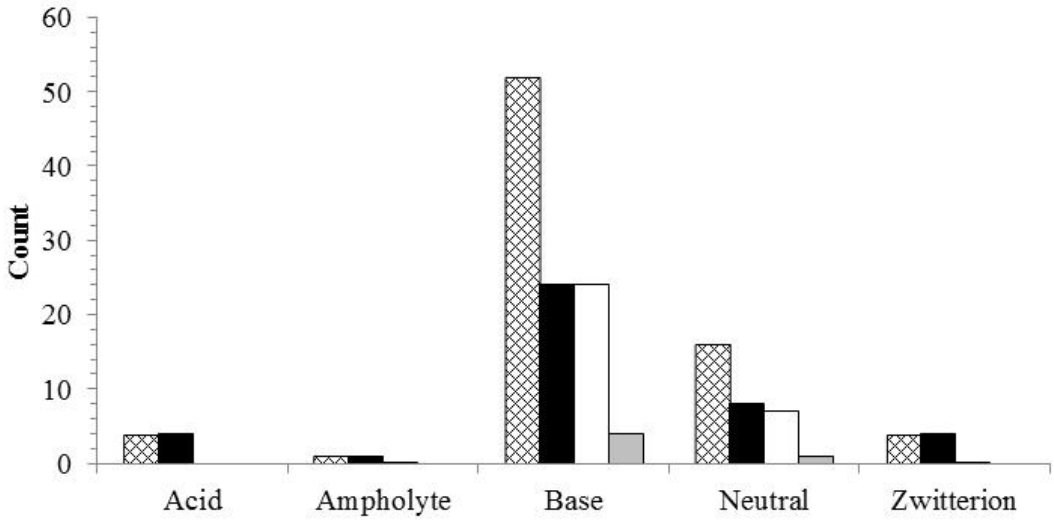

Hatched bars represent the total number of NCEs in each chemical class. Black bars represent the number of NCEs in each chemical class that were substrates of biliary efflux. White bars represent the number of NCEs in each chemical class that were non-substrates of biliary efflux. Grey bars represent the number of NCEs in each chemical class for which biliary efflux data could not be measured.

In the NCE set, approximately half of the neutral and basic compounds were efflux substrates, whereas all acids, ampholytes and zwitterions (of which they were far fewer in the NCE set) were efflux substrates.

6 CHAPTER SIX: RESULTS – SINGLE AND MULTIPLE PATHWAY IVIVE OF HEPATIC CLEARANCE INVOLVING ACTIVE TRANSPORT

6.1 Single pathway IVIVE of hepatic clearance involving active uptake

For the NCE set, uptake in cultured primary rat hepatocytes was measured at 37°C and 4°C and 41 out of the 77 NCEs were defined as substrates of active uptake (37°C:4°C uptake ratios >3). For these substrates of active uptake, a single pathway analysis of predicted clearance from metabolic intrinsic clearance ($CL_{int,met}$) in rat liver microsomes or total uptake intrinsic clearance ($CL_{int,upt}$) from cultured primary rat hepatocytes was compared with observed rat blood clearance (Figure 6-1).

Figure 6-1 Single pathway IVIVE analysis: Prediction of rat clearance for substrates of active uptake

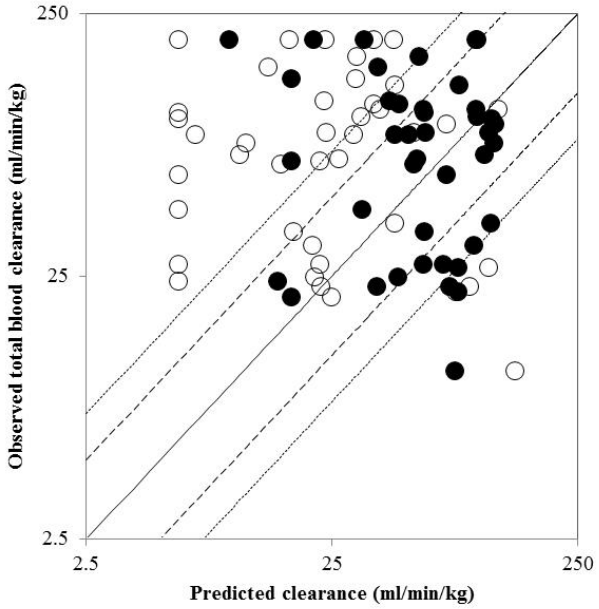

Prediction of rat clearance for substrates of active uptake (n=41). Open circles represent predicted clearance calculated from scaled $CL_{int,met}$ in rat liver microsomes. Filled circles represent predicted clearance calculated from scaled $CL_{int,upt}$ in cultured primary rat hepatocytes. The solid black line represents the line of unity and black dashed and dotted lines indicate 2-fold and 3-fold of unity respectively.

The statistical comparisons of these predictions are summarized in Table 6-1. In general, clearance appears to be better predicted from $CL_{int,upt}$ compared to $CL_{int,met}$ and there was a lower percentage of compounds falling outside 2-fold and 3-fold error of

observed which was consistent with the bias observed and the improved precision (lower *rmse* and *afe*). These data suggest uptake is a determinant factor in hepatic elimination and accounting for $CL_{int,upt}$ improved the clearance prediction, however the *afe* of the predictions was 2.9 indicating only modest precision of clearance predictions using this parameter. For some of the substrates of uptake, IVIVC disconnects still remain which suggest limitations with either the method (to accurately measure $CL_{int,upt}$) or with the IVIVE model (use of $CL_{int,upt}$ as a single parameter from which to predict clearance).

Table 6-1 Statistical data comparing the accuracy of clearance predictions for substrates of active uptake.

Clearance prediction	Predicted clearance model	
	$CL_{int,met}$	Total $CL_{int,upt}$
% Outside 2-fold	78	46
% Outside 3-fold	66	27
n	41	41
Bias	0.34	0.80
rmse	0.72	0.46
afe	5.2	2.9

n: sample number, *afe*: average fold error, *rmse*: root mean squared prediction error

6.2 Single pathway IVIVE of hepatic clearance involving biliary efflux

For the NCE set, biliary efflux in sandwich cultured rat hepatocytes was measured and 44 out of the 77 NCEs were defined as substrates of biliary efflux (BEI >10%). For the compounds that were substrates of biliary efflux, a single pathway analysis of predicted clearance from $CL_{int,met}$ in rat liver microsomes or $CL_{int,sec,}$ from sandwich cultured rat hepatocytes was compared with observed rat blood clearance (Figure 6-2).

Figure 6-2 Single pathway IVIVE analysis: Prediction of rat clearance for substrates of biliary efflux

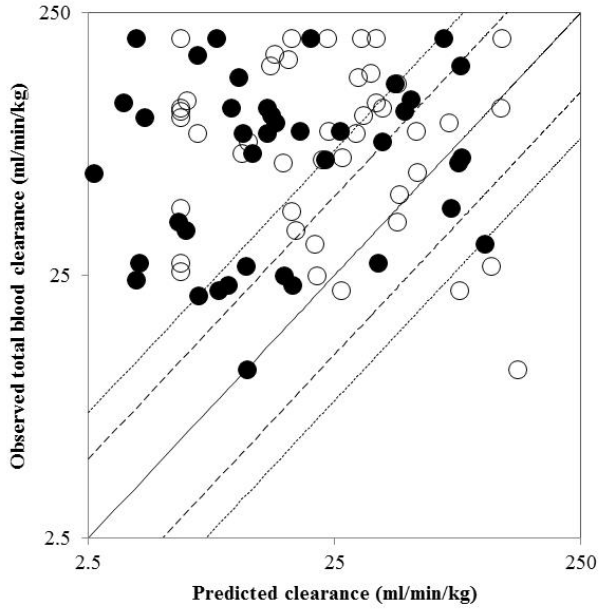

Prediction of rat clearance for substrates of active biliary efflux (n=44). Black open circles represent predicted clearance calculated from scaled $CL_{int,met}$ in rat liver microsomes. Black filled circles represent predicted biliary clearance calculated from $CL_{int,sec}$ in sandwich cultured rat hepatocytes. The solid black line represents the line of unity and black dashed and dotted lines indicate 2-fold and 3-fold of the unity respectively.

The statistical comparisons of these predictions are summarized in Table 6-2. In general, for substrates of biliary efflux, clearance was not better predicted from $CL_{int,sec}$ compared to $CL_{int,met}$. There was a higher percentage of compounds falling outside 2-fold and 3-fold error of observed clearance which was consistent with the bias observed and the precision was also lower (higher *rmse* and *afe*). However, as previously discussed in Section 5, the sandwich cultured rat hepatocyte model is not yet sufficiently established or robust for the quantitative prediction of biliary clearance. An underestimation of intrinsic biliary clearance may provide an explanation why *in vitro in vivo* clearance disconnects remain for this data set of biliary efflux substrates.

Table 6-2 Statistical data comparing the accuracy of clearance predictions for substrates of biliary efflux

Clearance prediction	Predicted clearance model	
	$CL_{int,met}$	$CL_{int,sec}$
% Outside 2-fold	77	82
% Outside 3-fold	64	66
n	44	44
Bias	0.29	0.19
rmse	0.75	0.92
afe	5.7	8.3

n: sample number, *afe*: average fold error, *rmse*: root mean squared prediction error

6.3 Multiple pathway IVIVE of hepatic clearance involving metabolism and transport

For the NCE set, predicted clearance based on metabolism as a single pathway analysis, resulted in a poor correlation between predicted and observed clearance (see Section 3.3.2). Whereas, clearance for substrates of active transport in rat hepatocytes were better predicted when the IVIVE model was based on $CL_{int,upt}$ but not $CL_{int,sec}$ as a single pathway. IVIVE models have evolved to describe hepatic drug elimination as an interplay of uptake, metabolism, biliary excretion and sinusoidal efflux (Camenisch and Umehara, 2012; Liu and Pang, 2005; Shitara et al., 2005). Sinusoidal efflux was not measured *in vitro* but considering the 3 remaining processes driving hepatic clearance, multiple pathway IVIVE of clearance was predicted and compared to single pathway analysis.

6.3.1 Multiple pathway IVIVE of hepatic clearance involving metabolism and active uptake

For substrates of active uptake and hepatic metabolising enzymes, a simple model for calculating intrinsic clearance was used (Webborn et al., 2007) where $CL_{int,met}$ is the intrinsic clearance in rat liver microsomes, $CL_{int,act}$ is the active uptake intrinsic clearance in primary rat liver hepatocytes. At the sinusoidal membrane, passive influx and efflux are assumed to be equivalent and parameterised as $CL_{int,pas}$:

$$CL_{int,app}(ml/min/kg) = CL_{int,met} * \frac{CL_{int,act} + CL_{int,pas}}{CL_{int,met} + CL_{int,pas}}$$

A direct scaling model was then used to calculate predicted clearance:

$$CL_H(ml/min/kg) = \frac{Q_H * CL_{int,app}}{Q_H + CL_{int,app}}$$

Although 41 out of the 77 NCE compounds were defined as substrates of active uptake in cultured primary rat hepatocytes (37°C:4°C uptake ratios >3), $CL_{int,pas}$ in cultured primary rat hepatocytes could not be measured for 14 compounds as analyte concentrations from the 4°C samples were <LOQ. Both $CL_{int,upt}$ and $CL_{int,pas}$ were measured for the remaining 27 compounds. A direct scaling model (Q_H 150 ml/min/kg, all binding disregarded) was then used to predict clearance values for all substrates of active uptake and the relationship between the predicted clearance from single pathway IVIVE models (accounting for metabolism or uptake) and a multiple pathway IVIVE models (accounting for metabolism and active and passive uptake data) were compared (Figure 6-3):

Figure 6-3 Comparison of single and multiple pathway IVIVE analysis: Prediction of rat clearance for substrates of active uptake

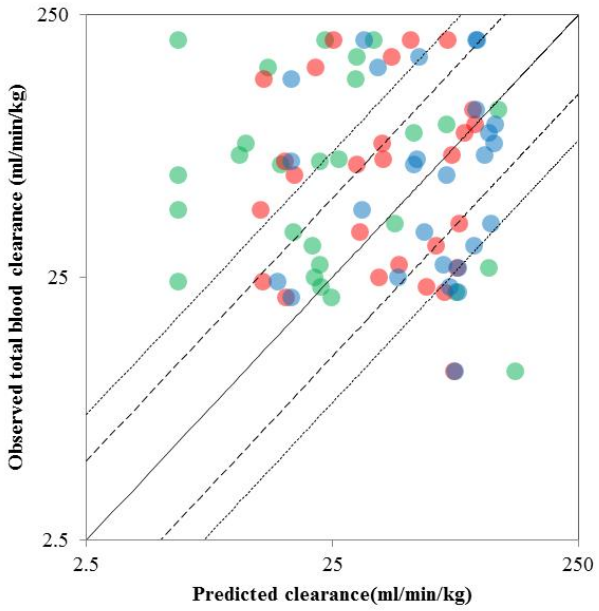

Prediction of rat clearance for substrates of active uptake (n=27). Green circles represent predicted clearance from single pathway IVIVE based on metabolism. Blue circles represent predicted clearance from single pathway IVIVE based on total uptake. Red circles represent predicted clearance from multiple pathway IVIVE based on metabolism and active and passive uptake. The black solid line indicates the line of unity whereas black dotted and dashed lines indicate 2-fold and 3-fold of unity respectively.

The statistical comparisons of these predictions are summarized in Table 6-3. For substrates of active uptake, in comparison to clearance predicted from $CL_{int,met}$, an improvement in precision and bias was achieved using the multiple pathway IVIVE method accounting for $CL_{int,act}$, $CLint_{,pas}$ and $CL_{int,met.}$ However, a single pathway IVIVE model based on $CL_{int,upt}$ only resulted in the lowest percentage of predicted clearance values falling outside 2-fold and 3-fold error which was consistent with the improved bias and precision (lower *rmse* and *afe*). Although this data set is small, it suggests that hepatocyte uptake is the rate determining step for elimination of these drugs and that clearance is best predicted using the simplest IVIVE model based on $CL_{int,upt.}$

Table 6-3 Statistical data comparing the accuracy of clearance predictions for substrates of active uptake: Comparison of single and multiple pathway IVIVE analysis.

	Predicted clearance based on eliminating process(es)		
Clearance prediction	Metabolism (Single pathway)	Total uptake: (Single pathway)	Metabolism and active uptake: (Multiple pathway)
% Outside 2-fold	67	52	59
% Outside 3-fold	59	33	37
n	27	27	27
Bias	0.42	1.00	0.69
rmse	0.68	0.43	0.49
afe	4.8	2.7	3.1

n: sample number, afe: average fold error, rmse: root mean squared prediction error

6.3.2 Multiple pathway IVIVE of hepatic clearance involving metabolism and biliary efflux

For compounds that were substrates of active efflux in sandwich cultured rat hepatocytes and metabolizing enzymes in rat liver microsomes, two multiple pathway IVIVE models for calculating intrinsic clearance were used which assume either biliary efflux or metabolism and biliary efflux are the primary processes driving hepatic clearance:

$$CL_{int,app}(ml/min/kg) = CL_{int,sec} * \frac{CL_{int,act} + CL_{int,pas}}{CL_{int,sec} + CL_{int,pas}}$$

$$CL_{int,app}(ml/min/kg) = CL_{int,met} + CL_{int,sec} * \frac{CL_{int,act} + CL_{int,pas}}{(CL_{int,met} + CL_{int,sec}) + CL_{int,pas}}$$

Where $CL_{int,met}$ is the intrinsic clearance in rat liver microsomes, $CL_{int,act}$ and $CL_{int,sec}$ are the active uptake intrinsic clearance in primary rat liver hepatocytes and secretory efflux clearance in sandwich cultured rat hepatocytes respectively. At the sinusoidal membrane, passive influx and efflux are assumed to be equivalent and parameterised as $CL_{int,pas}$.

A direct scaling model was then used to calculate predicted clearance:

$$CL_H\,(ml/min/kg) = \frac{Q_H * CL_{int,app}}{Q_H + CL_{int,app}}$$

Although 44 NCEs from the NCE set were defined as substrates of active biliary efflux in sandwich cultured rat hepatocytes (BEI > 10%), $CL_{int,pas}$ in cultured primary rat hepatocytes could not be measured for 14 compounds as analyte concentrations from the 4°C samples were <LOQ. For the remaining 30 substrates of biliary efflux, $CL_{int,sec}$, $CL_{int,upt}$ and $CL_{int,pas}$ could all be measured. A direct scaling model (Q_H 150 ml/min/kg, all binding disregarded) was then used to predict clearance values and the relationship between the predicted clearance from both single and multiple pathway IVIVE models (accounting for metabolism only or metabolism and transport data) were compared (Figure 6-4).

Figure 6-4 Comparison of single and multiple pathway IVIVE analysis: Prediction of rat clearance for substrates of biliary efflux

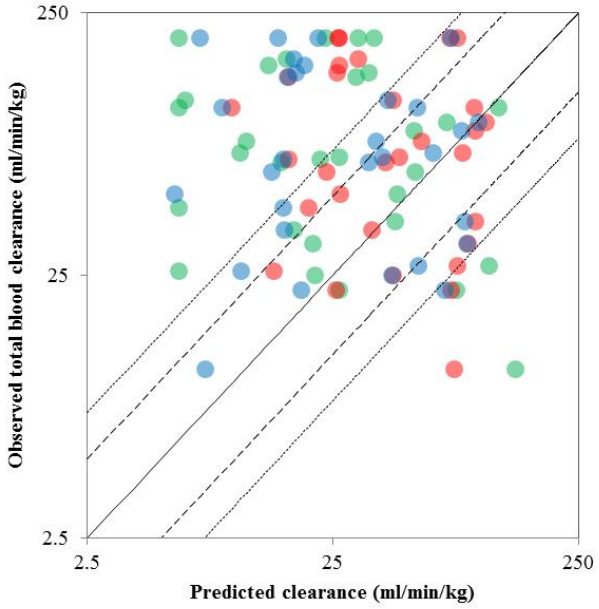

Prediction of rat clearance for substrates of biliary efflux for NCEs (n=30). Green circles represent predicted clearance from single pathway IVIVE based on metabolism. Blue circles represent predicted clearance from multiple pathway IVIVE assuming biliary secretion is a primary process driving hepatic clearance. Red circles represent predicted clearance from multiple pathway IVIVE assuming both metabolism and biliary secretion are primary processes driving hepatic clearance. The black solid line indicates the line of unity whereas black dotted and dashed lines indicate 2-fold and 3-fold of the unity respectively.

The statistical comparisons of these predictions are summarized in Table 6-4. For compounds that were substrates of active efflux, clearance predictions were improved using multiple pathway IVIVE models assuming either biliary efflux or metabolism and biliary efflux are the primary eliminating pathways. In comparison to a single pathway IVIVE model accounting for metabolism only, multi pathway IVIVE models showed a lower percentage of predicted clearance values falling outside 2-fold and 3-fold error which was consistent with the improved Bias and precision (lower rmse and afe).

Table 6-4 Statistical data comparing the accuracy of clearance predictions for substrates of biliary efflux: Comparison of single and multiple pathway IVIVE analysis

Clearance prediction	Predicted clearance based on eliminating process(es)		
	Metabolism (Single pathway)	Biliary secretion: (Multiple pathway)	Metabolism and biliary secretion: (Multiple pathway)
% Outside 2-fold	70	70	60
% Outside 3-fold	63	40	33
n	30	30	30
Bias	0.36	0.39	0.60
rmse	0.73	0.65	0.53
afe	5.4	4.5	3.4

n: sample number, *afe*: average fold error, *rmse*: root mean squared prediction error

In general for substrates of biliary efflux, an improvement in the clearance predictions was achieved when biliary efflux was accounted for, suggesting secretion of unchanged compound into the bile is a primary elimination process driving hepatic clearance for these compounds.

In summary, when comparing single pathway IVIVE analysis for the prediction of clearance of substrates of active transport, improvements were only made when the model accounted for $CL_{int,upt}$ but IVIVC disconnects remained which may be due to methodological limitations of the uptake and/or biliary efflux method. For substrates of active uptake, more complex multiple pathway models did not appear to offer any major advantage to improve predictions over the simpler single pathway models accounting for $CL_{int,upt}$, whereas clearance predictions for substrates of biliary efflux were improved using multiple pathway IVIVE models accounting for both $CL_{int,met}$ and $CL_{int,sec}$.

7 CHAPTER SEVEN: RESULTS – STRUCTURAL AND MOLECULAR ANALYSES OF HEPATIC DRUG TRANSPORT IN RAT

7.1 Structural analysis of hepatic drug transport using Bayesian Modelling

The set of 77 NCEs and 14 marketed drugs were used to develop Bayesian fragment-based classification models for prediction of active hepatic drug transport. Simplified Molecular Input Line Entry System or SMILES™ are a comprehensive chemical language which represent a unique string or identifiers for a specific chemical structure. Compound SMILES™ were retrieved from the Novartis database and their structures analysed and cut into fragments using proprietary software developed in-house. A probability model was constructed through a learning process with Bayesian statistics. Each independent fragment was assigned a fragment score based on its distribution between active (substrates of active transport) or inactive (non-substrate of active transport) molecules. A molecule activity score was calculated by summing up scores for all fragments in a molecule divided by the number of fragments in the molecule. The higher the score, the higher the probability the molecule is subjected to active transport.

7.1.1 Structural analysis of substrates of active uptake in cultured primary rat hepatocytes

Drug uptake into cultured primary rat hepatocytes was measured at 37ºC and 4ºC for the NCE and marketed drug set as discussed in Section 4.3. When the ratio of initial drug uptake (37ºC:4°C) in cultured primary rat hepatocytes was > 3, compounds were defined as substrates or 'active'. Conversely, when initial drug uptake ratios were < 3, compounds were defined as non-substrates or 'inactive'. Drug uptake in cultured primary rat hepatocytes was measured for all but 8 compounds which could not be quantified as drug levels were lower than the limit of quantification.

More than 1100 substructure fragments were identified in this 'uptake' training set. The activity score for active and inactive compounds was in the range –0.91 to 0.79 (Figure 7-1). The classification cut-off value of 0 was used as this score best divided the set of compounds into their activity class however it should be noted that values falling close to zero may have limited predictability. There were only 2 outliers in each of the active and inactive classes indicating good reliability of the model. In the active class, erythromycin, a large macrocyclic compound (MW 734) was a strong outlier with a

negative activity score of -0.61 whereas NCE 56 had an activity score of -0.03. In the inactive class, NCE 16 and NCE 71 had positive scores of 0.10 and 0.12 respectively.

Figure 7-1 Activity scores of active and inactive compounds of hepatic uptake transporters

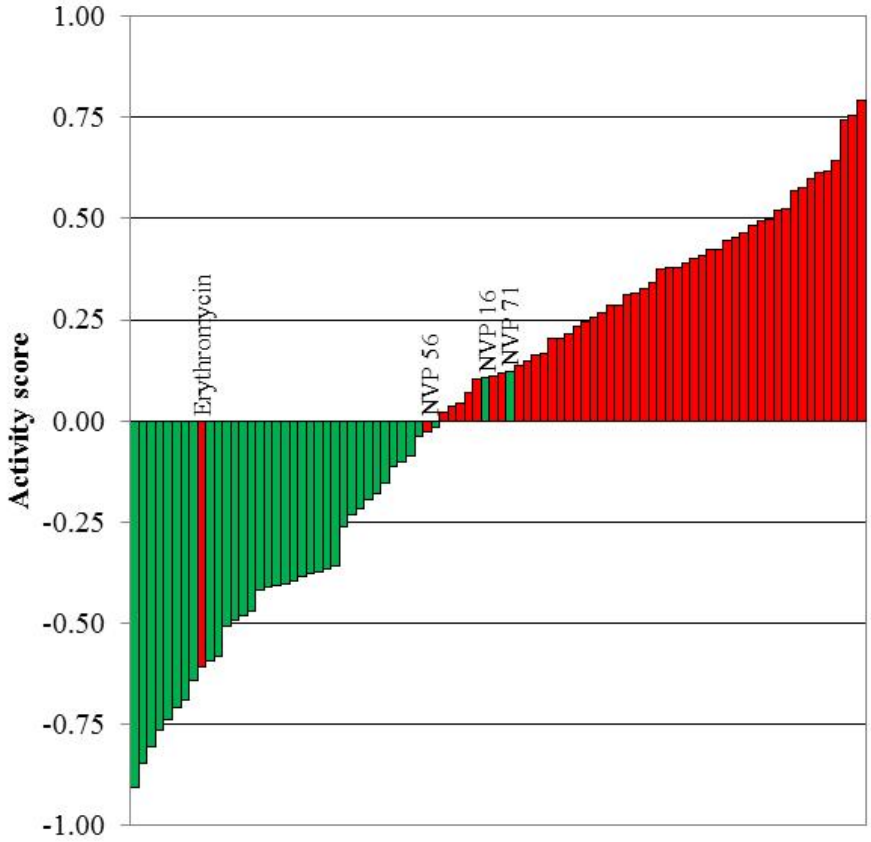

Activity scores of active and inactive molecules . Red bars denote the active molecules (substrates of active uptake) whilst green bars denote the inactive molecules (non-substrates of active uptake). From the active class, erythromycin and NCE 56 showed discrepant negative activity scores. From the inactive class, NCE 16 and 71 showed discrepant positive activity scores.

Structures of marketed drugs with high calculated activity scores for the active class are presented in Figure 7-2. Example fragments with high calculated fragment score for the active class are presented in Figure 7-3.

Figure 7-2 Structures of marketed drugs with high calculated activity score for hepatic uptake transporters

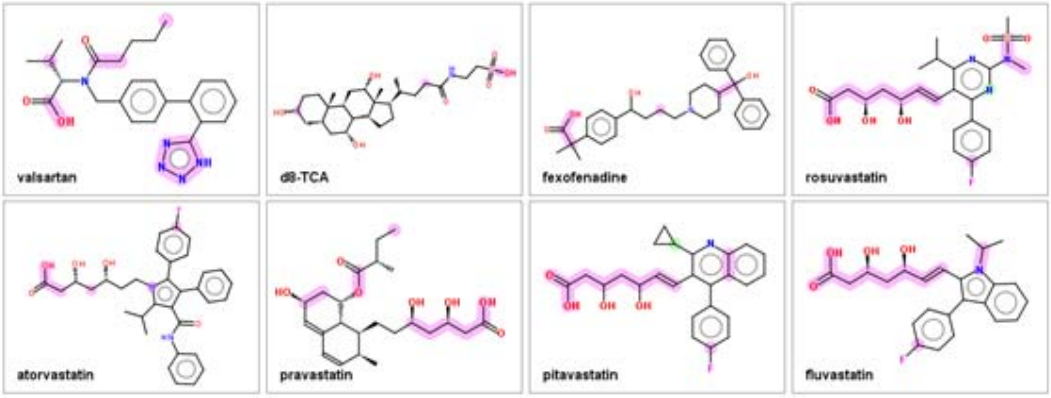

Parts of the molecule marked in magenta are predicted to be responsible for active uptake.

Figure 7-3 Example substructures with high calculated fragment score for hepatic uptake transporters

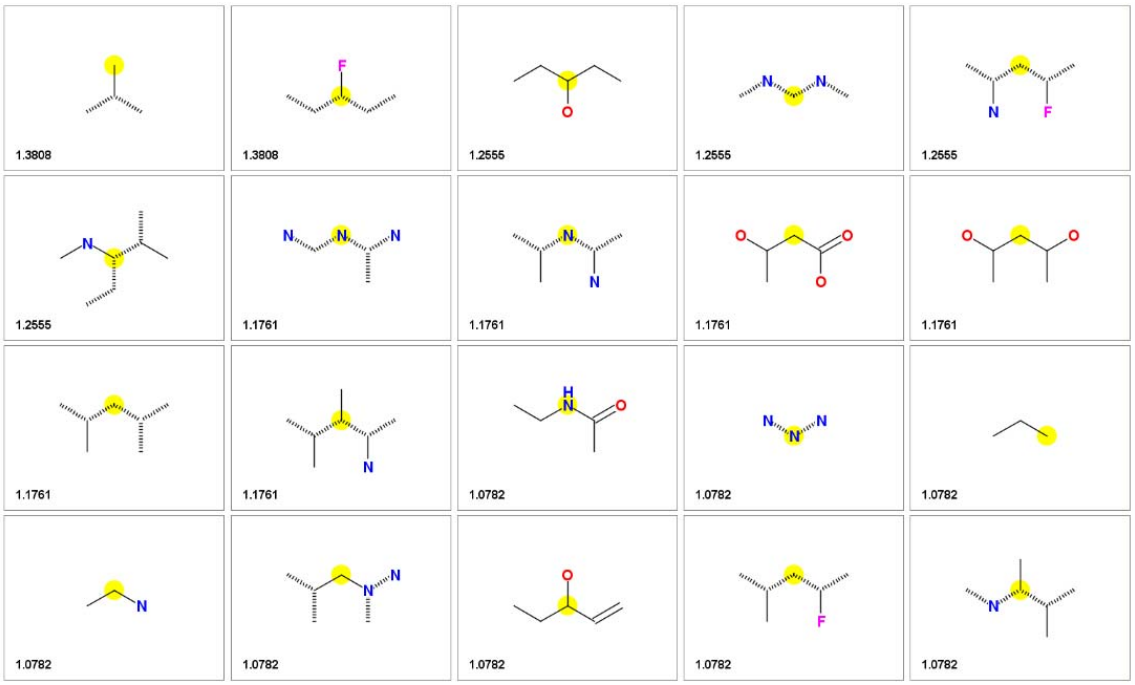

The yellow disc represents the central atom of the fragment. The calculated fragment scores are shown for the substructures.

The predictive performance of the uptake model was then evaluated in a 'leave one out' cross-validation study where 1 'test' compound at a time was deleted from the training set of 83 compounds and a new model created for the remaining structures which was used to predict an activity score for the test compound. Active compound erythromycin, which was a strong outlier in the training set, had a predicted activity score of -1.18. The predicted activity scores for the remainder of the active and inactive compounds were in the range -0.61 to 0.60 (Figure 7-4).

Figure 7-4 **Predicted activity score of active and inactive compounds of hepatic uptake transporters**

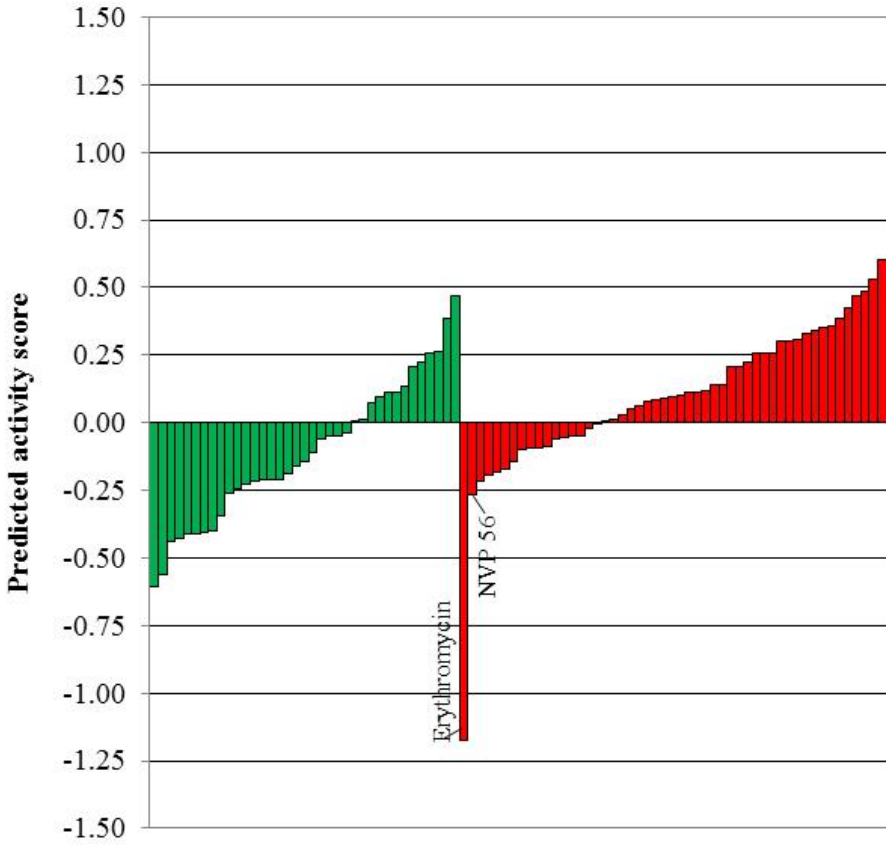

Predicted activity scores of active and inactive compounds. Red bars denote the active compounds whilst green bars denote the inactive compounds. Active and inactive compounds with predicted activity scores of < 0 or ≥ 0 respectively are poorly predicted by the cross validation model.

Whilst the data set used for this classification model is relatively small and diversity of chemical space may be limited, 67% of active and 63% of inactive compounds were correctly predicted when a classification cut-off value of 0 was applied, indicating modest to good model predictivity.

Table 7-1 Predictivity of the hepatic uptake classification model

Prediction	Active compounds	Inactive compounds
% Correct	67	63
% Incorrect	33	38
n	51	32

n = sample number

7.1.2 Structural analysis of substrates of biliary efflux in sandwich cultured rat hepatocytes

Biliary efflux in sandwich cultured rat hepatocytes was measured for the NCE and marketed drug set as discussed in Section 5.3. When the biliary efflux index (BEI) was > 10%, molecules were defined as substrates or 'active'. Conversely, when the BEI was < 10% molecules were defined as non-substrates or 'inactive'. Biliary efflux was assessed for all but 11 molecules which could not be measured due to experimental or analytical limitations. More than 1000 substructure fragments were identified in this 'biliary efflux' training set. The activity score for active and inactive molecules was in the range –1.14 to 0.89 (Figure 7-5). The classification cut-off value of 0 was used as this score best divided the set of molecules into their activity class however it should be noted that values falling close to zero may have limited predictability. There were only 5 outliers in the active class indicating good reliability of the model. Digoxin, a large glycoside (MW 781) and erythromycin, a large macrocyclic compound (MW 734) were strong outliers with negative activity scores of -1.03 and -0.30 respectively. Whereas NCEs 47, 28 and 25 had respective negative activity scores of – 0.09, -0.09 and -0.05. All molecules from the inactive class were predicted as inactive and had negative activity scores.

Figure 7-5 Activity scores of active and inactive molecules of biliary efflux

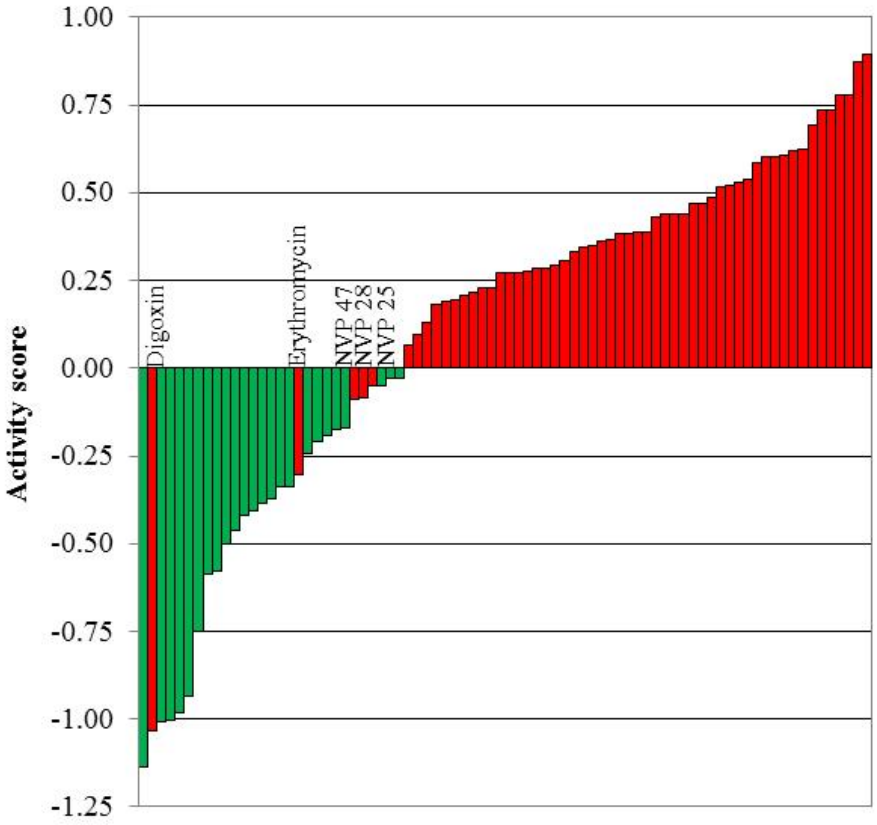

Activity scores of active and inactive molecules. Red bars denote the active molecules (substrates of biliary efflux) whilst green bars denote the inactive molecules (non-substrates of biliary efflux). From the active class, digoxin, erythromycin and NCEs 47, 28 and 25 showed discrepant negative activity scores.

Structures of marketed drugs with high calculated activity scores for the active class are presented in Figure 7-6. Example fragments with high calculated fragment score for the active class are presented in Figure 7-7.

Figure 7-6 Structures of marketed drugs with high calculated activity score for biliary efflux

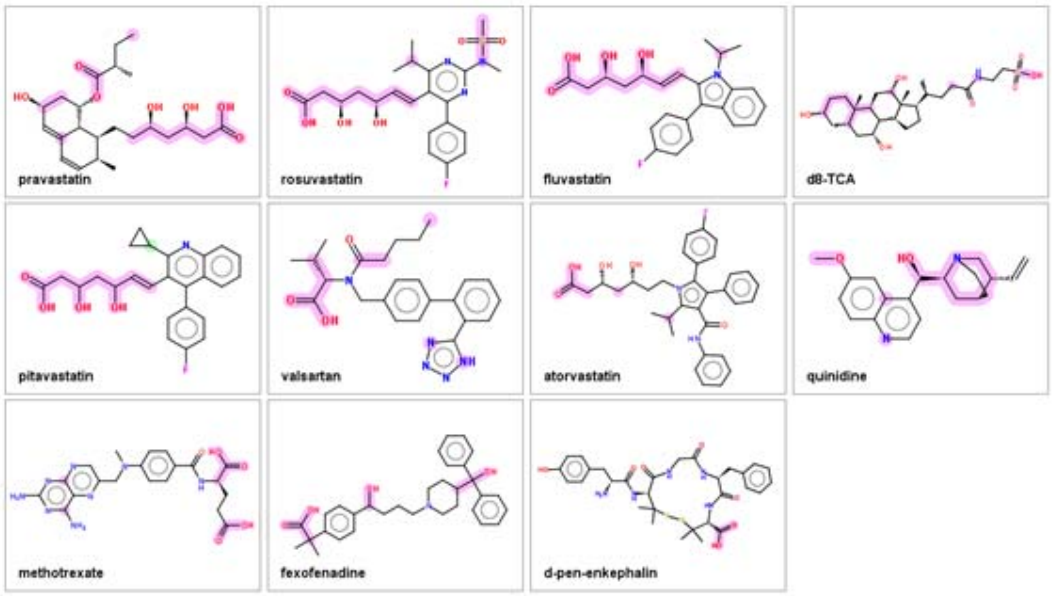

Parts of the molecule marked in magenta are predicted to be responsible for biliary efflux.

Figure 7-7 **Example substructures with high calculated fragment score for biliary efflux**

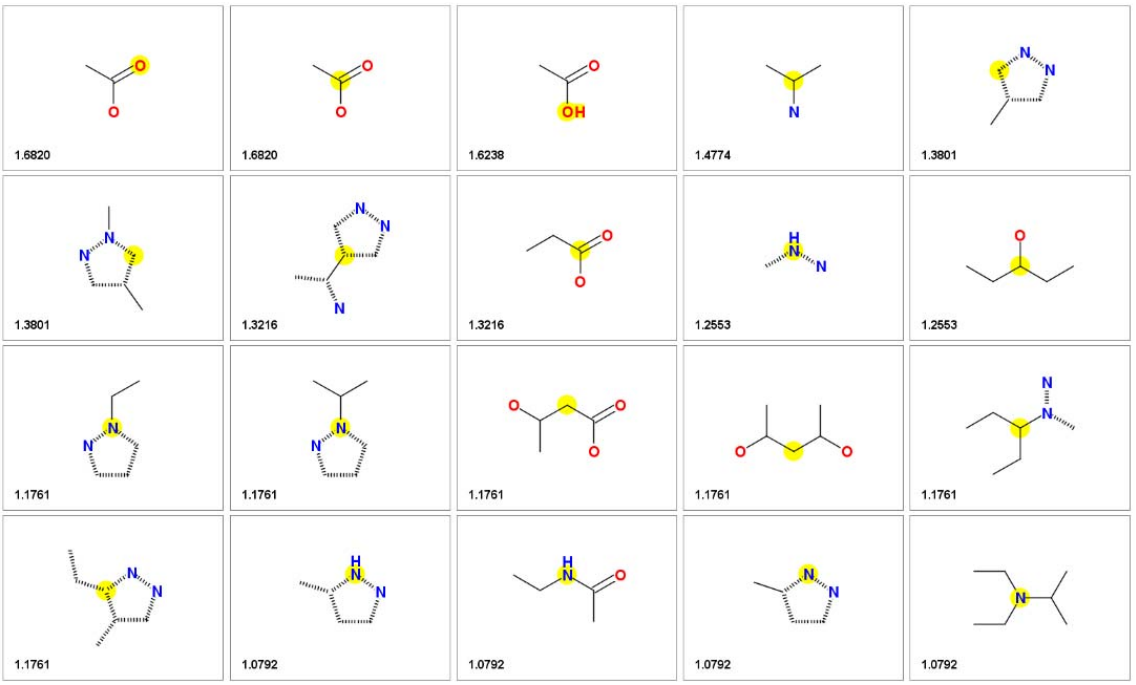

The yellow disc represents the central atom of the fragment. Calculated fragment scores are shown for the substructures.

The predictive performance of the biliary efflux model was then evaluated in a 'leave one out' cross-validation study where 1 'test' molecule at a time was deleted from the training set of 80 molecules and a new model created for the remaining structures which was used to predict an activity score for the test compound. Active molecules, digoxin and erythromycin which were strong outliers in the training set, had a predicted activity score of -1.66 and -0.76 respectively. Active molecules, NCEs 30, 28, 47 and 25 were also outliers in the training set and had respective predicted scores of -0.50, -0.32, 0.25 and -0.20. The predicted activity scores for the remainder of the active and inactive molecules were in the range -0.57 to 0.78 (Figure 7-8).

Figure 7-8 Predicted activity score of active and inactive molecules of biliary efflux

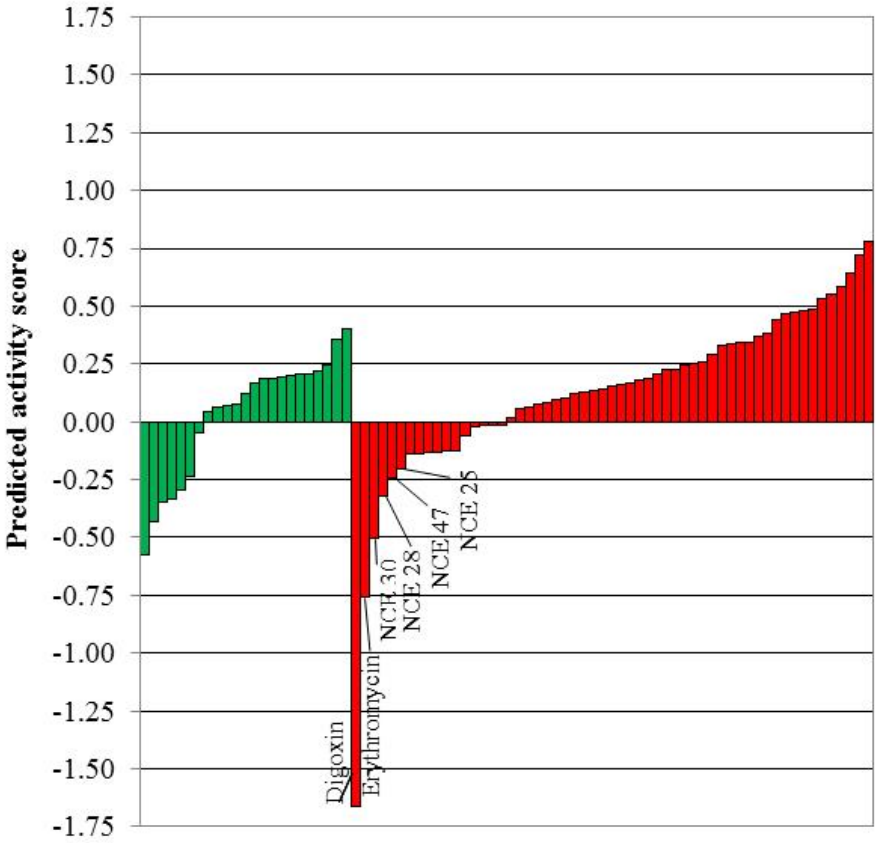

Predicted activity scores of active and inactive molecules. Red bars denote the active compounds (substrates of biliary efflux) whilst green bars denote the inactive molecules (non-substrates of biliary efflux). Active molecules with predicted activity scores of < 0 and inactive molecules with predicted activity scores of ≥ 0 are poorly predicted by the cross validation model.

The efflux data set used for this classification model is relatively small and diversity of chemical space may be limited. Using a classification cut-off value of 0, 70% of active molecules were correctly predicted but only 30% of inactive molecules were correctly predicted indicating only modest predictivity of this biliary efflux cross validation model (Table 7-2).

Table 7-2 Predictivity of the biliary efflux classification model

Prediction	Active compounds	Inactive compounds
% Correct	70	30
% Incorrect	30	70
n	57	23

n = sample number

7.2 Molecular analysis of hepatic drug transport using *in silico* computational modelling

The set of 77 NCEs were used to develop *in silico* computational models for prediction of active hepatic drug transport. Compound SMILES™ were retrieved from the Novartis database and imported into Volsurf+ (software version 1.0.7.1, Molecular Discovery, London UK), which reads the SMILES and converts 3D molecular fields into physic-chemically relevant molecular descriptors (Cruciani et al., 2000). These Volsurf+ descriptors along with physicochemical descriptors (both computed and measured) were then imported into SIMCA-P+ (software version 12.0.1.0, Umetrics, Malmö, Sweden) multivariate data analysis software to define discriminant *in silico* models describing active uptake and biliary efflux in rat hepatocytes.

7.2.1 Molecular analysis of substrates of drug uptake into cultured primary rat hepatocytes

Drug uptake into cultured primary rat hepatocytes was measured at 37ºC and 4ºC as discussed in Section 4. When the ratio of initial drug uptake (37ºC:4°C) in cultured primary rat hepatocytes was > 3, compounds were defined as substrates. Conversely, when initial drug uptake ratios were < 3, compounds were defined as non-substrates. Drug uptake in cultured primary rat hepatocytes was measured for all but 7 NCEs which could not be quantified as drug levels were lower than the limit of quantification. Based on the uptake data, the NCE data set was divided into 2 groups. A binary yes/no classification was assigned to compounds which were either substrates or non-substrates of active uptake if the drug uptake ratio (37°C:4°C) was either ≥ 3 or < 3 respectively. For the *in silico* modelling of active uptake, 128 Volsurf+ descriptors, 21 measured or computed physicochemical descriptors and the binary uptake classification were used to perform Principal Component Analysis or PCA using SIMCA-P+. The overall information was condensed into a PCA loading plot which shows how the descriptors are positioned in

relation to the binary substrate classification. The descriptor profile was then viewed in a coefficient plot which highlights the descriptors which maybe most influential to describe active uptake. Descriptors of least relevance were eliminated. Following this multiple linear regression analysis, a final principal least squares (PLS) model with a single principal component was defined by 4 descriptors as detailed in the final coefficient plot (Figure 7-9) that were important in influencing active uptake into rat hepatocytes was obtained:

1. PAMPA_FA indicates the calculated percentage fraction absorbed from the PAMPA permeability assay.
2. W1 is a hydrophilic volume descriptor in Volsurf+ which accounts for polarisability and dispersion forces.
3. W8 is hydrophilic volume descriptor in Volsurf+ which accounts for strong H-bond donor-acceptor regions.
4. IW4, a Volsurf+ descriptor of interaction energy (INTEGY) moments which describe the imbalance between the centre of a molecule mass and the barycentre of its hydrophilic and hydrophobic regions.

The coefficient plot of these descriptors demonstrates their inter-relationship with drug uptake where active drug transport into rat hepatocytes is favoured for compounds with increased hydrophilic volume and reduced permeability and INTEGY moments.

Figure 7-9 Coefficient plot of the 4 descriptors used to define the discriminant model of drug uptake

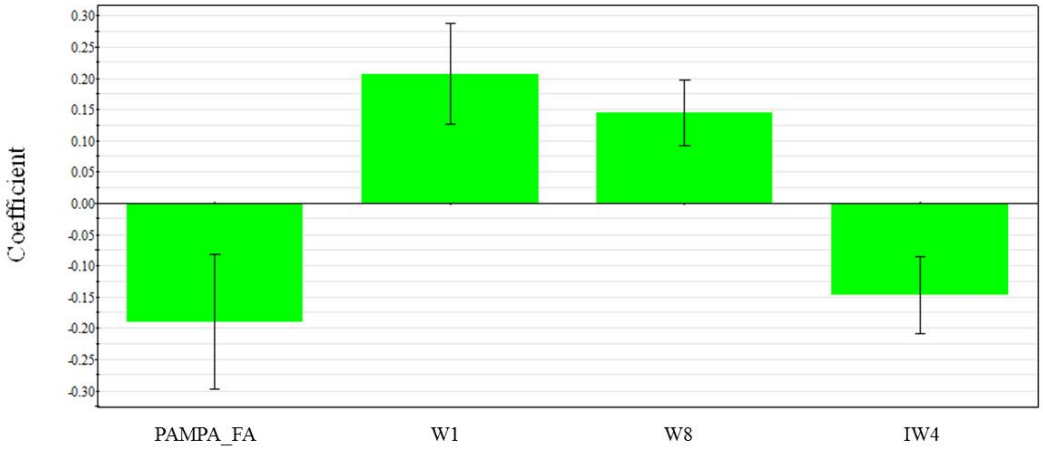

Coefficient plot of the 4 descriptors which define the discriminant model of drug uptake. The plot indicates that PAMPA_FA and IW4 are negatively correlated to active drug uptake whilst W1 and W8 are positively correlated to active drug uptake. The error bars indicate the variability for each descriptor.

This discriminant PLS model was applied to the 70 NCEs which resulted in a low correlation with the binary uptake classification ($r^2 = 0.24$) suggesting limited discriminant model predictivity of active uptake. The resultant PLS score plot shows modest discrimination between substrates and non-substrates of active uptake with >80% of substrates and ~50% of non-substrates of active uptake correctly predicted (Figure 7-10 and Table 7-3).

Figure 7-10 Discriminant PLS model of drug uptake into cultured primary rat hepatocytes

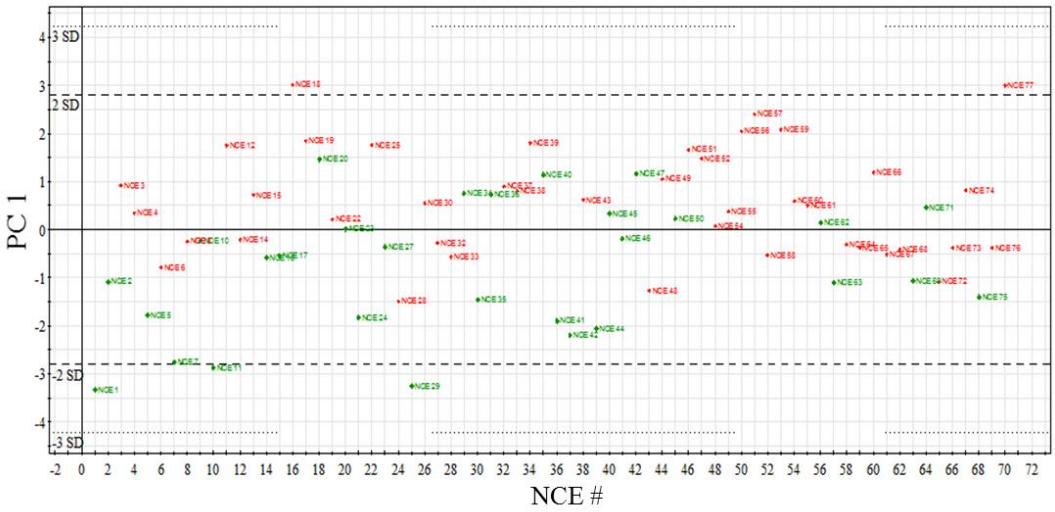

PLS score plot of the discriminant model of active uptake for 70 NCEs. Red text represents NCEs that were substrates of active uptake (measured) whilst green text denotes NCEs that were non-substrates of active uptake (measured). The solid horizontal line indicates the principal component axis, dashed and dotted horizontal lines indicate 2 and 3 standard deviations (SD) of the axis line respectively. Substrates of active uptake were correctly predicted if they lie above the principle component axis (zero) whereas non-substrates of active uptake were correctly predicted if they lie below this axis.

Table 7-3 Predictivity of the *in silico* model of drug uptake into cultured primary rat hepatocytes

Prediction	Substrates of active uptake	Non-substrates of active uptake
% Correct	83	55
% Incorrect	17	45
n	41	29

n = sample number

7.2.2 Molecular analysis of substrates of biliary efflux in sandwich cultured rat hepatocytes

From the NCE data set, biliary efflux in sandwich cultured rat hepatocytes was measured for 66 NCEs. Biliary efflux could not be quantified for 11 NCEs due to either experimental (high non-specific binding and/or poor mass balance) or analytical limitations (drug levels were lower than the limit of quantification). Based on the percentage biliary efflux index (BEI %), the NCE data set was divided into 2 groups. A binary yes/no classification was assigned to compounds which were either substrates or

non-substrates of biliary efflux if the BEI was either ≥ 10% or < 10% respectively. For the *in silico* modelling of biliary efflux, 97 Volsurf+ descriptors, 28 measured or computed physicochemical descriptors and the binary efflux classification were used to perform PCA using SIMCA-P+. The descriptors most influential to describe efflux were identified and a final PLS model with a single principal component was defined by 3 descriptors as detailed in the final coefficient plot (Figure 7-11) that were important in influencing biliary efflux in sandwich cultured rat hepatocytes was obtained:

1. PAMPA_FA indicates the calculated percentage fraction absorbed from the PAMPA permeability assay.
2. WO1 is a hydrogen bond donor volume descriptor in Volsurf+.
3. %FU10 represents the percentage unionized species at pH10.

The coefficient plot of these descriptors demonstrates their inter-relationship with biliary efflux where drug efflux into bile is favoured for compounds with increased hydrogen donor bond volume and reduced permeability and percentage fraction unionized at pH 10.

Figure 7-11 Coefficient plot of the 3 descriptors used to define the discriminant model of biliary efflux

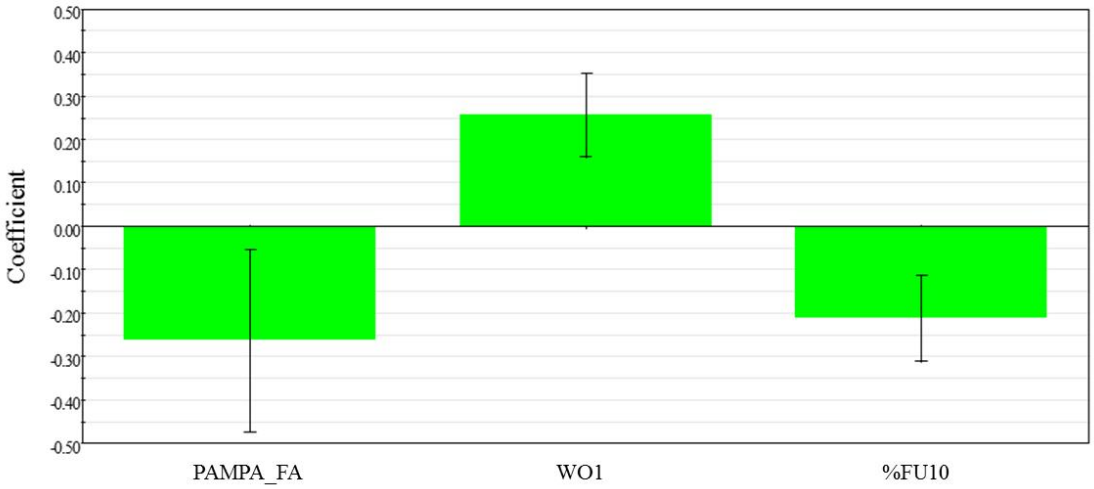

Coefficient plot of the 3 descriptors which define the discriminant model of biliary efflux. The plot indicates that PAMPA_FA and %FU10 are negatively correlated to biliary efflux whilst WO1 is positively correlated to biliary efflux. The error bars indicate the variability for each descriptor.

This discriminant PLS model was applied to the 66 NCEs which resulted in a low correlation with the binary biliary efflux classification (r^2 = 0.26) suggesting limited discriminant model predictivity of biliary efflux. The resultant PLS score plot shows modest discrimination between substrates and non-substrates of biliary efflux with >90% of substrates and ~50% of non-substrates of biliary efflux correctly predicted (Figure 7-12 and Table 7-4).

Figure 7-12 Discriminant PLS model of biliary efflux in sandwich cultured rat hepatocytes

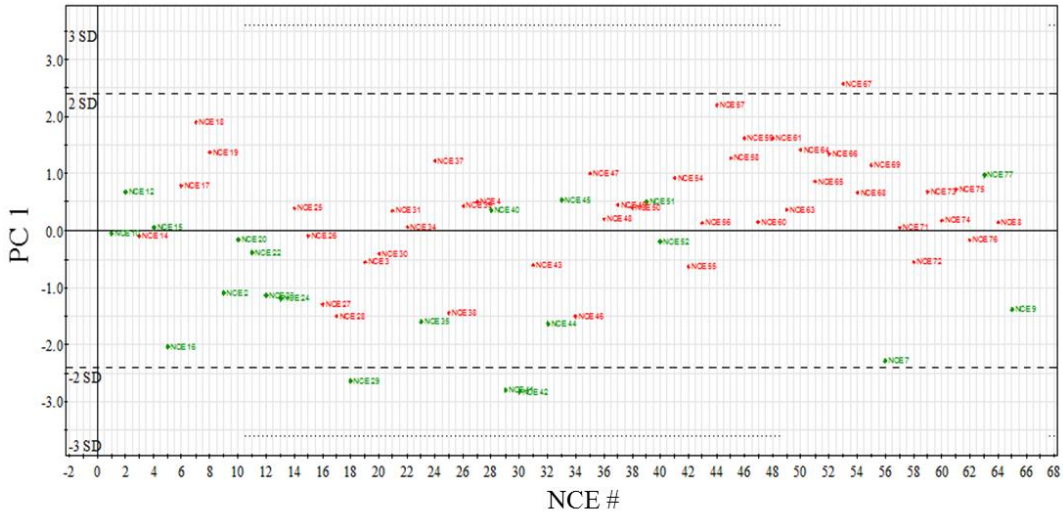

PLS score plot of the discriminant model of biliary efflux for 66 NCEs. Red text represents NCEs that were substrates of biliary efflux (measured) whilst green text denotes NCEs that were non-substrates of biliary efflux (measured). The solid horizontal line indicates the principal component axis, dashed and dotted horizontal lines indicate 2 and 3 standard deviations (SD) of the axis line respectively. Substrates of biliary efflux were correctly predicted if they lie above the principle component axis (zero) whereas non-substrates of biliary efflux were correctly predicted if they lie below this axis.

Table 7-4 Predictivity of the *in silico* model of biliary efflux in sandwich cultured rat hepatocytes

Prediction	Substrates of biliary efflux	Non-substrates of biliary efflux
% Correct	91	55
% Incorrect	9	45
n	44	22

n = sample number

In summary, both the classification and *in silico* models created to discriminate substrates and non-substrates of active uptake or biliary efflux show modest predictivity overall. Further characterisation with larger, more diverse data sets may be warranted in order to gain confidence and improve their predictive capacity.

8 CHAPTER EIGHT: RESULTS – INVESTIGATION OF THE RELATIONSHIP BETWEEN DRUG PHYSICOCHEMICAL PROPERTIES AND DISPOSITION PATHWAYS

8.1 Background

Based on literature data for marketed drugs with well characterised ADME properties, it is obvious that relationships between the physicochemical properties of drugs and disposition pathways exist with key determinants being permeability and lipophilicity (Wu and Benet, 2005). Simulations examining the interplay of passive diffusion, active uptake and metabolism on hepatic extraction ratios have been reported (Webborn et al., 2007). They indicated that the highest extractions result for poorly permeable compounds which are good substrates for active uptake transporters since active uptake balanced by passive diffusion can increase the liver: blood concentration ratio and exposure of the drug to the hepatic eliminating process. In this thesis, conventional IVIVE methods to predict drug clearance resulted in a high degree of under prediction. To investigate the potential causes for this under prediction, the relationships between predictability, active hepatic drug transport and physicochemical properties of a set of 77 NCEs was examined.

8.2 Relationship between clearance and permeability

The relationship between predictability of clearance and permeability was investigated for the NCE set (Figure 8-1). Prior validation of the cell permeability of marketed drugs with MDCKII LE cells indicated the assay to be robust and reproducible (see Appendix, Section 11.3). MDCKII LE cell permeability of the NCE set was then measured for all except 7 NCEs which remained undefined due to poor assay recovery (<70%). NCEs were grouped into low, medium and high passive permeability categories according to MDCKII LE P_{app} values with P_{app} values $< 5 \times 10^{-6}$ cm/s and $\geq 10 \times 10^{-6}$ cm/s indicating low and high permeability respectively. These cut off values were defined by the range of P_{app} values for marketed drugs classified as having either a low or high percentage of human intestinal absorption in the literature as detailed in Section 11.3 in the Appendix.

Figure 8-1 **Prediction of rat clearance from *in vitro* $CL_{int,met}$ for NCEs with low, medium and high passive permeability**

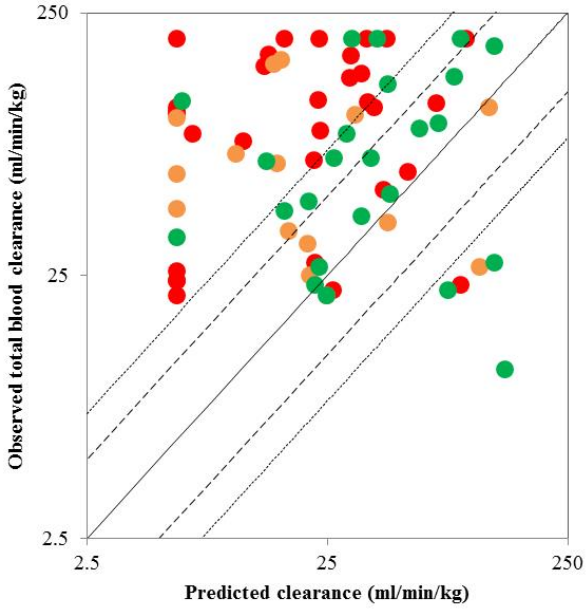

Prediction of rat clearance from *in vitro* $CL_{int,met}$ using rat liver microsomes for the NCE set (n=70). NCEs are colour coded according to their passive permeability category in MDCKII LE cells; red filled circles = low permeability, orange = medium permeability and green = high permeability. The solid black line represents the line of unity with black dashed and dotted lines indicating 2-fold and 3-fold of the unity respectively.

In general, using rat liver microsomes, the clearance of NCEs with high permeability was better predicted than the clearance of NCEs with low or medium permeability (Table 8-1). NCEs that were highly permeable had a lower percentage of predicted clearance falling outside 2-fold and 3-fold observed values in comparison to NCEs with medium or low permeability and this is consistent with the bias observed. Precision was also improved for high permeability compounds (lower *rmse and afe*).

Table 8-1 Statistical analysis of predictions of rat clearance from rat liver microsomes for low, medium and high permeability NCEs

Predicted clearance	MDCKII LE Permeability category		
	Low	Med	High
% Outside 2-fold	84	53	50
% Outside 3-fold	71	47	29
n	31	15	24
Bias	0.23	0.34	0.59
rmse	0.8	0.7	0.5
afe	6.1	5.0	3.5

n: sample number, *afe*: average fold error, *rmse*: root mean squared prediction error

8.3 Relationship between clearance and physicochemical parameters molecular weight, calculated partition coefficient, polar surface area and hydrogen bonding ability.

The relationship between predictability of clearance from rat liver microsomes and the physicochemical parameters molecular weight (MW), calculated partition coefficient (cLogP), polar surface area (PSA) and the sum number of hydrogen bond donors (HBD) and hydrogen bond acceptors (HBA) was investigated for the NCE set.

Table 8-2 Statistical analysis of predictions of rat clearance from rat liver microsomes: Relationship between predictability and physicochemical parameters

Predicted clearance	MW (Da)		cLogP		PSA (Å^2)		Sum of HBA & HBD	
	≤ 450	> 450	≤ 2	> 2	≤ 100	> 100	≤ 10	> 10
% within 3-fold	41	42	38	44	57	32	50	35
n	39	38	29	48	30	47	34	43
bias	0.29	0.37	0.23	0.40	0.36	0.30	0.42	0.27
rmse	0.72	0.69	0.74	0.68	0.57	0.78	0.60	0.78
afe	5.3	4.9	5.5	4.8	3.7	6.0	4.0	6.0

Da: Dalton, Å^2: Angstroms, n: sample number, *rmse*: root mean squared prediction error, *afe*: average fold error

There was a modest impact on predictability of clearance from rat liver microsomes when the cut-off values for each descriptor as detailed in Table 8-2 were

applied. Molecular weight appeared to have only a marginal effect on the precision of clearance predictions. However, the parameters cLogP, PSA and the sum of all HBA and HBD had a modest impact on clearance predictions. In general, precision and bias of clearance predictions were improved when NCEs had the following characteristic: MW > 450, cLogP > 2, PSA < 100 and the sum of all HBD and HBA was < 10.

8.4 Relationship between active drug transport and passive permeability

The relationship between active drug transport and permeability was investigated for the NCE set. Active uptake was measured in cultured primary rat hepatocytes and biliary efflux was measured in sandwich cultured rat hepatocytes as detailed in Sections 4.3 and 5.3 respectively. Apparent permeability (P_{app}) through cell monolayers was measured in MDCKII LE cells and the passive permeability of the NCEs were categorised as low, medium or high permeability using the classification detailed in Section 8.2.

8.4.1 Relationship between passive permeability and active uptake in cultured primary rat hepatocytes

Both apparent permeability and uptake data were obtained for 66 of the 77 NCEs. For the remaining 11 NCEs, permeability and/or uptake could not be measured due to technical issues. NCEs were defined as substrates of active uptake where uptake ratios (37ºC:4ºC) were ≥ 3. The average measured P_{app} values for substrates and non-substrates of active uptake were assessed and are illustrated in Figure 8-2:

Figure 8-2 **Range in measured passive permeability for non-substrates and substrates of active uptake in cultured primary rat hepatocytes**

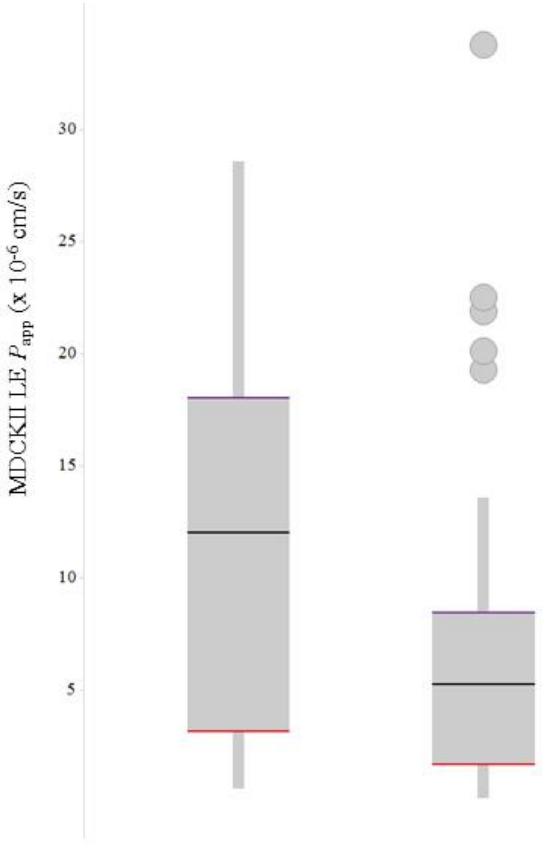

	Non-substrate	Substrate
Count	27	39
Median	12	5.3
Outliers	0	5

Box plot illustrating the range of MDCKII LE P_{app} values for non-substrates and substrates of active uptake in cultured primary rat hepatocytes. The purple and red horizontal lines represent the third quartile and first quartile respectively and the vertical lines (whiskers) extending from the boxes indicate variability outside the upper and lower quartiles. The grey circles represent outliers. Solid horizontal black lines indicate the median values (second quartile).

Non-substrates and substrates display a wide and overlapping range of measured P_{app} values. In comparison to non-substrates of active uptake, there is a trend towards lower P_{app} values for substrates of active uptake as indicated by a lower median P_{app} but the latter is skewed by 5 outliers which showed high permeability with $P_{app} \geq 19 \times 10^{-6}$ cm/s: NCEs 8, 28, 33 are lipophilic bases with PSA ~110 or less whereas NCEs 60 and 61 are

hydrophilic bases with higher PSA values of 130 and 141 respectively. For all 5 NCEs, hepatic extraction is likely dependent on a balance of passive diffusion, active uptake and removal by the eliminating process. Revisiting the IVIVE of rat clearance, hepatic metabolism is likely a key eliminating process for NCEs 8, 28 & 33 which showed good clearance predictions (within 2-fold of observed) from either rat liver microsomes or fresh hepatocytes but unlikely to be so important for NCEs 60 & 61 where observed clearance was > 2-fold under predicted.

Substrates and non-substrates of active uptake were grouped into low, medium and high permeability categories using the MDCKII LE P_{app} classification categories detailed in section 8.2. The majority of NCEs that were not substrates of active uptake had high passive permeability (59%) whereas, fewer substrates of active uptake had high passive permeability (18%) confirming a relationship between lower passive permeability and active uptake in rat hepatocytes (Table 8-3):

Table 8-3 Comparison of passive permeability category for substrates and non-substrates of active uptake in cultured primary rat hepatocytes

MDCKII LE P_{app} category	Non-substrates of active uptake		Substrates of active uptake	
	n	% of substrates	*n*	% of non-substrates
Low	9	33	19	49
Med	2	7	13	33
High	16	59	7	18

n: sample number

8.4.2 Relationship between passive permeability and biliary efflux in sandwich cultured rat hepatocytes

Both apparent permeability and biliary efflux data were obtained for 63 of the NCEs. For the remaining 14 NCEs, permeability and/or biliary efflux could not be measured due to technical issues. Compounds were defined as substrates of biliary efflux where the BEI ≥ 10%. The average measured P_{app} values for substrates and non-substrates of biliary efflux were assessed and are illustrated in Figure 8-3:

Figure 8-3 Range in measured permeability for non-substrates and substrates of biliary efflux in sandwich cultured rat hepatocytes

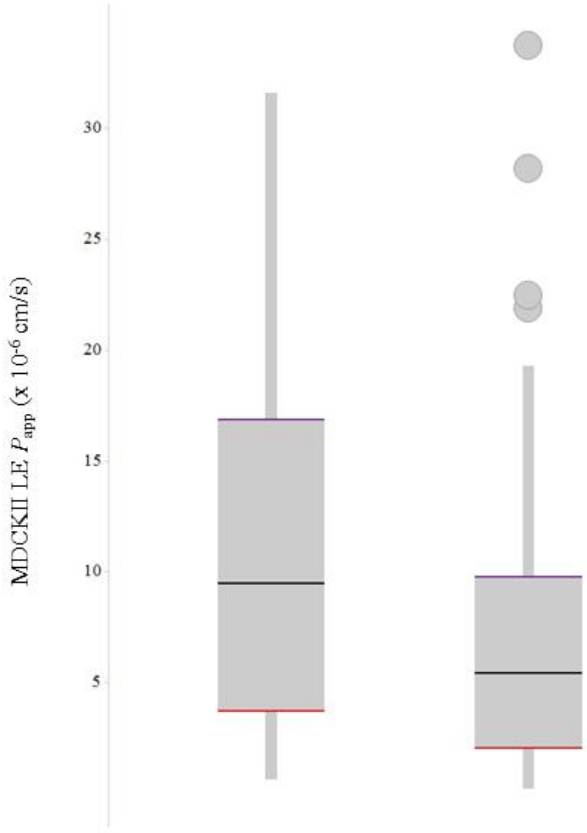

	Non-substrate	Substrate
Count	22	41
Median	9.5	5.4
Outliers	0	4

Box plot illustrating the range of MDCKII LE P_{app} values for non-substrates and substrates of biliary efflux in sandwich cultured rat hepatocytes. The purple and red horizontal lines represent the third quartile and first quartile respectively and the vertical lines (whiskers) extending from the boxes indicate variability outside the upper and lower quartiles. The grey circles represent outliers. Solid horizontal black lines indicate the median values (second quartile).

The range of measured P_{app} values for both non-substrates and substrates of biliary efflux is wide and overlapping. In comparison to non-substrates of biliary efflux, there is a trend towards lower P_{app} values for substrates of biliary efflux as indicated by a lower median P_{app} although it is skewed by 4 outliers which showed high passive permeability with P_{app} values > 20 x 10^{-6} cm/s: NCEs 8, 28 and 46 are lipophilic bases with PSA ~107 or less

whereas NCE 61 is a hydrophilic base with a higher PSA value of 141. For all 4 NCEs, hepatic extraction is likely dependent on a balance of passive diffusion, active uptake and removal by the eliminating process. Revisiting the IVIVE of rat clearance, hepatic metabolism is likely a key eliminating process for NCEs 8 & 28 which showed good clearance predictions (within 2-fold of observed) from either rat liver microsomes or fresh hepatocytes but unlikely to be so important for NCEs 46 & 61 where observed clearance was > 2-fold under predicted.

Substrates and non-substrates of biliary efflux were grouped into low, medium and high passive permeability categories using the MDCKII LE P_{app} classification categories detailed in section 8.2. Half of the NCEs that were not substrates of biliary efflux had high passive permeability (52%) whereas, fewer substrates of biliary efflux had high passive permeability (24%) confirming a relationship between lower passive permeability and biliary efflux in rat hepatocytes (Table 8-4):

Table 8-4 Comparison of passive permeability categories for substrates and non-substrates of biliary efflux in sandwich cultured rat hepatocytes

MDCKII LE P_{app} category	Non-substrates of biliary efflux		Substrates of biliary efflux	
	n	% of substrates	*n*	% of non-substrates
Low	8	36	19	46
Med	3	14	12	29
High	11	50	10	24

n: sample number

8.4.3 Cooperativity of active uptake and efflux processes in rat hepatocytes

Both active uptake and biliary efflux data were obtained for 63 of the NCEs. For the remaining 14 NCEs, uptake and/or biliary efflux could not be measured due to technical issues. The NCEs were defined as substrates of active uptake where uptake ratios (37ºC:4ºC) were ≥ 3 and substrates of biliary efflux where the BEI ≥ 10%. The NCEs were grouped into low, medium and high passive permeability categories using the MDCKII LE P_{app} classification categories detailed in Section 8.2. Intuitively, since uptake transporters may increase clearance by elevating the concentration at the site of the eliminating process (metabolism or biliary efflux), a degree of cooperativity between uptake and efflux processes would be expected and was demonstrated for 32 out of 63

NCEs which were substrates of both active and efflux processes in the hepatocyte (Table 8-5).

Table 8-5 Cooperativity of active uptake and biliary efflux processes in rat hepatocytes

	# Uptake substrates	# Uptake non-substrates
# Efflux substrates	32	10
# Efflux non-substrates	6	15

NCEs were defined as substrates of active uptake where uptake ratios (37ºC:4ºC) were ≥ 3 and substrates of biliary efflux where the BEI ≥ 10%. The number of NCEs where both active uptake and biliary efflux data were obtained = 63

This cooperative relationship of transport processes in the liver appears also to be influenced by compound passive permeability as illustrated in Figure 8-4.

Figure 8-4 Influence of passive permeability on the cooperative relationship of active transport processes in rat hepatocytes

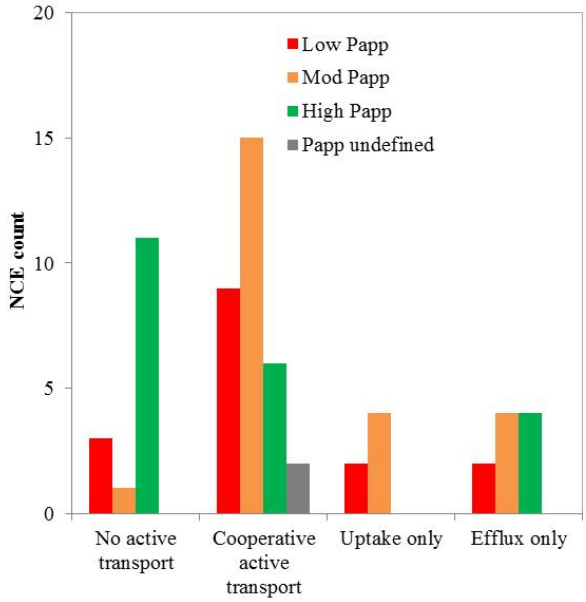

NCEs were defined as substrates of active uptake where uptake ratios (37ºC:4ºC) were ≥ 3 and substrates of biliary efflux where the BEI ≥ 10%. All 63 NCEs were grouped into low, medium and high passive permeability categories according to their Papp value: low: < 5 x 10^{-6} cm/s, medium: ≥ 5 and < 10 x 10^{-6} cm/s, high: ≥ 10 x 10^{-6} cm/s.

Fifteen NCEs were neither substrates of uptake nor efflux, 4 of which had low to moderate passive permeability and 11 with high passive permeability. From the thirty two NCEs that were substrates of both uptake and efflux, 24 had low to moderate passive permeability and only 6 had high passive permeability (P_{app} for 2 NCEs was undefined due to poor assay recovery). Six NCEs were substrates of uptake only and all had low to moderate passive permeability. Ten NCEs were substrates of biliary efflux only, 6 of which had low to moderate passive permeability and 4 with high passive permeability. In summary, higher passive permeability confers passive transport processes in rat hepatocytes whereas lower (i.e. low to moderate) passive permeability appears to confer active uptake and cooperativity between active uptake and biliary efflux. Conversely compound passive permeability appears to have a comparatively lower influence on efflux processes alone, since compounds with low, moderate and high passive permeability were subjected to efflux (however the number of compounds in this category is low).

8.5 Investigating disposition permeability relationships in rat

During the drug discovery process, if total clearance is well predicted from rat *in vitro* metabolic systems, there will probably be no need to specifically investigate alternative elimination routes as the IVIVE suggests metabolism is the key parameter driving clearance. When poor IVIVE are observed, mechanistic bile duct cannulated (BDC) rat studies are particularly useful for determining elimination pathways of unchanged drug and metabolites. Whilst direct elimination of unchanged drug can be quantified in blood and excreta, only a qualitative assessment of metabolite elimination profiles are typically possible in drug discovery due to limited availability of authentic metabolite standards.

Based on the IVIVE and permeability data from the original set of 77 NCEs, a small sub-set of these NCEs were selected to further explore direct (unchanged drug) elimination pathways in rats. The hypothesis proposed was that elimination of unchanged drug in excreta may be expected for NCEs that have lower permeability and a poor IVIVC (where predicted clearance from rat liver microsomes underestimates observed rat blood clearance > 2-fold) and less likely for NCEs with high passive permeability and good IVIVC. BDC rat data were retrieved from the internal database for NCEs 19, 24, 43, 52 and 69 and in these studies rats (1 animal per study) were all dosed at 3 mg/kg *i.v.* and excreta collected over 8 h. Additional BDC rat studies were conducted for NCEs 18, 26, 30, 41, 65, 66 and 71 in support of this research. For these additional studies rats (1 animal per study) were all dosed at 1 mg/kg *i.v.* and excreta collected over 8 h. In all rat

BDC studies, quantification of unchanged drug in blood samples and excreta was made using LC-MS/MS. Although only sparse blood sampling was conducted in the BDC studies, dose normalised blood concentration-time profiles data were found to be in a similar range in comparison to blood concentration-time profile data from the original *i.v.* pharmacokinetic studies from which total blood clearance was calculated (data not shown). The *in vivo, in vitro* and physicochemical properties for this subset of 12 NCEs are displayed in Table 8-6 which also includes percentage dose excreted as unchanged drug in bile, urine and faeces from BDC rat studies.

Table 8-6 *In vivo, in vitro* and physicochemical properties for the 12 NCEs profiled in BDC rat studies

NCE #	*Total blood clearance in rat (ml/min/kg)	Predicted clearance in RLM (ml/min/kg)	IVIVC disconnect in RLM	MDCKII LE Permeability Class	Active uptake substrate (*in vitro*, CRH)	Biliary efflux substrate (*in vitro*, SCRH)	cLogP	PSA ($Å^2$)	MW (Da)	Unchanged drug: % dose excreted in bile (*in vivo*)	Unchanged drug: % dose excreted in urine (*in vivo*)	Unchanged drug: % dose excreted in faeces (*in vivo*)
18	200	37	Yes	Low	Yes	Yes	3.7	124	527	25	<0.1	<0.1
19	200	6	Yes	Low	Yes	Yes	3.2	133	548	31	5	nr
26	174	14	Yes	Low	nd	Yes	0.2	126	451	15	34	7
52	200	44	Yes	Low	Yes	No	2.8	95	509	2.2	11	nr
71	147	35	Yes	Low	No	Yes	2.5	103	397	20	26	0.4
30	40	45	No	Mod	Yes	Yes	2.4	114	455	0.4	1.3	0.4
43	25	21	No	Mod	Yes	Yes	4.5	83	503	0.7	16	nr
65	73	10	Yes	Mod	Yes	Yes	1.8	92	417	36	13	0.7
66	100	6	Yes	Mod	Yes	Yes	4.9	120	565	64	0.1	<0.1
69	166	16	Yes	Mod	No	Yes	0.9	132	415	12	41	0.4
24	91	60	No	High	No	No	2.3	91	350	0.1	<0.1	nr
41	35	6	?	High	No	No	2.6	79	388	0.1	0.1	0.2

*Total blood clearance in rat capped at 200 ml/min/kg, RLM: rat liver microsomes, , CRH: cultured rat hepatocytes, SCRH: sandwich cultured rat hepatocytes, nr: no data

NCEs were identified as 1) having an IVIVE clearance disconnect if predicted clearance from rat liver microsomes was > 2-fold lower than the total blood clearance in rat (capped at 200 ml/min/kg), 2) active uptake substrates when *in vitro* uptake ratio (37:4ºC) in rat hepatocytes ≥3, 3) biliary efflux substrates when *in vitro* BEI % in SCRH ≥ 10%.

The IVIVC for these 12 NCEs is illustrated in Figure 8-5. All 12 NCEs were grouped into low, medium and high passive permeability categories (using the MDCKII LE P_{app} classification categories detailed in section 8.2).

Figure 8-5 Prediction of rat clearance using rat liver microsomes for the 12 NCEs profiled in bile duct-cannulated rat studies

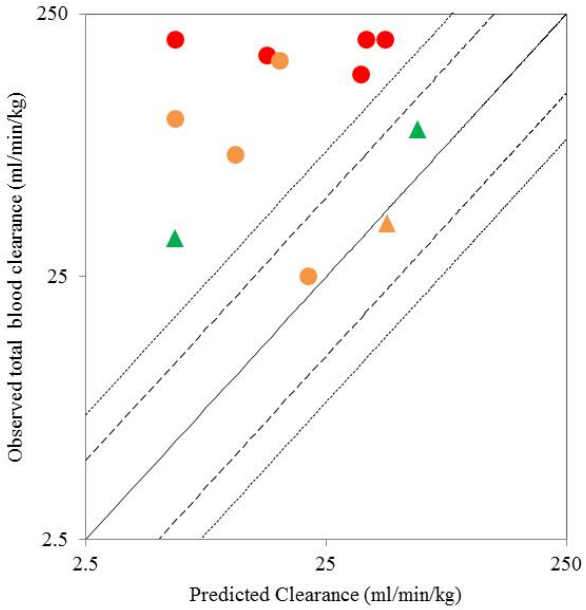

Prediction of rat clearance from *in vitro* $CL_{int,met}$ using rat liver microsomes for 12 NCEs. Circles denote NCEs where > 10% of the dose applied to bile duct cannulated rats was directly eliminated as unchanged drug in excreta whereas triangles denote NCEs where direct elimination of unchanged drug in excreta was minimal (< 10% of the dose applied). Compounds are colour coded according to their permeability category where red = low, orange = medium and green= high. The black solid line indicates the line of unity whereas black dashed and dotted lines indicate 2-fold and 3-fold of the unity line respectively.

Following quantification of parent compound in excreta of BDC rats, 9 NCEs were found to be directly eliminated in bile and/or urine in appreciable amounts (≥ 10% of the applied dose):

- NCEs 18, 19, 26, 52 and 71 with low permeability and NCEs 65, 66 and 69 with moderate permeability all indicated IVIVC disconnects in rat liver microsomes (and fresh rat hepatocytes) suggesting that hepatic metabolism is not a key elimination pathway. However, elimination of unchanged drug in bile and/or urine suggests a role for drug transporters in the overall clearance in rat. This was corroborated by *in vitro*

data as these 8 NCEs were also substrates of active uptake and/or biliary efflux in rat hepatocytes.

- NCE 43, a lipophilic base with a PSA of 83 Å^2 had a moderate permeability and the IVIVE of clearance indicated a good clearance prediction from rat liver microsomes (and fresh rat hepatocytes). Whilst the observed blood clearance in rat was low, metabolism appeared to be a key driving force in the overall elimination in rat. It was therefore surprising to see that this NCE was also directly eliminated in urine in appreciable amounts (16% of the dose directly excreted in urine). Looking more closely at the data generated for this NCE, it was found to be a substrate of active uptake and biliary efflux in rat hepatocytes, and Caco-2 data found in the internal database indicated an efflux ratio of 8 suggesting it is also a substrate of the P-gp transporter. Given the good IVIVC, it could be hypothesized that although NCE 43 undergoes first pass extraction in the liver, a portion of the parent compound in the systemic circulation directly enters the renal tubules from where it is directly excreted into the urine.

- With the exception of NCE 43, NCEs 26, 52, 65, 69 and 71, which were all directly eliminated into urine of BDC rats in appreciable amounts, were relatively lipophilic with cLogP <3, were not highly permeable and exhibited a disconnect in the IVIVC from rat liver microsomes (and fresh rat hepatocytes).

- NCEs qualitatively identified as substrates of biliary efflux from *in vitro* sandwich cultured rat hepatocyte studies appeared to be reasonably predictive of observed bile elimination in BDC rats. NCEs 18, 19, 26, 65, 66, 69 and 71 were all *in vitro* substrates of biliary efflux (BEI > 10%) which resulted in > 10% dose directly eliminated in bile. All seven of these NCEs had disconnects in the IVIVC from rat liver microsomes (and fresh rat hepatocytes) and were not highly permeable. NCEs 30 and 43 were exceptions to this and whilst identified as *in vitro* substrates of biliary efflux they were not directly eliminated in the bile of BDC rats in appreciable amounts. Although both NCEs were not highly permeable, the IVIVC from rat liver microsomes (and fresh rat hepatocytes) was good suggesting that hepatic metabolism was the key elimination process.

NCEs 24 and 41 were not directly eliminated in bile and or urine in appreciable amounts (≤ 10% of the applied dose): NCE 24 and 41 were highly permeable and

demonstrated good IVIVC from rat liver microsomes (and fresh rat hepatocytes) suggesting that hepatic metabolism is a key driver in the overall clearance.

In summary, the data from the BDC rat studies supports a disposition permeability hypothesis. When NCEs are not highly permeable and have a poor IVIVC from rat liver microsomes (which cannot be reconciled through the use of fresh rat hepatocytes) then transporter-mediated elimination of unchanged drug in excreta can be anticipated.

9 CHAPTER NINE: DISCUSSION

9.1 IVIVE methods for predicting hepatic metabolic clearance in rat

The primary aim of this PhD was to explore rat hepatobiliary disposition pathways of NCEs to elucidate causal relationships leading to the systematic under-prediction of drug clearance.

Optimisation of clearance is typically one of the more significant challenges in drug discovery which has driven the development of a range of robust *in vitro* tools and scaling methods. During early drug discovery, whilst liver microsomes and hepatocytes are common methods of choice, systematic under-prediction of drug clearance using conventional 'well-stirred' extrapolation methodology can result and has been well documented in the literature (Ito and Houston, 2004; Riley et al., 2005; Stringer et al., 2008).

Using a direct scaling method (all binding terms unaccounted for), comparison of observed rat blood clearance with predicted clearance from rat liver microsomes or fresh rat hepatocytes for the set of 77 NCEs used in this thesis indicated a high degree of under predictions. The predicted clearance of ~ 60% of the set of 77 NCEs was > 3-fold lower than observed clearance values. Statistical analysis of the predicted clearance data from both rat liver microsomes and fresh rat hepatocytes revealed that predictivity, precision and bias were marginally improved with rat liver microsomes which may be partly accounted for by permeability limited clearance in hepatocytes for a small number of NCEs.

IVIVE of rat clearance using well stirred models accounting for the fraction unbound in blood were investigated but precision of clearance predictions were significantly reduced in comparison to a direct scaling method and the *afe* increased from 5.1 to 28. These findings are consistent with Obach 1997 who also demonstrated that a direct scaling method provided a better estimate of *in vivo* clearance in comparison to the more conventional well stirred model accounting for fu_b or fu_p.

Correcting the blood binding terms with an ionisation factor, F_I (the ratio of unionized drug in blood to intracellular tissue water) was also investigated in this thesis but it did not improve the precision of rat clearance predictions in comparison to the well stirred model accounting only for fu_b. These findings are in contrast to data reported in the literature where the precision of human clearance predictions for marketed drugs were

improved when the blood binding terms were corrected for the F_I (Berezhkovskiy, 2011; Hallifax and Houston, 2012).

Accurate predictions of clearance can be made from microsomes and hepatocytes provided appropriate care and attention is made to the extrapolation methodology applied (Poulin et al., 2012a; Sohlenius-Sternbeck et al., 2012). However, methods more complex than direct scaling may also require additional fu_{inc}, fu_b and red blood cell partitioning data or in-depth knowledge of plasma protein binding partners or elimination pathways that are typically not available during early drug discovery. Additionally, these scaling methods may not be relevant for compounds with *in vivo* clearance approaching, or in excess of, liver blood flow.

It is also generally assumed that hepatic metabolic clearance is the key driver in elimination and transporter processes mediating drug uptake into hepatocytes and biliary efflux are neglected when conventional drug depletion protocols are employed. Hence alternative approaches were sought to explore hepatobiliary disposition of NCEs in rat and investigate the high incidence of under prediction of clearance.

9.2 Development and characterisation of a drug uptake model using cultured primary rat hepatocytes

Localisation of transporters on the sinusoidal membrane gives them a key 'gatekeeper' function in controlling the entry of substrates into the hepatocyte, access to metabolizing enzymes and excretory pathways (Shugarts and Benet, 2009). Primary hepatocytes, plated or in suspension, have become the system of choice for determining hepatic drug uptake (Menochet et al., 2012; Noe et al., 2007; Parker and Houston, 2008; Shimada et al., 2003). The hepatocyte uptake model should ideally be robust and amenable to assess if drug uptake into the hepatocyte could be a rate determining step in hepatic elimination for a diverse set of compounds.

Primary rat hepatocytes were successfully isolated from male Wistar rats and cultured based on a procedure reported in the literature (Menochet et al., 2012). Initial characterisation of the cultured primary rat hepatocyte uptake model indicated that uptake of d_8-taurocholic acid and pitavastatin (substrates of Oatp and Ntcp respectively) into rat hepatocytes at 37ºC was time and concentration dependent. The K_m and V_{max} for the uptake of pitavastatin in rat hepatocytes was 14µM and 1520 pmol/min/mg protein respectively which are consistent with kinetic parameters reported by Shimada et al, 2003

utilising an almost identical method with cultured primary rat hepatocytes and with kinetic parameters reported by Yabe et al, 2011 utilising primary rat hepatocytes in suspension.

In hepatocytes, passive processes are typically assessed in parallel incubations at 4ºC. Since membrane fluidity may decrease at lower temperatures, the effect of incubation temperature on the permeability in cultured primary rat hepatocytes was assessed for propranolol and alprenolol, compounds known to be highly permeable and highly absorbed in humans. For both drugs, the rate of uptake into cultured primary rat hepatocytes was linear and did not saturate at concentrations up to 100µM, although the rate of uptake at 37ºC was found to be approximately 2.5-fold higher compared to the uptake at 4ºC indicating that permeability is temperature dependent. These findings are consistent with Poirier et al, 2008 who demonstrated temperature dependent passive permeability in Chinese hamster ovary control cells and artificial membranes (PAMPA) and with Webborn et al, 2007 who reported temperature dependent uptake of propranolol in suspended rat hepatocytes. With this in mind, NCEs and marketed drugs were categorised as uptake substrates when the ratio of uptake rates at 37ºC and 4ºC was greater than the threshold value of 3.

Protocols in the literature describe primary hepatocyte uptake models that are varied in many respects including incubation time and concentration of compound used and whether cells are plated or used in suspension. It is known that isolated hepatocytes lose their cellular polarity rapidly upon isolation, resulting in the absence of the endogenous biochemical context for studying drug transport processes occurring at the sinusoidal and/or canalicular membrane domains (Hewitt et al., 2007). Loss of hepatocyte specific functions make this *in vitro* hepatocyte uptake model more static compared to the *in vivo* situation. Additionally, the assay validation indicated an incubation time of 120 seconds was a good compromise between a technically achievable incubation time and one in which the uptake velocity of uptake substrates, d_8-TCA and pitavastatin, had not yet reached equilibrium. Whilst not tested for each compound, it is assumed that cellular accumulation was measured within the linear uptake period to yield the initial uptake rate (pmol/min). Beyond this linear uptake period, which could potentially be shorter than 2 minutes for some compounds, efflux and metabolism could be become dominant so that cellular drug accumulation is no longer proportional to time (Pang, 2007). Loss of hepatocyte specific function and use of non-linear uptake periods are factors which may lead to an underestimation of the intrinsic uptake clearance.

9.3 Development and characterization of a drug efflux model using primary rat hepatocytes cultured in a sandwich configuration

Hepatobiliary excretion is an important route of elimination from the body for many drugs and several ABC efflux transporters, including Bcrp, Bsep, Mrp2 and P-gp located on the canalicular membrane, facilitate the energy dependent transport of substrates from the hepatocyte into bile against a concentration gradient. Following isolation, the polarity of hepatocytes is lost but can be regenerated following culturing of hepatocytes in a sandwich configuration between layers of collagen or Matrigel® (Liu et al., 1999a). This *in vitro* three-dimensional sandwich cultured rat hepatocyte (SCRH) model has been used for determining biliary efflux and predicting biliary clearance (Abe et al., 2008; Fukuda et al., 2008).

Primary rat hepatocytes were successfully isolated from male Wistar rats and cultured in a Collagen I/Matrigel® sandwich for 96 h based on a procedure reported in the literature (Wolf et al., 2008). The sandwich cultured rat hepatocytes exhibited liver-like cell morphology and formed bile canalicular networks consistent with the work of LeCluyse et al, 1994 who demonstrated the formation of extensive canalicular networks which acquired normal bile canalicular function in sandwich cultured rat hepatocytes. In this thesis, the functional activity of the bile canalicular network and excretory Mrp2 activity of SCRH was demonstrated with fluorescent carboxydichlorofluorescein (CDF) which was localised to both hepatocytes and bile canaliculi following pre-treatment with standard buffer. These findings are consistent with the work of LeCluyse et al, 1994 and other authors (Liu et al., 1999b; Nakakariya et al., 2012) who demonstrated normal bile canalicular function in SCRH with CDF.

Incubation of SCRH in Ca^{2+}-free buffer disrupts the barrier function of tight junctions and the bile network collapses. Biliary excretion of [^{3}H]TCA in SCRH was estimated as the difference in cellular accumulation in monolayers pre-incubated in standard buffer and $Ca^{2+/}Mg^{2+}$ buffer. Cellular accumulation of [^{3}H]TCA in standard buffer was approximately 5-fold higher than in $Ca^{2+/}Mg^{2+}$ buffer. These findings are consistent with Liu et al, 1999a who demonstrated that [^{3}H]TCA accumulation in SCRH in standard buffer was significantly higher than in Ca^{2+}-free buffer.

Initial characterisation studies in SCRH undertaken in this thesis evaluated the influence of extracellular matrix type, cell seeding density and plate well format on the cellular accumulation and biliary excretion index (BEI) of substrates of active uptake and

efflux in rat hepatocytes. The optimal protocol defined a seeding density of 250,000 freshly isolated rat hepatocytes per well in 12-well BioCoat™ Collagen I plates, an incubation time of 10 minutes and a substrate concentration of 5μM were suitable to generate a functional and robust rat *in vitro* model of biliary efflux. Biliary efflux index and predicted biliary clearance data generated for taurocholic acid, pitavastatin and rosuvastatin indicated good concordance with reference SCRH data in the literature (Abe et al., 2008; Wolf et al., 2008). Good assay reproducibility was also demonstrated for taurocholic acid, pitavastatin and propranolol. The coefficient of variation in BEI, $CL_{int,sec}$ and predicted biliary clearance from 3 individual experiments was acceptable at ≥ 35% for efflux substrates taurocholic acid and pitavastatin. Studies using propranolol, which is not a substrate of biliary efflux in SCRH, indicated acceptable assay variability in cellular accumulation with a 32% CV across 3 individual experiments.

The SCRH model was then used to screen a set of 14 marketed drugs. The biliary efflux index obtained in this thesis was found to be comparable to reference *in vitro* BEI data and predictive of observed biliary excretion (percentage dose excreted in rat bile) data reported in the literature. Although sandwich cultured rat hepatocyte models have been utilized for more than a decade to estimate rat CL_b (Abe et al., 2009; Fukuda et al., 2008; Liu et al., 1999a), in this thesis, the accurate prediction of biliary clearance was challenging and resulted in a high incidence of under prediction. These findings are consistent with Li et al, 2010 who reported that CL_b may be underestimated by 10-100-fold. The major caveats of this model which may limit the quantitative prediction of CL_b are (1) transporter protein expression changes after culturing and that absolute protein amount is a key determinant for biliary clearance (Li et al., 2009a), (2) the model lacks dynamic bile flow and (3) drug diffusion through the extracellular matrix layer may affect metabolic and transport rates (Treijtel et al., 2004). Use of universal and transporter-based correction factors to correct this underestimation have been reported in the literature for a small number of compounds with some success (Li et al., 2010; Zou et al., 2013), however, the sandwich cultured rat hepatocyte model is not yet sufficiently established or robust for the quantitative prediction of biliary clearance.

Cellular accumulation and biliary efflux data were generated in SCRH for the set of 77 NCEs which were categorized as substrates of biliary efflux if the BEI reached or exceeded the threshold value of 10%.

9.4 Analysis of single and multiple pathway IVIVE of hepatic clearance involving active transport

Drug elimination in the liver involves not only metabolism but also processes of uptake into the hepatocyte, biliary excretion and efflux back into the sinusoidal blood, which subsequently determine the hepatic elimination rate (Shitara et al., 2006). Single pathway analysis focusing on metabolism is often applied to predict *in vivo* hepatic clearance from *in vitro* data and can result in poor correlations between predicted and observed values (Ito and Houston, 2004; Riley et al., 2005). In this thesis, a range of IVIVE methods were applied to explore whether hepatic clearance of the set of 77 NCEs could be better predicted from the results of active uptake and biliary efflux assays in primary rat hepatocytes.

Following measurement of the rates of uptake at 37 and 4ºC in cultured primary rat hepatocytes, 41 of the 77 NCEs demonstrated uptake rate ratios (37:4ºC) ≥ 3 and were categorised as active uptake substrates. In general NCEs that were substrates of active uptake in cultured primary rat hepatocytes had lower permeability compared to the non-substrates (median P_{app} values of 5.3 x 10^{-6} cm/s and 12 x 10^{-6} cm/s for substrates and non-substrates respectively). For these 41 NCEs, single pathway IVIVE of clearance was improved using intrinsic uptake clearance ($CL_{int,upt}$) in comparison to metabolism ($CL_{int,met}$). The percentage of NCEs with predicted clearance falling outside 3-fold of observed clearance was reduced from 66 to 27% when $CL_{int,upt}$ was used suggesting uptake is a determinant factor for overall clearance, however IVIVC disconnects remain and limitations of the hepatocyte uptake method, as discussed in Section 9.2, could lead to an under estimation of $CL_{int,upt}$. Similar findings have been reported in the literature demonstrating improved predictions of rat hepatic clearance using $CL_{int,upt}$ for compounds with low permeability (Huang et al., 2012).

Biliary efflux in a sandwich cultured rat hepatocyte (SCRH) model was measured for the set of 77 NCEs. Forty four NCEs had a biliary efflux index (BEI) ≥ 10% and were categorised as biliary efflux substrates. For these 44 NCEs, single pathway IVIVE of clearance using intrinsic secretory clearance ($CL_{int,sec}$) offered no improvement compared to metabolism ($CL_{int,met}$). The SCRH model has previously been shown useful for studying hepatobiliary drug transport (Liu et al., 1999a; Swift et al., 2010). However, as previously discussed in Section 9.3, the SCRH model is not yet sufficiently established or robust for the quantitative prediction of biliary clearance which can be underestimated by 10-100-fold (Li et al., 2010). The initial validation studies in SCRH undertaken in this

thesis suggested a high incidence of under prediction of biliary clearance which may explain in part why *in vitro in vivo* disconnects in clearance remain for these substrates of biliary efflux.

Recent IVIVE methods reported in the literature have evolved to describe hepatic drug elimination as interplay of uptake into the hepatocyte, metabolism, biliary excretion and efflux back into the sinusoidal blood (Liu and Pang, 2005; Shitara et al., 2005). Whilst measurement of sinusoidal efflux was not undertaken in this thesis, the 3 remaining processes driving hepatic clearance were considered in multiple pathway IVIVE analysis and compared to single pathway analysis.

Clearance predictions for a sub-set of 27 NCEs from the original set of 77 NCEs which were identified as substrates of hepatic active uptake in cultured rat hepatocytes and for which passive uptake (uptake at 4°C) could also be measured, were further investigated. A multiple pathway IVIVE model accounting for $CL_{int,met}$, $CL_{int,act}$ and $CL_{int,pas}$ was used to derive predicted clearance values. In comparison to single pathway IVIVE based on $CL_{int,met}$, the multiple pathway IVIVE resulted in a reduction in the number of predicted clearance values falling outside 3-fold of observed clearance values (59% versus 37% respectively). However, a single pathway IVIVE based on total uptake intrinsic clearance ($CL_{int,upt}$) gave the best clearance predictions with 33% of predicted clearance values falling outside 3-fold of observed clearance values. In conclusion, accounting for active uptake in the IVIVE for these NCEs improves clearance predictions suggesting it is a key process influencing hepatic drug elimination.

Clearance predictions for a sub-set of 30 NCEs from the original set of 77 NCEs which were identified as substrates of biliary efflux in SCRH and for which active and/or passive uptake could also be measured in cultured rat hepatocytes, were further investigated. A multiple pathway IVIVE model accounting for metabolic ($CL_{int,met}$), active uptake ($CL_{int,act}$), passive uptake ($CL_{int,pas}$) and secretory ($CL_{int,sec}$) intrinsic clearances was used to derive predicted clearance values. In comparison to single pathway IVIVE based on metabolism, the multiple pathway IVIVE assuming biliary secretion is a primary elimination process (but also accounting for $CL_{int,act}$ and $CL_{int,pas}$) resulted in a reduction of the number of predicted clearance values falling outside 3-fold of observed clearance values (63% versus 40% respectively). However, the multiple pathway IVIVE assuming both metabolism and biliary secretion are primary elimination processes (but also accounting for $CL_{int,act}$ and $CL_{int,pas}$) appeared to be most predictive. The percent of predicted clearance values falling outside 3-fold of observed clearance values was lowest

at 33% which was consistent with the improved bias and precision of predictions. These data corroborate similar findings in the literature demonstrating that predictions of rat hepatic clearance were improved when both $CL_{int,upt}$ and $CL_{int,sec}$ were accounted for using a multiple pathway IVIVE method (Lundquist et al., 2014).

In summary, whilst improvements in clearance predictions were obtained when drug transport processes were included in the IVIVE method, more complex multiple pathway models only improved predictions for substrates of biliary efflux. None of these IVIVE methods resulted in a 1 to 1 correlation between predicted and observed clearances and limitations with the uptake and/or biliary efflux method used may be responsible. The data generated in this thesis suggests that the rat *in vitro* models of hepatocyte uptake and biliary efflux are fit for purpose to distinguish transporter substrates from non-substrates but accurate predictions using the intrinsic uptake or biliary efflux clearance values could not be obtained. Further characterisation of these systems and models with larger data sets may be warranted to gain confidence in their ability to predict clearance.

9.5 Structural and molecular analysis of hepatic drug transport

For more than two decades, prediction of clearance from microsomes and hepatocytes based on conventional 'well stirred' extrapolation methods have formed the cornerstone for the selection of drug candidates for further characterisation within the pharmaceutical industry. With the increasing awareness of the role of transporters in drug clearance, there are many instances where the conventional 'well stirred' assumptions are violated, particularly as chemistry efforts focused on reducing metabolic liability have led to an increased number of compounds which are reliant on non-cytochrome P450 dependent elimination routes. Hepatobiliary drug transport processes in rat were investigated in more detail for the set of 77 NCEs which highlighted drug uptake and efflux processes are determining factors for hepatic clearance. However, from a resource perspective, these studies would be difficult to integrate into early drug discovery screening strategies. It was of interest, therefore, to examine the potential for modelling hepatic drug transport based on structural and molecular analysis of the NCEs.

In vitro rat hepatocyte transport data and SMILES for the set of 77 NCEs and 14 marketed drugs were used to develop the Bayesian fragment-based classification model for the prediction of either active hepatic uptake or biliary efflux. The uptake and biliary efflux training sets indicated a clean division of substrates and non-substrates based on activity scores, with 5 or less outliers in each set. Using a 'leave one out' cross validation,

the predictive performance of the uptake and biliary efflux models were evaluated. Although the data sets used for the classification models were small and diversity in chemical space maybe somewhat limited, model predictivity was reasonably good. With the uptake model, more than 65% of compounds were correctly predicted as either substrates or non-substrates. However, for the biliary efflux model, whilst 70% of substrates were correctly predicted as substrates, only 30% of non-substrates were correctly predicted, suggesting this model may require further investment with larger and more structurally diverse compound sets in order to gain confidence in its predictivity.

Physicochemical molecular descriptors were generated from compound SMILES and imported together with measured physicochemical descriptors including permeability, solubility and pKa into SIMCA-P+ multivariate data analysis software to build discriminant *in silico* models to distinguish substrates from non-substrates of active uptake and biliary efflux in primary rat hepatocytes. As a first exploratory approach, descriptors were viewed in coefficient plots used to build PLS models to correlate substrates and non-substrates of active transport. The highest performance uptake and biliary efflux models were defined by 4 descriptors where drug uptake into cultured rat hepatocytes was favoured for NCEs with reduced permeability and increased hydrophilic volume. Biliary efflux in SCRH was favoured for NCEs with reduced permeability, reduced fraction unionized at pH10 and increased hydrogen bond donor volume. Both the uptake and biliary efflux models indicated good discrimination of substrates, as more than 80% were correctly predicted. However, there was a modest discrimination of non-substrates in either model with ~50% predicted correctly. This limited discrimination of non-substrates suggests these models are in need of refinement in order to improve predictions.

Whilst reports in the literature have demonstrated successful application of models to predict *in vivo* CL_b in rat (Chen et al., 2010; Varma et al., 2012; Yang et al., 2009), application of the structural and molecular properties models to predictively discriminate substrates and non-substrates of active transport from *in vitro* rat hepatocyte studies is novel. In general, both the structural and molecular properties models indicate potential utility in early drug discovery for predicting the likelihood that NCEs, to be tested further, or even prior to synthesis, are substrates of active drug transport processes in the liver. The information may be useful in deciding the most appropriate follow-up studies, especially if conventional IVIVE methods indicate poor predictions of clearance.

9.6 Investigation of the relationship between drug physicochemical properties and disposition pathways

In the research described in this thesis, the use of conventional IVIVE methods to predict drug clearance resulted in a high degree of under prediction. To investigate the potential causes for this, the relationships between predictability, active hepatic drug transport and physicochemical properties of the set of 77 NCEs was examined.

Analysis of the relationship between predictability of clearance and passive permeability indicated that the clearance of NCEs with high permeability was better predicted than the clearance of low or moderate permeability compounds using rat liver microsomes. A higher percentage of predicted clearances of NCEs with medium or low permeability fell outside 2-fold and 3-fold observed values compared to clearance of NCEs with high permeability. These findings are consistent with those of Huang et al, 2010 who demonstrated that rat clearance was dramatically under-predicted from rat liver microsomes for compounds with low passive permeability.

The impact of other physicochemical descriptors namely MW, cLogP, PSA and hydrogen bonding capacity on prediction of clearance was also assessed. Improved clearance predictions using conventional IVIVE methods were obtained for NCEs that were more lipophilic with reduced PSA and hydrogen bonding capacity. In general, these findings are aligned with principles of the BDDCS classification system (Wu and Benet, 2005) whereby lipophilic, permeable compounds are said to make good substrates for CYP enzymes and have hepatic metabolism as the major route of elimination. Conversely, metabolism is unlikely to be the key process driving hepatic elimination for more polar, less permeable compounds.

Relationships between passive permeability and active uptake into cultured primary rat hepatocytes or biliary efflux in SCRH was assessed for the NCE set. Whilst both substrates and non-substrates of active transport processes in rat hepatocytes displayed a wide and overlapping range of measured P_{app} values from MDCKII-LE cells, a trend towards lower P_{app} values was evident for substrates. Following binning of permeability P_{app} values into low, medium and high categories, the majority (> 50%) of non-substrates had high permeability, whereas fewer substrates had high permeability(< 25%), confirming an association between NCEs with lower permeability and active drug transport processes in rat hepatocytes. Additionally, a cooperative relationship between active uptake and biliary efflux processes in rat hepatocytes was observed for some

substrates. This is consistent with the role that uptake transporters have in modulating clearance by increasing the exposure of drug to elimination processes including biliary efflux transporters. Permeability also impacted this cooperative effect, since less than 20% of the NCEs that were substrates of both uptake and efflux in rat hepatocytes were highly permeable.

Given that metabolic clearance optimisation approaches in drug discovery commonly involve modulation of lipophilicity, a concurrent reduction in passive permeability could prove counterproductive. With lower lipophilicity and permeability, compounds may become substrates of hepatic uptake transporters, thereby increasing exposure to hepatic eliminating processes, potentially resulting in a higher extraction ratio.

9.7 Investigation of disposition permeability relationships in rat

The Biopharmaceutics Drug Disposition Classification System (BDDCS) centrally embraces solubility and permeability to allocate drugs into four classes categorising different routes of elimination in humans (Wu and Benet, 2005). In their research, Benet and co-workers recognised obvious disposition permeability relationships where BDDCS classes 1 and 2 compounds that are highly permeable compounds also tended to be highly metabolised whereas less permeable BDDCS class 3 and 4 compounds were primarily eliminated unchanged.

The original set of 77 NCEs were chosen to explore reasons for the high incidence of under prediction of clearance when conventional IVIVE methods and rat liver microsomes were used. Studies conducted in this thesis have demonstrated that passive permeability is a key property which influences whether a drug is actively transported into rat hepatocytes and the precision of clearance predictions from rat liver microsomes. It was of great interest to investigate if disposition permeability relationships played out *in vivo* in rat using mechanistic bile duct cannulated (BDC) rat studies and a small sub-set of original NCEs were selected to further explore the elimination pathways *in vivo*. The data obtained from these studies supported a disposition permeability hypothesis which is consistent with the BDDCS system concept reported by Wu and Bennet, 2005. When NCEs are not highly permeable and have a poor IVIVC of clearance from rat liver microsomes (which cannot be reconciled through the use of fresh rat hepatocytes) then transporter mediated elimination of unchanged drug in excreta can be anticipated.

10 CHAPTER TEN: CONCLUSIONS AND FUTURE WORK

The aim of this present study was to gain a more detailed understanding of the processes involved in rat hepatobiliary disposition of a set of 77 NCEs, for which ~60% were associated with > 3-fold under prediction of clearance using conventional 'well-stirred' extrapolation of intrinsic metabolic clearance. *In vitro* models of drug transport in rat hepatocytes were established to gain a more detailed understanding of the processes involved in rat hepatobiliary disposition for this set of 77 NCEs. The main findings and conclusions were:

- Characterisation of the model of drug uptake in cultured primary rat hepatocytes with marketed drugs indicated that this model was robust and functionally able to identify substrates of active hepatic drug uptake using a 2 minute incubation time. However a potential caveat which might preclude accurate estimation of intrinsic uptake clearance could be that the linear uptake period of NCEs could be shorter than the 2 minutes.
- Intrinsic uptake clearance in cultured rat hepatocytes was measured for the set of 77 NCEs and 41 were identified as substrates of active uptake (ratio of initial uptake at 37°C:4°C > 3).
- A model of biliary efflux in SCRH was established. Characterisation of this model with a marketed drug set indicated it was robust and functionally able to identify substrates of biliary efflux and that *In vitro* BEI data compared favourably with observed percentage dose excreted in rat bile. However, predicted biliary clearance was not a reliable estimate of observed biliary clearance in rat suggesting the SCRH model may not be sufficiently established for the quantitative prediction of biliary clearance.
- Biliary efflux index and intrinsic secretory clearance in SCRH was measured for the set of 77 NCEs and 44 were identified as substrates of biliary efflux (BEI >10%).

The next objectives of this research were to explore the use of extended clearance models to get an estimate of the effect of transporter involvement in hepatic disposition and to predict the overall hepatic clearance of a set of NCEs in rat. The main conclusions from these studies were:

- In general, for substrates of active uptake, clearance appeared to be better predicted from single pathway IVIVE using $CL_{int,upt}$ compared to $CL_{int,met}$. The data

suggested uptake is a rate determining step in hepatic elimination for some of these compounds. A more complex multiple pathway model did not appear to offer any major advantage to improve predictions over the simpler single pathway models accounting only for $CL_{int,upt.}$

- In general, for substrates of biliary efflux, clearance was not better predicted from single pathway IVIVE using $CL_{int,sec}$ compared to $CL_{int,met}$. However, improved predictions were obtained using more complex multiple pathway IVIVE models assuming either biliary efflux or biliary efflux and metabolism are primary processes driving hepatic clearance.
- None of these IVIVE methods resulted in a 1 to 1 correlation between predicted and observed clearances. The data generated in this thesis suggest that the rat *in vitro* models of hepatocyte uptake and biliary efflux are fit for purpose to identify transporter substrates from non-substrates but accurate predictions using the intrinsic uptake or biliary efflux clearance values could not be obtained.

Following on from this, it was of interest to identify relationships of active drug transport in rat hepatocytes with physicochemical, structural and molecular properties of the NCEs. The conclusions from these studies may be summarised as follows:

- Bayesian fragment-based classification models were established to predict active hepatic drug uptake and biliary efflux. The predictive performance of the uptake model was modest to good with ~70% of NCEs and marketed drugs correctly predicted as substrates and non-substrates. Whereas the predictive performance of the biliary efflux model was only modest. Around 70% of substrates were correctly identified but only 30% of non-substrates were correctly identified.
- *In silico* computational models were obtained for the prediction of active hepatic drug transport. The PLS models of drug uptake and biliary efflux showed modest discrimination between substrates and non-substrates with > 80% substrates and ~50% of non-substrates correctly predicted.
- The models used to predict the structural and molecular properties conferring active drug transport show promise for early drug discovery but further characterisation with larger, more diverse data sets may be warranted to gain confidence in their predictive capacity.

The final part of this study explored how passive permeability influences hepatobiliary drug disposition in rat. The main findings were that:

- NCEs possessing low or moderate permeability had a higher incidence of both under prediction of clearance using intrinsic metabolic clearance data and of active transport in rat hepatocytes. These data indicated the existence of disposition permeability relationships (DPR).
- Further supporting evidence of DPR was obtained from *in vivo* bile duct cannulated rat studies. When NCEs are not highly permeable and have a poor IVIVC from rat liver microsomes (which cannot be reconciled through the use of fresh rat hepatocytes), then transporter-mediated elimination of unchanged drug in excreta can be anticipated.

For drugs which undergo significant elimination of unchanged drug in excreta, it is highly unlikely that the traditional 'toolbox' to explore metabolic clearance will result in an improved IVIVC. Rather, reviewing physicochemical properties including lipophilicity and permeability and observing initial IVIVC from rat liver microsomes can provide insightful information on the likely disposition pathways of NCEs.

For new NCEs which are not highly permeable and show IVIVC disconnects in rat, the BDC rat *in vivo* model is a highly valuable tool for defining the key elimination pathways. If transporter–mediated elimination is prominent, then use of *in vitro* transporter assays using hepatocytes might be relevant to address high clearance issues within chemical scaffolds during drug discovery. Of particular interest is the identification of substrates of sinusoidal uptake transporters, since active uptake of drug into the hepatocyte together with drug removal by the eliminating process (metabolism or biliary) can generate a concentration gradient favourable to increase hepatobiliary drug elimination. The next steps will involve gaining more experience and confidence in predicting clearance with IVIVC models of hepatic elimination that incorporate permeability barriers.

The interplay of hepatic uptake, metabolism and biliary excretion was explored in this thesis with an aim of describing hepatic drug elimination. Further studies could investigate methods to measure passive and active sinusoidal efflux in rat hepatocytes to gain an understanding of the role of these processes in hepatobiliary disposition and in the prediction of hepatic clearance.

In addition, it would be of interest to explore the impact that incubation time has on the estimation of intrinsic uptake clearance for some of the NCEs, especially for those that are substrates of uptake transporters in rat hepatocytes. It was assumed that cellular accumulation was measured within a linear uptake period to yield initial uptake rates. However it is plausible that using a generic 2 minutes uptake incubation time, equilibrium between hepatocyte and medium concentration may have been reached sooner than for some NCEs and this could result in an underestimation of intrinsic uptake clearance.

The present study focused on exploring hepatobiliary drug disposition pathways using rat as the investigative species. There is no guarantee that clearance pathways relevant to rat will be similar to other preclinical species or even humans. Whilst pharmacokinetic data from dog or monkey is not readily available in early drug discovery, it is of interest to explore historical in-house IVIVC data in these species to see if disposition permeability relationships play out in higher species. Interrogating the IVIVC and diagnosing the cause of the disconnect can help identify appropriate tools and enhance confidence to predict human pharmacokinetic (PK) and disposition attributes. This is of particular importance, since data-driven opinions as to what the human pharmacokinetics would be prior to nomination of NCEs into the development phase have become the mainstay of drug discovery teams.

11 APPENDIX

11.1 *In vivo, in vitro* and *in silico* values for the NCE set

Table 11-1 *In vivo, in vitro* and *in silico* values for the NCE set

NCE # or drug name	*Total blood clearance in rat (ml/min/kg)	V_{ss} (L/kg)	Rat liver microsome CL_H (ml/min/kg)	Rat liver hepatocyte CL_H (ml/min/kg)	Fraction of unbound drug in rat plasma (fu_p)	Rat plasma stability (half-life, min)	MDCKII LE P_{app} (x 10^{-6} cm/s)	PAMPA: calculated % fraction absorbed	PAMPA P_e (x 10^{-6} cm/s)	Aqueous solubility pH 6.8 (mM)	Calculated LogP	Calculated LogD pH7.5	Calculated polar surface area (Å^2)	Calculated molecular weight	Calculated number of H-Bond Donors	Calculated number of H-bond Acceptors	Calculated % unionised species @ pH 7.4	Chemical class
NCE 1	86	5	48	113	nr	35	nr	100	200	< 0.01	3.2	3.2	72	389	2	5	100	N
NCE 2	28	2	123	63	0.01	>120	12	99	200	0.14	3.5	4.2	62	391	2	4	100	N
NCE 3	109	4	118	56	0.07	>120	8.8	31	2	0.03	4.3	2.6	83	504	1	7	100	N
NCE 4	11	2	138	69	0.04	>120	11	50	8	0.24	2.8	2.3	106	499	3	8	100	N
NCE 5	200	nr	90	140	nr	5	13	99	126	0.02	4.2	2.3	84	421	1	7	100	N
NCE 6	23	9	90	55	nr	>120	0.2	65	6	< 0.01	4.9	5.3	69	455	0	6	44	B
NCE 7	143	3	84	11	0.17	>120	20	100	398	0.56	2.0	2.5	68	254	1	5	100	B
NCE 8	22	3	80	37	0.01	>120	34	70	10	0.05	4.4	1.9	83	464	2	8	50	B
NCE 9	48	4	21	7	0.29	>120	32	95	50	0.01	1.3	0.0	132	402	3	11	100	B
NCE 10	21	5	25	7	0.53	>120	15	35	1	> 1	0.7	1.6	97	442	2	8	100	B
NCE 11	200	nr	95	132	0.10	>120	4.8	99	126	< 0.01	4.0	4.4	45	413	1	4	100	B
NCE 12	28	7	22	19	0.05	>120	1.2	32	1	0.58	4.2	1.9	100	477	3	7	6	B

NCE # or drug name	*Total blood clearance in rat (ml/min/kg)	V_{ss} (L/kg)	Rat liver microsome CL_H (ml/min/kg)	Rat liver hepatocyte CL_H (ml/min/kg)	Fraction of unbound drug in rat plasma (fu_p)	Rat plasma stability (half-life, min)	MDCKII LE P_{app} (x 10^{-6} cm/s)	PAMPA: calculated % fraction absorbed	PAMPA P_e (x 10^{-6} cm/s)	Aqueous solubility pH 6.8 (mM)	Calculated LogP	Calculated LogD pH7.5	Calculated polar surface area (Å^2)	Calculated molecular weight	Calculated number of H-Bond Donors	Calculated number of H-bond Acceptors	Calculated % unionised species @ pH 7.4	Chemical class
NCE 13	113	75	71	105	0.10	>120	1.0	78	13	< 0.01	4.4	4.1	72	419	2	5	100	N
NCE 14	27	2	108	47	0.01	>120	8.7	30	1	0.37	3.7	3.0	95	409	4	7	100	N
NCE 15	172	8	31	7	0.28	>120	3.4	35	0	0.08	1.1	1.3	118	420	3	9	67	B
NCE 16	160	12	15	38	0.02	>120	5.9	99	126	0.01	3.3	3.8	96	510	1	8	100	N
NCE 17	51	6	46	7	0.35	>120	16	33	0	0.04	-1.5	0.4	140	387	3	11	100	B
NCE 18	200	nr	37	28	0.30	>120	1.6	16	0	> 1	3.7	1.6	124	527	2	9	0	A
NCE 19	200	nr	6	14	0.10	>120	2.0	55	6	> 1	3.2	1.8	133	548	2	10	0	A
NCE 20	53	1	43	7	0.36	>120	1.3	28	0	0.31	1.1	0.9	126	468	3	9	99	B
NCE 21	200	30	10	40	0.10	>120	nr	52	4	< 0.01	4.6	4.6	72	421	2	5	100	N
NCE 22	61	5	6	7	0.19	>120	7.4	50	0	nr	1.5	1.7	114	387	3	8	91	B
NCE 23	187	4	123	37	0.02	>120	17	73	13	0.19	3.5	3.3	113	486	3	8	100	N
NCE 24	91	8	60	33	0.03	>120	12	99	200	0.01	2.3	1.8	91	350	2	7	83	B
NCE 25	89	3	23	35	0.27	>120	3.9	27	0	< 0.01	1.9	2.2	135	526	3	10	94	B
NCE 26	174	3	14	7	nr	>120	0.6	32	0	0.81	0.2	0.4	126	451	3	9	99	B
NCE 27	200	5	32	7	0.37	>120	11	58	5	> 1	0.8	1.3	100	450	1	8	99	B
NCE 28	95	5	72	110	0.01	>120	22	95	50	< 0.01	3.8	3.6	88	406	3	6	99	B
NCE 29	42	3	35	24	0.46	>120	23	92	32	> 1	1.8	1.8	94	301	0	6	100	B

NCE # or drug name	*Total blood clearance in rat (ml/min/kg)	V_{ss} (L/kg)	Rat liver microsome CL_H (ml/min/kg)	Rat liver hepatocyte CL_H (ml/min/kg)	Fraction of unbound drug in rat plasma (fu_p)	Rat plasma stability (half-life, min)	MDCKII LE P_{app} (x 10^{-6} cm/s)	PAMPA: calculated % fraction absorbed	PAMPA P_e (x 10^{-6} cm/s)	Aqueous solubility pH 6.8 (mM)	Calculated LogP	Calculated LogD pH7.5	Calculated polar surface area ($Å^2$)	Calculated molecular weight	Calculated number of H-Bond Donors	Calculated number of H-bond Acceptors	Calculated % unionised species @ pH 7.4	Chemical class
NCE 30	40	15	45	57	0.05	>120	5.9	51	3	0.02	2.4	2.7	114	455	3	8	67	B
NCE 31	200	6	119	119	0.10	>120	nr	22	0	0.02	4.5	3.1	113	590	1	11	99	B
NCE 32	24	9	6	7	0.10	>120	0.4	76	13	< 0.01	4.8	4.4	100	502	2	8	100	B
NCE 33	23	2	22	7	0.10	>120	20	84	20	< 0.01	4.7	3.4	111	502	2	9	100	B
NCE 34	62	1	54	21	0.17	>120	2.6	25	0	0.06	2.5	2.1	126	499	3	9	100	B
NCE 35	68	2	14	19	0.37	>120	29	80	8	> 1	1.1	1.0	90	322	1	7	99	B
NCE 36	200	nr	35	32	0.10	>120	nr	24	0	< 0.01	4.6	4.1	110	453	3	8	100	B
NCE 37	89	9	53	7	0.10	>120	nr	45	5	0.17	7.1	4.2	74	563	1	6	0	A
NCE 38	28	4	6	8	0.07	>120	nr	41	4	0.08	3.9	4.0	127	559	0	11	100	B
NCE 39	37	3	17	7	0.29	>120	6.2	22	1	0.26	1.6	2.1	135	538	3	10	100	B
NCE 40	24	18	6	10	0.05	>120	1.1	28	1	> 1	4.1	2.0	81	488	3	7	0	B
NCE 41	35	6	6	7	0.17	>120	16	99	398	0.15	2.6	1.6	79	388	0	7	100	B
NCE 42	27	5	23	14	0.06	>120	19	100	316	0.27	3.1	2.0	79	399	0	7	100	B
NCE 43	25	6	21	16	0.06	>120	5.3	61	8	0.94	4.5	2.0	83	503	3	7	1	B
NCE 44	70	14	38	56	0.24	>120	13	99	200	> 1	3.9	2.4	71	346	3	5	7	B
NCE 45	21	6	6	7	0.28	>120	0.6	19	0	> 1	4.6	2.2	98	516	2	8	0	B
NCE 46	44	3	17	29	0.26	>120	28	83	20	> 1	4.6	3.0	107	554	2	9	100	B

NCE # or drug name	*Total blood clearance in rat (ml/min/kg)	V_{ss} (L/kg)	Rat liver microsome CL_H (ml/min/kg)	Rat liver hepatocyte CL_H (ml/min/kg)	Fraction of unbound drug in rat plasma (fu_p)	Rat plasma stability (half-life, min)	MDCKII LE P_{app} (x 10^{-6} cm/s)	PAMPA: calculated % fraction absorbed	PAMPA P_e (x 10^{-6} cm/s)	Aqueous solubility pH 6.8 (mM)	Calculated LogP	Calculated LogD pH7.5	Calculated polar surface area (Å^2)	Calculated molecular weight	Calculated number of H-Bond Donors	Calculated number of H-bond Acceptors	Calculated % unionised species @ pH 7.4	Chemical class
NCE 47	22	5	26	7	0.31	>120	0.7	18	0	> 1	5.0	2.1	98	518	2	8	0	B
NCE 48	33	16	21	18	0.03	>120	5.8	79	13	0.06	1.9	-0.3	113	399	4	8	96	Z
NCE 49	67	2	15	36	0.04	>120	8.2	24	0	0.22	1.2	3.2	92	449	2	8	100	N
NCE 50	26	2	6	7	0.20	>120	3.3	45	3	0.81	1.4	0.2	131	453	4	9	100	N
NCE 51	21	8	25	51	0.10	>120	5.6	64	10	0.03	4.5	5.6	103	612	3	8	5	B
NCE 52	200	nr	44	11	0.74	>120	0.9	12	0	0.98	2.8	2.1	95	509	1	9	100	N
NCE 53	103	20	6	13	0.03	>120	4.6	67	10	0.10	4.0	2.7	132	545	4	10	1	B
NCE 54	142	29	31	10	nr	>120	3.9	47	1	> 1	3.1	-1.3	152	381	6	10	3	B
NCE 55	200	4	17	9	0.21	>120	0.7	44	3	0.27	2.4	2.2	101	491	2	10	98	B
NCE 56	87	2	7	7	0.80	>120	1.3	34	0	0.56	-0.4	0.1	146	476	3	11	100	B
NCE 57	102	5	33	24	0.03	>120	9.8	14	0	0.06	2.1	4.4	129	561	4	9	99	B
NCE 58	69	13	22	7	0.48	112	0.2	41	0	> 1	0.5	-1.7	133	413	5	9	5	Am
NCE 59	109	4	39	10	0.23	>120	1.0	30	3	0.56	1.3	3.8	142	562	4	10	100	B
NCE 60	134	4	45	35	nr	>120	19	33	2	0.01	1.0	2.3	130	481	2	10	99	B
NCE 61	87	3	30	13	0.10	>120	23	37	0	0.01	-0.1	0.3	141	425	3	10	100	B
NCE 62	200	10	41	120	0.01	>120	23	25	0	< 0.01	3.1	3.7	123	429	4	9	100	B
NCE 63	109	14	6	7	0.80	>120	1.5	53	2	> 1	-0.1	-2.0	122	357	4	9	1	B

NCE # or drug name	*Total blood clearance in rat (ml/min/kg)	V_{ss} (L/kg)	Rat liver microsome CL_H (ml/min/kg)	Rat liver hepatocyte CL_H (ml/min/kg)	Fraction of unbound drug in rat plasma (fu_p)	Rat plasma stability (half-life, min)	MDCKII LE P_{app} (x 10^{-6} cm/s)	PAMPA: calculated % fraction absorbed	PAMPA P_e (x 10^{-6} cm/s)	Aqueous solubility pH 6.8 (mM)	Calculated LogP	Calculated LogD pH7.5	Calculated polar surface area ($Å^2$)	Calculated molecular weight	Calculated number of H-Bond Donors	Calculated number of H-bond Acceptors	Calculated % unionised species @ pH 7.4	Chemical class
NCE 64	106	2	6	7	0.01	>120	2.3	34	1	> 1	1.6	0.0	101	409	2	6	0	A
NCE 65	73	2	10	12	0.01	>120	7.5	51	4	> 1	1.8	0.4	92	417	2	7	0	Z
NCE 66	100	13	6	7	0.01	>120	7.3	52	6	0.91	4.9	1.2	120	565	2	11	0	Z
NCE 67	81	4.9	11	7	0.02	>120	3.5	36	0	0.03	0.9	0.5	121	373	4	8	0	Z
NCE 68	114	13	37	7	0.55	>120	0.9	42	2	> 1	1.8	1.2	101	421	3	8	3	B
NCE 69	166	3	16	7	0.32	>120	5.6	44	3	0.04	0.9	0.8	132	415	3	9	100	B
NCE 70	200	nr	8	7	0.00	>120	nr	28	1	0.02	0.4	0.9	145	443	3	10	100	B
NCE 71	147	4	35	9	0.40	>120	3.0	36	0	0.25	2.5	1.9	103	397	3	9	83	B
NCE 72	200	nr	23	7	0.27	>120	3.8	57	0	0.33	2.4	2.3	90	298	3	7	100	N
NCE 73	157	5	14	7	0.34	>120	1.8	40	0	0.14	2.3	1.9	98	327	3	7	100	N
NCE 74	45	4	6	7	0.19	>120	5.4	32	2	0.12	2.1	-0.3	118	465	2	9	100	B
NCE 75	116	4	6	7	0.09	>120	19	67	8	0.04	2.5	2.0	101	428	3	8	100	B
NCE 76	70	3	27	9	0.22	>120	14	31	0	0.14	2.6	3.0	87	367	2	7	100	N
NCE 77	117	26	23	7	0.56	>120	4.8	0	1	> 1	0.8	0.7	130	544	2	11	3	B
atorvastatin	nr	nr	30	27	0.05	>120	5.3	57	8	> 1	4.5	3.1	114	559	4	7	0	A
d8-TCA	nr	nr	15	7	0.80	>120	nr	31	3	> 1	0.0	-2.0	144	516	5	8	0	A
digoxin	nr	nr	8	66	0.32	>120	nr	5	0	0.07	1.4	0.2	203	781	6	14	100	N

NCE # or drug name	*Total blood clearance in rat (ml/min/kg)	V_{ss} (L/kg)	Rat liver microsome CL_H (ml/min/kg)	Rat liver hepatocyte CL_H (ml/min/kg)	Fraction of unbound drug in rat plasma (fu_p)	Rat plasma stability (half-life, min)	MDCKII LE P_{app} (x 10^{-6} cm/s)	PAMPA: calculated % fraction absorbed	PAMPA P_e (x 10^{-6} cm/s)	Aqueous solubility pH 6.8 (mM)	Calculated LogP	Calculated LogD pH7.5	Calculated polar surface area (Å^2)	Calculated molecular weight	Calculated number of H-Bond Donors	Calculated number of H-bond Acceptors	Calculated % unionised species @ pH 7.4	Chemical class
d-pen-enkephalin	nr	nr	7	7	0.19	>120	1.2	nd	nd	nr		-0.2					0	Z
erythromycin	nr	nr	22	16	0.49	>120	0.4	51	8	> 1	1.6	0.5	194	734	5	14	5	B
fexofenadine	nr	nr	6	7	0.13	>120	1.8	18	1	1.0	2.0	0.5	81	502	3	5	0	Z
fluvastatin	nr	nr	24	7	0.10	>120	14	98	32	0.6	4.0	2.0	85	411	3	5	0	A
methotrexate	nr	nr	10	7	0.24	>120	0.3	28	1	> 1	-0.5	-0.2	211	454	7	13	0	Z
pitavastatin	nr	nr	15	18	0.10	>120	13	43	3	nr	3.6	-6.8	91	421	3	5	0	Z
pravastatin	nr	nr	11	2	0.26	>120	0.2	50	5	>1	2.0	0.5	124	425	4	7	0	A
propranolol	nr	nr	96	126	0.14	>120	24	100	398	>1	2.8	1.0	41	259	2	3	1	B
quinidine	nr	nr	110	106	0.36	>120	15	98	100	> 1	2.8	2.1	46	324	1	4	5	B
rosuvastatin	nr	nr	17	19	0.04	>120	0.9	16	0	0.77	1.9	-1.1	141	482	3	9	0	A
valsartan	nr	nr	6	7	0.02	>120	0.4	85	13	0.80	4.9	0.1	112	436	2	8	0	A

*Total blood clearance capped at 200 ml/min/kg, Nr: no result, A: acid, Am: ampholyte B: base, N: neutral, Z: zwitterion

11.2 Physicochemical properties of the marketed drug set

A small set of 14 marketed drugs were compiled for validating *in vitro* transporter studies. The distribution in chemical class in this marketed drug set is displayed in the pie chart below (Figure 11-1). Acids are the most common class (43%), followed by zwitterions (29%), bases (21%) and neutral compounds (7%).

Figure 11-1 Distribution of chemical class for the marketed drug set used to explore rat IVIVE of drug clearance

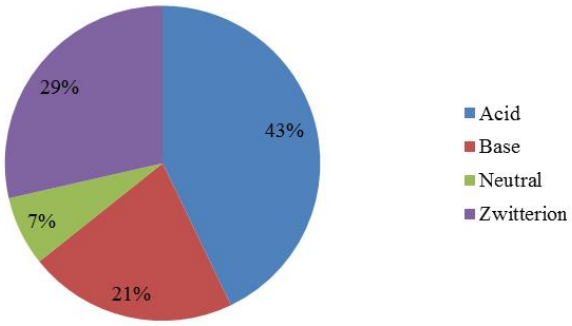

The range in lipohilicity (cLogP) and molecular weights for the marketed drug set are illustrated in Figure 11-2. The median calculated LogP was 2.0 and the median molecular weight was 468.

Figure 11-2 Lipophilicity and molecular weight range for the marketed drug set

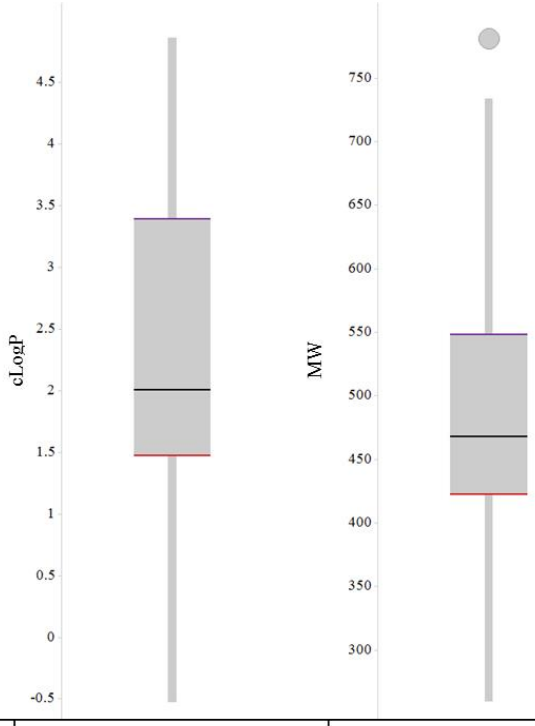

	cLogP	MW
Count	14	14
Median	2.0	468
Outliers	0	1

Box plot illustrating the range of lipophilicity (cLogP) values and molecular weights for the marketed drug set. The purple and red horizontal lines represent the third quartile and first quartile respectively and the vertical lines (whiskers) extending from the boxes indicate variability outside the upper and lower quartiles. The grey circles represent outliers. Solid horizontal black lines indicate the median values (second quartile).

11.2.1.1 Physicochemical property space of the marketed drug set

The set of 14 marketed drugs were projected onto ChemMAP, a tool to navigate the physicochemical property space of bioactive compounds, to determine their relative position in the score plot. Whilst they are few in number, the marketed drugs occupy a divergent property space.

Figure 11-3 Physiochemical property space for the marketed drug set

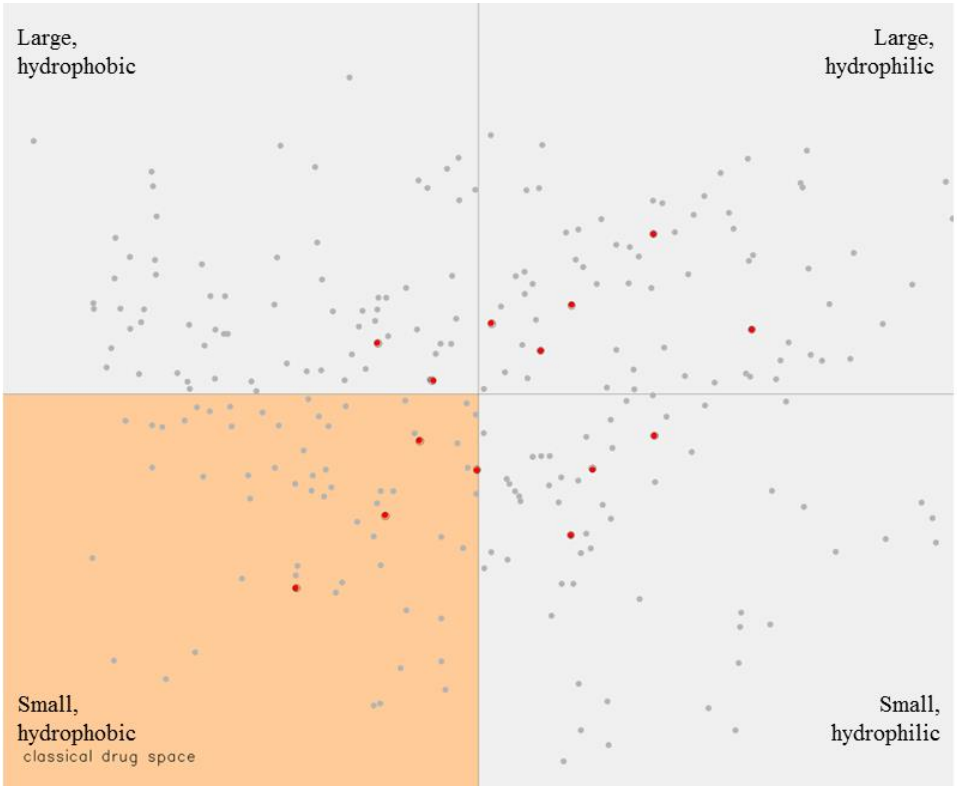

Physicochemical property space occupied by the marketed drug set. Red dots represent the 14 marketed drugs and grey dots represent background ChemMAP compounds. Classical drug space denotes the property space held by traditional small molecule drugs approved prior to 2002.

11.3 Transport of marketed drugs across MDCKII LE cells

Apparent permeability of NCEs was assessed using a subpopulation of low efflux cells from MDCKII wild type cells. The low efflux sub population of MDCKII cells (MDCKII LE) was previously identified and validated in-house using methodology detailed in Section 2.10.1, which is similar to that previously reported in the literature (Di et al., 2011).

The passive permeability (P_{app}) of 13 marketed drugs were measured in MDCKII LE cells and compared to MDCKII and MDCKII LE P_{app} data found in the literature (Table 11-2 and Figure 11-4. Eleven of these marketed drugs had previously been classified in the literature as having either high or low absorption based on their human intestinal absorption. As a guide, the passive permeability measured in MDCKII LE cells was referred to as high for P_{app} values $\geq 10x10^{-6}$ cm/s and low for P_{app} values $< 5x10^{-6}$ cm/s.

The assay reproducibility of P_{app} values for three QC standards, nadolol, furosemide and propranolol was assessed in MDCKII LE cells and is presented in Table 11-3. The coefficient of variation from 3 individual experiments was ≥ 20% for all 3 compounds indicating good assay robustness.

Table 11-2 Permeability results for marketed drugs with MDCKII LE cells and comparison to reference MDCKII P_{app} data and human intestinal absorption

			Reference data[#]			
	MDCKII LE P_{app} ($x10^{-6}$ cm/s)		MDCKII P_{app} ($x10^{-6}$ cm/s)		Human intestinal absorption	
Drugs	Mean	S.D.	Mean	S.D.	%	Rank
chlorpromazine	12	0.8	4.1	0.4	100	High
cimetidine	1.8	0.4	1.4	0.1	64	Low
furosemide	3.4	0.5	2.0	0.4	61	Low
labetalol	20	1.0	7.3	2.2	95	High
metoprolol	30	1.3	12	0.1	95	High
nadolol	0.7	0.03	0.8	0.1	35	Low
paroxetine	12	1.0	6.1	0.3	n.d.	
prazosin	14	1.0	11	2.2	100	High
propranolol	24	0.5	17	0.7	90	High
quinidine	15	1.0	13	2.7	80	High
ranitidine	0.9	0.1	1.0	0.0	50	Low
triprolidine	30	0.7	15	3.3	n.d.	
verapamil	17	3.5	10	0.2	95	High

[#]Reference data sourced from literature: P_{app} data generated in wild type MDCKII or MDCKII LE cells (Di et al., 2011; Feng et al., 2008; Irvine et al., 1999) and human intestinal data (Irvine et al., 1999; Thiel-Demby et al., 2009; Zhao et al., 2001; Zhu et al., 2002), n.d.: no data found in literature

Figure 11-4 Comparison of MDCKII LE P_{app} values with reference data for 13 marketed drugs

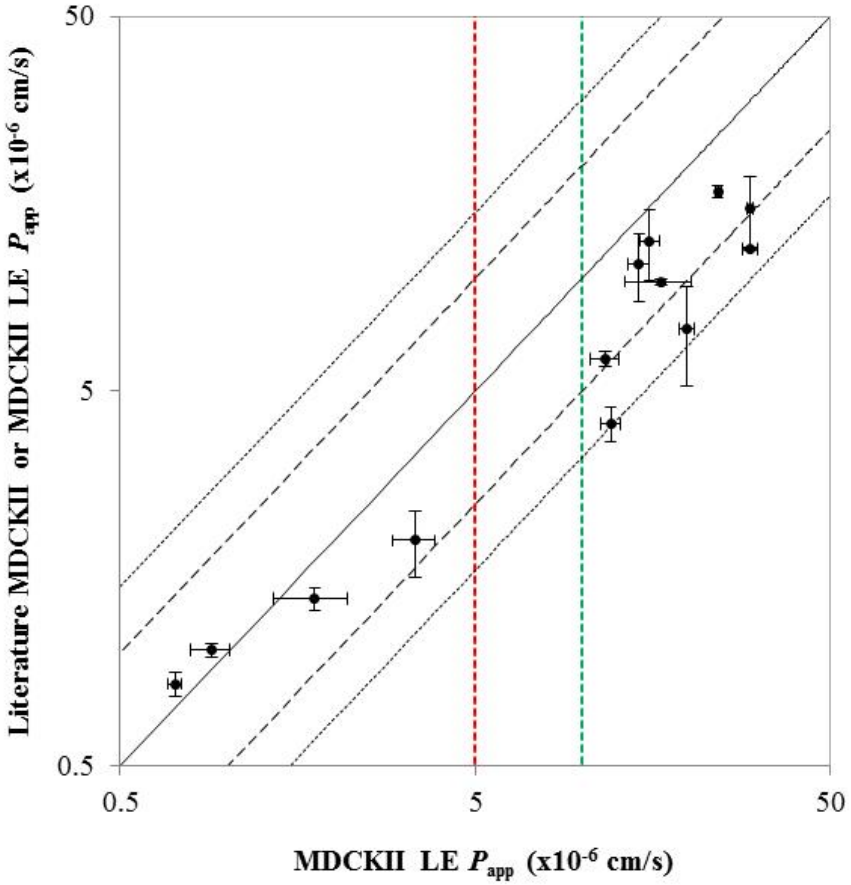

Correlation of MDCKII LE cellular permeability data with reference MDCKII or MDCKII LE P_{app} data for 13 marketed drugs presented in the literature (resultant $r^2 = 0.80$). The solid black line represents the line of unity whilst dashed and dotted black lines denote 2-fold and 3-fold deviation from the line of unity respectively. For reference, the P_{app} range used to classify low and high absorption potential is indicated by the red and green dashed vertical respectively (low < 5 x 10^{-6} and high ≥ 10 x 10^{-6} cm/s).

Table 11-3 Reproducibility of P_{app} values and percentage assay recovery of quality control standards in MDCKII LE cells

Drug	Experiment #	P_{app} (x10^{-6} cm/s)		% Recovery	
		Mean	S.D.	Mean	S.D.
nadolol	1	0.7	0.0	98	10
	2	0.5	0.2	98	2
	3	0.5	0.1	98	3
	Overall Mean	0.6		98	
	Overall SD	0.1		0.1	
	% CV	20		0.1	
furosemide	1	3.4	0.5	93	3.0
	2	3.0	0.6	84	4.4
	3	2.5	0.4	99	10
	Overall Mean	3.0		92	
	Overall SD	0.4		8	
	% CV	15		9	
propranolol	1	24	0.5	77	6
	2	25	6.1	80	10
	3	31	2.7	78	4
	Overall Mean	27		79	
	Overall SD	3.6		1.6	
	% CV	13		2.0	

Nadolol, furosemide and propranolol were included as QC standards in the MDCKII LE assay. On each experimental occasion, mean (± S.D.) P_{app} and % recovery data were calculated from 3 replicates. Data from 3 individual experiments were used to calculate the overall inter-assay mean (± S.D.) and % coefficient of variation (%CV) values of P_{app} and % recovery.

12 REFERENCES

Abe, K., A.S. Bridges, and K.L. Brouwer. 2009. Use of sandwich-cultured human hepatocytes to predict biliary clearance of angiotensin II receptor blockers and HMG-CoA reductase inhibitors. *Drug metabolism and disposition: the biological fate of chemicals*. 37:447-452.

Abe, K., A.S. Bridges, W. Yue, and K.L. Brouwer. 2008. In vitro biliary clearance of angiotensin II receptor blockers and 3-hydroxy-3-methylglutaryl-coenzyme A reductase inhibitors in sandwich-cultured rat hepatocytes: comparison with in vivo biliary clearance. *The Journal of pharmacology and experimental therapeutics*. 326:983-990.

Adson, A., P.S. Burton, T.J. Raub, C.L. Barsuhn, K.L. Audus, and N.F. Ho. 1995. Passive diffusion of weak organic electrolytes across Caco-2 cell monolayers: uncoupling the contributions of hydrodynamic, transcellular, and paracellular barriers. *Journal of pharmaceutical sciences*. 84:1197-1204.

Adson, A., T.J. Raub, P.S. Burton, C.L. Barsuhn, A.R. Hilgers, K.L. Audus, and N.F. Ho. 1994. Quantitative approaches to delineate paracellular diffusion in cultured epithelial cell monolayers. *Journal of pharmaceutical sciences*. 83:1529-1536.

Akashi, M., A. Tanaka, and H. Takikawa. 2006. Effect of cyclosporin A on the biliary excretion of cholephilic compounds in rats. *Hepatology research : the official journal of the Japan Society of Hepatology*. 34:193-198.

Amidon, G.L., H. Lennernas, V.P. Shah, and J.R. Crison. 1995. A theoretical basis for a biopharmaceutic drug classification: the correlation of in vitro drug product dissolution and in vivo bioavailability. *Pharmaceutical research*. 12:413-420.

Annaert, P., Swift, B., Jin, K. L. and Brouwer, K. L. R. 2007. Drug transport in the liver. In: Goufeng, Y and Morris, M. E. eds. *Drug Transporters: Molecular characterisation and role in drug disposition*. New Jersey: Wiley, pp.359-410.

Annaert, P., Z.W. Ye, B. Stieger, and P. Augustijns. 2010. Interaction of HIV protease inhibitors with OATP1B1, 1B3, and 2B1. *Xenobiotica; the fate of foreign compounds in biological systems*. 40:163-176.

Anzai, N., Y. Kanai, and H. Endou. 2006. Organic anion transporter family: current knowledge. *Journal of pharmacological sciences*. 100:411-426.

Austin, R.P., P. Barton, S.L. Cockroft, M.C. Wenlock, and R.J. Riley. 2002. The influence of nonspecific microsomal binding on apparent intrinsic clearance, and its prediction from physicochemical properties. *Drug metabolism and disposition: the biological fate of chemicals*. 30:1497-1503.

Bell, L.C., and J. Wang. 2012. Probe ADME and test hypotheses: a PATH beyond clearance in vitro-in vivo correlations in early drug discovery. *Expert opinion on drug metabolism & toxicology*. 8:1131-1155.

Berezhkovskiy, L.M. 2011. The corrected traditional equations for calculation of hepatic clearance that account for the difference in drug ionization in extracellular and intracellular tissue water and the corresponding corrected PBPK equation. *Journal of pharmaceutical sciences*. 100:1167-1183.

Boxenbaum, H. 1980. Interspecies variation in liver weight, hepatic blood flow, and antipyrine intrinsic clearance: extrapolation of data to benzodiazepines and phenytoin. *Journal of pharmacokinetics and biopharmaceutics*. 8:165-176.

Camenisch, G., and K. Umehara. 2012. Predicting human hepatic clearance from in vitro drug metabolism and transport data: a scientific and pharmaceutical perspective for assessing drug-drug interactions. *Biopharmaceutics & drug disposition*. 33:179-194.

Chen, C., and G.M. Pollack. 1997. Extensive biliary excretion of the model opioid peptide [D-PEN2,5] enkephalin in rats. *Pharmaceutical research*. 14:345-350.

Chen, Y., K. Cameron, A. Guzman-Perez, D. Perry, D. Li, and H. Gao. 2010. Structure-pharmacokinetic relationship of in vivo rat biliary excretion. *Biopharmaceutics & drug disposition*. 31:82-90.

Choi, Y.H., and A.M. Yu. 2014. ABC transporters in multidrug resistance and pharmacokinetics, and strategies for drug development. *Current pharmaceutical design*. 20:793-807.

Cruciani, G., M. Pastor, and W. Guba. 2000. VolSurf: a new tool for the pharmacokinetic optimization of lead compounds. *European journal of pharmaceutical sciences : official journal of the European Federation for Pharmaceutical Sciences*. 11 Suppl 2:S29-39.

Davies, B., and T. Morris. 1993. Physiological parameters in laboratory animals and humans. *Pharmaceutical research*. 10:1093-1095.

Dekeyser, J.G., Shou, M. 2012. Species differences in drug-metabolising enzymes. In: Lyubimov, A.V. ed. *Encyclopedia of Drug Metabolism and Interactions, 6-Volume Set, first edition.* New Jersey: Wiley, p.p. 1-38.

Di, L., C. Whitney-Pickett, J.P. Umland, H. Zhang, X. Zhang, D.F. Gebhard, Y. Lai, J.J. Federico, 3rd, R.E. Davidson, R. Smith, E.L. Reyner, C. Lee, B. Feng, C. Rotter, M.V. Varma, S. Kempshall, K. Fenner, A.F. El-Kattan, T.E. Liston, and M.D. Troutman. 2011. Development of a new permeability assay using low-efflux MDCKII cells. *Journal of pharmaceutical sciences*. 100:4974-4985.

Doring, B., T. Lutteke, J. Geyer, and E. Petzinger. 2012. The SLC10 carrier family: transport functions and molecular structure. *Current topics in membranes*. 70:105-168.

Faber, K.N., M. Muller, and P.L. Jansen. 2003. Drug transport proteins in the liver. *Advanced drug delivery reviews*. 55:107-124.

Faller, B., G. Ottaviani, P. Ertl, G. Berellini, and A. Collis. 2011. Evolution of the physicochemical properties of marketed drugs: can history foretell the future? *Drug discovery today*. 16:976-984.

Feng, B., J.B. Mills, R.E. Davidson, R.J. Mireles, J.S. Janiszewski, M.D. Troutman, and S.M. de Morais. 2008. In vitro P-glycoprotein assays to predict the in vivo interactions of P-glycoprotein with drugs in the central nervous system. *Drug metabolism and disposition: the biological fate of chemicals*. 36:268-275.

Fenner, K.S., H.M. Jones, M. Ullah, S. Kempshall, M. Dickins, Y. Lai, P. Morgan, and H.A. Barton. 2012. The evolution of the OATP hepatic uptake transport protein family in DMPK sciences: from obscure liver transporters to key determinants of hepatobiliary clearance. *Xenobiotica; the fate of foreign compounds in biological systems*. 42:28-45.

Frezard, F., and A. Garnier-Suillerot. 1998. Permeability of lipid bilayer to anthracycline derivatives. Role of the bilayer composition and of the temperature. *Biochimica et biophysica acta*. 1389:13-22.

Fukuda, H., R. Ohashi, M. Tsuda-Tsukimoto, and I. Tamai. 2008. Effect of plasma protein binding on in vitro-in vivo correlation of biliary excretion of drugs evaluated by sandwich-cultured rat hepatocytes. *Drug metabolism and disposition: the biological fate of chemicals*. 36:1275-1282.

Funk, C. 2008. The role of hepatic transporters in drug elimination. *Expert opinion on drug metabolism & toxicology*. 4:363-379.

Ganong, W.F. 1995. Review of Medical Physiology (Seventeenth edition). Appleton and Lange, Conneticut, USA. 459 pp.

Giacomini, K.M., S.M. Huang, D.J. Tweedie, L.Z. Benet, K.L. Brouwer, X. Chu, A. Dahlin, R. Evers, V. Fischer, K.M. Hillgren, K.A. Hoffmaster, T. Ishikawa, D. Keppler, R.B. Kim, C.A. Lee, M. Niemi, J.W. Polli, Y. Sugiyama, P.W. Swaan, J.A. Ware, S.H. Wright, S.W. Yee, M.J. Zamek-Gliszczynski, and L. Zhang. 2010. Membrane transporters in drug development. *Nature reviews. Drug discovery*. 9:215-236.

Godoy, P., N.J. Hewitt, U. Albrecht, M.E. Andersen, N. Ansari, S. Bhattacharya, J.G. Bode, J. Bolleyn, C. Borner, J. Bottger, A. Braeuning, R.A. Budinsky, B. Burkhardt, N.R. Cameron, G. Camussi, C.S. Cho, Y.J. Choi, J. Craig Rowlands, U. Dahmen, G. Damm, O. Dirsch, M.T. Donato, J. Dong, S. Dooley, D. Drasdo, R. Eakins, K.S. Ferreira, V. Fonsato, J. Fraczek, R. Gebhardt, A. Gibson, M. Glanemann, C.E. Goldring, M.J. Gomez-Lechon, G.M. Groothuis, L. Gustavsson, C. Guyot, D. Hallifax, S. Hammad, A. Hayward, D. Haussinger, C. Hellerbrand, P. Hewitt, S. Hoehme, H.G. Holzhutter, J.B. Houston, J. Hrach, K. Ito, H. Jaeschke, V. Keitel, J.M. Kelm, B. Kevin Park, C. Kordes, G.A. Kullak-Ublick, E.L. LeCluyse, P. Lu, J. Luebke-Wheeler, A. Lutz, D.J. Maltman, M. Matz-Soja, P. McMullen, I. Merfort, S. Messner, C. Meyer, J. Mwinyi, D.J. Naisbitt, A.K. Nussler, P. Olinga, F. Pampaloni, J. Pi, L. Pluta, S.A. Przyborski, A. Ramachandran, V. Rogiers, C. Rowe, C. Schelcher, K. Schmich, M. Schwarz, B. Singh, E.H. Stelzer, B. Stieger, R. Stober, Y. Sugiyama, C. Tetta, W.E. Thasler, T. Vanhaecke, M. Vinken, T.S. Weiss, A. Widera, C.G. Woods, J.J. Xu, K.M. Yarborough, and J.G. Hengstler. 2013. Recent advances in 2D and 3D in vitro systems using primary hepatocytes, alternative hepatocyte sources and non-parenchymal liver cells and their use in investigating mechanisms of hepatotoxicity, cell signaling and ADME. *Archives of toxicology*. 87:1315-1530.

Grime, K., and S.W. Paine. 2013. Species differences in biliary clearance and possible relevance of hepatic uptake and efflux transporters involvement. *Drug metabolism and disposition: the biological fate of chemicals*. 41:372-378.

Hallifax, D., and J.B. Houston. 2012. Evaluation of hepatic clearance prediction using in vitro data: emphasis on fraction unbound in plasma and drug ionisation using a database of 107 drugs. *Journal of pharmaceutical sciences*. 101:2645-2652.

Hewitt, N.J., M.J.G. Lechon, J.B. Houston, D. Hallifax, H.S. Brown, P. Maurel, J.G. Kenna, L. Gustavsson, C. Lohmann, C. Skonberg, A. Guillouzo, G. Tuschl, A.P. Li, E. LeCluyse, G.M.M. Groothuis, and J.G. Hengstler. 2007. Primary hepatocytes: Current understanding of the regulation of metabolic enzymes and transporter proteins, and pharmaceutical practice for the use of hepatocytes in metabolism, enzyme induction, transporter, clearance, and hepatotoxicity studies. *Drug Metab Rev*. 39:159-234.

Hillgren, K.M., D. Keppler, A.A. Zur, K.M. Giacomini, B. Stieger, C.E. Cass, and L. Zhang. 2013. Emerging transporters of clinical importance: an update from the International Transporter Consortium. *Clinical pharmacology and therapeutics*. 94:52-63.

Hirano, M., K. Maeda, S. Matsushima, Y. Nozaki, H. Kusuhara, and Y. Sugiyama. 2005. Involvement of BCRP (ABCG2) in the biliary excretion of pitavastatin. *Molecular pharmacology*. 68:800-807.

Hobbs, M., C. Parker, H. Birch, and K. Kenworthy. 2012. Understanding the interplay of drug transporters involved in the disposition of rosuvastatin in the isolated perfused rat liver using a physiologically-based pharmacokinetic model. *Xenobiotica; the fate of foreign compounds in biological systems*. 42:327-338.

Hoffmaster, K.A., R.Z. Turncliff, E.L. LeCluyse, R.B. Kim, P.J. Meier, and K.L. Brouwer. 2004. P-glycoprotein expression, localization, and function in sandwich-cultured primary rat and human hepatocytes: relevance to the hepatobiliary disposition of a model opioid peptide. *Pharmaceutical research*. 21:1294-1302.

Hoffmaster, K.A., M.J. Zamek-Gliszczynski, G.M. Pollack, and K.L. Brouwer. 2005. Multiple transport systems mediate the hepatic uptake and biliary excretion of the metabolically stable opioid peptide [D-penicillamine2,5]enkephalin. *Drug metabolism and disposition: the biological fate of chemicals*. 33:287-293.

Houston, J.B. 1994. Utility of in vitro drug metabolism data in predicting in vivo metabolic clearance. *Biochemical pharmacology*. 47:1469-1479.

Huang, L., L. Berry, S. Ganga, B. Janosky, A. Chen, J. Roberts, A.E. Colletti, and M.H. Lin. 2010. Relationship between passive permeability, efflux, and predictability of clearance from in vitro metabolic intrinsic clearance. *Drug metabolism and disposition: the biological fate of chemicals*. 38:223-231.

Huang, L., A. Chen, J. Roberts, B. Janosky, X. Be, L. Berry, and M.H. Lin. 2012. Use of uptake intrinsic clearance from attached rat hepatocytes to predict hepatic clearance for poorly permeable compounds. *Xenobiotica; the fate of foreign compounds in biological systems*. 42:830-840.

Huang, L., Y. Wang, and S. Grimm. 2006. ATP-dependent transport of rosuvastatin in membrane vesicles expressing breast cancer resistance protein. *Drug metabolism and disposition: the biological fate of chemicals*. 34:738-742.

HUGO. 2014. HUGO Gene Nomenclature Committee. [ONLINE] Available at: http://www.genenames.org/genefamilies. [Accessed 27 May 2014].

Ieiri, I., S. Suwannakul, K. Maeda, H. Uchimaru, K. Hashimoto, M. Kimura, H. Fujino, M. Hirano, H. Kusuhara, S. Irie, S. Higuchi, and Y. Sugiyama. 2007. SLCO1B1 (OATP1B1, an uptake transporter) and ABCG2 (BCRP, an efflux transporter) variant alleles and pharmacokinetics of pitavastatin in healthy volunteers. *Clinical pharmacology and therapeutics*. 82:541-547.

Imaoka, T., T. Mikkaichi, K. Abe, M. Hirouchi, N. Okudaira, and T. Izumi. 2013. Integrated approach of in vivo and in vitro evaluation of the involvement of hepatic uptake organic anion transporters in the drug disposition in rats using rifampicin as an inhibitor. *Drug metabolism and disposition: the biological fate of chemicals*. 41:1442-1449.

Irvine, J.D., L. Takahashi, K. Lockhart, J. Cheong, J.W. Tolan, H.E. Selick, and J.R. Grove. 1999. MDCK (Madin-Darby canine kidney) cells: A tool for membrane permeability screening. *Journal of pharmaceutical sciences*. 88:28-33.

Ito, K., and J.B. Houston. 2004. Comparison of the use of liver models for predicting drug clearance using in vitro kinetic data from hepatic microsomes and isolated hepatocytes. *Pharmaceutical research*. 21:785-792.

Iwatsubo, T., H. Suzuki, and Y. Sugiyama. 1997. Prediction of species differences (rats, dogs, humans) in the in vivo metabolic clearance of YM796 by the liver from in vitro data. *The Journal of pharmacology and experimental therapeutics*. 283:462-469.

Jemnitz, K., Z. Veres, M. Szabo, Z. Baranyai, F. Jakab, and L. Vereczkey. 2012. Differential inhibitory effect of cyclosporin A and bosentan on taurocholate uptake in human and rat hepatocytes as a function of culturing time. *Toxicology in vitro : an international journal published in association with BIBRA*. 26:174-181.

Jung, D., M.G. Elferink, F. Stellaard, and G.M. Groothuis. 2007. Analysis of bile acid-induced regulation of FXR target genes in human liver slices. *Liver international : official journal of the International Association for the Study of the Liver*. 27:137-144.

Kim, T.H., H.J. Park, and J.H. Choi. 2013. Functional Characterization of ABCB4 Mutations Found in Low Phospholipid-Associated Cholelithiasis (LPAC). *The Korean journal of physiology & pharmacology : official journal of the Korean Physiological Society and the Korean Society of Pharmacology*. 17:525-530.

Kitamura, S., K. Maeda, Y. Wang, and Y. Sugiyama. 2008. Involvement of multiple transporters in the hepatobiliary transport of rosuvastatin. *Drug metabolism and disposition: the biological fate of chemicals*. 36:2014-2023.

Koepsell, H., K. Lips, and C. Volk. 2007. Polyspecific organic cation transporters: structure, function, physiological roles, and biopharmaceutical implications. *Pharmaceutical research*. 24:1227-1251.

Kola, I., and J. Landis. 2004. Can the pharmaceutical industry reduce attrition rates? *Nature reviews. Drug discovery*. 3:711-715.

Lam, J.L., H. Okochi, Y. Huang, and L.Z. Benet. 2006. In vitro and in vivo correlation of hepatic transporter effects on erythromycin metabolism: characterizing the importance of transporter-enzyme interplay. *Drug metabolism and disposition: the biological fate of chemicals*. 34:1336-1344.

LeCluyse, E.L., K.L. Audus, and J.H. Hochman. 1994. Formation of extensive canalicular networks by rat hepatocytes cultured in collagen-sandwich configuration. *The American journal of physiology*. 266:C1764-1774.

Lepper, E.R., K. Nooter, J. Verweij, M.R. Acharya, W.D. Figg, and A. Sparreboom. 2005. Mechanisms of resistance to anticancer drugs: the role of the polymorphic ABC transporters ABCB1 and ABCG2. *Pharmacogenomics*. 6:115-138.

Leuthold, S., B. Hagenbuch, N. Mohebbi, C.A. Wagner, P.J. Meier, and B. Stieger. 2009. Mechanisms of pH-gradient driven transport mediated by organic anion polypeptide transporters. *American journal of physiology. Cell physiology*. 296:C570-582.

Li, L., P.J. Meier, and N. Ballatori. 2000. Oatp2 mediates bidirectional organic solute transport: a role for intracellular glutathione. *Molecular pharmacology*. 58:335-340.

Li, L., A. Nouraldeen, and A.G. Wilson. 2013. Evaluation of transporter-mediated hepatic uptake in a non-radioactive high-throughput assay: a study of kinetics, species difference and plasma protein effect. *Xenobiotica; the fate of foreign compounds in biological systems*. 43:253-262.

Li, N., Y.A. Bi, D.B. Duignan, and Y. Lai. 2009a. Quantitative expression profile of hepatobiliary transporters in sandwich cultured rat and human hepatocytes. *Molecular pharmaceutics*. 6:1180-1189.

Li, N., P. Singh, K.M. Mandrell, and Y. Lai. 2010. Improved extrapolation of hepatobiliary clearance from in vitro sandwich cultured rat hepatocytes through absolute quantification of hepatobiliary transporters. *Molecular pharmaceutics*. 7:630-641.

Li, N., Y. Zhang, F. Hua, and Y. Lai. 2009b. Absolute difference of hepatobiliary transporter multidrug resistance-associated protein (MRP2/Mrp2) in liver tissues and isolated hepatocytes from rat, dog, monkey, and human. *Drug metabolism and disposition: the biological fate of chemicals*. 37:66-73.

Lindahl, A., A. Sjoberg, U. Bredberg, H. Toreson, A.L. Ungell, and H. Lennernas. 2004. Regional intestinal absorption and biliary excretion of fluvastatin in the rat: possible involvement of mrp2. *Molecular pharmaceutics*. 1:347-356.

Lipinski, C.A., F. Lombardo, B.W. Dominy, and P.J. Feeney. 1997. Experimental and computational approaches to estimate solubility and permeability in drug discovery and development settings. *Advanced drug delivery reviews*. 23:3-25.

Liu, L., and K.S. Pang. 2005. The roles of transporters and enzymes in hepatic drug processing. *Drug metabolism and disposition: the biological fate of chemicals*. 33:1-9.

Liu, X., J.P. Chism, E.L. LeCluyse, K.R. Brouwer, and K.L. Brouwer. 1999a. Correlation of biliary excretion in sandwich-cultured rat hepatocytes and in vivo in rats. *Drug metabolism and disposition: the biological fate of chemicals*. 27:637-644.

Liu, X., E.L. LeCluyse, K.R. Brouwer, L.S. Gan, J.J. Lemasters, B. Stieger, P.J. Meier, and K.L. Brouwer. 1999b. Biliary excretion in primary rat hepatocytes cultured in a collagen-sandwich configuration. *The American journal of physiology*. 277:G12-21.

Liu, X., E.L. LeCluyse, K.R. Brouwer, R.M. Lightfoot, J.I. Lee, and K.L. Brouwer. 1999c. Use of Ca2+ modulation to evaluate biliary excretion in sandwich-cultured rat hepatocytes. *The Journal of pharmacology and experimental therapeutics*. 289:1592-1599.

Lombardo, F., R.S. Obach, M.Y. Shalaeva, and F. Gao. 2002. Prediction of volume of distribution values in humans for neutral and basic drugs using physicochemical measurements and plasma protein binding data. *Journal of medicinal chemistry*. 45:2867-2876.

Loo, T.W., and D.M. Clarke. 2005. Recent progress in understanding the mechanism of P-glycoprotein-mediated drug efflux. *The Journal of membrane biology*. 206:173-185.

Lowry, O.H., N.J. Rosebrough, A.L. Farr, and R.J. Randall. 1951. Protein measurement with the Folin phenol reagent. *The Journal of biological chemistry*. 193:265-275.

Lundquist, P., J. Loof, U. Fagerholm, I. Sjogren, J. Johansson, S. Briem, J. Hoogstraate, L. Afzelius, and T.B. Andersson. 2014. Prediction of in vivo rat biliary drug clearance from an in vitro hepatocyte efflux model. *Drug metabolism and disposition: the biological fate of chemicals*. 42:459-468.

Mahmood, I. 2012. Interspecies scaling of biliary excreted drugs: prediction of human clearance and volume of distribution. *Drug metabolism and drug interactions*. 27:157-164.

Mahmood, I., and J.D. Balian. 1996a. Interspecies scaling: predicting clearance of drugs in humans. Three different approaches. *Xenobiotica; the fate of foreign compounds in biological systems*. 26:887-895.

Mahmood, I., and J.D. Balian. 1996b. Interspecies scaling: predicting pharmacokinetic parameters of antiepileptic drugs in humans from animals with special emphasis on clearance. *Journal of pharmaceutical sciences*. 85:411-414.

Marion, T.L., E.M. Leslie, and K.L. Brouwer. 2007. Use of sandwich-cultured hepatocytes to evaluate impaired bile acid transport as a mechanism of drug-induced hepatotoxicity. *Molecular pharmaceutics*. 4:911-918.

Martignoni, M., G.M. Groothuis, and R. de Kanter. 2006. Species differences between mouse, rat, dog, monkey and human CYP-mediated drug metabolism, inhibition and induction. *Expert opinion on drug metabolism & toxicology*. 2:875-894.

Masuda, M., Y. I'Izuka, M. Yamazaki, R. Nishigaki, Y. Kato, K. Ni'inuma, H. Suzuki, and Y. Sugiyama. 1997. Methotrexate is excreted into the bile by canalicular multispecific organic anion transporter in rats. *Cancer research*. 57:3506-3510.

McGinnity, D.F., M.G. Soars, R.A. Urbanowicz, and R.J. Riley. 2004. Evaluation of fresh and cryopreserved hepatocytes as in vitro drug metabolism tools for the prediction of metabolic clearance. *Drug metabolism and disposition: the biological fate of chemicals*. 32:1247-1253.

Meier, P.J., A. St Meier-Abt, C. Barrett, and J.L. Boyer. 1984. Mechanisms of taurocholate transport in canalicular and basolateral rat liver plasma membrane vesicles. Evidence for an electrogenic canalicular organic anion carrier. *The Journal of biological chemistry*. 259:10614-10622.

Menochet, K., K.E. Kenworthy, J.B. Houston, and A. Galetin. 2012. Simultaneous assessment of uptake and metabolism in rat hepatocytes: a comprehensive mechanistic model. *The Journal of pharmacology and experimental therapeutics*. 341:2-15.

Milletti, F., L. Storchi, G. Sforna, and G. Cruciani. 2007. New and original pKa prediction method using grid molecular interaction fields. *Journal of chemical information and modeling*. 47:2172-2181.

Nakakariya, M., M. Ono, N. Amano, T. Moriwaki, K. Maeda, and Y. Sugiyama. 2012. In vivo biliary clearance should be predicted by intrinsic biliary clearance in sandwich-cultured hepatocytes. *Drug metabolism and disposition: the biological fate of chemicals*. 40:602-609.

Nezasa, K., K. Higaki, M. Takeuchi, M. Nakano, and M. Koike. 2003. Uptake of rosuvastatin by isolated rat hepatocytes: comparison with pravastatin. *Xenobiotica; the fate of foreign compounds in biological systems*. 33:379-388.

Ninomiya, M., K. Ito, R. Hiramatsu, and T. Horie. 2006. Functional analysis of mouse and monkey multidrug resistance-associated protein 2 (Mrp2). *Drug metabolism and disposition: the biological fate of chemicals*. 34:2056-2063.

Ninomiya, M., K. Ito, and T. Horie. 2005. Functional analysis of dog multidrug resistance-associated protein 2 (Mrp2) in comparison with rat Mrp2. *Drug metabolism and disposition: the biological fate of chemicals*. 33:225-232.

Nishimuta, H., T. Nakagawa, N. Nomura, and M. Yabuki. 2013. Species differences in hepatic and intestinal metabolic activities for 43 human cytochrome P450 substrates between humans and rats or dogs. *Xenobiotica; the fate of foreign compounds in biological systems*. 43:948-955.

Noe, J., R. Portmann, M.E. Brun, and C. Funk. 2007. Substrate-dependent drug-drug interactions between gemfibrozil, fluvastatin and other organic anion-transporting peptide (OATP) substrates on OATP1B1, OATP2B1, and OATP1B3. *Drug metabolism and disposition: the biological fate of chemicals*. 35:1308-1314.

Nordell, P., P. Svanberg, J. Bird, and K. Grime. 2013. Predicting metabolic clearance for drugs that are actively transported into hepatocytes: incubational binding as a consequence of in vitro hepatocyte concentration is a key factor. *Drug metabolism and disposition: the biological fate of chemicals*. 41:836-843.

Obach, R.S. 1997. Nonspecific binding to microsomes: impact on scale-up of in vitro intrinsic clearance to hepatic clearance as assessed through examination of warfarin,

imipramine, and propranolol. *Drug metabolism and disposition: the biological fate of chemicals*. 25:1359-1369.

Obach, R.S. 1999. Prediction of human clearance of twenty-nine drugs from hepatic microsomal intrinsic clearance data: An examination of in vitro half-life approach and nonspecific binding to microsomes. *Drug metabolism and disposition: the biological fate of chemicals*. 27:1350-1359.

Osypiw, J.C., R.L. Allen, and D. Billington. 1994. Subpopulations of rat hepatocytes separated by Percoll density-gradient centrifugation show characteristics consistent with different acinar locations. *The Biochemical journal*. 304 (Pt 2):617-624.

Oude Elferink, R.P., and C.C. Paulusma. 2007. Function and pathophysiological importance of ABCB4 (MDR3 P-glycoprotein). *Pflugers Archiv : European journal of physiology*. 453:601-610.

Paine, S.W., A.J. Parker, P. Gardiner, P.J. Webborn, and R.J. Riley. 2008. Prediction of the pharmacokinetics of atorvastatin, cerivastatin, and indomethacin using kinetic models applied to isolated rat hepatocytes. *Drug metabolism and disposition: the biological fate of chemicals*. 36:1365-1374.

Pang, L.S., Sun, H., and Liu, S. 2007. Interplay of drug transporters and enzymes on hepatic drug processing. *In* Drug Transporters: Molecular characterisation and role in drug disposition. Y. Guofeng, and Morris, M., editor. John Wily & Sons, Hoboken, New Jersey. 709-745.

Parker, A.J., and J.B. Houston. 2008. Rate-limiting steps in hepatic drug clearance: comparison of hepatocellular uptake and metabolism with microsomal metabolism of saquinavir, nelfinavir, and ritonavir. *Drug metabolism and disposition: the biological fate of chemicals*. 36:1375-1384.

Poirier, A., T. Lave, R. Portmann, M.E. Brun, F. Senner, M. Kansy, H.P. Grimm, and C. Funk. 2008. Design, data analysis, and simulation of in vitro drug transport kinetic experiments using a mechanistic in vitro model. *Drug metabolism and disposition: the biological fate of chemicals*. 36:2434-2444.

Poulin, P., C.E. Hop, Q. Ho, J.S. Halladay, S. Haddad, and J.R. Kenny. 2012a. Comparative assessment of In Vitro-In Vivo extrapolation methods used for predicting hepatic metabolic clearance of drugs. *Journal of pharmaceutical sciences*. 101:4308-4326.

Poulin, P., J.R. Kenny, C.E. Hop, and S. Haddad. 2012b. In vitro-in vivo extrapolation of clearance: modeling hepatic metabolic clearance of highly bound drugs and comparative assessment with existing calculation methods. *Journal of pharmaceutical sciences*. 101:838-851.

Prentis, R.A., Y. Lis, and S.R. Walker. 1988. Pharmaceutical innovation by the seven UK-owned pharmaceutical companies (1964-1985). *British journal of clinical pharmacology*. 25:387-396.

Riley, R.J., D.F. McGinnity, and R.P. Austin. 2005. A unified model for predicting human hepatic, metabolic clearance from in vitro intrinsic clearance data in hepatocytes and

microsomes. *Drug metabolism and disposition: the biological fate of chemicals*. 33:1304-1311.

Rioux, N., E. Bellavance, H. Poirier, M. Dupuis, M. Garneau, M.D. Ribadeneira, and J. Duan. 2013. A strategy to reduce biliary clearance in early drug discovery. *Journal of pharmacological and toxicological methods*. 68:346-348.

Rollins, D.E., and C.D. Klaassen. 1979. Biliary excretion of drugs in man. *Clinical pharmacokinetics*. 4:368-379.

Ros, J.E., L. Libbrecht, M. Geuken, P.L. Jansen, and T.A. Roskams. 2003. High expression of MDR1, MRP1, and MRP3 in the hepatic progenitor cell compartment and hepatocytes in severe human liver disease. *The Journal of pathology*. 200:553-560.

Saito, H., H. Hirano, H. Nakagawa, T. Fukami, K. Oosumi, K. Murakami, H. Kimura, T. Kouchi, M. Konomi, E. Tao, N. Tsujikawa, S. Tarui, M. Nagakura, M. Osumi, and T. Ishikawa. 2006. A new strategy of high-speed screening and quantitative structure-activity relationship analysis to evaluate human ATP-binding cassette transporter ABCG2-drug interactions. *The Journal of pharmacology and experimental therapeutics*. 317:1114-1124.

Sasaki, M., H. Suzuki, J. Aoki, K. Ito, P.J. Meier, and Y. Sugiyama. 2004. Prediction of in vivo biliary clearance from the in vitro transcellular transport of organic anions across a double-transfected Madin-Darby canine kidney II monolayer expressing both rat organic anion transporting polypeptide 4 and multidrug resistance associated protein 2. *Molecular pharmacology*. 66:450-459.

Seglen, P.O. 1976. Preparation of isolated rat liver cells. *Methods in cell biology*. 13:29-83.

Shilling, A.D., F. Azam, J. Kao, and L. Leung. 2006. Use of canalicular membrane vesicles (CMVs) from rats, dogs, monkeys and humans to assess drug transport across the canalicular membrane. *Journal of pharmacological and toxicological methods*. 53:186-197.

Shimada, S., H. Fujino, T. Morikawa, M. Moriyasu, and J. Kojima. 2003. Uptake mechanism of pitavastatin, a new inhibitor of HMG-CoA reductase, in rat hepatocytes. *Drug metabolism and pharmacokinetics*. 18:245-251.

Shitara, Y., T. Horie, and Y. Sugiyama. 2006. Transporters as a determinant of drug clearance and tissue distribution. *European journal of pharmaceutical sciences : official journal of the European Federation for Pharmaceutical Sciences*. 27:425-446.

Shitara, Y., H. Sato, and Y. Sugiyama. 2005. Evaluation of drug-drug interaction in the hepatobiliary and renal transport of drugs. *Annual review of pharmacology and toxicology*. 45:689-723.

Shugarts, S., and L.Z. Benet. 2009. The role of transporters in the pharmacokinetics of orally administered drugs. *Pharmaceutical research*. 26:2039-2054.

Smith, D.A., B.C. Jones, and D.K. Walker. 1996. Design of drugs involving the concepts and theories of drug metabolism and pharmacokinetics. *Medicinal research reviews*. 16:243-266.

Soars, M.G., K. Grime, J.L. Sproston, P.J. Webborn, and R.J. Riley. 2007. Use of hepatocytes to assess the contribution of hepatic uptake to clearance in vivo. *Drug metabolism and disposition: the biological fate of chemicals*. 35:859-865.

Soars, M.G., P.J. Webborn, and R.J. Riley. 2009. Impact of hepatic uptake transporters on pharmacokinetics and drug-drug interactions: use of assays and models for decision making in the pharmaceutical industry. *Molecular pharmaceutics*. 6:1662-1677.

Sohlenius-Sternbeck, A.K. 2006. Determination of the hepatocellularity number for human, dog, rabbit, rat and mouse livers from protein concentration measurements. *Toxicology in vitro : an international journal published in association with BIBRA*. 20:1582-1586.

Sohlenius-Sternbeck, A.K., C. Jones, D. Ferguson, B.J. Middleton, D. Projean, E. Floby, J. Bylund, and L. Afzelius. 2012. Practical use of the regression offset approach for the prediction of in vivo intrinsic clearance from hepatocytes. *Xenobiotica; the fate of foreign compounds in biological systems*. 42:841-853.

Song, S., H. Suzuki, R. Kawai, and Y. Sugiyama. 1999. Effect of PSC 833, a P-glycoprotein modulator, on the disposition of vincristine and digoxin in rats. *Drug metabolism and disposition: the biological fate of chemicals*. 27:689-694.

Stringer, R., P.L. Nicklin, and J.B. Houston. 2008. Reliability of human cryopreserved hepatocytes and liver microsomes as in vitro systems to predict metabolic clearance. *Xenobiotica; the fate of foreign compounds in biological systems*. 38:1313-1329.

Strober, W. 2001. Trypan blue exclusion test of cell viability. *Current protocols in immunology / edited by John E. Coligan ... [et al.]*. Appendix 3:Appendix 3B.

Swift, B., N.D. Pfeifer, and K.L. Brouwer. 2010. Sandwich-cultured hepatocytes: an in vitro model to evaluate hepatobiliary transporter-based drug interactions and hepatotoxicity. *Drug Metab Rev*. 42:446-471.

Tahara, H., H. Kusuhara, E. Fuse, and Y. Sugiyama. 2005. P-glycoprotein plays a major role in the efflux of fexofenadine in the small intestine and blood-brain barrier, but only a limited role in its biliary excretion. *Drug metabolism and disposition: the biological fate of chemicals*. 33:963-968.

Thiel-Demby, V.E., J.E. Humphreys, L.A. St John Williams, H.M. Ellens, N. Shah, A.D. Ayrton, and J.W. Polli. 2009. Biopharmaceutics classification system: validation and learnings of an in vitro permeability assay. *Molecular pharmaceutics*. 6:11-18.

Tonsberg, H., R. Holm, T.G. Bjerregaard, J.B. Boll, J. Jacobsen, and A. Mullertz. 2010. An updated and simplified method for bile duct cannulation of rats. *Laboratory animals*. 44:373-376.

Treijtel, N., A. Barendregt, A.P. Freidig, B.J. Blaauboer, and J.C. van Eijkeren. 2004. Modeling the in vitro intrinsic clearance of the slowly metabolized compound tolbutamide determined in sandwich-cultured rat hepatocytes. *Drug metabolism and disposition: the biological fate of chemicals*. 32:884-891.

Tsujii, H., J. Konig, D. Rost, B. Stockel, U. Leuschner, and D. Keppler. 1999. Exon-intron organization of the human multidrug-resistance protein 2 (MRP2) gene mutated in Dubin-Johnson syndrome. *Gastroenterology*. 117:653-660.

Turncliff, R.Z., X. Tian, and K.L. Brouwer. 2006. Effect of culture conditions on the expression and function of Bsep, Mrp2, and Mdr1a/b in sandwich-cultured rat hepatocytes. *Biochemical pharmacology*. 71:1520-1529.

Umehara, K., and G. Camenisch. 2012. Novel in vitro-in vivo extrapolation (IVIVE) method to predict hepatic organ clearance in rat. *Pharmaceutical research*. 29:603-617.

van de Waterbeemd, H., and E. Gifford. 2003. ADMET in silico modelling: towards prediction paradise? *Nature reviews. Drug discovery*. 2:192-204.

Varma, M.V., G. Chang, Y. Lai, B. Feng, A.F. El-Kattan, J. Litchfield, and T.C. Goosen. 2012. Physicochemical property space of hepatobiliary transport and computational models for predicting rat biliary excretion. *Drug metabolism and disposition: the biological fate of chemicals*. 40:1527-1537.

Watanabe, T., H. Kusuhara, K. Maeda, H. Kanamaru, Y. Saito, Z. Hu, and Y. Sugiyama. 2010. Investigation of the rate-determining process in the hepatic elimination of HMG-CoA reductase inhibitors in rats and humans. *Drug metabolism and disposition: the biological fate of chemicals*. 38:215-222.

Watkins, J.B., 3rd, and T.P. Dykstra. 1987. Alterations in biliary excretory function by streptozotocin-induced diabetes. *Drug metabolism and disposition: the biological fate of chemicals*. 15:177-183.

Webborn, P.J., A.J. Parker, R.L. Denton, and R.J. Riley. 2007. In vitro-in vivo extrapolation of hepatic clearance involving active uptake: theoretical and experimental aspects. *Xenobiotica; the fate of foreign compounds in biological systems*. 37:1090-1109.

Wilkinson, G.R., and D.G. Shand. 1975. Commentary: a physiological approach to hepatic drug clearance. *Clinical pharmacology and therapeutics*. 18:377-390.

Williams, J.A., R. Hyland, B.C. Jones, D.A. Smith, S. Hurst, T.C. Goosen, V. Peterkin, J.R. Koup, and S.E. Ball. 2004. Drug-drug interactions for UDP-glucuronosyltransferase substrates: a pharmacokinetic explanation for typically observed low exposure (AUCi/AUC) ratios. *Drug metabolism and disposition: the biological fate of chemicals*. 32:1201-1208.

Wohnsland, F., and B. Faller. 2001. High-throughput permeability pH profile and high-throughput alkane/water log P with artificial membranes. *Journal of medicinal chemistry*. 44:923-930.

Wolf, K.K., K.R. Brouwer, G.M. Pollack, and K.L. Brouwer. 2008. Effect of albumin on the biliary clearance of compounds in sandwich-cultured rat hepatocytes. *Drug metabolism and disposition: the biological fate of chemicals*. 36:2086-2092.

Wolf, K.K., S. Vora, L.O. Webster, G.T. Generaux, J.W. Polli, and K.L. Brouwer. 2010. Use of cassette dosing in sandwich-cultured rat and human hepatocytes to identify drugs

that inhibit bile acid transport. *Toxicology in vitro : an international journal published in association with BIBRA*. 24:297-309.

Wu, C.Y., and L.Z. Benet. 2005. Predicting drug disposition via application of BCS: transport/absorption/ elimination interplay and development of a biopharmaceutics drug disposition classification system. *Pharmaceutical research*. 22:11-23.

Yabe, Y., A. Galetin, and J.B. Houston. 2011. Kinetic characterization of rat hepatic uptake of 16 actively transported drugs. *Drug metabolism and disposition: the biological fate of chemicals*. 39:1808-1814.

Yamashiro, W., K. Maeda, M. Hirouchi, Y. Adachi, Z. Hu, and Y. Sugiyama. 2006. Involvement of transporters in the hepatic uptake and biliary excretion of valsartan, a selective antagonist of the angiotensin II AT1-receptor, in humans. *Drug metabolism and disposition: the biological fate of chemicals*. 34:1247-1254.

Yang, X., Y.A. Gandhi, D.B. Duignan, and M.E. Morris. 2009. Prediction of biliary excretion in rats and humans using molecular weight and quantitative structure-pharmacokinetic relationships. *The AAPS journal*. 11:511-525.

Zamek-Gliszczynski, M.J., H. Xiong, N.J. Patel, R.Z. Turncliff, G.M. Pollack, and K.L. Brouwer. 2003. Pharmacokinetics of 5 (and 6)-carboxy-2',7'-dichlorofluorescein and its diacetate promoiety in the liver. *The Journal of pharmacology and experimental therapeutics*. 304:801-809.

Zhao, Y.H., J. Le, M.H. Abraham, A. Hersey, P.J. Eddershaw, C.N. Luscombe, D. Butina, G. Beck, B. Sherborne, I. Cooper, and J.A. Platts. 2001. Evaluation of human intestinal absorption data and subsequent derivation of a quantitative structure-activity relationship (QSAR) with the Abraham descriptors. *Journal of pharmaceutical sciences*. 90:749-784.

Zhou, F., and G. You. 2007. Molecular insights into the structure-function relationship of organic anion transporters OATs. *Pharmaceutical research*. 24:28-36.

Zhu, C., L. Jiang, T.M. Chen, and K.K. Hwang. 2002. A comparative study of artificial membrane permeability assay for high throughput profiling of drug absorption potential. *European journal of medicinal chemistry*. 37:399-407.

Zou, P., X. Liu, S. Wong, M.R. Feng, and B.M. Liederer. 2013. Comparison of in vitro-in vivo extrapolation of biliary clearance using an empirical scaling factor versus transport-based scaling factors in sandwich-cultured rat hepatocytes. *Journal of pharmaceutical sciences*. 102:2837-2850.